UNIVERSITY OF SOUTHAMPTON

MID-FREQUENCY VIBRATION ANALYSIS OF BUILT-UP STRUCTURES

by

Lin Ji

SUBMITTED FOR THE DEGREE OF

DOCTOR OF PHILOSOPHY

INSTITUTE OF SOUND AND VIBRATION RESEARCH

FACULTY OF ENGINEERING AND APPLIED SCIENCE

SEPTEMBER 2003

UNIVERSITY OF SOUTHAMPTON

ABSTRACT

FACULTY OF ENGINEERING AND APPLIED SCIENCE

INSTITUTE OF SOUND AND VIBRATION RESEARCH

Doctor of Philosophy

MID-FREQUENCY VIBRATION ANALYSIS OF BUILT-UP STRUCTURES

by Lin Ji

The thesis concerns the vibration analysis of built-up structures at frequencies where neither standard, low-frequency deterministic methods nor high-frequency statistical methods are appropriate, i.e. the so-called 'mid-frequency' vibration region. The system model considered is a typical form of such complex built-up structures, composed of a long-wavelength (low mode-count) source and a short-wavelength (high mode-count) receiver. The interfaces might be either discrete-point couplings or continuous couplings. The thesis is presented in four parts.

The first part concerns discrete point coupling cases between a stiff source and a flexible receiver. A concept of 'power modes' is introduced to estimate the power transmitted to a flexible receiver. It allows expressions for the upper and lower bounds and the mean value of the transmitted power to be developed in a simple manner. The second part involves three cases of straight-line coupling of beam-stiffened plates. A hybrid Mode/FT approach and locally reacting impedance method are presented to predict simply and accurately the frequency response of the beam and the power transmitted to the plate, as well as the effective mass and damping loaded to the beam by the presence of the plate. The third part concerns an arbitrary continuous coupling between the long- and short-wavelength substructures. A mode-based approach is described, which is able to accommodate both deterministic and statistical models. Relevant results are compared to those of 'Resound' and 'Fuzzy' structure theory. Following the numerical examples presented in the previous parts, the main theoretical developments are experimentally verified in Part IV. Good agreements are observed.

ACKNOWLEDGEMENTS

The author wishes to thank Dr B. R. Mace and Dr R. J. Pinnington for their guidance and encouragement. She also gratefully acknowledges the support, both academic and financial, from ISVR, especially the Dynamics Group. Tremendous tributes are paid to the family members, who support the author in a quiet manner and watch her gradually making progress with great patience. Mr J. Han, beloved husband and also the best friend, deserves all the best words in the world.

CONTENTS

LIST OF TABLES

LIST OF FIGURES

GLOSSARY OF SYMBOLS

$\mathbf{A_r}$ dynamic correlation matrix between the receiver and the interface

$\mathbf{A_s}$ dynamic correlation matrix between the source and the interface

b_n nth modal receptance of the uncoupled beam

b_n' nth modal receptance of the coupled beam

D_b complex stiffness of the beam

D_p complex stiffness of the plate

$\mathbf{D_C}$ scaling matrix

F_0 amplitude of an external excitation harmonic point force

$f(x)$ force distribution

$f_e(x_b^e)$ amplitude of the external time-harmonic forces acting on the beam

$f_{e,n}$ nth modal forces corresponding to external force on the source structure

$f_I^b(x_b)$ amplitude of the interface time-harmonic forces acting on the beam

$f_{I,k}$ kth generalized interface force coordinate

$f_{I,m}^r$ mth modal force corresponding to the interface force on the receiver structure

$f_{I,n}^s$ nth modal forces corresponding to the interface force on the source structure

$f_I^p(x_p^I, y_p^I)$ amplitude of the interface time-harmonic forces acting on the plate

$\mathbf{f_{e,n}}$ column vectors composed of $f_{e,n}$

$\mathbf{f_{I,k}}$ column vectors composed of $f_{I,k}$

$\mathbf{f_{I,m}^r}$ column vectors composed of $f_{I,m}^r$

$\mathbf{f_{I,n}^s}$ column vectors composed of $f_{I,n}^s$

$F(k)$ Fourier Transform of $f(x)$

$F_e\left(\mathbf{x}_s^e\right)$ external force acting at the local coordinate $\mathbf{x}_s^e$

$F_I\left(\mathbf{x}_I\right)$ interface force at the local coordinate $\mathbf{x}_I$

$F_I^r\left(\mathbf{x}_r^I\right)$ interface force at the local coordinate $\mathbf{x}_r^I$

$F_I^s\left(\mathbf{x}_s^I\right)$ interface forces acting at the local coordinates $\mathbf{x}_s^I$

$\mathbf{F}$ vector of amplitudes of the forces

$\mathbf{F}_I$ interface force vector

H conjugate transpose

k wavenumber

k_b free wavenumber of the beam

k_b' wavenumber of the beam after coupling to the plate

k_p free wavenumber of the plate

k_x wavenumber in the x-direction

k_y wavenumber in the y-direction

$K(k)$ line dynamic stiffness of the plate

$\mathbf{K}$ stiffness matrix of a continuous structure

L_b length of the beam

m_b mass distribution of the beam (mass per unit length)

m_k, m_n, m_n' effective mass (density)

m_p mass distribution of the plate (mass per unit area)

m_r mass distribution of the receiver structure (mass per unit length/area/volume)

m_s mass distribution of the source structure (mass per unit length/area/volume)

$\mathbf{M}$ real part of the complex mobility matrix

$\bar{\mathbf{M}}$ complex mobility matrix

$\mathbf{M}_C$ scalled dimensionless mobility matrix

$\bar{\mathbf{M}}_R$ mobility matrix of the receiver at the interface points

$\mathbf{M}_R$ the real part of the mobility matrix $\bar{\mathbf{M}}_R$

$\bar{\mathbf{M}}_S$ mobility matrix of the source at the interface points

$\bar{\mathbf{M}}_{RS}$ complex Hermitian matrix combined by $\bar{\mathbf{M}}_S$ and $\bar{\mathbf{M}}_R$

P , P' transmitted power

$\bar{P}$ frequency averaged power

P_{low} , P'_{low} lower bound of the transmitted power

P_{up} , P'_{up} upper bound of the transmitted power

p_m mth modal receptance of the plate

$\mathbf{Q}$ power mode force vector

$\mathbf{T}_r$ transformation matrix between the local coordinates $\mathbf{x}_r^I$ and $\mathbf{x}_I$

$\mathbf{T}_s$ transformation matrix between the local coordinates $\mathbf{x}_s^I$ and $\mathbf{x}_I$

V_I region of the interface

V_r^I region of the receiver occupied by the interface

V_s^e the region of the source over which the external force loadings act

V_s^I the region of the source over which the interface force loadings act

$\mathbf{V}$ vector of amplitudes of the velocities

$\mathbf{V}_{sf}$ free velocity vector of the source substructure at the interface points

w displacement

$w_{b,n}$ modal coordinate of the nth mode of the beam

$w_{I,k}$ kth generalized interface displacement coordinate

$w_{r,m}$ modal coordinate of the mth mode of the receiver structure

$w_{s,n}$ modal coordinate of the nth mode of the source structure

$w_b(x)$ displacement of the beam

$w_p(x, y)$ displacement of the plate

$w_I(\mathbf{x_I})$ interface displacement

$\mathbf{w_{r,m}}$ column vectors composed of $w_{r,m}$

$\mathbf{w_{s,n}}$ column vectors composed of $w_{s,n}$

$W_b(k)$ Fourier Transform of $w_b(x)$

$W_p(k_x, k_y)$ Fourier Transform of $w_p(x, y)$

x_b local coordinate of the beam

(x_p, y_p) local coordinates of the plate

(x_p^I, y_p^I) interface locations on the plate

$\mathbf{x}$ a general location of a structure

$\mathbf{x_I}$ local coordinate of the interface

$\mathbf{x_r}$ a general location of a receiver structure

$\mathbf{x_s}$ a general location of a source structure

$Y_{b,n}$ nth modal receptance of the uncoupled beam

$Y'_{b,n}$ nth modal receptance of the coupled beam

$Y_{r,m}$ mth modal receptance of the uncoupled receiver

$Y_{s,n}$ nth modal receptance of the uncoupled source

$Y(k_x)$ line receptance of the plate

$\mathbf{Y_n}$ diagonal matrix composed of the modal dynamic receptance of the structure

$\mathbf{Y_{r,m}}$ diagonal matrix composed of $Y_{r,m}$

$\mathbf{Y_{s,n}}$ diagonal matrix composed of $Y_{s,n}$

Z_n plate-loaded modal impedance

Z_p , Z'_p line impedance of the plate

$\boldsymbol{\alpha}_{\mathbf{r}}$, $\boldsymbol{\beta}_{\mathbf{r}}$ modal correlation matrices between $\Psi_{r,m}$ and $\mathrm{X}_{I,k}$

$\boldsymbol{\alpha}_{\mathbf{s}}$, $\boldsymbol{\beta}_{\mathbf{s}}$ modal correlation matrices between $\Phi_{s,n}$ and $\mathrm{X}_{I,k}$

$\eta_n^{(b)}$ nth modal loss factor of the beam

η_k , η_n , η'_n effective loss factor

θ attachment angle of the beam on the plate

$\theta_{r,\kappa}$ phase angle of a natural mode of the receiver structure

κ the number of the dimensions of the receiver structure

$\overline{\lambda}$ the mean value of λ_n

λ_n eigenvalues of $\mathbf{M}$

$\lambda_{\max}^{RS}$ maximum eigenvalue of $\overline{\mathbf{M}}_{\mathbf{RS}}$

$\lambda_{\min}^{R}$ minimum eigenvalue of $\mathbf{M}_{\mathbf{R}}$

$\boldsymbol{\Lambda}$, $\boldsymbol{\Lambda}_{\mathbf{RS}}$ real and non-negative diagonal matrix

ρ mass density

σ standard deviation of λ_n

$\phi_{b,n}(x)$ nth normalized mode shape function of the beam

$\hat{\phi}_{b,n}(x)$ new set of orthogonal functions by extending $\phi_{b,n}$ in $-\infty < x < +\infty$

$\Phi_{b,n}(k)$ Fourier Transform of $\hat{\phi}_{b,n}(x)$

$\Phi_{s,n}$ nth mass-normalized unloaded mode shape function of the source structure

$\boldsymbol{\Phi}$ unitary matrix

$\mathrm{X}_k(\mathbf{x}_{\mathbf{I}})$ kth interface basis functions

$\chi_r(y)$ rth normalized mode shape functions of the plate along y-direction

$\psi_k(x)$ kth normalized mode shape functions of the plate along x-direction

$\varphi_m(x, y)$ mth normalized mode shape of the plate

$\Psi_{r,m}$ mth unloaded mass-normalized mode shape of the receiver

$\mathbf{\Psi}$ orthogonal matrix composed of the eigenvectors of matrix $\mathbf{M}$

ω frequency

$\omega_{b,n}$, $\omega_n^{(b)}$ nth natural frequency of the beam

$\omega_{r,m}$ mth natural frequency of the receiver structure

$\omega_{s,n}$ nth natural frequency of the source structure

Chapter 1

INTRODUCTION

1.1 MID-FREQUENCY VIBRATION PROBLEMS: THE LIMITATIONS OF LOW-FREQUENCY DETERMINISTIC AND HIGH-FREQUENCY STATISTICAL METHODS

The analysis of vibration transmission in complex built-up structures is relevant to many practical structural-acoustic systems of engineering interest, such as occur in vehicles, aircraft structures, mechanical equipment, etc. Usually these complex systems can be viewed as being fabricated from many components, with quite different vibration properties, joined together at their interfaces. One common example of such an arrangement is a beam-stiffened plate structure, being broadly representative of machine foundations in ships. The beam is usually well-defined with long-wavelengths and/or low modal density, while the plate has relatively short-wavelengths and/or high modal density with complex boundary conditions. The mismatch between the local dynamic properties of the components may then present a number of challenges to predicting the vibrations of the coupled system, due to the limitations between the low-frequency deterministic methods and the high-frequency statistical methods. These vibration issues are therefore defined as the 'mid-frequency' vibration problem [1-8].

In principle, subsystems of arbitrary complexity can be modelled across the entire frequency range using deterministic descriptions of the subsystem dynamics, using, for example, finite elements (FE). However, at high frequencies, in what might be termed the 'mid-frequency' range, it becomes difficult to devise a precise mathematical model that can adequately capture the complex response pattern. This is because, in the context of FEA [9-10], it is generally considered that approximately four to eight elements (depending on the related vibration shape functions) must be used adequately to resolve each structural wavelength. As the wavelengths of interest become shorter, more and more degrees of freedom are therefore typically required to provide a deterministic description of the dynamic of a subsystem. This can and does lead to unfeasibly large models at high frequencies. Computational limitations therefore may place a restriction on the highest frequency at which such a description can be maintained, for a given subsystem.

Computational cost is not the sole issue for a deterministic FE model. Actually, even if it is possible to extend the FE model to the mid-frequency range at the expense of rapidly increasing demands in terms of the size of the model and consequent analysis time and cost, the results of deterministic prediction of frequency response might be very unreliable. This is because the system response becomes increasingly sensitive to geometrical imperfections as frequency increases [11], so that even a very detailed deterministic mathematical model based on the nominal system properties may not yield a reliable response prediction.

The statistical energy analysis (SEA) method has been successfully applied to the high-frequency vibration analysis of coupled systems [12-17]. Vibration energy as an independent variable is taken to mean the time-average sum of the kinetic and potential energies under stationary random excitation and vibration inputs are expressed in terms of time-average input powers, rather than in terms of external forces or displacements. The primary aim of the analysis is to estimate the distribution of vibration energy among the coupled subsystems, and for this purpose energy balance equations are set up which involve expressions for power flowing from one subsystem to another. However, it requires that each subsystem ideally contains a number of resonant modes within the analysis frequency band of interest, which implies that the wavelength of the subsystem deformation is of the same order as, or less than, the dimensions of the subsystem [1]. In the mid-frequency range, however, this requirement may be only partly met, i.e. the frequencies are not high enough to make the wavelengths of all subsystems to be sufficiently short. As a result, the energy-based approach may become too broad-brush and lose all details of the system vibration behaviour.

Given the difficulties arising from the limitations of a deterministic FE model and a statistical SEA model, there is a desire to predict the mid-frequency vibrations of built-up structures in a simple manner but with acceptable accuracy.

1.2 LITERATURE REVIEW OF RELEVANT EXISTING METHODS

Concerning the above mid-frequency vibration issue, some effort has been made in this research area and a number of model reduction and specialist methods have been developed. The foremost amongst them are briefly reviewed below.

The component-mode-synthesis (CMS) method is one of the most commonly used model reduction methods, and is very useful if all the subsystems of a built-up structure have at most modest levels of component modal uncertainty [3]. The principle of CMS is

to divide the system into subsystem models and then assemble them together by the interface boundary conditions of the subsystems, thus the size of the system model can be reduced greatly. CMS models can be set up both in the time-domain and in the frequency-domain, and these two kinds of model can be transferred between each other and to incorporate measured data.

Frequency-domain CMS approaches involve coupling subsystem frequency response function (FRF) matrices by enforcing compatibility and equilibrium between the interface degrees of freedom (DOFs) and forces. This involves inverting an FRF matrix and subsequent manipulations on a frequency-by-frequency basis rather than solving an algebraic eigenvalue problem. These approaches have the advantage of being able to incorporate experimental FRFs directly into its spectral formulations without a knowledge of the system modes, which can be very difficult to compute accurately especially for the higher order ones. However, these inherently require several matrix inversion calculations, and hence can be very time-consuming for large interface DOF cases, e.g., line or surface couplings.

In time-domain approaches, the response of a subsystem is described in terms of shape functions, or modes. The most common approaches include fixed and free interface normal modes of vibration together with constraint or attachment modes and perhaps also rigid body modes [18]. Other component modes are also suggested in [19-20]. Subsystem models are coupled together and solved for the global modes in terms of the local shape functions. These approaches can be potentially very useful to deal with the difficulties of many interface DOFs by the use of generalized interface DOFs, such as suggested in [21-22], so as to alleviate the computational issue. But more research has to be done in this area.

One other relevant study is that of [23-24] where FRF descriptions of subsystems (modelled using free interface modes without residuals) were coupled, solved and used to determine the vibration behaviour of the coupled system. Again they are problematic for coupling cases with many interface DOFs.

Structural model reduction can also be realized by the wave-based approach [25], in which the vibration fields of subsystems are represented in terms of a superposition of travelling waves. The relationship between the subsystem wavenumbers can be determined by the trace-matching of the travelling waves at the junctions. Then the parameters can be determined to model the response of each subsystem plus its boundary conditions. Furthermore the parameters can be determined to model the response of the

complete structure by combining the separate responses of the subsystems. This approach is especially useful for infinite structures.

Except for these above mentioned model reduction methods, there are also some specialist numerical/analytical methods developed by different authors to deal with the couplings of long-wavelength (low modal density) and short-wavelength waves (high modal density). The significant ones include 'Resound' theory [1], the local modal/perturbational (LM/P) method [3], fuzzy structure theory [4-6], a combination of FEA and analytical impedances [26-28] and multipole theory [29-30].

In the 'Resound' approach [1], the vibration analysis of complex dynamic systems is based on partitioning the system DOFs into a 'global' and a 'local' set. The global equations of motion are formulated and solved in a standard deterministic manner with due account being taken of the presence of the local DOFs. The local equations of motion are formulated and solved by using SEA methods with due account being taken of power input from the global DOFs. This hybrid approach forms a flexible framework within which a number of existing analytical techniques can be devised, and has been found to yield good results for a relatively simple system comprising two coupled rods. The application of this method to more complex systems, however, is still ongoing.

In [3], a local modal/perturbational (LM/P) method is described which enables estimations to be made of the statistics of frequency functions of a system whose properties are uncertain. The global modes of the baseline system are found in terms of the subsystem modes by using CMS method. Uncertainty is assumed to exist in the local modal properties of the subsystems. A perturbation is found which relates small changes in the local modal properties to those in the global modal properties. This method can be efficiently used to determine the variability in the dynamic responses of a system caused by the inherent variability of its properties. But it requires that the random statistical distributions of the modal properties of the subsystems are known.

Fuzzy structure theory [5-6] models a deterministic master substructure coupled to a fuzzy substructure modelled statistically as a continuous set of light oscillators. The key result of fuzzy structure theory is that the attached items act mainly to provide damping to the master structure, and furthermore the level of this damping is (surprisingly) independent of the dissipation factor of the attachments. These results agree well with those obtained from the resound theory. However, the fuzzy structure theory has been based on special examples so far rather than with a somewhat general class of cases.

In [26-27], it is established that for a beam/plate coupled structure, if the wavenumber of the plate is at least twice that of the beam, the short-wavelength plate presents a locally reacting impedance to the long-wavelength beam at the joints. Consequently, such a locally reacting plate model can be incorporated into a standard sub-structuring procedure to predict the vibration response of a beam-stiffened plate system by splitting the coupled structure into a beam attached to a set of independent narrow strips of the plate. The corresponding solution, however, may still be very time-consuming since the calculation still requires many connecting points between the beam and the plates.

In [29-30], the vibration power transmitted by N forces can be regarded as the power transmitted by N independent poles of vibration. The source of vibration can thus be taken as moving in a set of vibrational poles and the receiver be defined by a set of polar mobilities and impedances, provided the structure is symmetric or if the power transmission by each pole is independent. This technique is extremely useful in measurement. In [7], it is found that the multipole theory is particularly suitable for the following cases: (1) both the source and the receiver structures are fully symmetric with respect to the common boundary; (2) the source structure is fully symmetric and the receiver has high modal overlap with non-distinct resonant behaviour; and (3) the source structure is much stiffer than the receiver, which has high modal overlap with non-distinct resonant behaviour. For other situations, the multipole method has no advantages over the conventional FRF based sub-structuring (frequency-domain CMS) method.

It is true to say that more research is required before generally accepted methods are fully developed to couple long- and short-wavelength substructures in the so-called 'mid-frequency' region. This provides the motivations of the present research.

1.3 AIMS OF THE RESEARCH

This research is directed at the development of new and appropriate methods for the mid-frequency vibration analysis of built-up structures, which are composed of both long-wavelength (low modal density) and short-wavelength (high modal density) substructures. The emphasis is put on estimating as accurately as possible the coupling energy flow between the long wave and short wave substructures. Because the number of the interface DOFs might be very large in many cases (e.g. line or surface coupling), computational cost will be a very real issue. Various possible model reduction (mainly for interface DOF model reduction) and approximate techniques are therefore investigated. The key is the ability to couple subsystems of different forms within the same system model, e.g.

different components may be modelled using different techniques, the choice being determined by the characteristics of the individual component and its properties.

The system model considered is composed of a stiff source and a flexible receiver, being a typical form of a built-up structure. The interfaces might be either discrete-point couplings (e.g. a machine resiliently mounted to a flexible foundation) or continuous couplings (e.g. the beam-stiffened plate machinery foundation of a ship). Conventional FRF-based sub-structuring method, Fourier Transform (FT), modal analysis and wave methods are used as appropriate. By introducing some techniques for simplifying, decomposing and approximating different coupling models, new methodologies are then developed based on these conventional approaches in certain hybrid forms of different theoretical models.

For a better understanding of the whole vibration properties of the coupled system, the FRFs of the stiff source and the power transmitted to the flexible receiver are particularly of interest. (The predicted power can then be input to a SEA model, by assuming energy conservation of the system, i.e., the power transmitted to the receiver P_{tr} equals to the power dissipated by the receiver P_{diss}, so that the mean-square velocity response of the receiver structure $\left\langle \overline{v_r^2} \right\rangle$ can be predicted from $\left\langle \overline{v_r^2} \right\rangle = P_{tr}/(\eta_r \omega M_r)$, where η_r and M_r are respectively the damping loss factor and the total mass of the receiver, and ω is the vibration frequency of interest [11].) The dynamic interactions between the long wave and short wave substructures will be investigated at the same time. The performance of the newly developed approaches will be assessed against conventional methods, e.g. the FRF-based sub-structuring method, by numerical examples, together with comparisons to some specialist approaches, e.g. the 'Resound' and fuzzy structure theory. Since many practical built-up structures are essentially assembled by thin plates and beams joined in many different ways, the numerical models involved will be beam/plate coupled systems, where a stiff beam (long wave model) coupled to a flexible plate (short wave model), an external time-harmonic point force being applied directly to the beam. Finally the main theoretical developments will be experimentally verified by laboratory measurements.

It is expected that a general framework can be formed for coupling different types of subsystem models and for developing interface reduction methods for the mid-frequency vibration predictions.

1.4 THESIS STRUCTURE

The thesis is presented in four parts after this introduction. The first part concerns the discrete-point coupling cases for which a new technique, the power mode method, is developed. Two chapters are involved in this part of thesis. In Chapter 2, the concept of power modes is introduced and used to estimate the power transmission to a structure from multiple sources. In Chapter 3, this power mode approach is extended to estimating the power transmission between a stiff source and a flexible receiver through discrete coupling, where the system may be subjected to multi-directional and rotational vibrations. Both are presented with numerical examples.

In the second part of the thesis, three special cases of beam-stiffened plates with straight-line couplings are considered, being an infinite beam attached to an infinite plate, a finite beam attached to an infinite plate, and a finite beam attached to a finite plate where the beam and the plate modal shapes are the same along the coupling. These are described, respectively, in Chapters 4-6. A number of methods, either conventional (Fourier Transform (FT), wave analysis, and FRF-based sub-structuring methods) or newly developed (the approximate Mode/FT and locally reacting impedance methods as well as the analytical mode-based method), are investigated and compared. Although only special cases of beam/plate coupling systems are considered in this part of thesis, it provides new methodologies, both analytical and approximate, on which the vibration of a general stiff beam/flexible plate system can be predicted in certain ways much more simply. This finally leads to Part III for predicting the vibration of a stiff source/flexible receiver system with general continuous couplings.

Based on the methodologies provided in Part II, a so-called 'mode-based' approach is developed in Part III to deal with general continuous coupling cases between a stiff source and a flexible receiver, together with the Mode/FT and locally reacting methods. The theoretical procedures of this mode-based approach, either analytical or approximate, are described in Chapter 7. A technique of transferring the physical DOFs into generalized DOFs is used to reduce the system DOFs. In addition, modelling of different subsystems by different appropriate coupling techniques is made, the choice being determined by the locally dynamic properties of the individual subsystem of interest. Numerical applications of the mode-based approach are given in Chapter 8 for beam-stiffened plate models, where the rectangular plate attached is relatively very flexible compared to the source beam, and the beam may be either straight or L-shaped.

Laboratory measurements, as the final part of this thesis, are arranged to experimentally verify the main theoretical developments of the research. These are given in Chapter 9.

1.4.1 Original contributions of the thesis

Much of the work presented in this thesis is original. These mainly include the power mode approach described in Chapters 2 and 3, the Mode/FT approach and the locally reacting impedance method in Chapter 5, and the Mode-based approach in Chapters 6-7. The predicted results are then compared with those of the conventional FRF-based sub-structuring method as well as some lab measurements. Moreover, the dynamic interactions between the components of the built-up complex structures are investigated as a general class of cases rather than a specific example. Expressions are given for the dynamic stiffness modification matrix, effective mass and effective damping induced to the dynamics of the source by the presence of the receiver. The results are then compared with the 'Resound' and fuzzy structure theory in the cases of a relatively very flexible receiver (fuzzy-attachment) loaded on a stiff source (master-structure). All the comparisons show fairly good agreement.

Part I

DISCRETE-POINT COUPLINGS: POWER MODES

An issue which is frequently the focus of noise and vibration control procedures is the prediction and control of the power transmitted from a resiliently mounted machine to a flexible foundation via a multiple point interface. A common arrangement of such a vibration system can be modelled as a stiff source connected to a flexible receiver through discrete point couplings. The difficulty in providing a complete solution of the transmitted power, due to the complex nature of the coupled system, has been widely recognised. Although different techniques [29-30, 32, and 36] are available to simplify the problem, there are certain limitations in their application (e.g. as described in section 1.2). More general techniques are required to predict the transmitted power in a simple manner but with acceptable accuracy.

With this in mind, a concept of 'power modes' is introduced to approximate the broad features of the transmitted power rather than attempted to describe the detailed response precisely. This is the so-called 'power mode approach'. In Chapter 2, the approach is used to estimate the power transmission from multiple sources. Then in Chapter 3 it is further extended for more general cases, namely a stiff source attached to a flexible receiver through discrete-point couplings. In principle, the power mode approach has two main advantages: first, it allows expressions for the upper and lower bounds and the mean value of the transmitted power to be developed in a simple manner; and secondly, it can involve both the translational and rotational motions of the system.

Chapter 2

A POWER MODE APPROACH TO ESTIMATING POWER TRANSMISSION FROM MULTIPLE SOURCES

2.1 INTRODUCTION

Generally, the prediction of the power transmission from multiple sources requires full knowledge of both the strength of the source excitations and the dynamic properties of the receiver. It tends to be quite problematic when there is a large number of excitation points and/or when the receiver structure involves some dynamic uncertainties.

On account of the difficulties arising from an exact description of the transmitted power, a so-called 'power mode approach' is described in this chapter for estimating the power transmission from multiple sources in a simple manner. A set of force sources is transformed into arrays of force distributions. The transformation involves the eigenvalues and eigenvectors of the real part of the mobility matrix of the receiver. As a result, the vibrational power transmitted by N forces can be considered as being transmitted by N independent contributions, i.e., power modes, with each of them related only to one set of force distribution (eigenvector) and one eigenvalue. Thus N terms contribute to the power, rather than the N^2 terms involving the original forces. This eigen-decomposition technique was first suggested in [32]. Here it is further extended and approximations are developed for the maximum and minimum possible values and the mean value of the transmitted power.

The 'multipole' approach of [29-30] is somewhat similar, except that the transformation matrices are pre-selected 'Hadamard' matrices, so that the polar mobilities can be regarded as monopole, dipole, quadrupole terms, etc. Using this approach, the power injected by many of the cross terms is often negligible. However, the receiver structure must be geometrically symmetrical or the source a set of uncorrelated outputs.

There are two main advantages to the power mode approach. First, it allows expressions for the upper and lower bounds and the mean value of the transmitted power to be developed in a simple manner. Secondly, this approach can be used for cases where both force and moment excitations are involved.

In the next section the power mode theory is developed for an array of point forces applied to a region of a structure whose properties are uniform and homogeneous. Then various approximations are developed. Following this, more general situations are considered. These include the case of combined force and moment sources and that of velocity source excitations. Finally some numerical examples are presented.

2.2 POWER MODE THEORY

Suppose an array of N time harmonic forces are applied to a structure at a frequency ω. The time averaged power transmitted to the receiver can be expressed as

$$P = \frac{1}{2}\mathrm{Re}\left\{\mathbf{F}^H\mathbf{V}\right\}, \mathbf{V} = \bar{\mathbf{M}}\mathbf{F} \tag{2.1}$$

where $\mathbf{F}$ is the vector of amplitudes of the forces, $\mathbf{V}$ is the vector of amplitudes of the velocities of the receiving structure at the excitation points, $\bar{\mathbf{M}}$ is the complex mobility matrix of the receiver structure, and the superscript H denotes the conjugate transpose. Equation (2.1) can be written as

$$P = \frac{1}{4}\mathrm{Re}\left\{\mathbf{F}^H\mathbf{V} + \mathbf{V}^H\mathbf{F}\right\} = \frac{1}{4}\mathrm{Re}\left\{\mathbf{F}^H\left(\bar{\mathbf{M}} + \bar{\mathbf{M}}^H\right)\mathbf{F}\right\} \tag{2.2}$$

Since $\left(\bar{\mathbf{M}} + \bar{\mathbf{M}}^H\right) = 2\,\mathrm{Re}\left\{\bar{\mathbf{M}}\right\}$, the transmitted power becomes

$$P = \frac{1}{2}\mathbf{F}^H\mathbf{M}\mathbf{F} \tag{2.3}$$

where $\mathbf{M}$ is the real part of the complex mobility matrix $\bar{\mathbf{M}}$. Equation (2.3) shows that the power transmission depends only on the real part of the mobility matrix, whose imaginary part can therefore be ignored as far as power transmission is concerned.

Since equation (2.3) is in a non-negative definite quadratic form, $\mathbf{M}$ is a real, symmetric and non-negative definite matrix. By matrix theories [33-34], $\mathbf{M}$ can be decomposed into the form

$$\mathbf{M} = \mathbf{\Psi}\mathbf{\Lambda}\mathbf{\Psi}^T \tag{2.4}$$

where $\mathbf{\Lambda}$ is a real and non-negative diagonal matrix of the eigenvalues λ_n of $\mathbf{M}$, $\mathbf{\Psi}$ is the orthogonal matrix composed of the corresponding eigenvectors (in columns), so that $\mathbf{\Psi}\mathbf{\Psi}^T = \mathbf{\Psi}^T\mathbf{\Psi} = \mathbf{I}$, and the superscript T denotes the transpose. The eigenvalues are arranged in descending order, i.e.,

$$\lambda_1 \geq \lambda_2 \geq \cdots \geq \lambda_N \geq 0 \tag{2.5}$$

The eigenvalues satisfy the following relations [34]

$$\sum_{n=1}^{N} \lambda_n = \sum_{n=1}^{N} M_{nn} \tag{2.6}$$

$$\sum_{n=1}^{N} \lambda_n^2 = \sum_{m=1}^{N} \sum_{n=1}^{N} M_{mn}^2 = \|M\|_2 \tag{2.7}$$

where $\|M\|_2$ is the second order norm of matrix $\mathbf{M}$. From equations (2.6) and (2.7), the mean value of λ_n and its standard deviation σ are found to be

$$\overline{\lambda} = \sum_{n=1}^{N} M_{nn} \Big/ N \tag{2.8}$$

$$\sigma = \sqrt{\frac{\|M\|_2}{N} - \frac{1}{N^2}\left(\sum_{n=1}^{N} M_{nn}\right)^2} \tag{2.9}$$

Let the force vector $\mathbf{F}$ now be weighted by $\mathbf{\Psi}$ so as to give a new set of forces defined by

$$\mathbf{Q} = \mathbf{\Psi}^T \mathbf{F} \tag{2.10}$$

It follows that

$$\sum_{n=1}^{N} |Q_n|^2 = \sum_{n=1}^{N} |F_n|^2 \tag{2.11}$$

Combining equations (2.3), (2.4) and (2.10), the power transmitted to the receiver can then be re-written as

$$P = \frac{1}{2}\mathbf{Q}^H \mathbf{\Lambda} \mathbf{Q} = \frac{1}{2}\sum_{n=1}^{N} |Q_n|^2 \lambda_n \tag{2.12}$$

Equation (2.12) shows that the vibrational power transmitted to the receiver by N forces can be regarded as the power transmitted by N independent contributions, each of them related only to one set of force distributions (eigenvectors) and one eigenvalue. In [35], 'radiation modes' have been used to describe the power radiated by a vibrating surface into a surrounding acoustic medium, in which the sound power radiation from a set of velocity distributions (radiation modes) on the structure is independent of the amplitudes of the other velocity distributions. Therefore, by analogy to the 'radiation modes', equation (2.12) may be defined as a set of independent 'power modes'. The force vector $\mathbf{Q}$ may thus be called the power mode force vector, which is given in terms of $\mathbf{F}$ and the

eigenvectors of the real part of the mobility matrix, and the eigenvalue λ_n called power mode mobilities. Equation (2.12) involving a sum of N terms is in contrast to equation (2.3) where the power is given by a sum of N^2 terms involving the physical forces $\mathbf{F}$.

Conceptually equation (2.12) is useful. However, it does not provide any practical advantages over equation (2.3) since full knowledge of $\mathbf{M}$ is required to determine its eigenproperties. However, advantages do occur because simple approximations can be developed for the transmitted power based on power mode theory. These are developed in the next section.

2.3 POWER TRANSMISSION APPROXIMATION BASED ON THE POWER MODE APPROACH

As mentioned in Section 2.1, it is often more appropriate to approximate the main properties of the transmitted power rather than attempt to predict precisely the detailed response, especially if the properties of the receiver structure are not known exactly. Therefore in this section the power mode theory is used to find simple approximations for the transmitted power. These give estimates of upper and lower bounds for the transmitted power, as well as its mean value. The actual power thus lies in some range between these upper and lower bounds.

2.3.1 Upper and lower bounds of the transmitted power

Expressions for the upper and lower bounds of the transmitted power can be derived from power mode theory. Combining equations (2.5), (2.11), and (2.12), strict upper and lower bounds are given by

$$P_{up} = \frac{1}{2}\left(\sum_{n=1}^{N}|F_n|^2\right)\lambda_1 \tag{2.13}$$

$$P_{low} = \frac{1}{2}\left(\sum_{n=1}^{N}|F_n|^2\right)\lambda_N \tag{2.14}$$

It is seen that the bounds on power depend only on the maximum and minimum power mode mobilities of the receiver structure λ_1 and λ_N as well as the magnitudes of the force sources $|F_n|$, regardless of the distribution and the relative phases of the force sources [32]. Therefore it is a good simplification to estimate the transmitted power using upper and lower bounds. Since the usefulness of such an approximate approach depends on the width of the range formed by the upper and lower limits, equations (2.13) and (2.14) are

very suitable for cases where the maximum and minimum power mode mobilities of the receiver structures are comparable. It should be noted here the upper- and lower-bounds in equations (2.13) and (2.14) refer to variations in force distribution but not ensemble of structures.

Generally the correlation between the individual excitation points of the receiver becomes of decreasing importance as the wavelength of the structure decreases. Therefore when the wavelength of the receiver structure is very short, it is reasonable to neglect the correlations between the individual excitations, at least when frequency averaged, so that each individual excitation is taken to be independent. If it is also assumed that the local driving point properties of the receiver have the same order of magnitude, the eigenvalues λ_n typically are then of the same order of magnitude. As a result, both λ_1 and λ_N will often lie within, say, one standard deviation of the mean $\overline{\lambda}$, so that they can be simply approximated, using equations (2.8) and (2.9), as

$$\lambda_1 \approx \left(\overline{\lambda} + \sigma\right) \tag{2.15}$$

$$\lambda_N \approx \left(\overline{\lambda} - \sigma\right) \tag{2.16}$$

As a result, equations (2.13) and (2.14) can be rewritten as

$$P_{up} \approx \frac{1}{2}\left(\sum_{n=1}^{N}\left|F_n\right|^2\right)\left(\overline{\lambda} + \sigma\right) \tag{2.17}$$

$$P_{low} \approx \frac{1}{2}\left(\sum_{n=1}^{N}\left|F_n\right|^2\right)\left(\overline{\lambda} - \sigma\right) \tag{2.18}$$

So far the upper and lower bounds for the power transmitted to a short-wavelength structure can be approximated using equations (2.17) and (2.18). In such cases, many or all power modes contribute significantly to the transmitted power rather than just a few of them. In particular, when the receiver structure is very flexible (e.g. such that $kl >> 1$ where k is the wavenumber and l the distance between the excitation points), so that each forcing point can be taken as uncorrelated with the others, the power mode mobilities and the power mode forces can be simply approximated by

$$\lambda_n \approx M_{nn} \tag{2.19}$$

$$Q_n \approx F_n \tag{2.20}$$

Equation (2.12) then becomes

$$P \approx \sum_{n=1}^{N}\left(\frac{1}{2}|Q_n|^2 \lambda_n\right) \approx \sum_{n=1}^{N}\left(\frac{1}{2}|F_n|^2 M_{nn}\right) \tag{2.21}$$

The above expression indicates that each power mode contributes significantly to the total power transmission at high frequencies.

In other cases, however, e.g. if the wavelength is very long, individual excitations may be strongly correlated. For example, when the response is dominated by a single resonant mode, then at the resonance frequency, the driving point mobility tends to be quite close to the transfer mobility [29], i.e.,

$$\mathrm{O}[M_{nn}] \approx \mathrm{O}[M_{mn}], m \neq n \tag{2.22}$$

Here it is still assumed that the local driving point properties of the receiver have the same orders of magnitude. As a result, the maximum power-mode mobility λ_1 can be much larger than the minimum one λ_N, which implies that only a few of the lower power modes give significant power transmission. Then the power range formed by equations (2.13) and (2.14) will be too broad to be of practical value, due to a very small lower bound. Under such circumstances, it is more useful to replace the lower bound by the approximation for the power associated with only the first power mode which plays a dominant role in the total power transmission, while the upper bound is still approximated using equation (2.17).

Equation (2.22) implies that the eigenvector ψ_1 has the approximate form

$$\psi_1 \approx \frac{1}{\sqrt{N}}[1 \quad 1 \quad \cdots \quad 1]^T \tag{2.23}$$

When λ_1 is still approximated using equation (2.15), the power transmitted by the first power mode can then be approximated as

$$P_1 \approx \frac{1}{2N}\left|\sum_{n=1}^{N} F_n\right|^2 \left(\bar{\lambda}+\sigma\right) \tag{2.24}$$

Thus the power transmitted to a long-wavelength receiver can be estimated using the range formed by equations (2.17) and (2.24).

Especially in very low frequency range such that $kl << 1$, all forces are in effect applied at same point. It then follows that

$$\lambda_1 \approx \sum_{n=1}^{N} M_{nn}, \lambda_{2,3,\ldots,N} \approx 0 \tag{2.25}$$

$$|Q_1|^2 \approx \frac{1}{N}|F_1 + F_2 + \cdots + F_N|^2 \tag{2.26}$$

Equation (2.12) then becomes

$$P \approx \frac{1}{2}|Q_1|^2 \lambda_1 \approx \frac{1}{2}\left(\left|\sum_{n=1}^{N} F_n\right|^2\right)\sum_{n=1}^{N} M_{nn} \Big/ N \tag{2.27}$$

Equation (2.27) shows that in the low-frequency range the power can be regarded as being transmitted by the first-order power mode only, i.e., one power mode dominates. This is similar to the monopole in the multipole approach.

2.3.2 Mean value of the transmitted power

In the above subsection, upper and lower bounds of the transmitted power were found which define a fairly narrow range within which the transmitted power lies. It is also useful to estimate the mean value of the power over a range of frequencies. An estimate of the mean value of the transmitted power can be found by taking the average over all the power modes.

The mean square power mode force can be found from equation (2.11) to be

$$E\left[|Q_n|^2\right] = \frac{1}{N}\sum_{n=1}^{N}|F_n|^2 \tag{2.28}$$

The mean power modal mobility is given by equation (2.6). The mean value of the transmitted power, when averaged over all the power modes, can thus be approximated in terms of the mean square force and the mean point mobility as

$$E[P] = \frac{N}{2}\left(\frac{1}{N}\sum_{n=1}^{N}|F_n|^2\right)\left(\frac{1}{N}\sum_{n=1}^{N}M_{nn}\right) \tag{2.29}$$

Equation (2.29) is in a very simple form, being equivalent to approximating the mean of a product by the product of their means, and gives an estimate of the frequency average of the transmitted power. This result was also given in [36].

Thus the power transmitted to a receiver structure by an array of point forces can be described in terms of upper and lower bounds and a mean value.

2.4 COMBINED FORCE AND MOMENT EXCITATIONS

The translational motion normal to the surface of the seating is usually the dominant mechanism of power transmission from a machine source to a flexible supporting structure

[36]. However, it is known that in many cases of practical interest, vibration sources apply moments as well as forces. The power transmitted by moment excitations is generally greater at higher frequencies [37-38]. Therefore it is necessary to consider also moment excitations.

Suppose the source array $\mathbf{F}$ is formed partly by a set of forces and partly by a set of moments. The real part of the mobility matrix $\mathbf{M}$ of the receiver structure is now composed of force and moment point mobilities and transfer mobilities, and the transmitted power can be written in the same form as equation (2.3). However, since both $\mathbf{F}$ and $\mathbf{M}$ consist of elements with different units, the approximations developed in Section 2.3 are no longer applicable. In this section, a scaling technique to deal with this problem is described [39-40]. The main principle of this scaling technique is to scale the mobility matrix $\mathbf{M}$ by a specified diagonal matrix to give a new "dimensionless" matrix, and then to weight the physical force vector using the same diagonal matrix to give a new set of forces with the same units. As a result, the power mode approach described in the previous sections can then be applied.

Let $\mathbf{M}$ be scaled by such a real diagonal matrix $\mathbf{D}_C$ defined as

$$D_{C,nn} = \frac{1}{\sqrt{M_{nn}}} \tag{2.30}$$

where $D_{C,nn}$ and M_{nn} are the nth diagonal elements of $\mathbf{D}_C$ and $\mathbf{M}$, respectively, so that

$$\mathbf{M}_C = \mathbf{D}_C \mathbf{M} \mathbf{D}_C \tag{2.31}$$

Let $\mathbf{F}$ be weighted by $\mathbf{D}_C^{-1}$ so as to give a new set of forces defined by

$$\mathbf{F}_C = \mathbf{D}_C^{-1} \mathbf{F} \tag{2.32}$$

Combining equations (2.31) and (2.32) with (2.3) gives

$$P = \frac{1}{2} \mathbf{F}_c^{\,H} \mathbf{M}_c \mathbf{F}_c \tag{2.33}$$

Since the scaled mobility matrix $\mathbf{M}_C$ is real, symmetric, non-negative and dimensionless and $\mathbf{F}_C$ is a vector of the scaled forces with the same units, equation (2.33) then meets all the requirements of the power mode theory.

$\mathbf{M}_C$ is decomposed into the form

$$\mathbf{M}_C = \mathbf{\Psi}_C \mathbf{\Lambda}_C \mathbf{\Psi}_C^T \tag{2.34}$$

where $\mathbf{\Lambda}_C$ is the real and non-negative diagonal matrix of the eigenvalues of $\mathbf{M}_C$, and $\mathbf{\Psi}_C$ is the orthogonal matrix composed of the corresponding eigenvectors (in columns). Let the scaled force vector $\mathbf{F}_C$ be weighted by $\mathbf{\Psi}_C$. A new set of scaled power mode forces can then be written as

$$\mathbf{Q}_C = \mathbf{\Psi}_C{}^T \mathbf{F}_C = \mathbf{\Psi}_C{}^T \mathbf{D}_C^{-1} \mathbf{F} \tag{2.35}$$

Consequently, equation (2.33) can be written in terms of the power modes as

$$P = \frac{1}{2} \mathbf{Q}_C{}^H \mathbf{\Lambda}_C \mathbf{Q}_C = \frac{1}{2} \sum_{n=1}^{N} \left| Q_{C,n} \right|^2 \lambda_{C,n} \tag{2.36}$$

where $\lambda_{C,n}$ is the n th diagonal element of $\mathbf{\Lambda}_C$.

As a result, approximate expressions for the upper and lower bounds as well as the mean value are then developed by analogy with equations (2.17), (2.18) (or (2.24)) and (2.29), with $\mathbf{F}$ being replaced by $\mathbf{F}_C$ and $\mathbf{M}$ by $\mathbf{M}_C$.

The above scaling technique in effect scales the individual excitations by a factor equal to the square root of the real part of the input mobility so that the elements of $\mathbf{F}_C$ have the same units. An alternative scaling procedure can be used, with the scaling matrix $D_{C,n}$ being given by

$$D_{C,nn} = \frac{1}{\sqrt{M_{nn}^{\infty}}} \tag{2.37}$$

where M_{nn}^{∞} is the characteristic point mobility of the receiver structure, i.e., the point mobility if the receiver structure is extended to infinity. Comparing equation (2.30) with (2.37), one can expect that the former give better estimates of the transmitted power while the latter allows for uncertainties in the properties of the receiver structure, e.g. the boundary conditions.

Since the scaling matrices described in equations (2.30) and (2.37) are all frequency-dependent, different scaling matrices may have different influences on the performance of the power approximations.

2.4.1 Other cases

Similar results can be obtained for velocity/rotational velocity excitations in the same manner as that described above for force/moment sources. In this case, however, the

mobility matrix of the receiver structure is replaced by the corresponding impedance matrix, with the roles of the force and velocity vectors being reversed.

In some cases there may also be force excitations which act in different directions on the receiver (e.g. in-plane and out-of-plane forces), so that the corresponding input mobilities M_{nn} may have different orders of magnitude – in-plane motion is usually much stiffer than out-of-plane motion, for example. If such excitations input significant power, then this situation can be treated using the same scaling approach described above.

2.5 NUMERICAL EXAMPLES

Numerical examples are considered in this section. The system model chosen is a thin rectangular plate with four simply supported edges. The material of the plate is chosen to be Perspex, whose material properties are given in Table 2.1. The plate is first assumed to be excited by point forces, and then by co-located force/moment excitations. Both the dimensions of the plate and the excitation points are given in Table 2.2. All the point and transfer mobilities of the plate are calculated using modal summation with analytical modal shapes and natural frequencies. These are given in Appendix I. A running frequency average has been taken over a frequency band of 10Hz width, which is about three times the mean modal spacing, to illustrate the broader features of the power transmission. The exact results are found using equation (2.3), i.e., the classical mobility matrix method.

2.5.1 Plate with force excitations

First the plate is assumed to be excited by three point forces $F_1 = 1$, $F_2 = 2e^{j\pi/3}$ and $F_3 = 0.5e^{-j\pi/4}$ at the three given positions, respectively. Since here there are three point forces, there are consequently three power modes.

Using equation (2.4) a receiver structure can be characterised by a set of power mode mobilities. Figure 2.1 shows the three power mode mobilities of the plate as a function of frequency. The first power mode tends to be much larger than the others at lower frequencies, but becomes comparable to the other power mode mobilities as frequency increases. This implies that the transmitted power is usually dominated by the first power mode at lower frequencies while more power modes give significant contributions at higher frequencies.

This trend is further illustrated in Figure 2.2, which shows the power transmitted by each power mode together with the total power. It can be seen that the power transmitted by the first power mode dominates the total power transmission for the low modal overlap area (e.g. below 70 Hz where the modal overlap factor is less than unity), but the significance of the other two power modes increases as the modal overlap of the receiver increases. Therefore it is quite reasonable to estimate the lower power bound using the first power mode approximation for a stiff and low modal overlap receiver. It should be noted that the power associated with an individual power mode depends on both the power mode mobility and the corresponding power mode force, the latter being determined by not only the excitation forces themselves, but also the forcing positions, as given in equation (2.10). Thus there may be a small power mode mobility and a large power mode force, or vice versa. As a result, the lower order power modes do not necessarily transmit more power than the higher order ones, as shown in Figure 2.2.

In Section 2.3, approximations for the upper and lower bounds and the mean of the transmitted power were developed. Figure 2.3 shows the power transmitted to the plate together with these approximations. It can be seen that the mean power expression in equation (2.29) gives a fairly good approximation to the transmitted power. The upper and the lower bounds expressed by equations (2.17) and (2.18) are very useful approximations for the transmitted power, provided the modal overlap factor of the receiver structure is high enough (e.g. more than 3 (above 200 Hz) in Figure 2.3). Below this frequency the lower bound is more accurately approximated by the power transmitted by the first power mode, given in equation (2.24).

2.5.2 Simultaneous force/moment excitations

The power mode approach can be applied to cases where both force and moment excitations are involved using the scaling technique described in Section 2.4. This is investigated here by assuming the point force sources comprise not only the forces of the previous example, but also consist of co-located moment excitations $M_{x1} = 0.05Nm$, $M_{x2} = 0.075e^{j2\pi/3}Nm$ and $M_{x3} = 0.05jNm$. Figure 2.4 shows the power transmitted to the plate and the approximations when the scaling matrix of equations (2.30) is used. It is seen that the bounds provide a narrow range for the power and the mean value is a good approximation.

Figure 2.5 shows the power transmitted to the plate and the approximations when the scaling matrix of equation (2.37) is used. It is seen that the expressions plotted in Figure

2.4 give better estimates of the transmitted power than Figure 2.5, as we would expect. This is because the scaling approach for Figure 2.4 needs exact information of the point mobilities M_{nn} of the receiver, but the scaling approach for Figure 2.5 only needs the characteristic point mobility terms M_{nn}^{∞} of the receiver. However, the latter scaling approach can be more useful when the receiver structures have some uncertainties, e.g. boundary condition uncertainties.

2.6 SUMMARY

In this chapter a power mode method for estimating the power transmitted to a flexible receiver by an array of point force excitations was described. Based on power mode theory, the vibrational power transmitted by N discrete point forces was regarded as the power transmitted by N independent power modes following eigen-decomposition of the real part of the mobility matrix of the receiving structure. Simple expressions were developed for approximating the upper and lower bounds and the mean value of the transmitted power in terms of these power modes. It also has been shown that these approximations can be extended to more general cases, including that where both force and moment excitations are applied to the structure and where there are velocity source excitations. Finally numerical results were presented for the case of a plate excited at a number of points.

It is known that only under ideal, limiting cases, such as are considered here, can the source mobilities be neglected. In practice, however, the mobilities of the source may be important and thus have to be included. This leads to the application of the power mode technique to estimating the power transmission between a stiff source and a flexible receiver through discrete couplings. This is given in Chapter 3.

Table 2.1 Material properties of the rectangular plate

Young's modulus (GN/m^2)	Poisson's ratio	Loss factor	Density (kg/m^3)
4.4	0.38	0.05	1152

Table 2.2 Plate dimensions and the excitation points

Plate dimensions	Length=2m (x -direction); Width=0.9m (y -direction) Thickness=0.005m
Excitation points	$(x_1, y_1) = (0.37, 0.45)m$ $(x_2, y_2) = (0.89, 0.45)m$ $(x_3, y_3) = (1.34, 0.45)m$

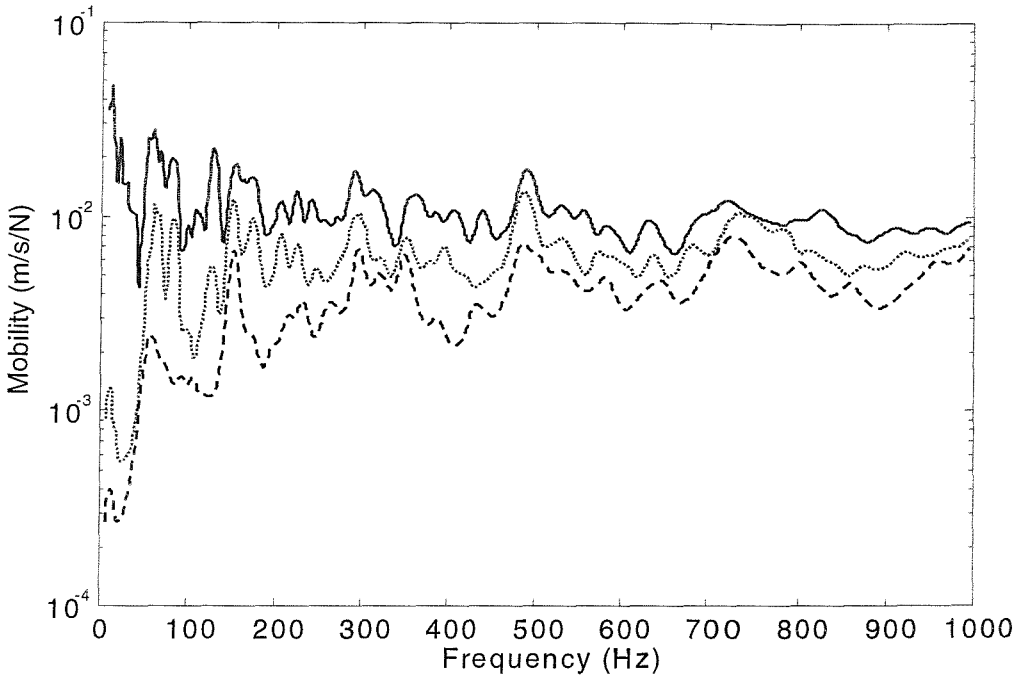

Figure 2.1 Power mode mobilities of the plate: first order (____), second order (·····), and third order (- - - -).

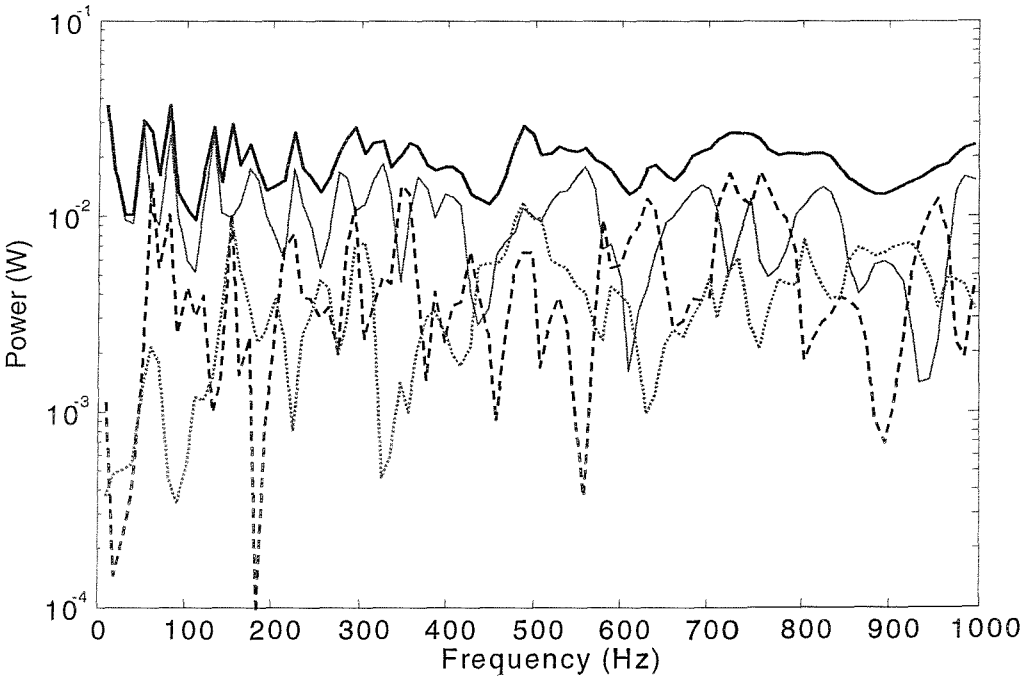

Figure 2.2 Total power transmission and that from each power mode: total power transmission (____ , equation (2.3)); power transmitted from the first (____), second (- - - -) and third (·····) power modes (equation (2.12)).

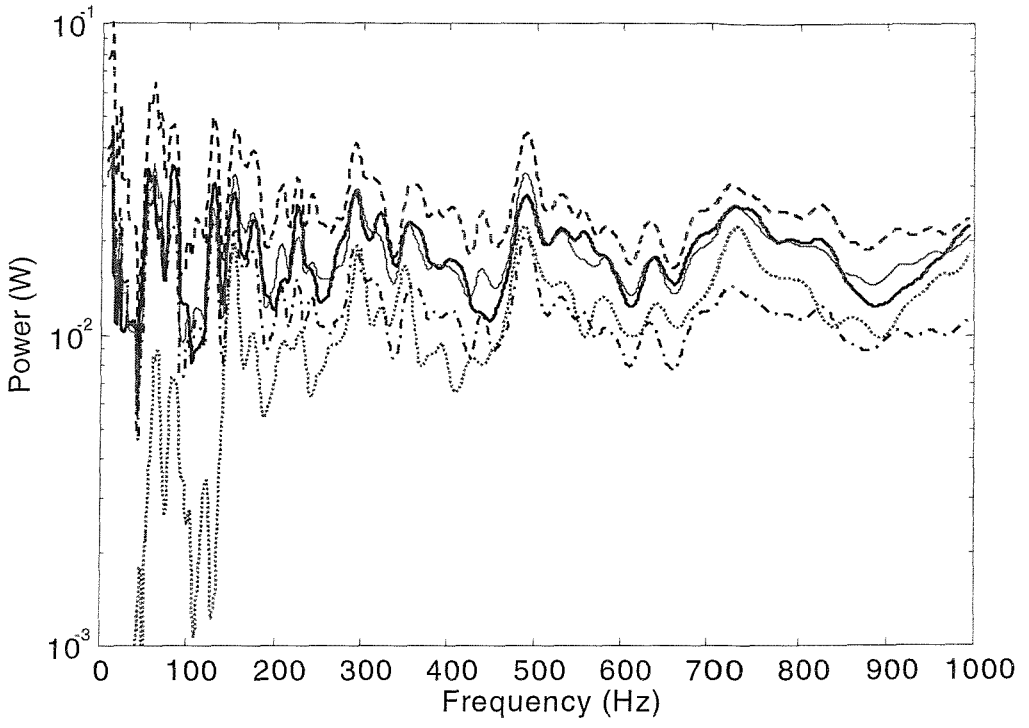

Figure 2.3 Exact and approximate power transmissions to the plate subjected to point forces: exact value (——, equation (2.3)); approximations for the mean (——— , equation (2.29)), upper bound (- - - - , equation (2.17)), lower bound (..... , equation (2.18)), and first power mode (_.._.. , equation (2.24)).

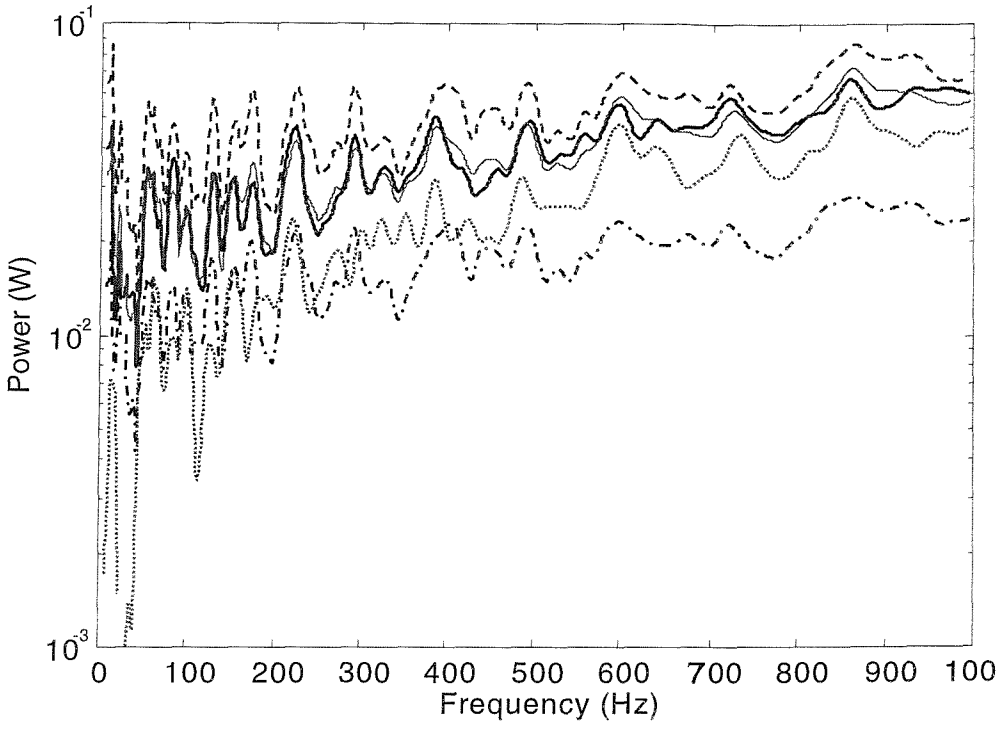

Figure 2.4 Exact and approximate power transmissions to the plate subjected to co-located force/moment excitations (scaled by equation (2.30)): exact value (——— , equation (2.3)); approximations for the mean (——— , equation (2.29)), upper bound (- - - - , equation (2.17)), lower bound (..... , equation (2.18)), and first power mode (-·-·- , equation (2.24)).

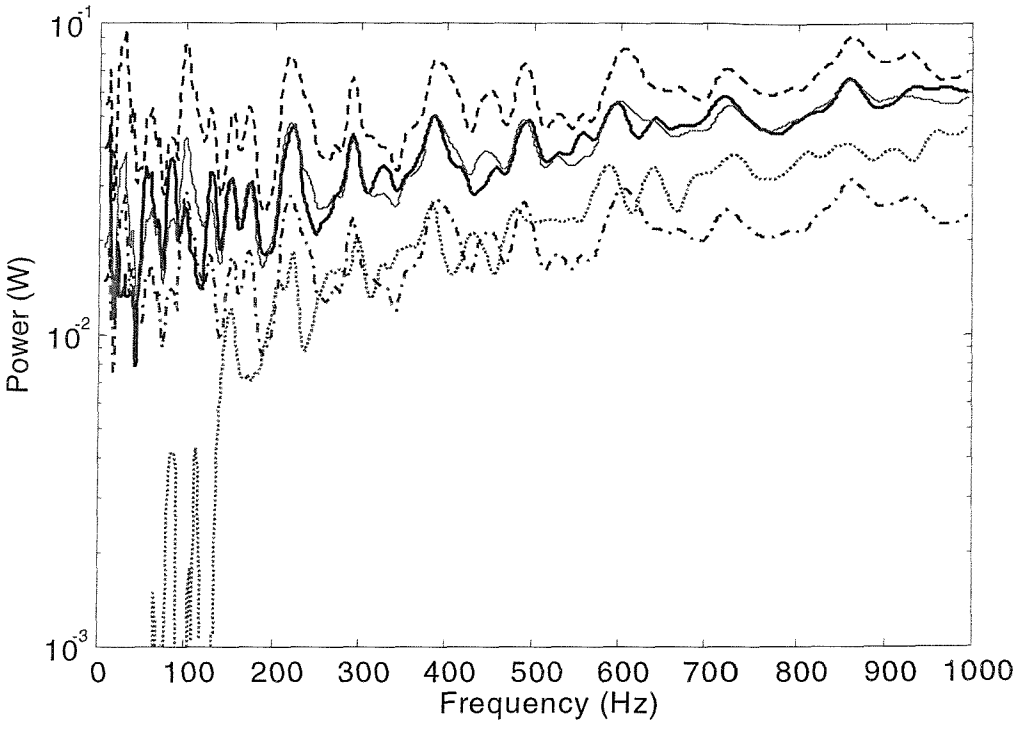

Figure 2.5 Exact and approximate power transmissions to the plate subjected to co-located force/moment excitations (scaled by equation (2.37)): exact value (——— , equation (2.3)); approximations for the mean (——— , equation (2.29)), upper bound (- - - - , equation (2.17)); lower bound (····· , equation (2.18)), and first power mode (_·_·_ , equation (2.24)).

Chapter 3

APPLICATION OF THE POWER MODE APPROACH TO ESTIMATING POWER TRANSMISSION BETWEEN A STIFF SOURCE AND A FLEXIBLE RECEIVER

3.1 INTRODUCTION

In Chapter 2, a power mode approach was developed for estimating the power transmission to a flexible receiver from multiple sources, where ideal force and/or moment excitations were assumed. However, most realistic sources depart from these ideal excitation sources. It is usually necessary to consider a general linear source [11, 41], that is the outputs of the source depend on both the properties of the source structure and the receiver structure. In this chapter, therefore, the power mode approach is extended to the estimation of the power transmitted to a flexible receiver from a stiff source through discrete point couplings. The coupling degrees of freedom (DOFs) may involve both translational and rotational motions, and there may be simultaneous force and moment excitations. The difference of this chapter from the previous one is that the influences of the dynamics of the source structure on the transmitted power are considered.

In the next section a general expression for the power transmission between a source and a receiver through discrete points is described by the FRF-based sub-structuring approach. In Section 3.2.1, the coupling DOFs at the interface points are assumed to be of the same type, e.g. the translational motion due to force coupling. Approximations are made for the upper and lower bounds and the frequency average of the transmitted power, which require less information than an exact description. Then in Section 3.2.2 a matrix scaling technique is introduced to extend these approximations for more general cases where the coupling DOFs of the system may involve different types, e.g. simultaneous translational and rotational motions. Finally, numerical examples are presented concerning a multi-point coupled beam/plate model with force and moment excitations.

3.2 POWER TRANSMISSION BETWEEN A STIFF SOURCE AND A FLEXIBLE RECEIVER

Suppose a source structure is coupled to a receiver structure through N discrete points. The power transmitted from the source to the receiver can be written as

$$P = \frac{1}{2}\mathbf{F}_{\mathrm{I}}{}^{H}\mathbf{M}_{\mathrm{R}}\mathbf{F}_{\mathrm{I}} \tag{3.1}$$

where $\mathbf{M}_{\mathrm{R}}$ is the real part of the mobility matrix $\bar{\mathbf{M}}_{\mathrm{R}}$ of the receiver at the interface points before coupling and $\mathbf{F}_{\mathrm{I}}$ is the interface force vector caused by the interaction between the source and the receiver. By using the conventional FRF-based sub-structuring method [18-19], the interface force vector is given by

$$\mathbf{F}_{\mathrm{I}} = \left(\bar{\mathbf{M}}_{\mathrm{S}} + \bar{\mathbf{M}}_{\mathrm{R}}\right)^{-1}\mathbf{V}_{\mathrm{sf}} \tag{3.2}$$

Here $\bar{\mathbf{M}}_{\mathrm{S}}$ is the complex mobility matrix of the source at the interface points before coupling, and $\mathbf{V}_{\mathrm{sf}}$ is the free velocity vector of the source substructure at the interface points when the source substructure is uncoupled from the receiver, given by

$$\mathbf{V}_{\mathrm{sf}} = \bar{\mathbf{M}}_{\mathrm{es}}\mathbf{F}$$

where $\mathbf{F}$ is a vector corresponding to the set of external force excitations, and $\bar{\mathbf{M}}_{\mathrm{es}}$ is the mobility matrix composed of the transfer-mobilities (of the source structure) between the force excitation points and the interface points. Here free velocity is used to define the source strength, which has the advantage of allowing simple comparisons between different sources [36].

As a result, a general expression for the power transmission within the system can be written as

$$P = \frac{1}{2}\mathrm{Re}\left\{\mathbf{V}_{\mathrm{sf}}{}^{H}\left[\left(\bar{\mathbf{M}}_{\mathrm{S}} + \bar{\mathbf{M}}_{\mathrm{R}}\right)^{-1}\right]^{H}\bar{\mathbf{M}}_{\mathrm{R}}\left(\bar{\mathbf{M}}_{\mathrm{S}} + \bar{\mathbf{M}}_{\mathrm{R}}\right)^{-1}\mathbf{V}_{\mathrm{sf}}\right\} \tag{3.3}$$

Obviously equation (3.3) will be inconvenient if the number of interface DOFs is very large, and/or the required FRF data are not known to sufficient accuracy, due to some uncertainty of the receiver properties, for example. Approximations for the upper and lower bounds and the frequency average power are thus of interest, especially if these require less information than an exact description. In this section, the power mode approach is used in two stages: first, the coupling forces are assumed to involve only

translational motion at the coupling DOFs, and secondly, there may be both translational and rotational coupling DOFs.

3.2.1 Translational coupling motion only

In this case it is assumed that the coupling DOFs of the source/receiver system all act in the same direction, e.g. normal to the surface of a plate-like receiver. This can be further defined to be where all the coupling forces and DOFs are dynamically similar, e.g. all out-of-plane, bending vibrations of a flexible plate

3.2.1.1 Approximations to the upper and lower bounds of the transmitted power

Similar to equation (2.14), a strict lower bound for the transmitted power of equation (3.1) can be expressed as

$$P_{low} = \frac{1}{2}\left(\sum_{n=1}^{N}\left|F_{1,n}\right|^2\right)\lambda_{\min}^{R} \tag{3.4}$$

where $\lambda_{\min}^{R}$ is the minimum eigenvalue (power mode mobility) of $\mathbf{M}_{\mathbf{R}}$. From equation (3.2), it follows that

$$\sum_{n=1}^{N}\left|F_{1,n}\right|^2 = \mathbf{V}_{\mathbf{sf}}{}^{H}\bar{\mathbf{M}}_{\mathbf{RS}}^{-1}\mathbf{V}_{\mathbf{sf}} \tag{3.5}$$

where

$$\bar{\mathbf{M}}_{\mathbf{RS}} = \left(\bar{\mathbf{M}}_{\mathbf{R}} + \bar{\mathbf{M}}_{\mathbf{S}}\right)\left(\bar{\mathbf{M}}_{\mathbf{R}} + \bar{\mathbf{M}}_{\mathbf{S}}\right)^{H} \tag{3.6}$$

is given by the combination of mobility matrices of the source and the receiver. (Note that $\bar{\mathbf{M}}_{\mathbf{RS}}$ here does not represent a mobility matrix.) It is seen that $\bar{\mathbf{M}}_{\mathbf{RS}}$ is a Hermitian matrix, and thus can be decomposed into a diagonal form

$$\bar{\mathbf{M}}_{\mathbf{RS}} = \mathbf{\Phi}\mathbf{\Lambda}_{\mathbf{RS}}\mathbf{\Phi}^{\mathbf{H}} \tag{3.7}$$

Since equation (3.5) is a positive semi-definite quadratic form, $\mathbf{\Lambda}_{\mathbf{RS}}$ is a real and non-negative diagonal matrix, and $\mathbf{\Phi}$ is a unitary matrix ($\mathbf{\Phi}\mathbf{\Phi}^{-1} = \mathbf{\Phi}^{-1}\mathbf{\Phi} = \mathbf{I}$). Then a strict lower bound for $\sum_{n=1}^{N}\left|F_{1,n}\right|^2$ is

$$\sum_{n=1}^{N}\left|F_{1,n}\right|^2 \geq \left(\sum_{n=1}^{N}\left|V_{sf,n}\right|^2\right)\frac{1}{\lambda_{\max}^{RS}} \tag{3.8}$$

where $\lambda_{\max}^{RS}$ is the maximum eigenvalue of matrix $\bar{\mathbf{M}}_{\mathbf{RS}}$, and satisfies [42]

$$\sqrt{\lambda_{\max}^{RS}} \le \max_{n} \left| \bar{M}_{R,nn} + \bar{M}_{S,nn} \right| + \sqrt{\sum_{n \ne m} \sum \left| \bar{M}_{R,nm} + \bar{M}_{S,nm} \right|^2} \tag{3.9}$$

Combining equations (3.4), (3.8) and (3.9), a strict lower bound of the transmitted power is then given by

$$P_{low} = \frac{\frac{1}{2}\left(\sum_{n=1}^{N} \left| V_{sf,n} \right|^2 \right) \lambda_{\min}^{R}}{\left(\max_{n} \left| \bar{M}_{R,nn} + \bar{M}_{S,nn} \right| + \sqrt{\sum_{n \ne m} \sum \left| \bar{M}_{R,nm} + \bar{M}_{S,nm} \right|^2} \right)^2} \tag{3.10}$$

Physically, the minimum power transmission occurs either if the free-velocity distribution of the source structure is proportional to the eigenvector corresponding to the largest eigenvalue of $\bar{\mathbf{M}}_{\mathbf{RS}}$ (equations (3.5) and (3.4)), or if the interface force distribution is proportional to the eigenvector corresponding to the smallest eigenvalue of $\mathbf{M}_{\mathbf{R}}$ (equation (3.1)).

It is difficult to find an expression for the upper bound of the transmitted power, similar to equation (2.13), using the above eigen-decomposition approach. However, a convenient approximation to the maximum transmitted power can be estimated by simply assuming the mobility matrix $\bar{\mathbf{M}}_{\mathbf{S}}$ in equation (3.3) is zero. As a result, the upper bound of the transmitted power can be written as

$$P_{up}' \approx \frac{1}{2} \mathrm{Re}\left\{ \mathbf{V}_{\mathbf{sf}}{}^{H} \bar{\mathbf{M}}_{\mathbf{R}}^{-1} \mathbf{V}_{\mathbf{sf}} \right\} \tag{3.11}$$

Although it is not a strict maximum, it tends to be a good, somewhat conservative approximation which is rarely exceeded in practice. Physically equation (3.11) means that the maximum power transmission occurs when the source can almost be treated as a set of free velocities.

A flexible receiver structure usually implies a relatively short wavelength and/or high modal overlap. In such cases, as mentioned above, the correlations between the individual driving points are often relatively small, at least when frequency averaged, so that the local driving point properties of the receiver at different coupling points can be regarded as being uncorrelated. Under such circumstances, one can write the approximate relations

$$\lambda_{\min}^{R} \approx \min_{n} \left\{ M_{R,nn} \right\} \tag{3.12}$$

$$M_{R,mn} \approx 0, \; m \neq n \tag{3.13}$$

Hence, the upper and lower bounds of the transmitted power can be approximated as

$$P'_{up} \approx \frac{1}{2} \sum_{n=1}^{N} \frac{\left|V_{sf,n}\right|^2}{M_{R,nn}} \tag{3.14}$$

$$P'_{low} \approx \frac{1}{2} \left(\sum_{n=1}^{N} \left|V_{sf,n}\right|^2 \right) \frac{\min_n \left\{M_{R,nn}\right\}}{\left(\max_n \left|\bar{M}_{R,nn}\right| + \left(1+\sqrt{N(N-1)}\right) \max_n \left|\bar{M}_{S,nn}\right| \right)^2} \tag{3.15}$$

It is seen from equations (3.14) and (3.15) that these approximations for the upper and lower bounds depend only on the diagonal elements of the mobility matrices of the source and receiver. Although these approximations are less conservative than the corresponding exact results, they are much easier to predict since the amount of data required is substantially reduced.

From equations (3.14) and (3.15), it is seen that the width of the range of power is closely related to the mobility mismatch between the source and the receiver. The lower the mobility of the source compared to that of the receiver, or the stiffer the source compared to the receiver, the narrower is the range between these limits. If it is assumed that the local driving point mobilities of the receiver points are approximately equal, or at least of comparable magnitudes, the approximations to both the upper and lower bounds of the transmitted power can be quite close to the "exact" value, provided that the mobility mismatch between the source and the receiver is big enough. If the receiver structure is much more flexible than the source so as to meet the condition

$$\max_n \left|\bar{M}_{R,nn}\right| >> \left(1+\sqrt{N(N-1)}\right) \max_n \left|\bar{M}_{S,nn}\right| \tag{3.16}$$

the approximations to both the upper and lower limits of the power can then be very close to the exact value. Under such circumstances, the power can actually be treated as that transmitted by a set of free velocities $\mathbf{V}_{sf}$, i.e.,

$$P \approx \frac{1}{2} \sum_{n=1}^{N} \left|V_{sf,n}\right|^2 \frac{1}{M_{R,nn}} \tag{3.17}$$

Equation (3.16) actually gives the condition under which the flexibility of the source structure itself may be neglected, so that the power transmitted to the receiver can be regarded as that by a set of ideal velocities, i.e., a set of point-velocities uncorrelated with each other. Therefore, provided the mobility-mismatch of the system meets the condition

of equation (3.16), the approximations developed in section 2 may be quite useful for estimating the power transmitted to a receiver structure which is not flexible enough to meet the conditions of equations (3.12) and (3.13).

3.2.1.2 Approximation to the frequency average transmitted power

In the above subsection, the upper bound is estimated by assuming that the mobilities of the source structure at the interface points are zero, while the approximation for the lower bound was made when both the mobility terms of the source and receiver at the interface are included. The upper bound given in equation (3.14) tends to be more conservative than the lower bound given in equation (3.15), especially when the local driving properties of the receiver at each coupling point are similar. This implies that the latter approximation is likely to be closer to the exact value than the former. It is also known that the frequency average of the real part of the point mobility of a structure approximates that of the characteristic point mobility, i.e., the point mobility of the equivalent infinite structure [11]. Therefore, one can write an approximation to the frequency average of the transmitted power as

$$\overline{P} \approx \frac{1}{2}\left(\sum_{n=1}^{N}\left|V_{sf,n}\right|^2\right)\frac{\mathrm{Re}\left\{\overline{M}^{\infty}_{R,nn}\right\}}{\left(\left|\overline{M}^{\infty}_{R,nn}\right|+\left(1+\sqrt{N(N-1)}\right)\max_{n}\left|\overline{M}_{S,nn}\right|\right)^2} \tag{3.18}$$

where $\overline{M}^{\infty}_{R,nn}$ is the characteristic point mobility of the receiver structure. This relation is particularly valid for non-tonal excitation or for tonal excitation if the modal overlap of the receiver is large enough, i.e., if the excitation excites resonant response in at least a few receiver modes.

Generally, equation (3.18) is accurate if the source/receiver system has a big enough mobility mismatch. Otherwise, equation (3.18) tends to underestimate the true frequency average.

3.2.2 Translational and rotational coupling

In many cases of practical interest the vibration source may apply moments as well as forces. The power transmitted to the receiver then arises partly from the translational and partly from the rotational motions. The former is usually the largest, but the latter can be substantial at higher frequencies [37-38]. Therefore, it is important to consider combined translational and rotational motions of the coupling DOFs.

Under such circumstances, however, $\mathbf{V}_{sf}$, $\bar{\mathbf{M}}_S$ and $\bar{\mathbf{M}}_R$ are composed of elements with different units. The approximations made above can no longer be applied. Nevertheless, this problem of dimensional incompatibility can be overcome by using a matrix scaling technique similar to that of Section 2.4. This is described in the following subsections. Similar scaling approaches can be extended for more general cases where the coupling DOFs are of different types, e.g. the simultaneous in-plane and out-of-plane vibrations of a structure.

3.2.2.1 Approximations to the upper and lower bounds of the transmitted power

Let the mobility matrices $\bar{\mathbf{M}}_S$ and $\bar{\mathbf{M}}_R$ be scaled by a real diagonal matrix $\mathbf{D}'_C$ whose nth diagonal element is defined as

$$D'_{C,nn} = \frac{1}{\sqrt{\left|\bar{M}_{R,nn}\right|}} \tag{3.19}$$

so as to give two dimensionless matrices $\bar{\mathbf{M}}_S^C$ and $\bar{\mathbf{M}}_R^C$ as

$$\bar{\mathbf{M}}_S^C = \mathbf{D}'_C \bar{\mathbf{M}}_S \mathbf{D}'_C \tag{3.20}$$

$$\bar{\mathbf{M}}_R^C = \mathbf{D}'_C \bar{\mathbf{M}}_R \mathbf{D}'_C \tag{3.21}$$

It is seen from equation (3.20) that

$$\left|\bar{M}^C_{R,nn}\right| = 1 \tag{3.22}$$

Let $\mathbf{F}_I$ and $\mathbf{V}_{sf}$ be weighted by $\mathbf{D}'_C$ to give a new set of forces and a new set of free velocities, whose elements all have the same units, as

$$\mathbf{F}_I^C = \mathbf{D}'^{-1}_C \mathbf{F}_I \tag{3.23}$$

$$\mathbf{V}_{sf}^C = \mathbf{D}'_C \mathbf{V}_{sf} \tag{3.24}$$

The power transmission in equation (3.3) can then be re-written as

$$P = \frac{1}{2}\mathrm{Re}\left\{\mathbf{V}_{sf}^{C^H}\left[\left(\bar{\mathbf{M}}_S^C + \bar{\mathbf{M}}_R^C\right)\right]^{-1^H} \bar{\mathbf{M}}_R^C \left(\bar{\mathbf{M}}_S^C + \bar{\mathbf{M}}_R^C\right)^{-1} \mathbf{V}_{sf}^C\right\} \tag{3.25}$$

Consequently the approximations for the upper and lower bounds of the transmitted power can be made in analogy to equations (3.14) and (3.15), with $\mathbf{V}_{sf}$, $\bar{\mathbf{M}}_S$ and $\bar{\mathbf{M}}_R$ being replaced by $\mathbf{V}_{sf}^C$, $\bar{\mathbf{M}}_S^C$ and $\bar{\mathbf{M}}_R^C$.

By replacing the terms of $M_{R,nn}^{C}$ by its maximum possible value of unity (given by equation (3.22)), the approximations for the upper and lower bounds of the power can be further simplified as

$$P'_{up} \approx \frac{1}{2}\sum_{n=1}^{N}\left|V_{sf,n}^{C}\right|^2 \tag{3.26}$$

$$P'_{low} \approx \frac{1}{2}\left(\sum_{n=1}^{N}\left|V_{sf,n}^{C}\right|^2\right)\frac{1}{\left(1+\left(1+\sqrt{N(N-1)}\right)\max_{n}\left|\bar{M}_{S,nn}^{C}\right|\right)^2} \tag{3.27}$$

So far, the bounds of the power transmission for a stiff source/flexible receiver system with both translational and rotational motions of coupling DOFs can be estimated by equations (3.26) and (3.27).

3.2.2.2 Approximation to the frequency average transmitted power

A similar scaling approach can be used to approximate the frequency average of the transmitted power. Here the scaling matrix $\mathbf{D}_{\mathrm{C}}^{\prime\infty}$ is used where

$$D_{C,nn}^{\prime\infty} = \frac{1}{\sqrt{\left|\bar{M}_{R,nn}^{\infty}\right|}}, D_{C,nm}^{\prime\infty} = 0, n \neq m \tag{3.28}$$

and where $\bar{M}_{R,nn}^{\infty}$ is the characteristic point mobility of the receiver. Then the approximation for the frequency average of the transmitted power can be written in a form similar to equation (3.18) as

$$\bar{P} \approx \frac{1}{2}\left(\sum_{n=1}^{N}\left|V_{sf,n}^{C_\infty}\right|^2\right)\frac{1}{\left(1+\left(1+\sqrt{N(N-1)}\right)\max_{n}\left|\bar{M}_{S,nn}^{C_\infty}\right|\right)^2} \tag{3.29}$$

where $V_{sf,n}^{C_\infty}$ are a new set of scaled free velocities of the source structure, given by

$$\mathbf{V}_{\mathbf{sf}}^{\mathbf{C}_\infty} = \mathbf{D}_{\mathrm{C}}^{\prime\infty}\mathbf{V}_{\mathbf{sf}} \tag{3.30}$$

and $\bar{M}_{S,nn}^{C_\infty}$ is the (n,n)th element of the scaled matrix

$$\bar{\mathbf{M}}_{\mathrm{S}}^{\mathrm{C}_\infty} = \mathbf{D}_{\mathrm{C}}^{\prime\infty}\bar{\mathbf{M}}_{\mathrm{S}}\mathbf{D}_{\mathrm{C}}^{\prime\infty} \tag{3.31}$$

The approximations of equations (3.26), (3.27) and (3.29) are thus related only to the scaled point mobility terms of the source and the receiver.

Similar scaling approaches can be extended for more general cases, where the transmitted power is associated with more than two different directional and/or rotational coupling DOFs.

3.3 NUMERICAL EXAMPLES

Numerical examples are presented here to demonstrate the approach developed in Section 3.2. Since many of the basic features of structures of practical concern can be reduced to relatively simple configurations of beams and plates, the numerical model considered here is a beam/plate system coupled by four evenly spaced points, as shown in Figure 3.1. The beam is chosen to be relatively stiff and with a low modal density compared to that of the plate. Both the beam and the plate are simply supported for simplicity. External time harmonic force and moment excitations act at a distance ξ from one end of the beam. The dimensions of the system and the coupling positions are listed in Table 3.1. The material properties of the system are those of Perspex as given in Table 2.1. Three different plate thicknesses of 0.010m, 0.005m and 0.002m are used to vary the stiffness of the plate receiver, which give three wavenumber ratios of the beam and the plate $k_p/k_b = 2.5$, 3.5 and 5.6. ($k_p = \sqrt{m_p\omega^2/D_p}$ and $k_b = \sqrt{m_b\omega^2/D_b}$, where m_p (m_b) is the mass per unit area (length) of the plate (beam), and D_p (D_b) is the bending stiffness of the plate (beam)).

For convenience, here, the frequency-independent wavenumber ratio k_p/k_b is used to indicate the dynamic mismatch of the plate and the beam, instead of the frequency-dependent mobility ratio of the system. Such a representation is valid provided that the beam and the plate satisfy the condition $m_b >> 2m_p/k_p$, so that the wavelengths of the beam, before and after it is coupled with the plate, are comparable. (Please refer to equations A4.4-A4.8 in Appendix IV.) If it is not the case, e.g., the width of the beam is very small, k_p/k_b should not be used to represent the dynamic mismatch between the plate and the beam.

Approximations to the transmitted power from the beam to the plate are made under the following two circumstances: first, only translational coupling DOFs are involved; secondly, both translational and rotational coupling DOFs are considered. These relevant equations have been given in Sections 3.2.1 and 3.2.2, respectively. The calculations for the input- and transfer mobilities of a simply supported plate, a simply supported beam and an infinite plate can be found in Appendices I-III. The approximate results are

compared to exact results found using the conventional FRF-based sub-structuring technique, which is given in Appendix V. A running frequency average, i.e., smoothing technique has been used for all figures given in this section to determine the broad features of the transmitted power. The plate modal densities are 0.15, 0.30 and 0.74 mode/Hz when the plate thickness is 0.010m, 0.005m and 0.002m, respectively. The bandwidth used in the smoothing is 10 Hz so that each band consists of a few (plate) vibration modes.

3.3.1 Transmitted power with translational coupling DOFs only

When the system is assumed have only translational coupling DOFs, the beam and the plate generally rotate through different angles, and the coupling moments are zero. Under such circumstances, the transmitted power only has contributions from the translational coupling DOFs, so that the estimates for the power transmitted to the plate can be found using the expressions given in section 3.2.1. Figures 3.2-3.4 compare the exact and the approximate results for the transmitted power, when a time harmonic force of magnitude 1 is applied to the beam, where $k_p/k_b = 2.5$, 3.5 and 5.6, respectively. It is seen clearly that the accuracy of the approximations increases as the mobility mismatch between the beam and the plate increases, as expected. When the plate is much more flexible than the beam, the transmitted power can be simply approximated by that transmitted by a set of free velocities, as shown in Figure 3.4.

The above upper and lower bound calculations need the point-mobilities of the plate at all the interface DOFs to be known exactly. In principle, this requires detailed knowledge of the modal properties of the plate. In many cases, however, this is impractical, or it may even be impossible to find these values accurately. In such cases, the plate receiver may be approximated by regarding it as extending uniformly to infinity in a manner analogous to that described in section 3.3.2. The upper bound can then be approximated by replacing $M_{R,nn}$ in equation (3.14) by $\mathrm{Re}\{\bar{M}^{\infty}_{R,nn}\}$, while the lower bound expression of equation (3.15) becomes equation (3.18). Figure 3.5 shows such approximations for the case where $k_p/k_b = 2.5$. By comparison with Figure 3.2, it can be seen that this further approximation gives reasonable results even for this case of modest wavenumber mismatch. When the plate receiver is relatively very flexible compared to the beam, however, one needs use only equation (3.18) to get good estimates for the transmitted power, as shown in Figures 3.3-3.4.

3.3.2 Transmitted power with both translational and rotational coupling DOFs

When the system has both translational and rotational coupling DOFs, the translation and the rotation $\partial w/\partial y$ of the beam and the plate at the interface DOFs are equal. (There is assumed to be no coupling between the torsion in the beam and the rotation $\partial w/\partial x$ in the plate.) Under such a circumstance, the transmitted power has contributions from both translational and rotational coupling DOFs, and thus can be approximated by the expressions described in section 3.2.2.2. Figures 3.6-3.8 compare the exact transmitted power to the approximations, when a time harmonic force and moment of magnitudes 1 and 0.5, respectively, are applied to the beam at the point $\xi = 0.73$, where $k_p/k_b = 2.5$, 3.5 and 5.6, respectively. Once again the approximations become closer to the exact values as the wavenumber ratio increases.

The plate receiver may also be simply approximated as being an infinite structure when it is difficult to determine the exact values of the relevant point mobilities. Consequently, the upper bound of the transmitted power can be estimated by replacing $V_{sf,n}^{C}$ in equation (3.26) by $V_{sf,n}^{C_\infty}$, while the lower bound is now given by equation (3.27). When the plate receiver is relatively very flexible compared to the beam, as shown in Figure 3.8, only equation (3.29) is needed to approximate the transmitted power accurately. If that is not the case, however, equation (3.26) (where $V_{sf,n}^{C} = V_{sf,n}^{C_\infty}$) can be used together with equation (3.27) to roughly approximate the broad features of the transmitted power. This is shown in Figure 3.9 for the case.

3.4 SUMMARY

In this chapter a power mode approach to estimating the power transmitted to a receiver structure from multiple sources was extended to the case of power transmission between a stiff source and a flexible receiver through discrete couplings.

In the first instance, the coupling DOFs at the interface points were assumed to be of a dynamically similar type, e.g., the translational motion due to force coupling. Then more general source/receiver systems were considered where the coupling DOFs could be of different types, e.g. the simultaneous translational and rotational motions. A matrix scaling technique was introduced. Approximations were developed for the upper and lower bounds and the frequency average of the transmitted power. These approximations were

found depending only on the point mobilities of the source and receiver, and thus the amount of data required can be reduced substantially compared to an exact description.

This power mode approach is particularly useful when the dynamic mismatch between the source and the receiver is big enough.

Table 3.1 System dimensions and coupling positions

	Dimensions (m)	**Coupling positions** (m)	**Excitation position** (m)
Beam	Length=2; Width=0.059; Height=0.068.	$x_1 = 0.40$, $x_2 = 0.80$ $x_3 = 1.20$, $x_4 = 1.60$	$\xi = 0.73$
Plate	Length=2; Width=0.9; Thickness=0.010, 0.005, 0.002.	$(x_1, y_1) = (0.40, 0.45)$ $(x_2, y_2) = (0.80, 0.45)$ $(x_3, y_3) = (1.20, 0.45)$ $(x_4, y_4) = (1.60, 0.45)$	

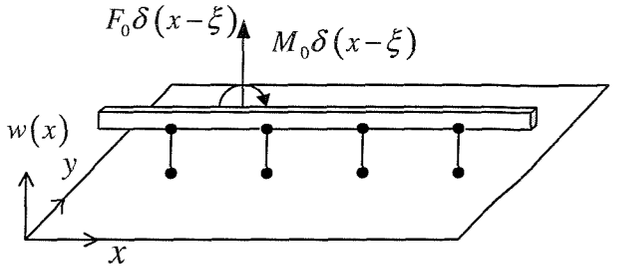

Figure 3.1 Multipoint-coupled beam/plate system

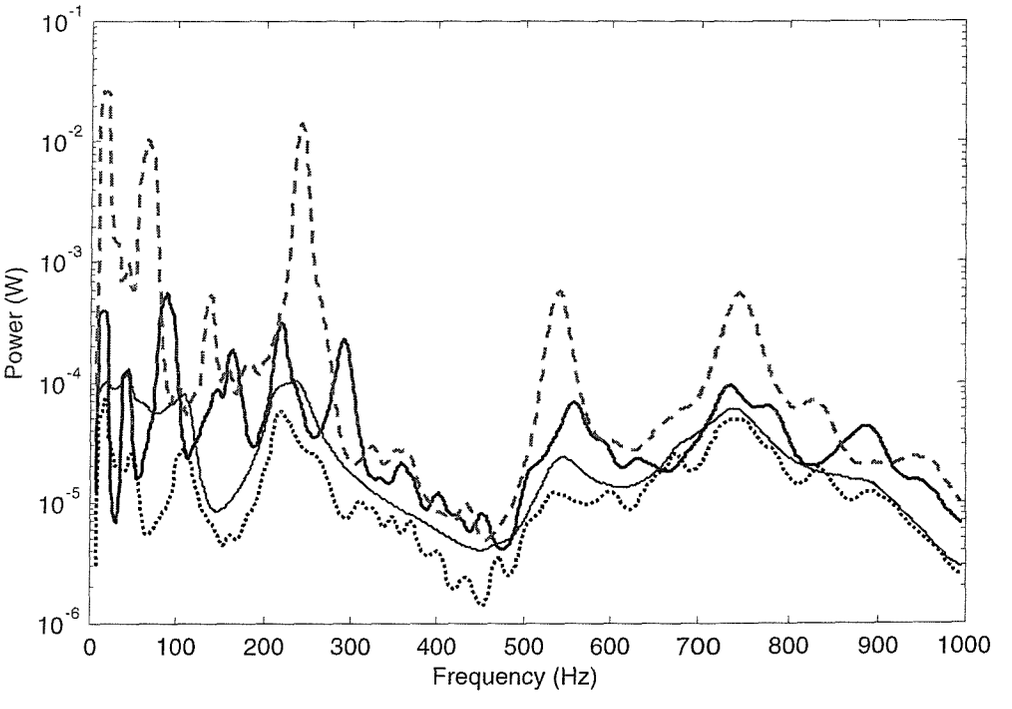

Figure 3.2 Power transmitted to the plate when only translational coupling DOFs are assumed ($k_p/k_b = 2.5$): exact (____ , equation (3.3)); approximations to the upper bound (_ _ _ , equation (3.14)), lower bound (..... , equation (3.15)) and frequency average (____ , equation (3.18)).

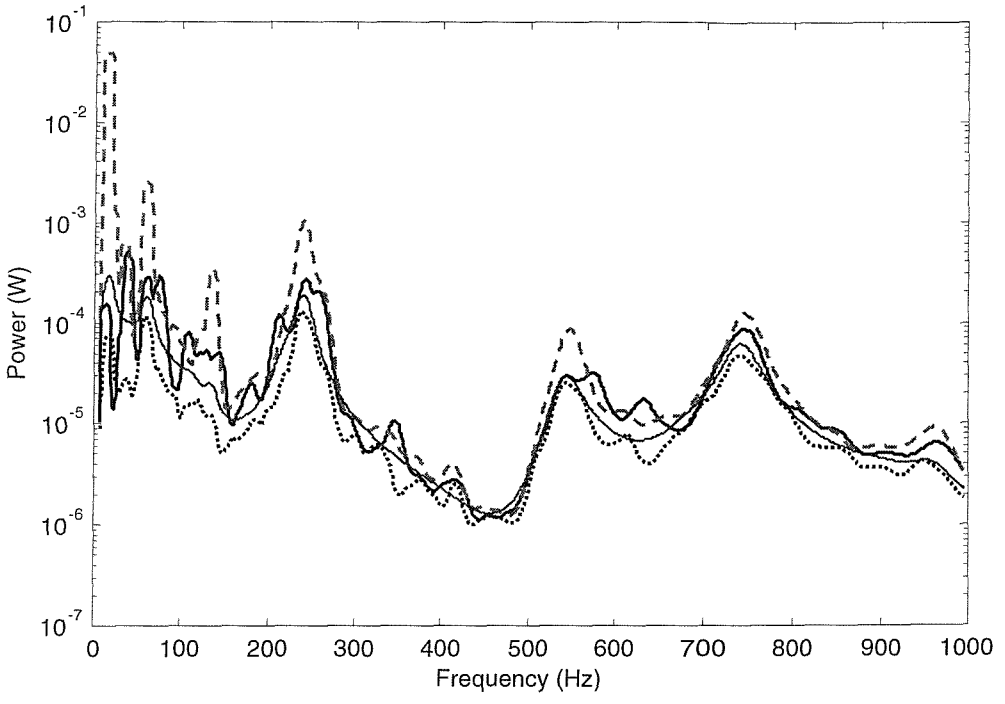

Figure 3.3 Power transmitted to the plate when only translational coupling DOFs are assumed ($k_p/k_b = 3.5$): exact (——— , equation (3.3)), approximations to the upper bound (_ _ _ , equation (3.14)), lower bound (..... , equation (3.15)) and frequency average (——— , equation (3.18)).

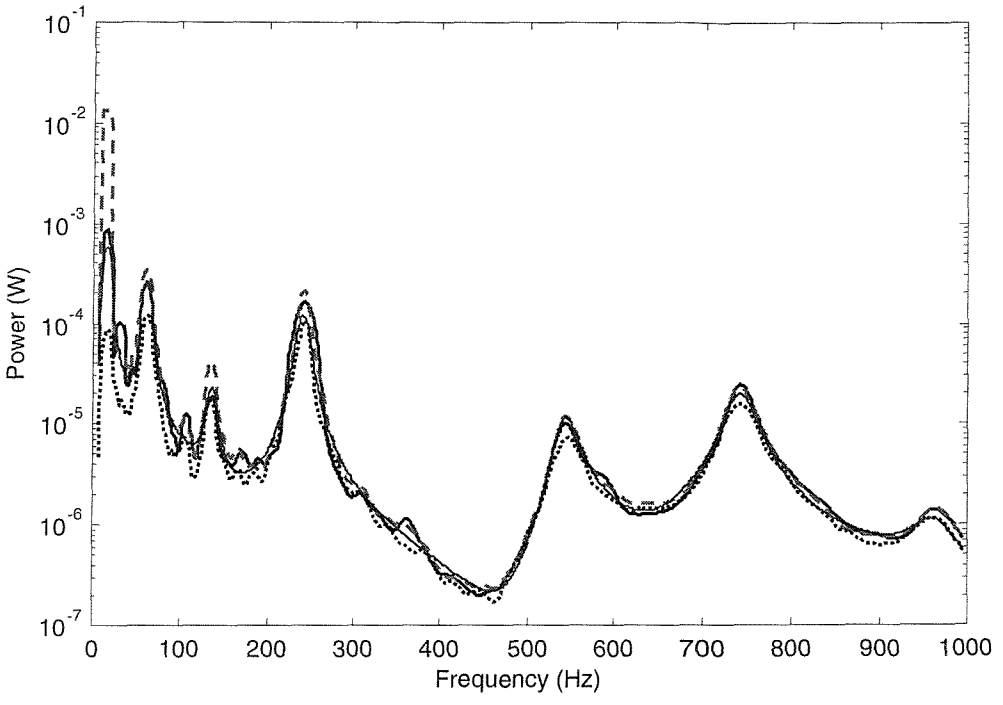

Figure 3.4 Power transmitted to the plate when only translational coupling DOFs are assumed ($k_p/k_b = 5.6$): exact (_____ , equation (3.3)), approximations to the upper bound (_ _ _ , equation (3.14)), lower bound (..... , equation (3.15)) and frequency average (_____ , equation (3.18)).

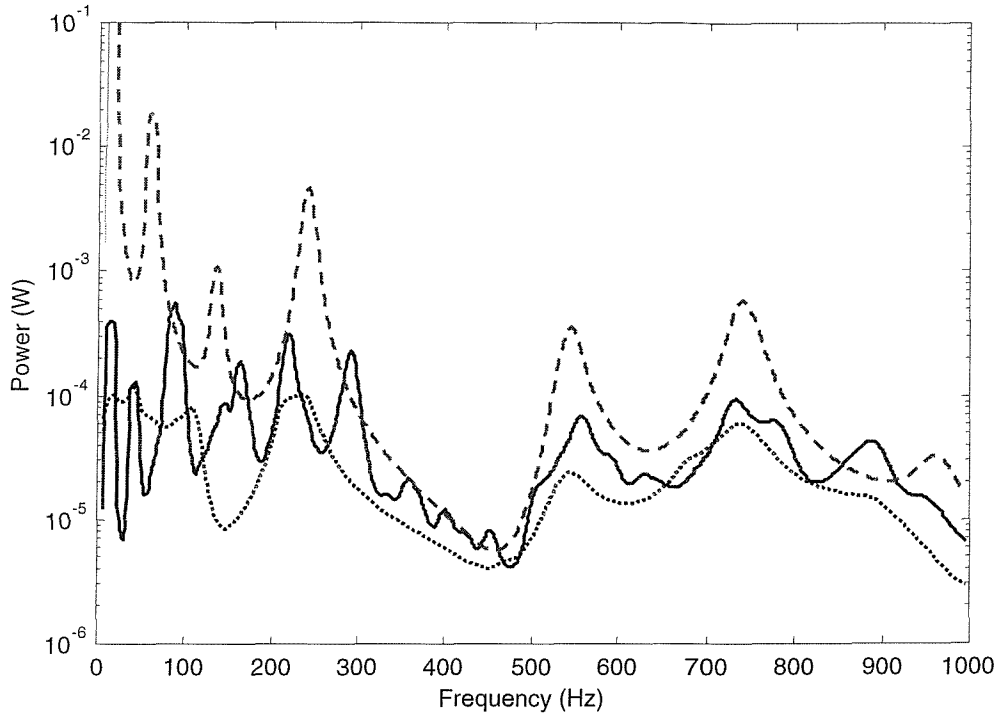

Figure 3.5 Power transmitted to the plate when only translational coupling DOFs are assumed and the plate is approximated as being infinite ($k_p/k_b = 2.5$): exact (——— , equation (3.3)), approximations to the upper bound (_ _ _ , equation (3.14)) and lower bound (..... , equation (3.15)).

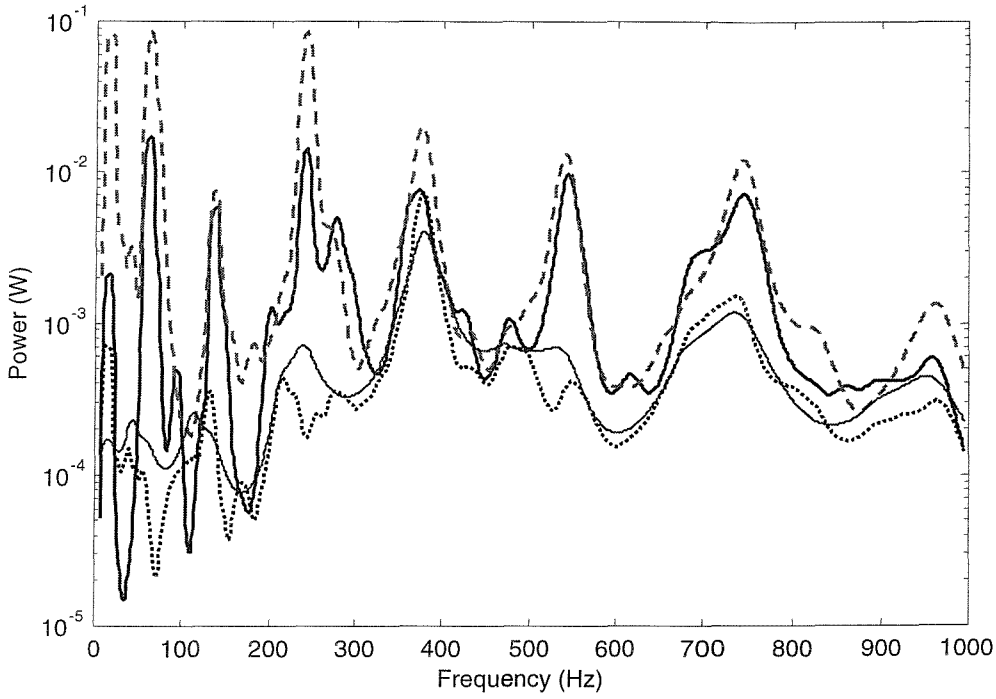

Figure 3.6 Power transmitted to the plate when both translational and rotational coupling DOFs are considered ($k_p/k_b = 2.5$): exact (——— , equation (3.3)), approximations to the upper bound (_ _ _ , equation (3.26)), lower bound (..... , equation (3.27)) and frequency average (——— , equation (3.29)).

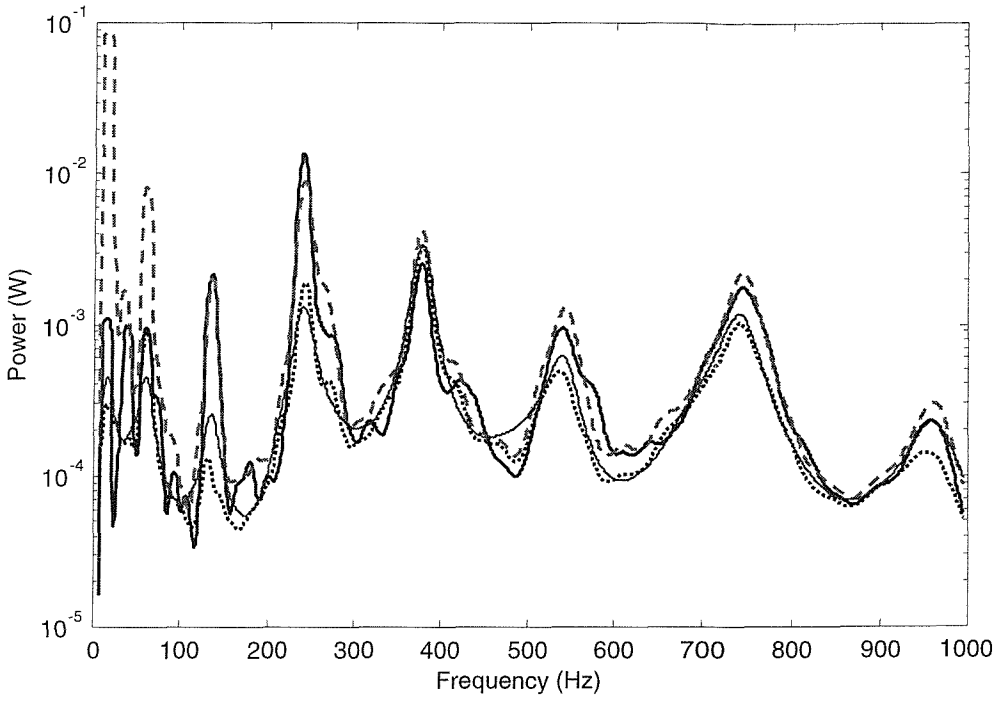

Figure 3.7 Power transmitted to the plate when both translational and rotational coupling DOFs are considered ($k_p/k_b = 3.5$): exact (——— , equation (3.3)); approximations to the upper bound (_ _ _ , equation (3.26)), lower bound (..... , equation (3.27)) and frequency average (——— , equation (3.29)).

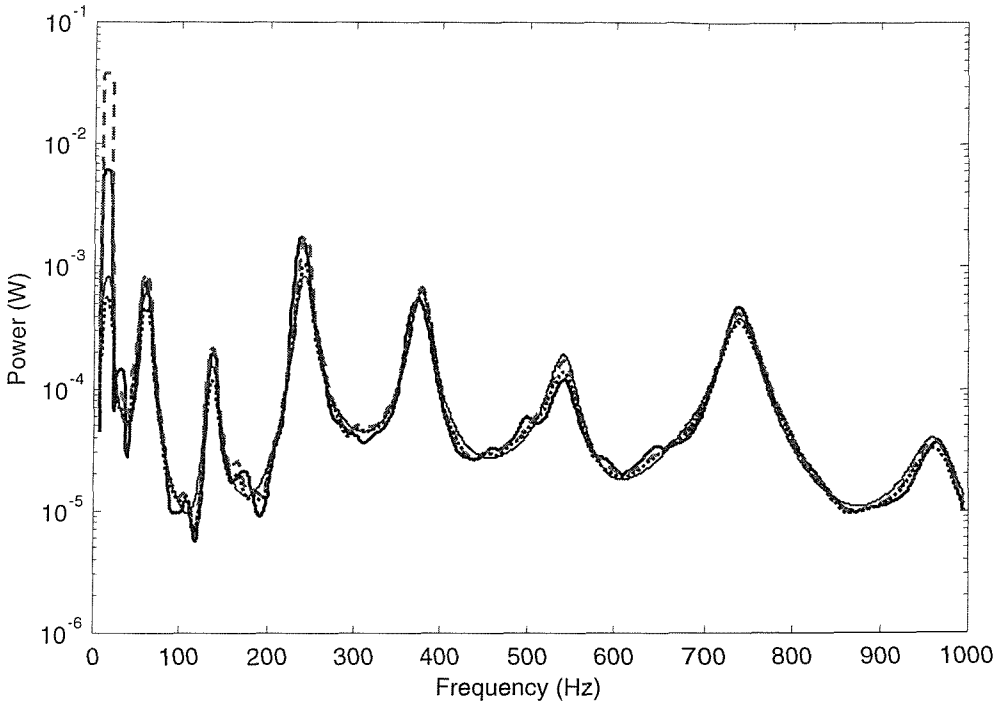

Figure 3.8 Power transmitted to the plate when both translational and rotational coupling DOFs are considered ($k_p/k_b = 5.6$): exact (——— , equation (3.3)); approximations to the upper bound (_ _ _ , equation (3.26)), lower bound (..... , equation (3.27)) and frequency average (——— , equation (3.29)).

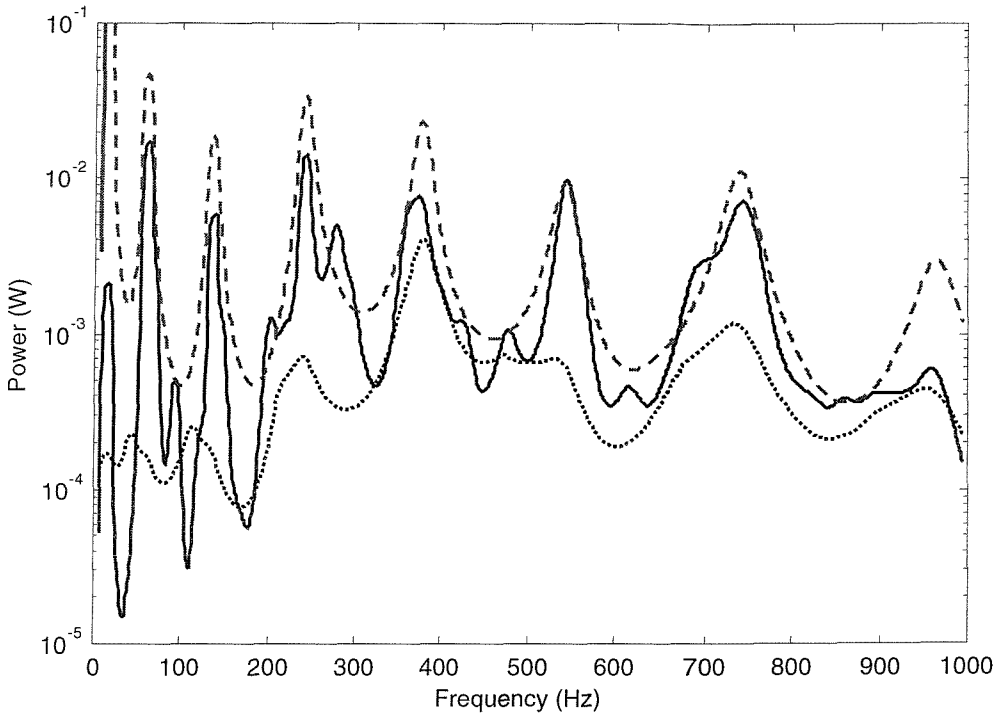

Figure 3.9 Power transmitted to the plate when both translational and rotational coupling DOFs are considered and the plate is approximated as being infinite ($k_p/k_b = 2.5$): exact (——— , equation (3.3)), approximations to the upper bound (_ _ _ , equation (3.26)) and lower bound (..... , equation (3.27)).

Part II

STRAIGHT LINE COUPLINGS: SPECIAL CASES

Many practical engineering structures are built up from beams and plates with straight-line couplings. One such structure is the machinery foundation of a ship, which is constructed from a collection of large stiff beams and flexible plates. Usually heavy vibration sources are supported by the stiff beams. Therefore, as an important part for the continuous coupling studies in this thesis, vibration problems of beam-stiffened plates are particularly of interest. Being broadly representative of the machinery foundation, the system model considered is composed of a directly excited stiff beam and an attached large flexible plate.

First of all, long-wavelength waves can be generated in the beam by applying external sources. As the long-wavelength waves propagate along the beam, short-wavelength waves can then be generated in the attached flexible plate and hence transmit some of the energy from the beam to the plate [26-27]. When the difference between the wavelengths of the beam and the plate is very large, (which is very often for many relevant practical cases), the vibration around the structure is largely controlled by the long-wavelength stiff beam, but with some modifications or damping effects from the attached short-wavelength flexible plate. Under such circumstances, the frequency response functions (FRFs) of the source beam and the power transmitted to the plate are most important for a better understanding of the whole vibration properties of the coupled system.

This part of the thesis is concerned with three special cases of a plate-stiffened beam system: (1) an infinite beam attached to an infinite plate, (2) a finite beam attached to an infinite plate and (3) a finite beam attached to a finite plate where the beam and the plate have the same mode shapes along the coupling. Certain analytical/approximate methods are developed to predict simply and accurately the frequency response of the stiff beam and the power transmitted to the plate. Meanwhile, the interacting effects between the beam and the plate are investigated, being the effective mass and damping added to beam arising from the presence of the plate.

Although only special cases of beam/plate coupling systems are involved in this part of study, it provides new methodologies, both analytical and approximate, on which the

vibration of a general stiff beam/flexible plate system can be predicted in a much simpler way. This will finally lead to Part III for predicting the vibration of a stiff source/flexible receiver system with arbitrary continuous couplings.

Chapter 4

VIBRATION OF AN INFINITE BEAM ATTACHED TO AN INFINITE PLATE

4.1 INTRODUCTION

In this chapter, a foundation consisting of an infinite beam attached to an infinite plate is studied, as shown in Figure 4.1. It can be viewed as the simplest form of a beam-stiffened plate system due to the infinite extent of both the beam and the plate substructures. In this case, conventional Fourier Transform (FT) and wave analysis methods can be used to give analytical solutions for the dynamic response of the coupled system. These methods are described separately in subsections 4.2.1 and 4.2.2. Based on these analytical solutions, the dynamic interactions between the beam and the plate are furthermore investigated. It allows the loading effects of the plate on the beam to be equivalently simulated as adding effective mass and damping. Numerical examples are presented in section 4.5.

This chapter provides important theoretical background for determining the vibration response of a finite beam attached to an infinite plate, which will be considered in the next chapter.

4.2 VIBRATION ANALYSIS OF AN INFINITE BEAM/PLATE SYSTEM

4.2.1 Fourier Transform (FT) method

Let the beam component in Figure 4.1 be excited directly by a harmonic external point force F_0 with frequency ω acting at $x=0$, and the beam drive the plate with a force per unit length $f(x)$ along the line $y=0$. The force loadings on the beam and the plate may be shown as in Figures 4.2 and 4.3, respectively. The equations of motion of the beam and the plate then can be written as

$$D_b \frac{\partial^4 w_b(x)}{\partial x^4} - m_b \omega^2 w_b(x) = F_0 \delta(x) - f(x) \tag{4.1}$$

$$D_p \nabla^4 w_p(x,y) - \omega^2 m_p w_p(x,y) = f(x)\delta(y) \tag{4.2}$$

where D_b and D_p are, respectively, the complex bending stiffness of the beam and of the plate, and m_b and m_p are the mass per unit length of the beam and mass per unit area of the plate, and ∇^4 is given by

$$\nabla^4 = \frac{\partial^4}{\partial x^4} + 2\frac{\partial^4}{\partial x^2 \partial y^2} + \frac{\partial^4}{\partial y^4} \tag{4.3}$$

In [43], the one-dimensional Fourier Transforms are defined by

$$G(\beta) = \int_{-\infty}^{+\infty} g(x) e^{-j\beta x} dx \tag{4.4}$$

$$g(x) = \frac{1}{2\pi} \int_{-\infty}^{+\infty} G(\beta) e^{j\beta x} d\beta \tag{4.5}$$

The two-dimensional Fourier Transforms are defined by

$$G(\beta,\gamma) = \int_{-\infty}^{+\infty}\int_{-\infty}^{+\infty} g(x,y) e^{-j\beta x} e^{-j\gamma y} dxdy \tag{4.6}$$

$$g(x,y) = \frac{1}{4\pi^2} \int_{-\infty}^{+\infty}\int_{-\infty}^{+\infty} G(\beta,\gamma) e^{j\beta x} e^{j\gamma y} d\beta d\gamma \tag{4.7}$$

Applying one-dimensional and two-dimensional Fourier Transforms, respectively, to both sides of equation (4.1) and (4.2), it gives

$$D_b k^4 W_b(k) - m_b \omega^2 W_b(k) = F_0 - F(k) \tag{4.8}$$

$$D_p \left(k_x^2 + k_y^2\right)^2 W_p(k_x, k_y) - m_p \omega^2 W_p(k_x, k_y) = F(k_x) \tag{4.9}$$

From a physical view, these are beam and plate equations in the wavenumber domain. By the definitions given in equations (4.4)-(4.7), a positive k_x or k_y actually represent the waves travelling in negative directions. From equation (4.9), it follows that

$$W_p(k_x, k_y) = \frac{F(k_x)}{D_p\left(k_x^2 + k_y^2\right)^2 - m_p\omega^2} \tag{4.10}$$

Then the inverse Fourier transform of the plate, by equation (4.7), is given by

$$w_p(x,y) = \frac{1}{4\pi^2} \iint_{\infty} W_p(k_x, k_y) e^{jk_x x} e^{jk_y y} dk_x dk_y \tag{4.11}$$

Equation (4.11) yields

$$w_p(x,0)=\frac{1}{4\pi^2}\iint_{\infty} W_p(k_x,k_y)e^{jk_x x}dk_x dk_y \tag{4.12}$$

The integral over k_y can then be performed to give

$$W_p(k_x)=\frac{1}{2\pi}\int_{-\infty}^{+\infty} W_p(k_x,k_y)dk_y \tag{4.13}$$

Substituting equation (4.10) into (4.13), the displacement response of the plate at $y=0$ in the wave-number domain can finally be expressed as

$$W_p(k_x)=F(k_x)\left(\frac{1}{2\pi}\int_{-\infty}^{+\infty}\frac{1}{D_p\left(k_x^2+k_y^2\right)^2-m_p\omega^2}dk_y\right) \tag{4.14}$$

From the above equation, the line receptance of the plate can then be written as

$$Y(k_x)=\frac{W(k_x)}{F(k_x)}=\frac{1}{2\pi}\int_{-\infty}^{+\infty}\frac{1}{D_p\left(k_x^2+k_y^2\right)^2-m_p\omega^2}dk_y \tag{4.15}$$

Equation (4.15) finally yields

$$Y(k_x)=\frac{1}{4D_p k_p^2}\left(\frac{1}{\sqrt{k_x^2-k_p^2}}-\frac{1}{\sqrt{k_x^2+k_p^2}}\right) \tag{4.16}$$

where $k_p=\sqrt[4]{m_p\omega^2/D_p}$ is the wavenumber of the plate. Since in this case $k=k_x$, combining equations (4.8), (4.14) and (4.16) the dynamic displacement of the beam can be derived in the wavenumber domain as

$$W_b(k)=\frac{F_0}{D_b k^4-m_b\omega^2+K(k)} \tag{4.17}$$

where $K(k)$ is the line dynamic stiffness of the plate, i.e., the inverse of equation (4.16) as

$$K(k)=2D_p\sqrt{k^4-k_p^4}\left(\sqrt{k^2+k_p^2}+\sqrt{k^2-k_p^2}\right) \tag{4.18}$$

The general expression for the power transmission to the plate is given by

$$P=\frac{1}{2}\mathrm{Re}\left\{\int_{-\infty}^{+\infty} f^*(x)\,j\omega w_b(x)dx\right\} \tag{4.19}$$

Equation (4.19) is equivalent, by Ref. [7], to

$$P = \frac{1}{2}\mathrm{Re}\left\{\frac{1}{2\pi}\int_{-\infty}^{+\infty} F^*(k)\, j\omega W_b(k)\, dk\right\} = \frac{\omega}{4\pi}\mathrm{Im}\left\{\int_{-\infty}^{+\infty} K(k)\left|W_b(k)\right|^2 dk\right\} \tag{4.20}$$

So far the power transmission has also been expressed in the wavenumber domain.

It is seen from equation (4.18) that when the small damping of the plate is neglected

$$\mathrm{Im}(K) \approx 0,\ |k| \geq k_p \tag{4.21}$$

Therefore equation (4.20) can be re-expressed as

$$P \approx \frac{\omega}{4\pi}\mathrm{Im}\left\{\int_{-k_p}^{+k_p} K(k)\left|W_b(k)\right|^2 dk\right\} \tag{4.22}$$

Physically the above expression indicates that only the wave terms with $|k| < |k_p|$ can radiate power to the plate, and thus only the wave terms with wavenumber less than k_p should be taken into account to estimate the power transmission from the beam to the plate. This provides a good simplification to predict the power transmission within the system.

4.2.2 Wave analysis method

Similarly, an analytical solution for the dynamic response of such a coupled beam/plate system can also be obtained by wave analysis method [26-27].

For uncoupled infinite beam, its displacements along the x-direction is expressed

$$w_b(x) = Ae^{-jk_b x} \tag{4.23}$$

After coupling, the equation of motion of the beam, being driven by $f(x)$, becomes

$$D_b \frac{\partial^4 w_b(x)}{\partial x^4} + m_b \frac{\partial^2 w_b(x)}{\partial t^2} = -f(x) \tag{4.24}$$

The equation of motion of the plate is

$$D_p \nabla^4 w_p(x, y) + m_p \frac{\partial^2 w_p(x, y)}{\partial t^2} = 0 \tag{4.25}$$

The boundary conditions at the beam/plate joint are

$$w_b(x) = w_p(x,0) \tag{4.26}$$

$$\theta_x = \left.\frac{\partial w_p}{\partial y}\right|_{y=0} = 0 \tag{4.27}$$

$$Q_y = D_p \frac{\partial}{\partial y}\left(\frac{\partial^2 w_p}{\partial y^2} + (2-\nu)\frac{\partial^2 w_p}{\partial x^2}\right) = \frac{f(x)}{2} \tag{4.28}$$

The displacements of the plate after coupling can be written as

$$w_{p+} = \left(Be^{-jk_y y} + Ce^{-k_e y}\right)e^{-jk_b' x}, \quad y \geq 0 \tag{4.29}$$

$$w_{p-} = \left(Be^{jk_y y} + Ce^{k_e y}\right)e^{-jk_b' x}, \quad y < 0 \tag{4.30}$$

where k_b' is the wavenumber of the beam after coupling. Combining equations (4.26), (4.29) and (4.30), gives

$$A = B + C \tag{4.31}$$

Combining equations (4.27), (4.29) and (4.30), gives

$$jk_y B + k_e C = 0 \tag{4.32}$$

From equations (4.25), (4.29) and (4.30), this yields

$$k_y = \sqrt{k_p^2 - k_b'^2} \tag{4.33}$$

$$k_e = \sqrt{k_p^2 + k_b'^2} \tag{4.34}$$

where the first expression represents the trace-matching of the travelling waves at the joint. Combining equations (4.29) to (4.34), gives

$$D_p A e^{-jk_b' x} k_e k_y (-k_y + jk_e) = \frac{f(x)}{2} \tag{4.35}$$

The equation of motion of the beam after coupling becomes

$$D_b k_b'^4 w_b(x) - m_b \omega^2 w_b(x) = -f(x) \tag{4.36}$$

where $w_b(x) = Ae^{-jk_b' x}$.

Combining equations (4.35) and (4.36), it follows that

$$D_b k_b'^4 = m_b \omega^2 + 2D_p k_e k_y \left(k_y - jk_e\right) \tag{4.37}$$

The above equation is the general dispersion relation for an infinite beam coupled to an infinite plate. And also the line impedance of the plate can then be expressed as

$$Z_p = \frac{f(x)}{j\omega w_b(x)} = \frac{2D_p}{\omega}(k_e k_y)(k_e + jk_y) \tag{4.38}$$

Substituting equations (4.33) and (4.34) into (4.38), gives

$$Z_p = \frac{2m_p\omega}{k_p}\sqrt{1-\left(\frac{k_b'}{k_p}\right)^4}\left(\sqrt{1+\left(\frac{k_b'}{k_p}\right)^2} + j\sqrt{1-\left(\frac{k_b'}{k_p}\right)^2}\right) \tag{4.39}$$

Multiplying $j\omega$ to both sides of equation (4.39), it is seen then that $j\omega Z_p$ is formally identical to $K(k)$ which is given in equation (4.18) derived from the Fourier Transform approach.

4.3 VIBRATION APPROXIMATION BASED ON A LOCALLY REACTING PLATE MODEL

The difference between the wavelengths of the long wave stiff beams and the short wave flexible plates is very often very large so that k_b'/k_p is quite small. When $(k_b'/k_p)^2 << 1$, equation (4.39) can be approximated by

$$Z_p \approx \frac{2m_p\omega}{k_p}(1+j) \tag{4.40}$$

Equation (4.40) shows that provided the plate wavenumber is much larger than the coupled beam wavenumber, the line impedance of the plate is independent of the beam properties, and also the plate can be regarded as locally reacting [26-27]. In Ref. [27] a locally reacting plate model is considered to be valid for cases of $k_p/k_b' > 2$.

Having determined the condition under which the plate can be considered locally reacting, it is appropriate to consider the dispersion relation for a beam coupled to a general locally reacting receiver plate. In this case, the general dispersion relation is given by [8]

$$D_b k_b'^4 \approx m_b\omega^2 - j\omega Z_p \tag{4.41}$$

Equation (4.41) shows that in effect the presence of the plate loads the dynamic response of the beam. As a result, the dynamic response and the power transmission of the coupled beam/plate system can then be approximated simply.

When subjected to point force excitation $F_0\delta(x)$, the displacement response at point x, before coupling with the plate, is given by [11]

$$w_b(x) = \frac{F_0}{j4D_b k_b^3}\left(e^{-jk_b x} - je^{-k_b x}\right),\ x \geq 0 \tag{4.42}$$

$$w_b(x) = \frac{F_0}{j4D_b k_b^3}\left(e^{jk_b x} - je^{k_b x}\right),\ x < 0 \tag{4.43}$$

where $k_b = \sqrt[4]{m_b\omega^2/D_b}$ is the free wavenumber of the beam. After coupling the wavenumber of the beam becomes

$$k_b' \approx \sqrt[4]{\frac{m_b\omega^2 - j\omega Z_p}{D_b}} \tag{4.44}$$

In Appendix IV, the approximate relation between k_b' and k_b, when the beam is attached to a locally reacting plate, is given by

$$\frac{k_b'}{k_b} \approx \sqrt[4]{1 + \frac{m_p\lambda_p}{m_b\pi}} \tag{4.45}$$

The coupled response of the beam can then be approximated as

$$w_b(x) \approx \frac{F_0}{j4D_b k_b'^3}\left(e^{-jk_b' x} - je^{-k_b' x}\right),\ x \geq 0 \tag{4.46}$$

$$w_b(x) \approx \frac{F_0}{j4D_b k_b'^3}\left(e^{jk_b' x} - je^{k_b' x}\right),\ x < 0 \tag{4.47}$$

Hence the transmitted power from the beam to the plate can be approximated by

$$P \approx \frac{1}{2}\mathrm{Re}\left\{2\omega^2 \int_0^{+\infty} Z_p \left|w_b(x)\right|^2 dx\right\} \tag{4.48}$$

4.4 THE INTERACTIONS BETWEEN THE BEAM AND THE PLATE

The dynamic interactions between the beam and the plate can be quantified based on the dynamic analysis of the beam/plate system in Section 4.2.1. These are given below.

Equation (4.17) yields

$$W_b(k) = \frac{F_0}{D_b k^4 - m_b\omega^2 + \mathrm{Re}\{K(k)\} + j\,\mathrm{Im}\{K(k)\}} \tag{4.49}$$

The above equation can then be re-written as

$$W_b(k) = \frac{F_0}{D_b\left[1 + j(\eta_b + \eta_k)\right]k^4 - [m_b + m_k]\omega^2} \tag{4.50}$$

where

$$m_k = -\frac{\mathrm{Re}(K)}{\omega^2} \tag{4.51}$$

$$\eta_k = \frac{\mathrm{Im}(K)}{D_b k^4} \tag{4.52}$$

Equation (4.50) implies that when the beam vibrates with a wave propagation of wavenumber k, the presence of the plate is equivalent to adding a mass (density) m_k and a loss factor η_k to this wave propagation, as given in equations (4.51) and (4.52). Therefore, the interacting effects between the beam and the plate can be viewed as adding an effective mass and an effective damping to each wave propagation of the beam. The energy 'dissipated' by η_k represents the energy transmitted from the beam to the plate.

When $|k| < k_p$ and also the plate has a small damping η_p, equation (4.18) gives

$$\mathrm{Re}(K) \approx -2D_p\left(k_p^2 - k^2\right)\sqrt{k_p^2 + k^2} \tag{4.53}$$

$$\mathrm{Im}(K) \approx 2D_p\left(k_p^2 + k^2\right)\sqrt{k_p^2 - k^2} \tag{4.54}$$

Then the effective mass and effective loss factor can be respectively expressed as

$$m_k \approx \frac{2D_p\left(k_p^2 - k^2\right)\sqrt{k_p^2 + k^2}}{\omega^2} \tag{4.55}$$

$$\eta_k \approx \frac{2D_p\left(k_p^2 + k^2\right)\sqrt{k_p^2 - k^2}}{D_b k^4} \tag{4.56}$$

From equations (4.55) and (4.56), it is seen that the effective loss factor added by loading the plate to the beam depends on both the properties of the beam and of the plate but regardless of the internal damping of the plate. However, the mass added to the beam by the plate tends to depend on the plate properties only. Especially when $|k| << k_p$, these expressions reduce to

$$\eta_k \approx \frac{2D_p}{D_b k_p}\left(\frac{k_p}{k}\right)^4 \approx \frac{2m_p}{m_b k_p} = \frac{m_p \lambda_p}{m_b \pi} \tag{4.57}$$

$$m_k \approx \frac{2m_p}{k_p} = \frac{m_p \lambda_p}{\pi} \tag{4.58}$$

From equation (4.57) one may reasonably suppose that when a set of waves travels along the beam, the waves with fast wave velocity (k is very small) can transmit most of their energy to the plate. Equation (4.58) shows that the mass added to the beam is almost equivalent to the plate mass in a strip of width equal to one third of the plate wavelength. When the plate receiver is much more flexible than the source beam (e.g. behaves in a 'Fuzzy' manner to the beam), it is seen then the induced effective loss factor of the beam by coupling the plate depends only on the wavenumber of the plate and the mass ratio between the beam and the plate, and is independent of the internal damping of the plate. This is in good agreement with the fuzzy structure theory [5-6].

It should be noted, however, that equations (4.53) and (4.54) are only valid when the plate damping η_p is relatively very small. Otherwise the contributions of η_p to $\mathrm{Re}(K)$ and $\mathrm{Im}(K)$ must be considered in equations (4.53) and (4.54). Under such circumstances, the plate internal damping η_p may have a quite obvious influence on both the effective damping and effective mass, especially when η_p is very big. Therefore fuzzy structure theory tends to be more valid when the fuzzy attachment has a relatively small damping.

When $|k| \geq k_p$, however, equation (4.18) yields

$$\mathrm{Im}(K) = 0 \tag{4.59}$$

$$\mathrm{Re}(K) = 2D_p\sqrt{k^4 - k_p^4}\left(\sqrt{k^2 + k_p^2} + \sqrt{k^2 - k_p^2}\right) \tag{4.60}$$

Combining equations (4.51) and (4.52), gives

$$\eta_k = 0 \tag{4.61}$$

$$m_k = -\frac{2D_p\sqrt{k^4 - k_p^4}\left(\sqrt{k^2 + k_p^2} + \sqrt{k^2 - k_p^2}\right)}{\omega^2} \tag{4.62}$$

It is seen that no effective damping but effective (negative) mass is added to the beam by the plate when $|k| > k_p$. Physically it means that waves travelling along the beam with wavenumber greater than the plate wavenumber cannot radiate power to the plate. The

influence of the plate on the beam vibration, therefore, can be taken as mainly adding an effective mass. The negative value of equation (4.62) means that the beam mass density has in effect been reduced by the presence the plate. When $|k| >> k_p$, this reduced mass density may be estimated as

$$m_k \approx -\frac{D_p m_b \lambda_b}{D_b \pi} \tag{4.63}$$

Alternatively, from equations (4.49), (4.59) and (4.60), the dynamic interaction between the beam and plate in the case of $|k| > k_p$ can be more reasonably taken as the plate loading effective stiffness to the beam. The effective stiffness is given by

$$D_k = \frac{2D_p\sqrt{k^4 - k_p^4}\left(\sqrt{k^2 + k_p^2} + \sqrt{k^2 - k_p^2}\right)}{k^4} \tag{4.64}$$

When $|k| >> k_p$, equation (4.64) simply gives

$$D_k \approx \frac{4D_p}{k} = \frac{2D_p\lambda_b}{\pi} \tag{4.65}$$

Therefore, it is seen that when $|k| < k_p$ the plate loads the beam with effective mass and damping, while when $|k| > k_p$ the plate loads the beam with effective stiffness.

4.5 NUMERICAL EXAMPLES

In Section 4.2, an analytical solution of the power transmission has been given in the wavenumber domain as equation (4.22). Moreover in Section 4.3 it has shown that if the plate receiver is so flexible that $\left(k_p/k_b\right)^2 >> 1$, the plate may then be reasonably regarded as locally reacting, as given in equation (4.40). Consequently, the power transmission to the plate from the source beam can be approximated simply by equation (4.48). In this section, numerical models of an infinite beam-stiffened plate are set up to investigate how the wavenumber ratio k_p/k_b affects the accuracy of the approximation based on the locally reacting theory. An external harmonic point force of amplitude 1 is introduced directly on the beam at the point $x = 0$. All the relevant parameters of the numerical models are listed in Tables 4.1 and 4.2. Three different wavenumber ratios are investigated

by varying the thickness of the plate. These are $k_p/k_b = 1.8$, 2.5, and 3.5, corresponding to the plate thickness 0.020m, 0.010m and 0.005m, respectively.

Figures 4.4-4.6 compare the point mobilities at the driving point of the beam after coupling with the plate, predicted both by the analytical FT approach (solid line) and by the locally reacting method (dotted line), corresponding to $k_p/k_b = 1.8$, 2.5 and 3.5, respectively. It is seen that the locally reacting method gives very good approximations for the dynamic response of the coupled beam, even when $k_p/k_b = 1.8$. The bigger the wavenumber ratio k_p/k_b is, the more accurate the locally reacting prediction is.

Figures 4.7-4.9 compare the power transmission results from the analytical prediction of equation (4.22) and the approximations of equation (4.48). It can also be seen that the locally reacting approximation agrees well with the analytical result, provided the plate wavenumber is big enough, say, at least twice that of the beam.

Figures 4.4-4.6 also give the modulus of the input mobility of the beam when it is uncoupled from the plate. It is seen that the point mobility of the beam after coupling decreases in a manner which can be viewed as the beam being loaded with effective mass as well as damping by the presence of the plate. Actually, the dynamic response of the coupled beam tends to be less affected as the plate flexibility increases. This implies the interacting effects between the beam and the plate decrease when the plate receiver is more flexible.

4.6 SUMMARY

In this chapter, an infinite beam-stiffened plate model was considered (i.e., an infinite beam attached to an infinite plate). Both Fourier Transform (FT) and wave analysis methods were used to give an analytical solution for the dynamic response of the coupled system. It has been shown that only the wave terms (propagating along the beam) with $k_b' < k_p$ should be taken into account for predicting the power transmission to the plate. When the wavenumber ratio between the beam and the plate is big enough, e.g. $k_p/k_b' > 2$, the locally reacting plate model can be used to approximate simply and accurately both the dynamic response of the beam and the power transmission to the plate. Moreover, it has been shown that when $k_b' < k_p$ the plate adds effective mass and damping to the beam, while when $k_b' > k_p$ the plate adds effective stiffness to the beam. The energy dissipated by the effective damping represents the energy transmitted from the beam to the

plate. When the plate receiver is much more flexible than the source beam (e.g. behaves in a fuzzy manner to the beam), the induced effective loss factor depends only on the wavenumber of the plate and the mass ratio between the beam and the plate, regardless of the internal damping of the plate. This is in good agreement with the fuzzy structure theory [5-6]. The effective mass is almost equivalent to the plate mass in a strip of width equal to one third of the plate wavelength in this case. Since the mass distribution of the plate m_p is usually relatively very small, the effective mass added is very small (depending on ω) consequently. Therefore, the main effect of loading a fuzzy-like plate to a stiff beam can be viewed as adding effective damping to the beam vibrations.

Table 4.1 Material properties for the beam/plate system

Young's modulus (GN/m^2)	Poisson's ratio	Loss factor	Density (kg/m^3)
4.4	0.38	0.05	1152

Table 4.2 System dimensions and coupling positions

Structure	Beam	Plate
Dimensions (m)	Width=0.059m; Height=0.068m	Thickness=0.020m/0.010m /0.005m

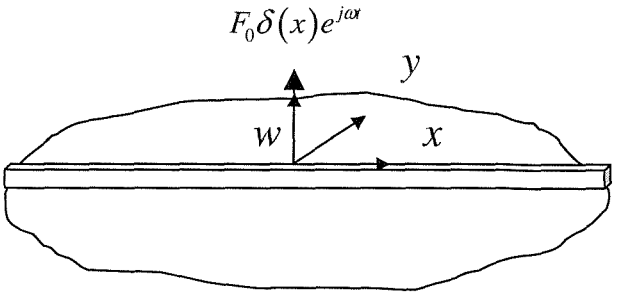

Figure 4.1 An infinite beam-stiffened plate model.

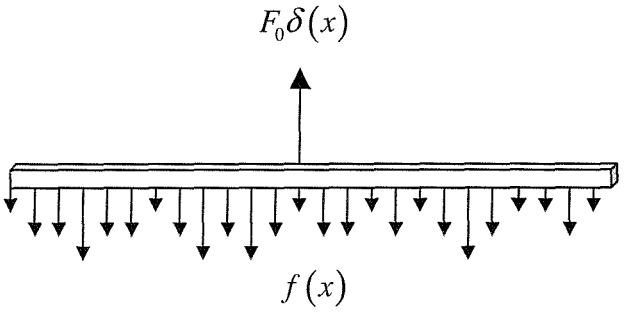

Figure 4.2 The infinite beam and its force loadings.

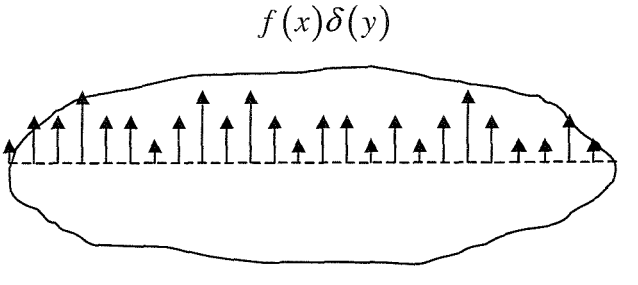

Figure 4.3 The infinite plate and its force loadings.

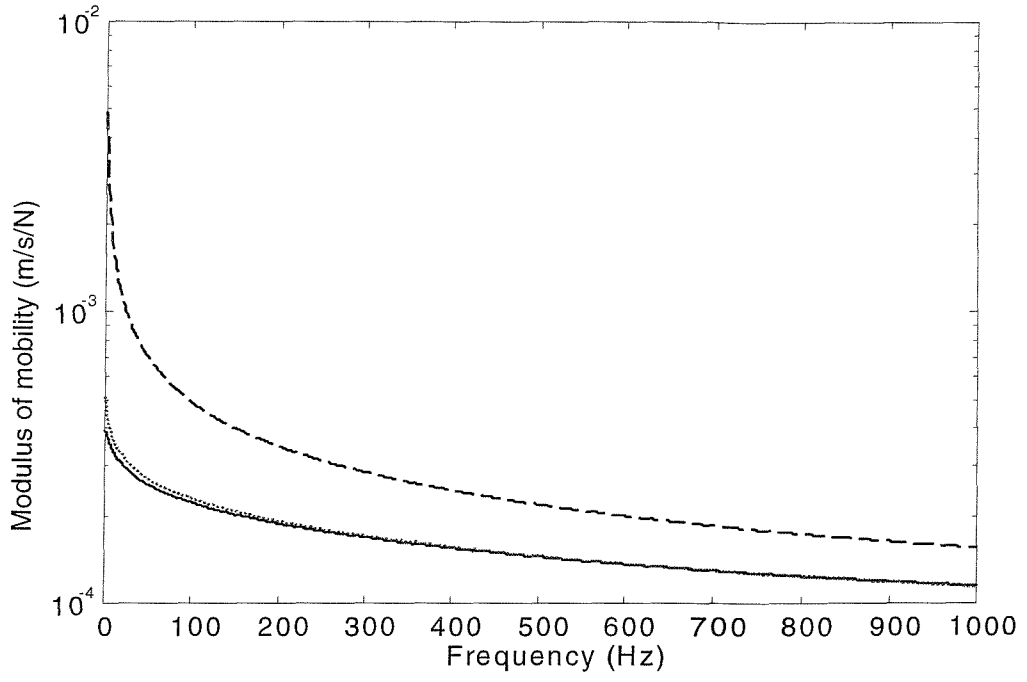

Figure 4.4 Point mobility at excitation point of the beam when the plate thickness is 0.020m: Fourier Transform analytical result, _____ ; locally reacting approximate result, ... ; uncoupled result, _ _ _ _ .

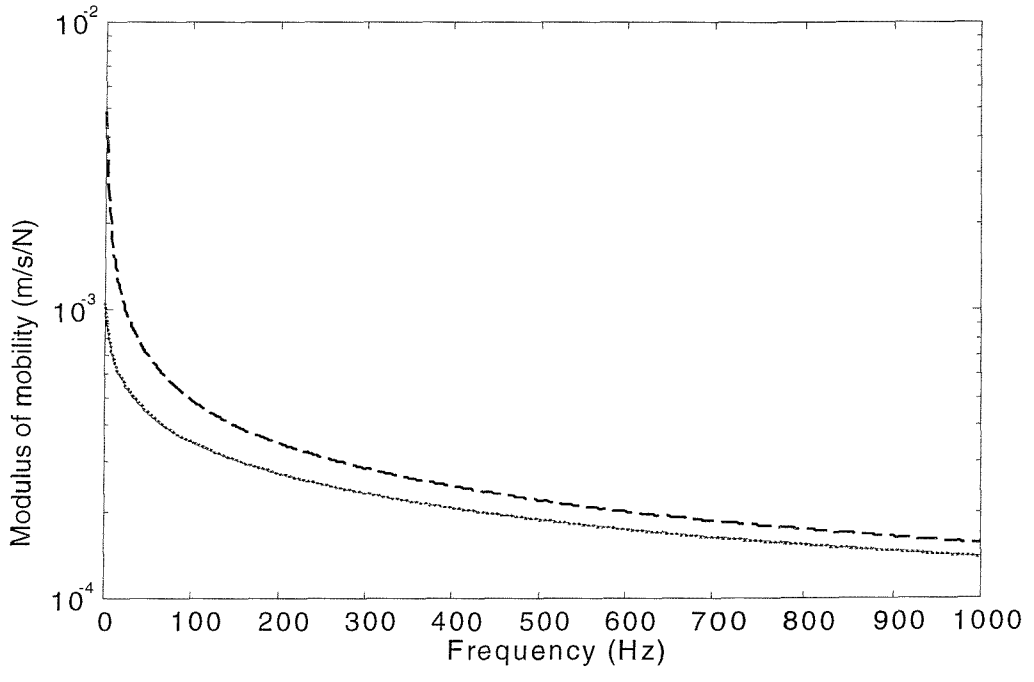

Figure 4.5 Point mobility at excitation point of the beam when the plate thickness is 0.010m: Fourier Transform analytical result, _____ ; locally reacting approximate result, ... ; uncoupled result, _ _ _ _ .

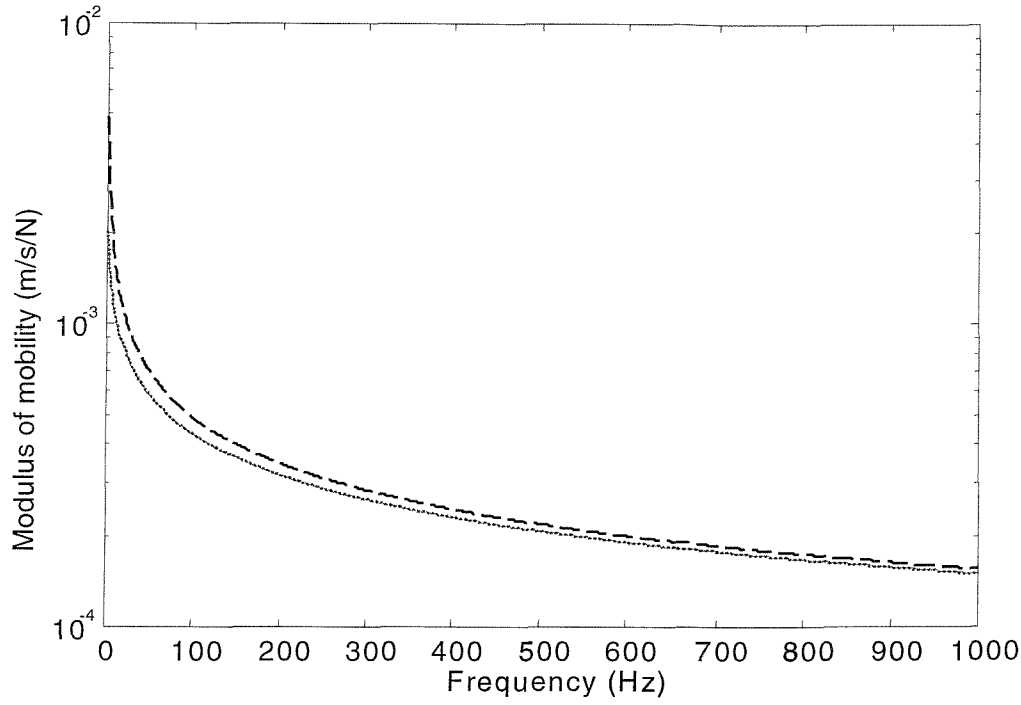

Figure 4.6 Point mobility at excitation point of the beam when the plate thickness is 0.005m: Fourier Transform analytical result, ——— ; locally reacting approximate result, ... ; uncoupled result, – – – – .

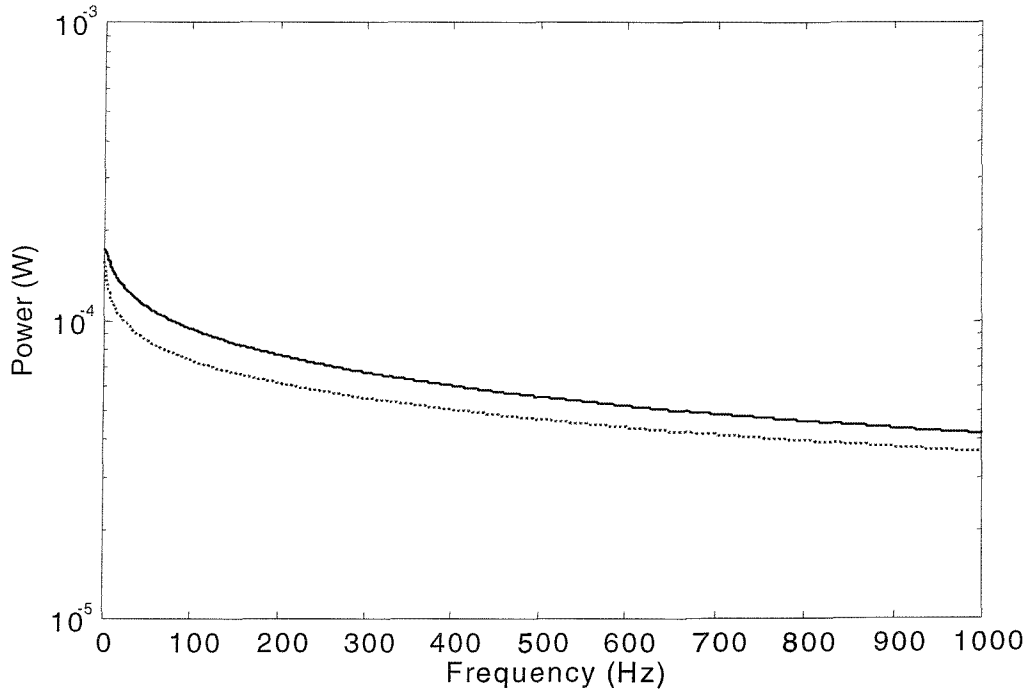

Figure 4.7 Power transmission to the plate when the plate thickness is 0.020m: Fourier Transform analytical result, ——— ; locally reacting result, ...

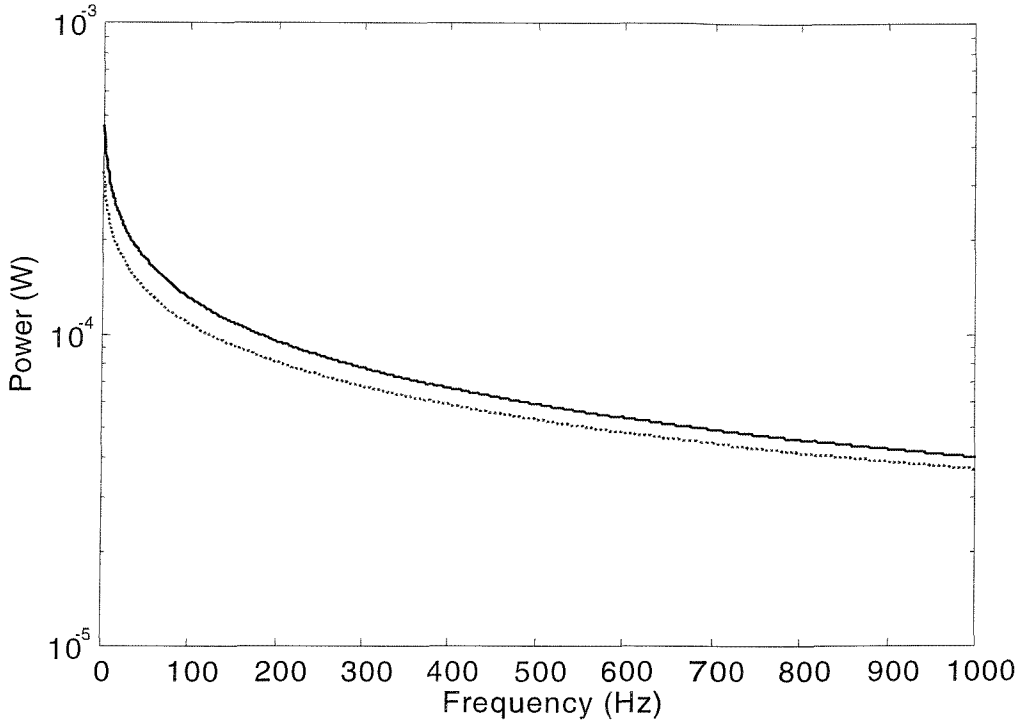

Figure 4.8 Power transmission to the plate when the plate thickness is 0.010m: Fourier Transform analytical result, ——— ; locally reacting result, ...

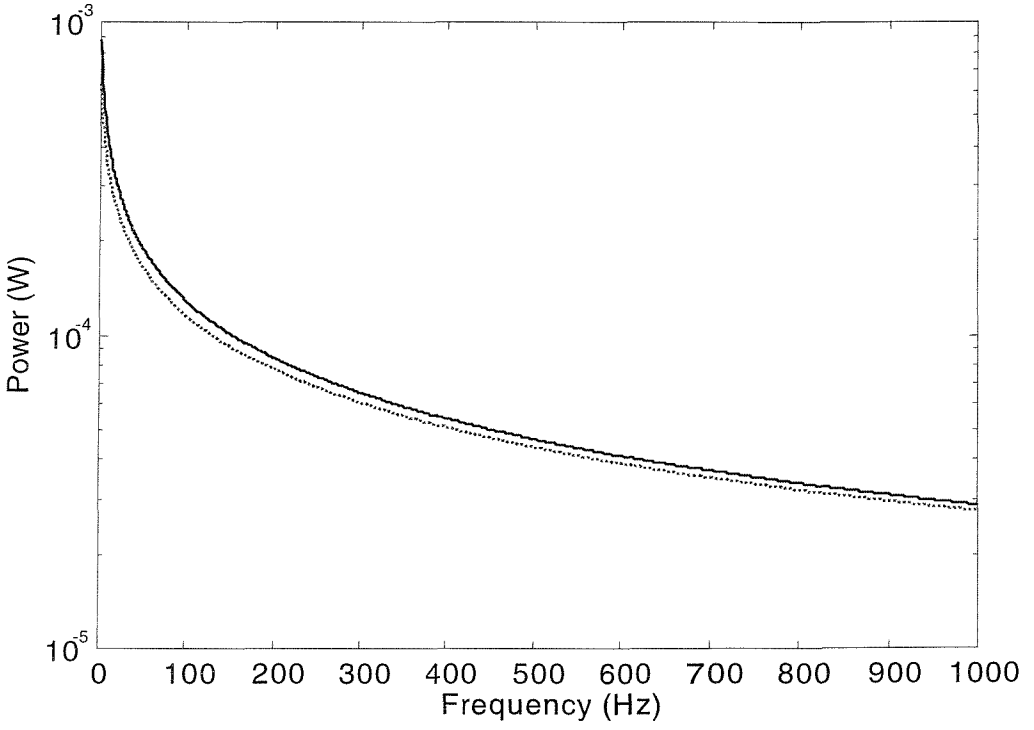

Figure 4.9 Power transmission to the plate when the plate thickness is 0.005m: Fourier Transform analytical result, ——— ; locally reacting result, ...

Chapter 5

VIBRATION OF A FINITE BEAM ATTACHED TO AN INFINITE PLATE

5.1 INTRODUCTION

As far as an infinite beam/plate model is concerned, both Fourier Transform (FT) and wave analysis methods can be used in a straightforward way to provide analytical solutions for the vibration response of the coupled system, as described in Chapter 4. In this case, waves have been treated as propagating along the beam without any changes. However, when the beam/plate system considered is composed of a finite beam attached to an infinite plate, waves that propagate in the beam encounter changes at both ends of the beam, in directions, amplitudes and phase, and often even the basic characters [11]. Wave descriptions in the finite beam are now very complicated, so that the direct application of the above conventional methods becomes quite troublesome or problematic. In such cases, the source beam is more conveniently described in terms of natural frequencies and natural modes instead of waves.

In this chapter, therefore, a hybrid approach is described to approximate in a simple and accurate way the dynamic response of a finite beam attached to an infinite plate, as shown in Figure 5.1. The beam wavelength is usually relatively much longer than that of the plate. Both the beam and the plate are here assumed as uniform and homogenous for simplicity. The finite beam is defined by its modal properties while the infinite plate is defined by wave terms. This is the so-called 'Mode/FT approach' which combines both the modal analysis and Fourier Transform methods. The prediction is mainly concerned the FRFs of the beam and the power transmitted to the plate, as well as the dynamic interactions between the modal properties of the beam and wave motion in the plate. Expressions are given for the effective mass (density) and damping added to each mode of the beam.

When a locally reacting plate model is incorporated into the Mode/FT procedure, a simpler 'locally reacting impedance method' can be developed. The results are then discussed and compared to fuzzy structure theory [5-6].

It is expected that the Mode/FT approach can provide a useful methodology for predicting the vibrations of beam/plate coupled structures, in that it is able to deal with the large dynamic mismatch between the beam and plate components and at the same time can overcome the practical difficulty in determining the exact dynamic properties of the large, flexible plate. In addition, it gives insight into the vibration and coupling of general built-up structures comprising substructures which are dynamically mismatched.

5.2 VIBRATION APPROXIMATION BASED ON A COMBINATION OF MODAL ANALYSIS AND FOURIER TRANSFORM METHODS

Central to the Mode/FT approach is to enforce the equilibrium and continuity conditions by approximate means along the interface between the beam and the plate. This is done in the wavenumber domain. The dynamic interactions between the modal properties of the beam and the wave motions of the plate can then be determined, and hence both the FRFs of the stiff beam and power transmitted to the large flexible plate, as well as the dynamic interactions within the beam-stiffened plate system, can be found. These are given below.

5.2.1 Modal analysis of the beam

Figure 5.2 shows the beam and its force loadings, where x_b is the local coordinate of the beam, and $f_e\left(x_b^e\right)$ and $f_I^b\left(x_b\right)$ are the amplitudes of the external and interface time-harmonic forces acting on the beam, respectively. Time dependent behaviour of the form $\exp\left(j\omega t\right)$ is assumed, and the explicit time dependence will henceforth be suppressed. By conventional modal analysis [11] the beam displacement response $w_b\left(x_b\right)$ can be defined in terms of its uncoupled natural modes, as

$$w_b\left(x_b\right)=\sum_n w_{b,n}\phi_{b,n}\left(x_b\right) \tag{5.1}$$

where $w_{b,n}$ is the modal coordinate of the nth mode of the beam, and $\phi_{b,n}$ is the nth normalized mode shape function of the beam when it is separated from the plate, so that

$$\int_0^{L_b}\phi_{b,n}\left(x\right)\phi_{b,m}\left(x\right)dx=\begin{cases}1, n=m\\0, n\neq m\end{cases} \tag{5.2}$$

where L_b is the length of the beam. From [11], $w_{b,n}$ is given by

$$w_{b,n}=Y_{b,n}\left(f_{e,n}+f_{I,n}^b\right) \tag{5.3}$$

where $Y_{b,n}$ is the nth modal receptance of the uncoupled beam, and $f_{e,n}$ and $f_{I,n}^{s}$ are, respectively, the nth modal forces corresponding to $f_e\left(x_b^e\right)$ and $f_I^b\left(x_b\right)$. These terms are given by

$$Y_{b,n} = \frac{1}{m_b} \frac{1}{\omega_{b,n}^2\left(1+j\eta_{b,n}\right)-\omega^2} \tag{5.4}$$

$$f_{e,n} = \int_0^{L_b} f_e(x)\phi_{b,n}(x)dx \tag{5.5}$$

$$f_{I,n}^b = \int_0^{L_b} f_I^b(x)\phi_{b,n}(x)dx \tag{5.6}$$

Here m_b is the mass per unit length of the beam, $\omega_{b,n}$ and $\eta_{b,n}$ are the nth natural frequency and modal loss factor of the uncoupled beam, respectively.

5.2.2 Wave analysis of the infinite plate

Figure 5.3 shows the plate and its force loadings along the interface, where $\left(x_p, y_p\right)$ are the local coordinates of the plate, and $\left(x_p^I, y_p^I\right)$ and $f_I^p\left(x_p^I, y_p^I\right)$ are, respectively, the interface locations on the plate, and interface force distribution.

If it is assumed that the interface starts from the point $\left(x_p^I, y_p^I\right)=\left(x_p, y_p\right)=(0,0)$ and ends at $\left(x_p^I, y_p^I\right)=\left(x_p, y_p\right)=(L_b,0)$ along the line $y_p^I = y_p = 0$, the interface forces acting on the plate can be expressed as

$$f_I^p\left(x_p^I, y_p^I\right)=\begin{cases} f_I^p\left(x_p\right)\delta\left(y_p\right) & 0 \le x_p \le L_b \\ 0 & x_p < 0 \cup x_p > L_b \end{cases} \tag{5.7}$$

By using the Fourier Transform given in equation (4.4), the above equation can be expressed in the wavenumber domain as

$$F_I^p\left(k_x\right)=\int_0^{L_b} f_I^p\left(x_p\right)e^{-jkx_p}dx_p \tag{5.8}$$

The interface displacements can then be related with interface force loading by

$$W_p\left(k_x\right)=\frac{F_I^p\left(k_x\right)}{j\omega Z_p\left(k_x\right)} \tag{5.9}$$

where $W_p\left(k_x\right)$ is the Fourier Transforms of $w_p\left(x_p,0\right)$, given by

$$W_p(k_x) = \int_{-\infty}^{+\infty} w_p(x_p, 0) e^{-jkx_p} dx_p \tag{5.10}$$

and $Z_p(k_x)$ is the line impedance of the plate along the interface $y_p = 0$. From equation (4.18), it is seen that

$$Z_p(k_x) = \frac{1}{j\omega} 2D_p \sqrt{k_x^4 - k_p^4} \left(\sqrt{k_x^2 + k_p^2} + \sqrt{k_x^2 - k_p^2} \right) \tag{5.11}$$

If the damping of the plate is negligible, the above equation is such that

$$\mathrm{Re}\left[Z_p(k_x) \right] = 0, \quad |k_x| \geq k_p \tag{5.12}$$

Equation (5.12) implies that only the waves propagating faster than the wave motion in the plate can transmit energy into the plate. Hence it is reasonable to assume that energy transmitting, non-reactive interaction between a beam and an infinite plate mainly involves wavenumbers within the range $|k_x| < |k_p|$.

5.2.3 Vibration response of the coupled system

From the above description, it is seen that the local coordinates of the beam and plate are related such that $x_p^I = x_p = x_b = x$, where $0 \leq x \leq L_b$. The equilibrium and continuity conditions along the interface between the beam and the plate are

$$f_I^p(x)\delta(y) = -f_I^b(x) \quad 0 \leq x \leq L_b \tag{5.13}$$

$$w_p(x, 0) = w_b(x) \quad 0 \leq x \leq L_b \tag{5.14}$$

A new set of orthogonal functions is now defined as

$$\hat{\phi}_{b,n}(x) = \begin{cases} \phi_{b,n}(x) & 0 \leq x \leq L_b \\ 0 & x < 0 \cup x > L_b \end{cases} \tag{5.15}$$

The interface force $f_I^p(x)\delta(y)$ may then be decomposed into the form

$$f_I^p(x)\delta(y) = \left[\sum_n f_{I,n} \hat{\phi}_{b,n}(x) \right] \delta(y) \tag{5.16}$$

Taking the Fourier Transform of the above equation ($k = k_x$) gives

$$F_I^p(k) = \sum_n f_{I,n} \Phi_{b,n}(k) \tag{5.17}$$

where $\Phi_{b,n}(k)$ is the Fourier Transform of $\hat{\phi}_{b,n}(x)$ in the range of $-\infty < x < +\infty$, which is equivalent to the Fourier Transform of $\phi_{b,n}(x)$ in the range of $0 \le x \le L_b$. Substituting equation (5.17) into (5.9), gives

$$\sum_n f_{I,n}\Phi_{b,n}(k) = j\omega Z_p(k)W_p(k) \tag{5.18}$$

From equations (5.1) and (5.15), $w_b(x)$ may be re-written as

$$w_b(x) = \sum_n w_{b,n}\hat{\phi}_{b,n}(x) \tag{5.19}$$

The above equation then yields

$$W_b(k) = \sum_n w_{b,n}\Phi_{b,n}(k) \tag{5.20}$$

where $W_b(k)$ is the Fourier Transforms of $w_b(x)$, given by

$$W_b(k) = \int_0^{L_b} w_b(x)e^{-jkx}dx \tag{5.21}$$

It is now assumed that the displacement of the plate outside of the interface region is set equal to zero by applying fictitious forces acting on the plate model, i.e.,

$$w_p(x,0) \approx 0 \quad x < 0 \cup x > L_b \tag{5.22}$$

Substituting equation (5.22) into (5.10) and the combining with equations (5.14) and (5.21), it follows that

$$W_p(k) \approx W_b(k) \tag{5.23}$$

Equation (5.23) is the displacement continuity condition of the beam-stiffened plate in the wavenumber domain. Physically, equation (5.23) means that when the displacements of the beam and the plate (along coupling) are decomposed into wave components, each beam wave component are almost the same as that of the plate.

The assumption of equation (5.22) is therefore equivalent to assuming that the plate displacement wave components $W_p(k)$ are dominated by the contribution from $w_p(x,0)$ in the range of $0 \le x \le L_b$. Substituting equation (5.20) into (5.23) and then into (5.18), yields

$$\sum_n f_{I,n}\Phi_{b,n}(k) \approx j\omega Z_p(k)\sum_n w_{b,n}\Phi_{b,n}(k) \tag{5.24}$$

The orthogonal property of $\hat{\phi}_{b,n}(x)$ in equation (5.15) gives, by Ref. [43],

$$\begin{aligned}\int_{-\infty}^{+\infty} \hat{\phi}_{b,n}(x)\hat{\phi}_{b,m}(x)dx &= \int_{0}^{L_b} \phi_{b,n}(x)\phi_{b,m}(x)dx \\ &= \frac{1}{2\pi}\int_{-\infty}^{+\infty} \Phi^{*}_{b,n}(k)\Phi_{b,m}(k)dk = \begin{cases}1, n = m \\ 0, n \neq m\end{cases}\end{aligned} \tag{5.25}$$

where $*$ denotes the complex conjugate. Let both sides of equation (5.24) be multiplied by $\Phi^{*}_{b,n}(k)$ and integrated over k from $-\infty$ to $+\infty$. If it is assumed that $Z_p(k)$ changes slowly compared to $\Phi_{b,n}(k)$ so that the cross couplings between the modes of the beam can be ignored, it follows that

$$f_{1,n} \approx j\omega w_{b,n} Z_n \tag{5.26}$$

where

$$Z_n = \frac{1}{2\pi}\int_{-\infty}^{+\infty} \left|\Phi_{b,n}(k)\right|^2 Z_p(k)dk \tag{5.27}$$

Physically, equation (5.27) shows the coupling relations between the line-impedance of the plate $Z_p(k)$ and the mode shapes of the beam. Hence the interactions between the wave motion in the plate and the modal properties of the beam can be determined.

Substituting equation (5.26) into (5.16) then into (5.13) and finally into (5.6) and (5.3), the nth modal amplitude of the beam, $w_{b,n}$, after coupling to the plate, can be expressed as

$$w_{b,n} \approx \frac{Y_{b,n}}{1 + j\omega Y_{b,n} Z_n} f_{e,n} \approx \frac{1}{\frac{1}{Y_{b,n}} + j\omega Z_n} f_{e,n} \tag{5.28}$$

Equation (5.28) shows that the nth modal impedance of the beam, after coupling to the plate, is increased by Z_n. Hence Z_n may be called the 'plate-loaded modal impedance', which depends on both the plate properties k_p and D_p, and the beam property $\phi_{b,n}(x)$, by the relations given in equations (5.11) and (5.27). Note that in equation (5.28) it is implicitly assumed that the plate loads each beam mode independently and hence that the cross-mode loading is negligible.

Combining equations (5.1) and (5.28), the beam displacement can then be expressed as

$$w_b(x) \approx \sum_n \frac{f_{e,n}}{\frac{1}{Y_{b,n}} + j\omega Z_n} \phi_{s,n}(x) \tag{5.29}$$

The power transmission from the beam to the plate is given by

$$P = \frac{1}{2}\mathrm{Re}\left\{ \int_0^{L_b} \left[\sum_n f_{I,n}\phi_{b,n}(x) \right]^* j\omega \left[\sum_n w_{b,n}\phi_{b,n}(x) \right] dx \right\} \tag{5.30}$$

Combining equations (5.25)-(5.27), the transmitted power can be expressed as

$$P \approx \frac{1}{2}\mathrm{Re}\left\{ j\omega \sum_n f_{I,n}^* w_{b,n} \right\} \approx \frac{1}{2}\omega^2 \sum_n \left| w_{b,n} \right|^2 \mathrm{Re}\{Z_n\} \tag{5.31}$$

From equations (5.11) and (5.27), it is seen that

$$\mathrm{Re}\{Z_n\} \approx 0\,,\ |k| \geq k_p \tag{5.32}$$

Therefore, equation (5.32) indicates that only the components of the mode shapes of the beam with wavelengths bigger than the plate wavelength can transmit significant power to the plate. Otherwise, the components generally only cause near-field wave motions in the plate.

In summary, the Mode/FT approach can be briefly divided into the following steps: (1) The beam model is defined in terms of its uncoupled natural modes (section 5.2.1), while the plate model is described in the wavenumber domain by a line-impedance (section 5.2.2). (2) By introducing a new set of orthogonal functions $\hat{\phi}_{b,n}$ in the range $-\infty < x < +\infty$ based on the beam modes $\phi_{b,n}$ in the range $0 < x < L_b$ (equation (5.15)), the plate interface force can then be decomposed in terms of $\hat{\phi}_{b,n}$ (equation (5.16)). As a result, a new relation between the plate interface force and displacement can be given (equation (5.18)). (3) When the plate displacement outside of the interface region is ignored (equation (5.22)), an estimate can then be made of the relation between displacements of the plate (along the interface) and beam in the wavenumber domain (equation (5.23)). Consequently, an approximate relation between the plate interface force and the beam displacement can be established (equation (5.24)). (4) Assume the line-impedance of the plate changes slowly with k compared to $\Phi_{b,n}(k)$. By the orthogonal properties of $\phi_{b,n}$ and hence $\hat{\phi}_{b,n}$, the interface force and displacement relation can then be simply estimated (equation (5.26)).

Finally, the beam displacement and the power transmitted to the plate can be predicted in a simple manner.

In step (4) the cross-mode coupling interaction has been ignored. Such a simplification is quite reasonable if the uncoupled mode shape $\phi_{b,n}$ has a strong sinusoidal component at a given wavenumber (as it generally will for a uniform, straight beam), so that $|\Phi_{b,n}(k)|^2$ is sharply peaked in the wavenumber domain. These cross-mode coupling terms are expected to be less important for the higher modes of the beam.

5.2.4 Dynamic interactions between the beam and the plate

The dynamic interactions between the beam and the plate are given by equation (5.28). The modal receptance $Y_{b,n}$ of an uncoupled beam is given in equation (5.4), while the modal receptance $Y'_{b,n}$ of the beam after coupling to the plate becomes

$$Y'_{b,n} \approx \frac{Y_{b,n}}{1+j\omega Y_{b,n} Z_n} \tag{5.33}$$

Substituting equation (5.4) into (5.33), it follows that

$$Y'_{b,n} \approx \frac{1}{\left[m_b\omega_{b,n}^2\left(1+j\eta_{b,n}\right)-m_b\omega^2\right]+j\omega Z_n} \tag{5.34}$$

The term $j\omega Z_n$ can be separated into real and imaginary parts

$$j\omega Z_n = -K_{n1} + jK_{n2} \tag{5.35}$$

where K_{n1} and K_{n2} are given, respectively, as

$$\begin{aligned} K_{n1} = {} & \frac{D_p}{\pi}\int_{-\infty}^{+\infty}\left|\Phi_{b,n}(k)\right|^2\left(k_p^2-k^2\right)\sqrt{k_p^2+k^2}\,dk \\ & +\frac{D_p}{\pi}\int_{-\infty}^{-k_p}\left|\Phi_{b,n}(k)\right|^2\left(k_p^2+k^2\right)\sqrt{k^2-k_p^2}\,dk \\ & +\frac{D_p}{\pi}\int_{+k_p}^{+\infty}\left|\Phi_{b,n}(k)\right|^2\left(k_p^2+k^2\right)\sqrt{k^2-k_p^2}\,dk \end{aligned} \tag{5.36}$$

$$K_{n2} = \frac{D_p}{\pi}\int_{-k_p}^{+k_p}\left|\Phi_{b,n}(k)\right|^2\left(k_p^2+k^2\right)\sqrt{k_p^2-k^2}\,dk \tag{5.37}$$

Equation (5.34) can then be re-written as

$$Y'_{b,n} \approx \frac{1}{m_b \omega_{b,n}^2 \left[1 + j\left(\eta_{b,n} + \eta_n\right)\right] - \left(m_b + m_n\right)\omega^2} \tag{5.38}$$

where

$$m_n \approx \frac{K_{n1}}{\omega^2} \tag{5.39}$$

$$\eta_n \approx \frac{K_{n2}}{m_b \omega_{b,n}^2} \tag{5.40}$$

Equation (5.38) indicates that the plate in effect adds mass m_n and damping η_n to each mode of the beam. The energy dissipated by the induced effective damping corresponds the energy transmitted from the beam to the plate. It is seen from equation (5.40) that $\eta_n \to \infty$ when $\omega_{b,n} = 0$. This means that the rigid modes of the beam can be greatly damped by the plate.

5.2.4.1 Approximations for K_{n1} and K_{n2}

Equations (5.39) and (5.40) give the approximations for the effective mass and damping added to the beam by the plate. These two expressions can be further simplified under certain circumstances, which are described below. This gives insight into the coupling behaviour and allows comparisons with the locally reacting models of Ref [26-27].

Suppose that the uncoupled mode shape $\phi_{b,n}$ of a uniform, straight beam has a strong sinusoidal component at a given wavenumber, e.g.

$$\phi_{b,n}(x) = \sqrt{\frac{2}{L_b}} \sin\left(\frac{n\pi x}{L_b} + \theta\right) \tag{5.41}$$

where θ represents a phase constant which is determined by the exact boundary conditions of the beam. Under such circumstances $\left|\Phi_{b,n}(k)\right|^2$ tends to be sharply peaked in the wavenumber domain around the value of $k_{b,n} \approx \sqrt[4]{m_b \omega_{b,n}^2 / D_b}$ but converge quickly to zero as $|k| \to \infty$. If it is assumed that the other terms in the integrands in equations (5.36) and (5.37) vary slowly with k compared to $\left|\Phi_{b,n}(k)\right|^2$, K_{n1} and K_{n2} can, respectively, be simply approximated as

$$K_{n1} \approx 2D_p \left(k_p^2 - k_{b,n}^2\right)\sqrt{k_p^2 + k_{b,n}^2} \tag{5.42}$$

$$K_{n2} \approx 2D_p \left(k_p^2 + k_{b,n}^2\right)\sqrt{k_p^2 - k_{b,n}^2} \tag{5.43}$$

Here the orthogonality condition of equation (37) has been applied.

As a special case, when the beam is relatively very stiff compared to the plate such that $k_{b,n} << k_p$, the above equations become

$$K_{n1} \approx K_{n2} \approx 2D_p k_p^3 \tag{5.44}$$

The effective mass and damping in equations (5.39) and (5.40) can then be estimated in a much simpler manner. Physically, equation (5.44) represents a 'locally reacting' case [26-27]. The relevant details will be discussed in the section below.

5.3 DISCUSSION

In the above section, a hybrid Mode/FT approach is used to provide simple estimates of the vibrations of beam-stiffened plate systems, together with the approximations for the dynamic interactions between the source beam and the plate receiver. In this section, the limiting case where the beam-stiffened plate system has a very big dynamic mismatch will be considered, i.e., the plate is relatively very much more flexible than the beam. It then behaves as a locally reacting model [26-27] or a set of fuzzy attachments [5-6]. These discussions illustrate various features of the vibrations and coupling of a beam-stiffened plate.

5.3.1 Locally reacting impedance method

In [26-27], it was seen that when the plate wavenumber is much bigger than that of the beam (typically $k_p/k_b > 2$), the plate can be considered as being locally reacting. The locally reacting impedance is given by

$$Z_p' \approx \frac{2m_p\omega}{k_p}(1+j) \tag{5.45}$$

Such a plate model was then incorporated into a standard sub-structuring procedure to predict the vibration response of a beam-stiffened plate system by splitting the coupled structure into a beam attached to a set of independent narrow strips of the plate [27]. The corresponding solution, however, may still be very time-consuming since the calculation still requires many connecting points between the beam and the plates. However, this locally reacting plate model can be incorporated easily into the Mode/FT approach to predict the response of the beam-stiffened plate system.

When equation (5.45) is substituted into (5.27), it follows that

$$Z_n \approx Z'_p \approx \frac{2m_p\omega}{k_p}(1+j) \tag{5.46}$$

Equation (5.46) implies that the plate-loaded impedance (by a locally reactive plate) to each mode of the beam tends to be the same. It depends only on the plate properties k_p and m_p, regardless of the beam properties since the beam is of relatively very high impedance. Substituting equation (5.46) into (5.28), the modal amplitudes of the beam are approximated by

$$w'_{b,n} \approx \frac{Y_{b,n}}{1+j\omega Y_{b,n}Z'_p} f_{e,n} \approx \frac{1}{1/Y_{b,n}+j\omega Z'_p} \tag{5.47}$$

Consequently, the power transmitted to the plate can be simply determined by

$$P' \approx \frac{\omega^3 m_p}{k_p}\sum_n \left|w'_{b,n}\right|^2 \tag{5.48}$$

From the above it is seen that the locally reacting impedance method can provide predictions of the vibration response of a beam/plate system in a much simpler manner.

Similarly, the effective mass and loss factor added to each mode of the beam by the locally reacting plate model is given, from equation (5.46), by

$$m'_n \approx \frac{m_p\lambda_p}{\pi} = \frac{2m_p}{k_p} \tag{5.49}$$

$$\eta'_n \approx \frac{m_p\omega^2\lambda_p}{m_b\omega_n^2\pi} \tag{5.50}$$

The above equations indicate that the effective loss factor (for a given mode) increases with frequency but the effective mass decreases. Also the effective loss factor depends on both beam and plate properties whereas the effective mass depends on only the plate properties, regardless of the orders of the beam modes.

5.3.2 Comparison with fuzzy structure theory

In [5-6], fuzzy structure theory was used to investigate the dynamic coupling relations between a large deterministic 'master' substructure and a continuous set of light oscillators, i.e., 'fuzzy attachments'. It was found that the attached items act mainly to provide damping to the master structure. Moreover, the level of this damping is

independent of the dissipation factor of the attachments. Similar conclusions were also given in Ref. [1]

When the plate receiver is relatively much more flexible than the source beam, the former behaves like 'fuzzy attachments' to the latter. By equation (5.49), it is seen that in this case the ratio of m_n'/m_b can be very small since $m_p\lambda_p/m_b$ is usually very small for a fuzzy-like plate. As a result, the plate in effect only adds damping to each mode of the beam. Equation (5.50) indicates that the effective damping is independent of the internal damping of the plate itself. These conclusions are consistent with those of fuzzy structure theory.

It is worth noting from equation (5.50) that the effective loss factor added to each mode of the beam by a fuzzy-like plate attachment can be simply estimated as $\eta_n' \approx m_p\lambda_p/m_b\pi$ due to the continuity of the natural frequencies of the plate.

5.4 NUMERICAL EXAMPLES

Numerical examples of a finite beam attached to an infinite plate are presented to investigate the validity of the combined mode/FT approximation method. The same perspex material is used in the numerical model as that in Chapter 4. All the other relevant parameters are listed in Table 5.1. The beam boundary conditions are simply supported. Four plate thicknesses of 0.020m, 0.010m, 0.005m and 0.002m are considered, corresponding to wavenumber ratios $k_p/k_b = 1.8$, 2.5, 3.5 and 5.6, respectively. A time harmonic point force of unit amplitude acts at a distance $\xi = 0.73m$ from one end of the beam. Results are obtained for both the point mobility of the beam at the driving point and the power transmitted to the plate, as well as the plate-loaded effective mass and damping to the first 3 modes of the beam.

5.4.1 Exact results from the conventional FRF-based sub-structuring method

First the FRF-based sub-structuring method is used, where the line interface between the beam and the plate is modelled using many discrete points. A description for the FRF-based sub-structuring method is given in Appendix V. Analytical solutions for the input- and transfer mobilities of the beam and the plate have been given in Appendices II and III. Numerical tests are conducted to find out how many points should be used to ensure the FRF-based approach converged. Figures 5.4-5.5 compare the calculated results for the point mobility of the beam at the driving point and the power transmitted to a 0.010m

thick infinite plate, respectively, when the line coupling is simulated by discrete points spaced at a half, one-third, one-fourth and one-fifth of the plate wavelength λ_p. It is seen that the conventional sub-structuring method can provide accurate predictions for the vibration response of the coupled system when the discrete points are spaced at no more than a quarter of the plate wavelength apart. The same conclusion holds for the other three cases when $k_p/k_b = 1.8$, 3.5 and 5.6. (The relative figures are not shown here.) However, this FRF-based sub-structuring method can be prohibitive when very large numbers of interface points are needed. For example, when the plate thickness is 0.002m, at least 93 connecting points between the beam and the plate are required at the frequency 1kHz.

5.4.2 Comparisons between the exact and approximate results

In this subsection, the performance of the Mode/FT approach is assessed against the benchmark given by the FRF-based sub-structuring method, where the line coupling is modelled as discrete points spaced at a quarter of the plate wavelength. The approximate results from the former are compared to the exact ones from the latter in Figures 5.6-5.11 for the point mobility of the beam at the driving point and the power transmitted to the plate when $k_p/k_b = 1.8$, 2.5 and 3.5. It is seen that the Mode/FT approach can provide fairly good approximations both for the dynamic response of the beam and for the power transmission to the plate, and also the accuracy of these approximations increases as the flexibility of the plate increases.

Figures 5.6-5.11 also give the estimated results from the locally reacting impedance method. It is quite obvious that the locally reacting method is less accurate than the Mode/FT approach when the plate is not flexible enough compared to the beam, e.g. $k_p/k_b = 1.8$ in Figures 5.6 and 5.7. However, when the plate is flexible enough such that $k_p/k_b \geq 2$, both the Mode/FT approach and the locally reacting impedance method can be used to predict the vibration response of the coupled beam/plate system, as shown in Figures 5.8-5.11, where $k_p/k_b = 2.5$ and 3.5, respectively.

It is worth noting that the Mode/FT approach, and hence the locally reacting impedance method, are developed by neglecting the displacements of the plate outside of the interface region. However, this assumption tends to be invalid when the plate wavelength is comparable to length of the interface (e.g. at very low frequencies), since relatively large displacements may occur in a quite large region of the plate, at and around the interface

region. This explains why relatively larger errors are observed in Figures 5.6-5.11 in the lower frequency range.

The advantages of the Mode/FT approach and the locally reacting impedance method over the conventional sub-structuring method are particularly significant when the plate has a very short wavelength. For example, when the plate thickness is 0.005m, the computational time needed by the mode/FT approach is only about one twentieth of that of the FRF-based sub-structuring method, and the locally reacting impedance method is even more attractive than the Mode/FT approach when very flexible plate receivers are considered.

5.4.3 Effective loss factor and effective mass

In Section 5.2.4, the dynamic interactions between the beam and the infinite plate were generally described as the plate introducing effective mass and damping on each mode of the beam. These influences on the dynamic properties of the beam can be demonstrated well in Figure 5.12, which shows the point mobility results of the beam before and after it is coupled to the plate in the case of $k_p/k_b = 1.8$, 2.5 and 3.5, respectively. It is seen that the beam resonance frequencies are shifted downwards due to the induced effective mass and the resonant response is significantly decreased due to the induced effective damping. Moreover, it is observed that these effective mass and damping decrease as the flexibility of the plate increases.

Figures 5.13-5.14 show the effective loss factor and effective mass induced to the first three modes of the beam when it is attached to the 0.005m thick plate ($k_p/k_b = 3.5$), using the expressions given in equations (5.40) and (5.39), respectively. In Figure 5.14, a dimensionless mass is used which is defined as m_n'/m_b. Two general trends can be found from Figures 5.13-5.14: first, the added damping in a given mode increases and the added mass decreases, as frequency increases; secondly, the lower the orders of the beam modes are, the bigger the induced loss factor and effective mass are, which implies that large interacting effects occur to the lower orders of modes of the beam.

When the beam structure is attached to a relatively very flexible plate, e.g. the plate thickness is 0.002m such that $k_p/k_b = 5.6$, the plate-loaded dynamic effect on the beam tends to be mainly adding damping, as shown in Figure 5.15. This can be explained well from Figures 5.16 and 5.17, where the effective loss factor and dimensionless effective mass added to the first three modes of the beam are given by equations (5.40) and (5.39),

respectively. It is seen that the added mass is less than 3 percent of m_b for the frequencies above 130Hz. Therefore it is quite reasonable to neglect the induced mass but consider the induced damping only. Figures 5.16 and 5.17 also show the results corresponding to equations (5.50) and (5.49)where the plate is treated as a locally reacting model. Very good agreements are observed. This indicates again the validity of the locally reacting impedance method in estimating the vibration response of a beam attached to a relatively very flexible plate.

Since the damping effects are really only important at the beam resonances, the effective damping η_n in equation (5.50) can be taken as $(m_p/m_b)(\lambda_p/\pi)$, where λ_p corresponds to the plate wavelength at $\omega \approx \omega_{b,n}$. These values are shown in Figure 5.18 by the points marked * corresponding to the first fourteen resonance frequencies. It indicates that the lower the order of the beam mode is, the larger the added effective loss factor.

It should be pointed out that although in the above numerical examples the beam modes used have a zero displacement at both ends, the Mode/FT approach can also give fairly good approximations for coupled beam-plate cases where the beam modes are not zero at its ends, e.g. a free-free beam, but perhaps with a little bigger errors at lower frequencies. This will be demonstrated in Chapter 9.

5.5 SUMMARY

In this chapter, a combined Mode/FT approach was developed to predict the vibration response of a coupled system consisting of a finite straight beam attached to an infinite thin plate. Then a locally reacting plate model was incorporated into the Mode/FT procedure to give the locally reacting impedance method in an even simpler way. The performance of this Mode/FT approach was assessed numerically against the conventional FRF-based sub-structuring method, by modelling the interface as discrete point couplings spaced at no more than a quarter of the plate wavelength. Fairly good agreements were observed in the case of $k_p/k_b > 2$ while the computational cost is very low. This advantage is particularly significant when the plate receiver has a very short wavelength. The close relations between the Mode/FT approach and the locally reacting impedance method were also discussed. It was found that the results of these two methods agree very well when the plate receiver is relatively very flexible compared to the beam, as we expected.

Meanwhile, it was seen that the dynamic interaction between the beam and the plate could be interpreted as the plate adding effective mass and damping to each mode of the beam. When the plate behaves like fuzzy attachments to the beam, the plate can be taken as mainly adding damping to each mode of the beam. Moreover, the effective damping is independent of the internal damping of the plate itself. These are in good agreement with the results of fuzzy structure theory. The numerical investigations also indicated that relatively more damping is added to the lower orders of modes of the beam.

Table 5.1 Parameters of the numerical finite beam and infinite plate model

Structure	Beam	Plate
Dimensions (m)	Length=2; Width=0.059; Height=0.068	Thickness=0.020, 0.010, 0.005, 0.002
Wavenumber ratio	$k_p/k_b = 1.8, 2.5, 3.5, 5.6$	

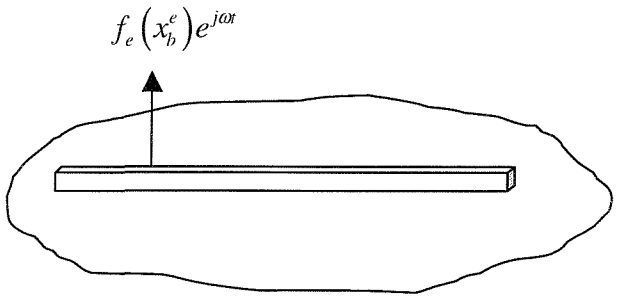

Figure 5.1 A beam attached to an infinite plate.

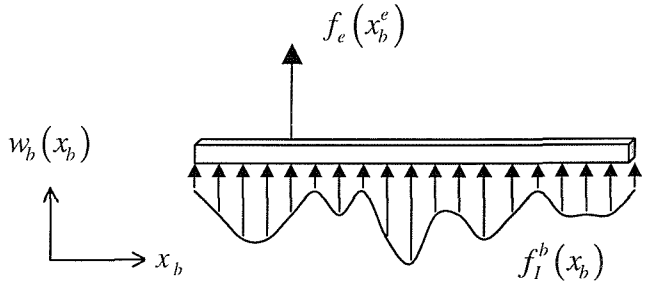

Figure 5.2 The beam and its loadings.

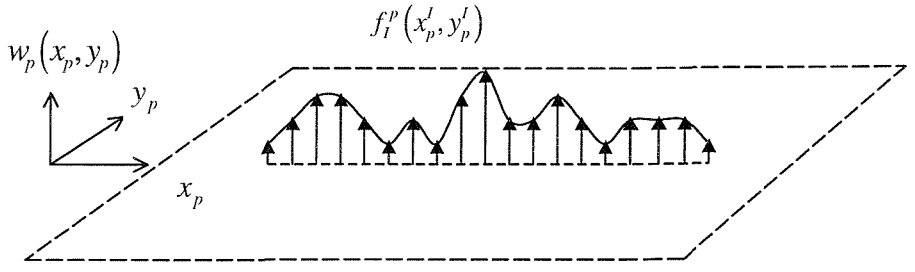

Figure 5.3 The plate and its loadings.

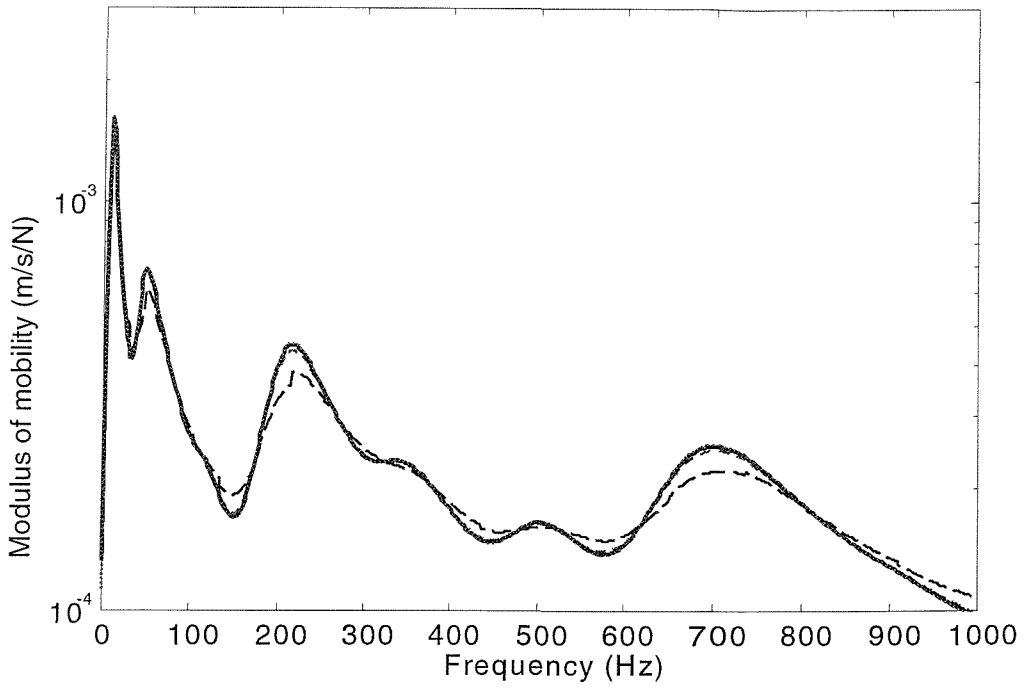

Figure 5.4 Point mobilities of the beam at the driving point when coupled to the 0.010m plate by discrete points spaced at: $\lambda_p/2$, ---- ; $\lambda_p/3$, ... ; $\lambda_p/4$ and $\lambda_p/5$, ____ .

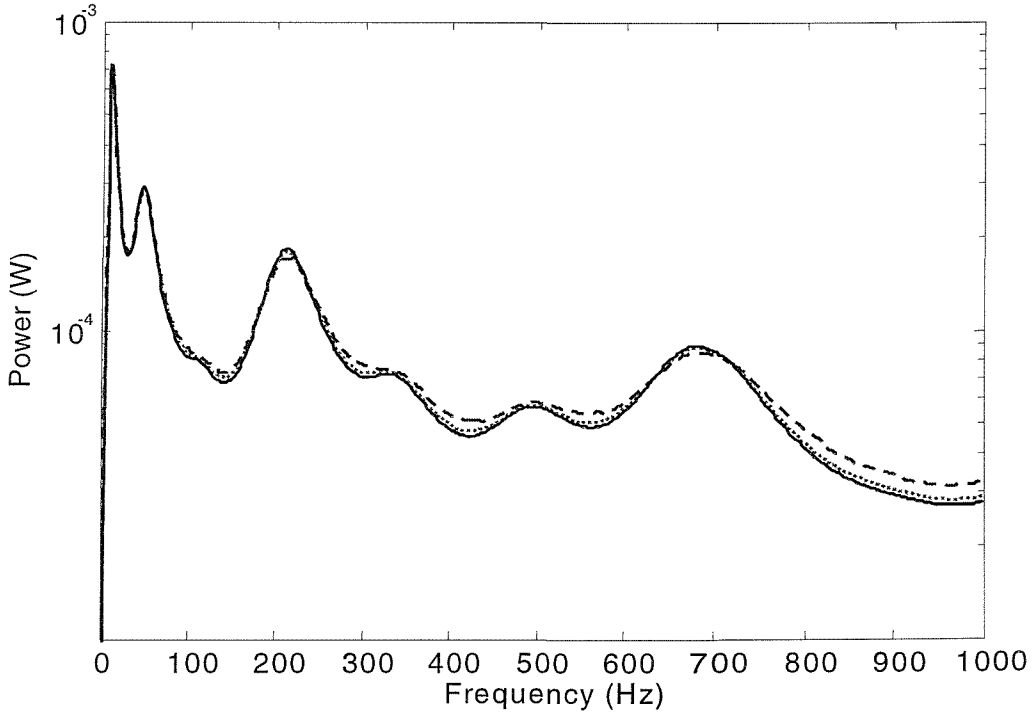

Figure 5.5 Power transmitted to the 0.010m plate when the discrete points spaced at: $\lambda_p/2$, ---- ; $\lambda_p/3$, ... ; $\lambda_p/4$ and $\lambda_p/5$, ____ .

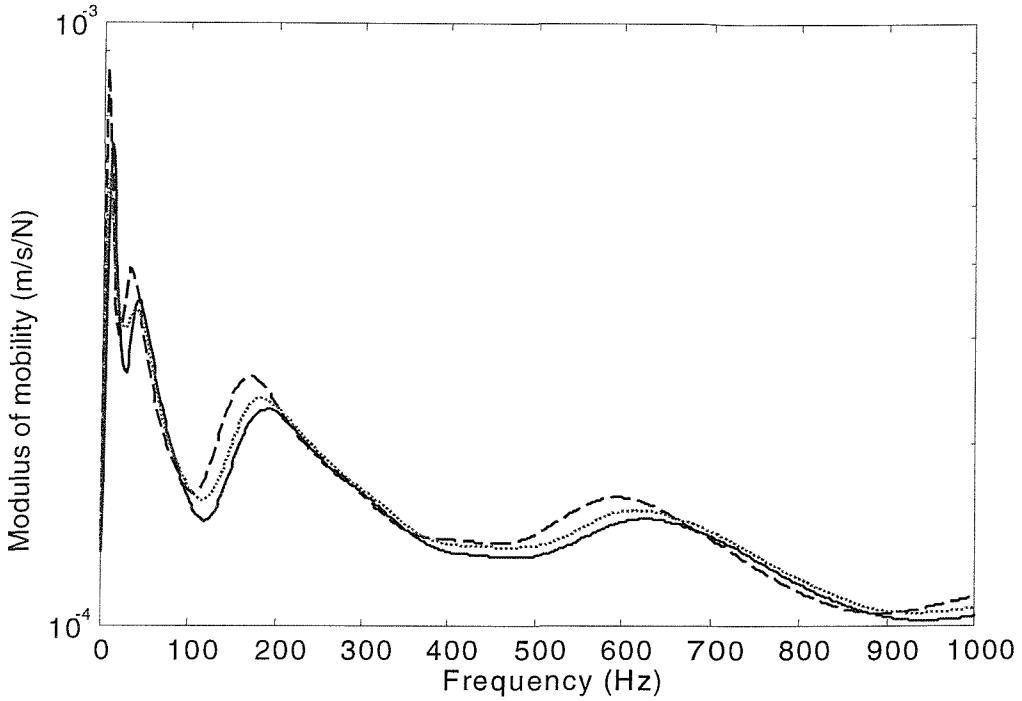

Figure 5.6 Point mobility of the beam at the driving point when the plate thickness is 0.020m ($k_p/k_b = 1.8$): exact, ——— ; Mode/FT, ... ; locally reacting, – – – .

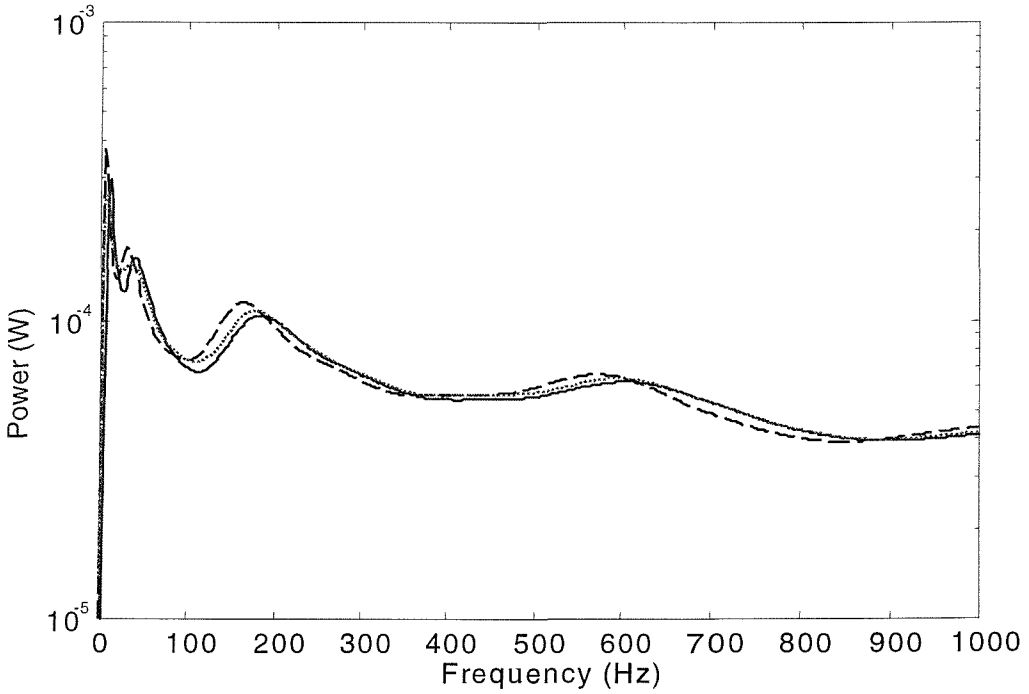

Figure 5.7 Power transmitted from the beam to the 0.020m thick plate ($k_p/k_b = 1.8$): exact, ——— ; Mode/FT, ... ; locally reacting, – – – – .

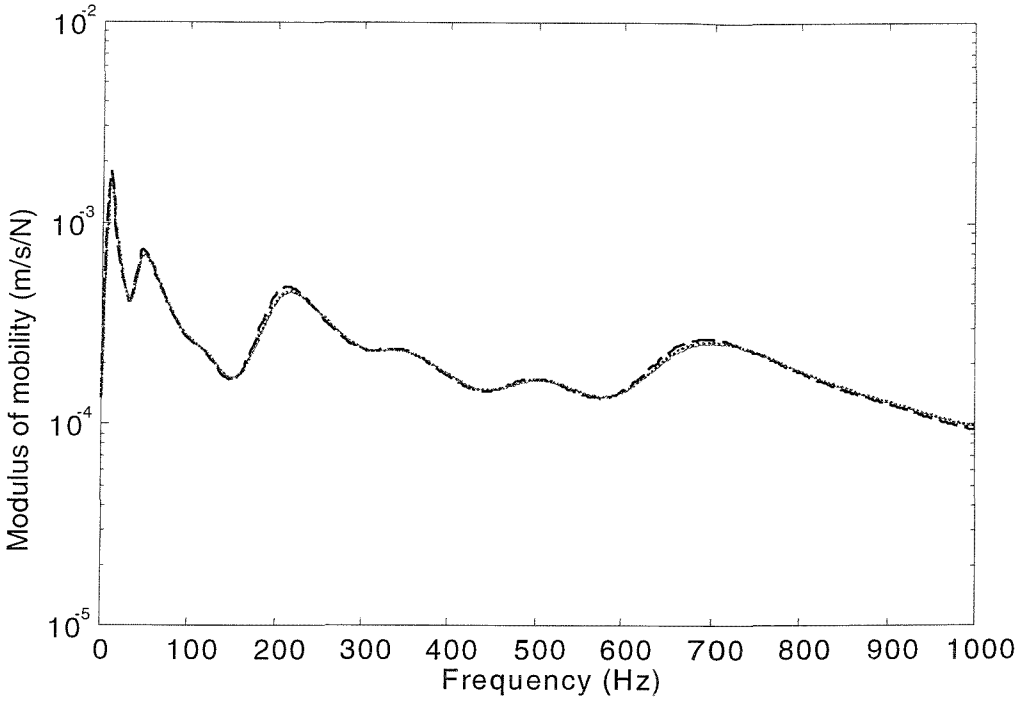

Figure 5.8 Point mobility of the beam at the driving point when the plate thickness is 0.010m ($k_p/k_b = 2.5$): exact, ——— ; Mode/FT, ... ; locally reacting, – – – .

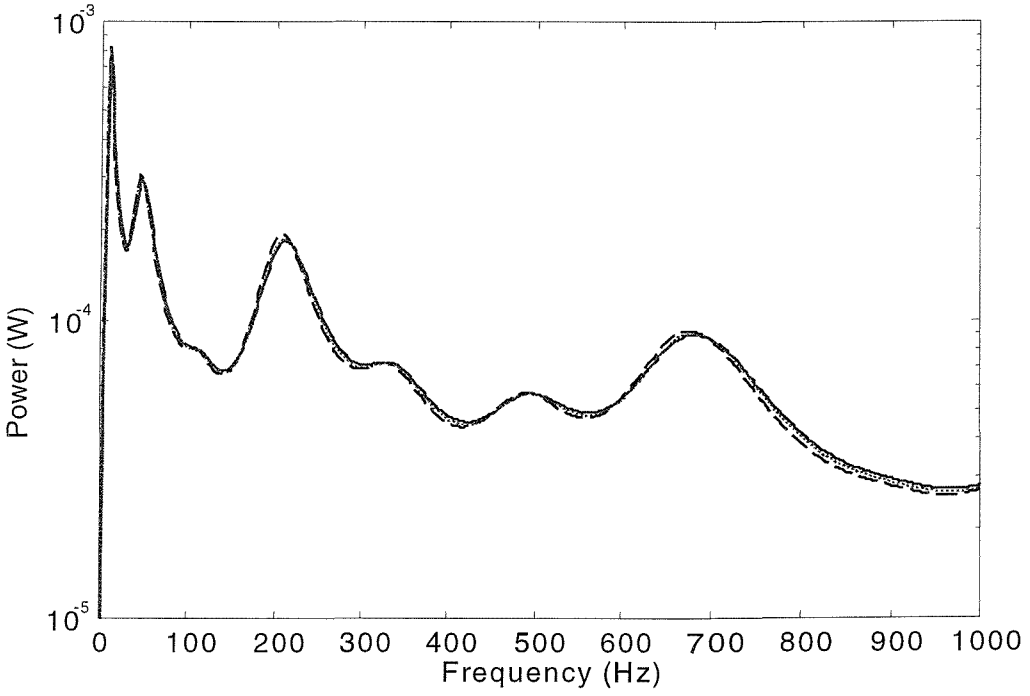

Figure 5.9 Power transmitted from the beam to the 0.010m thick plate ($k_p/k_b = 2.5$): exact, ——— ; Mode/FT, ... ; locally reacting, – – – – .

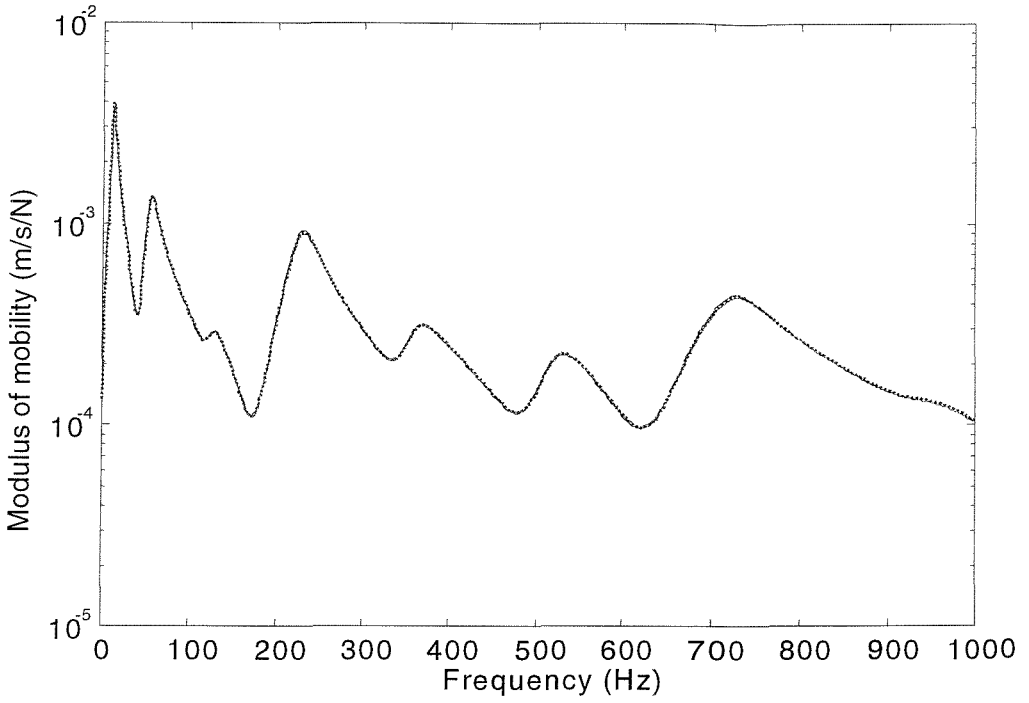

Figure 5.10 Point mobility of the beam at the driving point when the plate thickness is 0.005m ($k_p/k_b = 3.5$): exact, ——— ; Mode/FT, ... ; locally reacting, – – – .

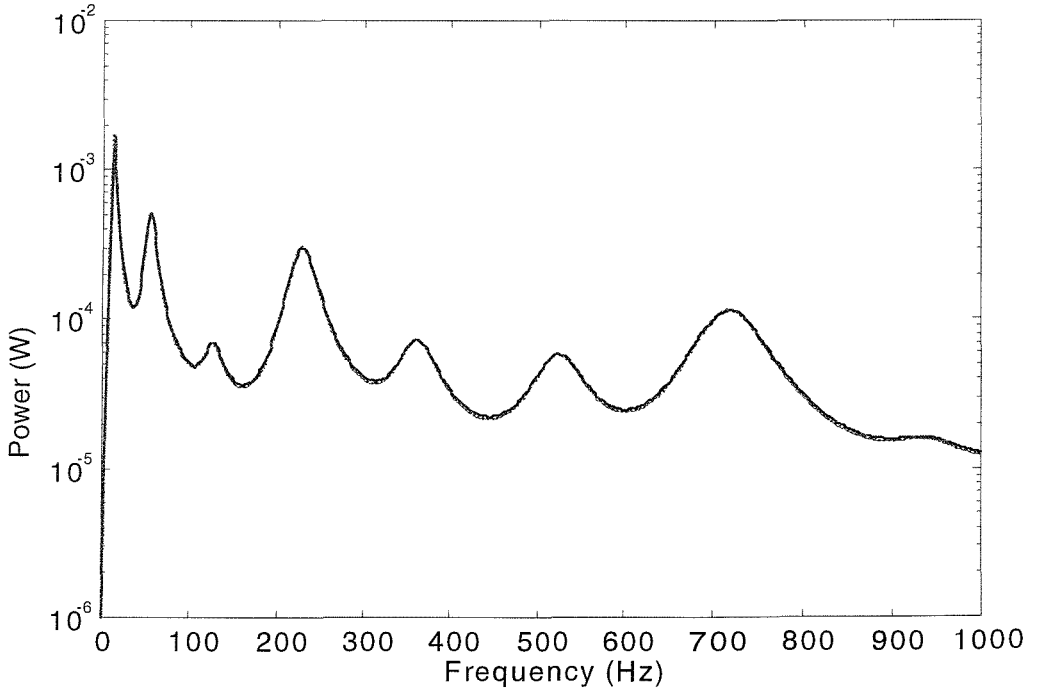

Figure 5.11 Power transmitted from the beam to the 0.005m thick plate ($k_p/k_b = 3.5$): exact, ——— ; Mode/FT, ... ; locally reacting, – – – – .

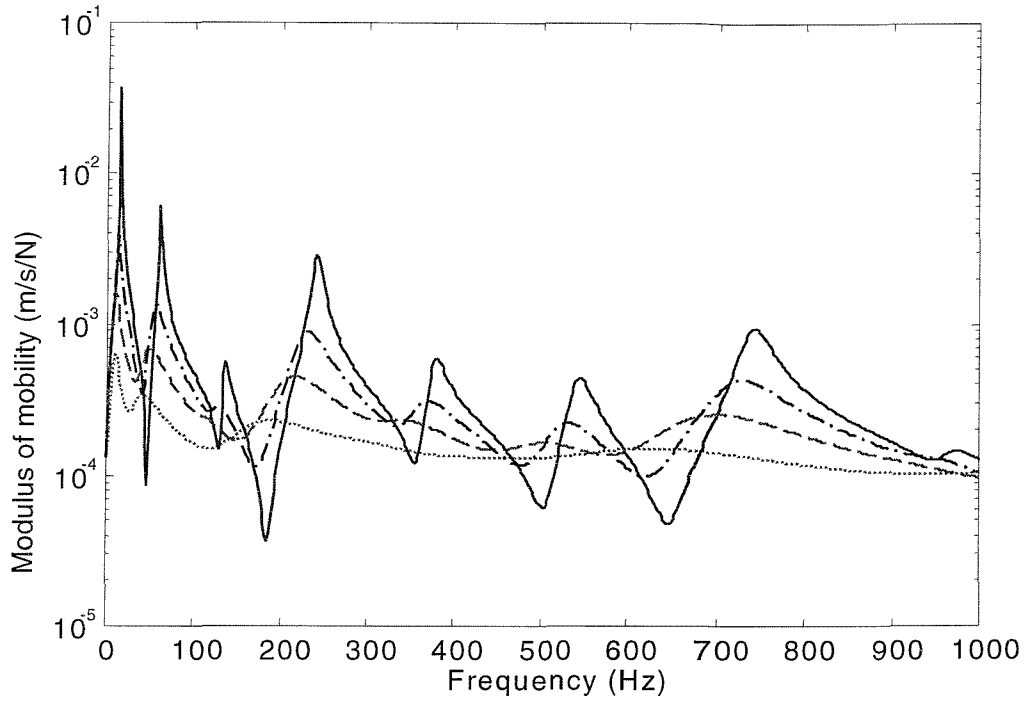

Figure 5.12 Point mobility of the beam at the driving point: before coupling to a plate (———); after coupling to a plate ($k_p/k_b = 1.8$, ... ; $k_p/k_b = 2.5$, – – – ; $k_p/k_b = 3.5$, –.–.–).

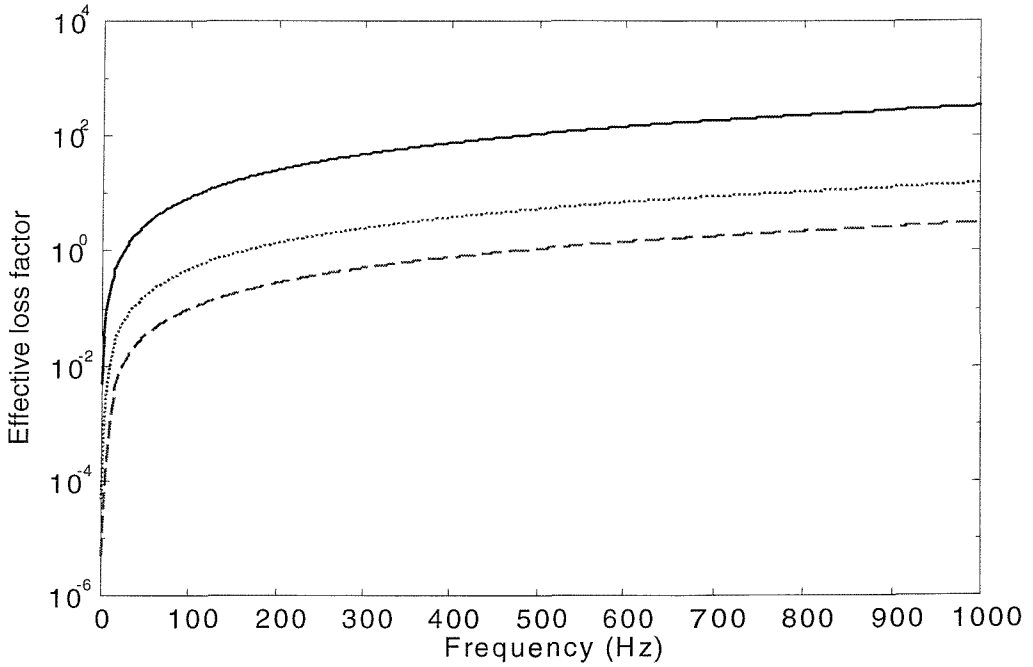

Figure 5.13 Effective loss factors induced to the first three modes of the beam when $k_p/k_b = 3.5$: 1st, ——— ; 2nd, ... ; 3rd, – – – .

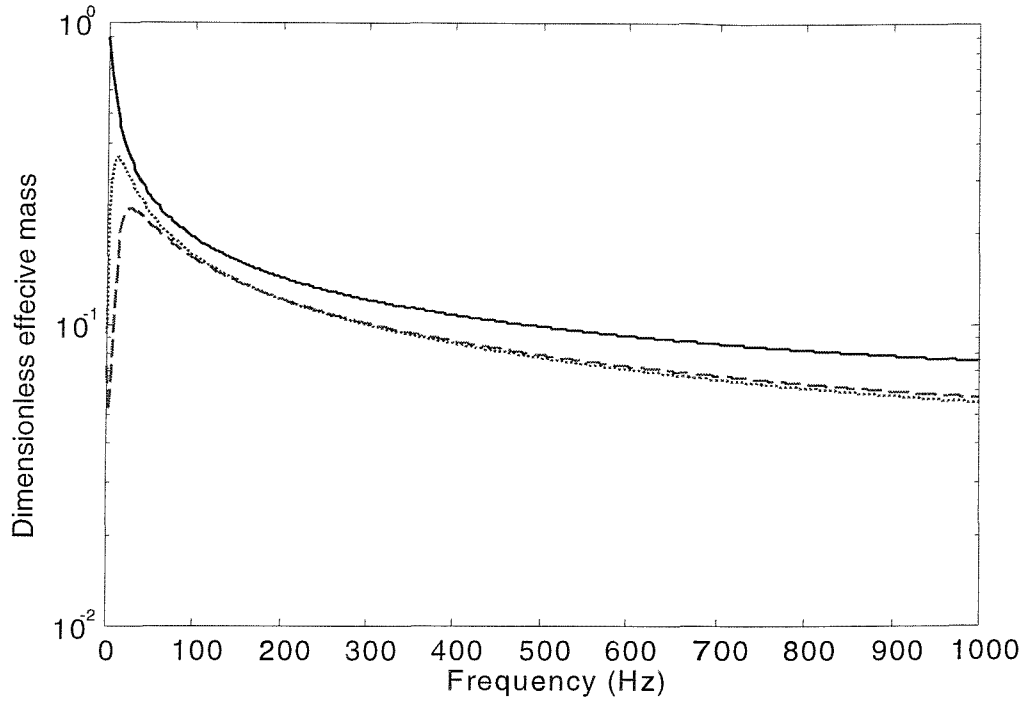

Figure 5.14 Dimensionless effective mass induced to the first three modes of the beam when $k_p/k_b = 3.5$: 1st, ____ ; 2nd, ... ; 3rd, ---- .

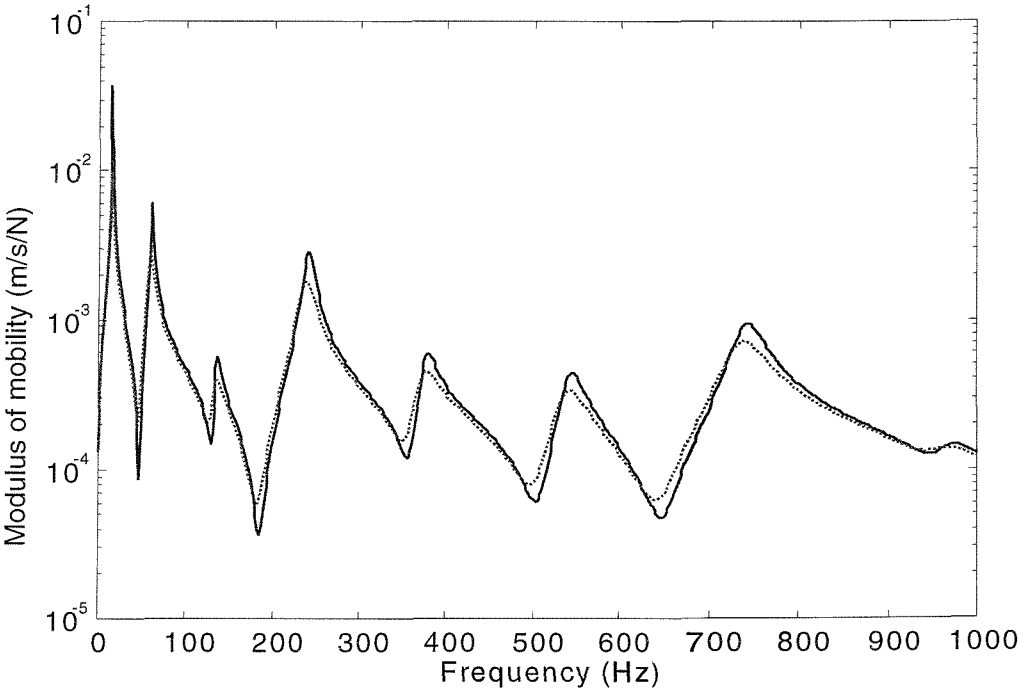

Figure 5.15 Point mobility of the beam at the driving point: before coupling, ——— ; after coupling ($k_p/k_b = 5.6$), ...

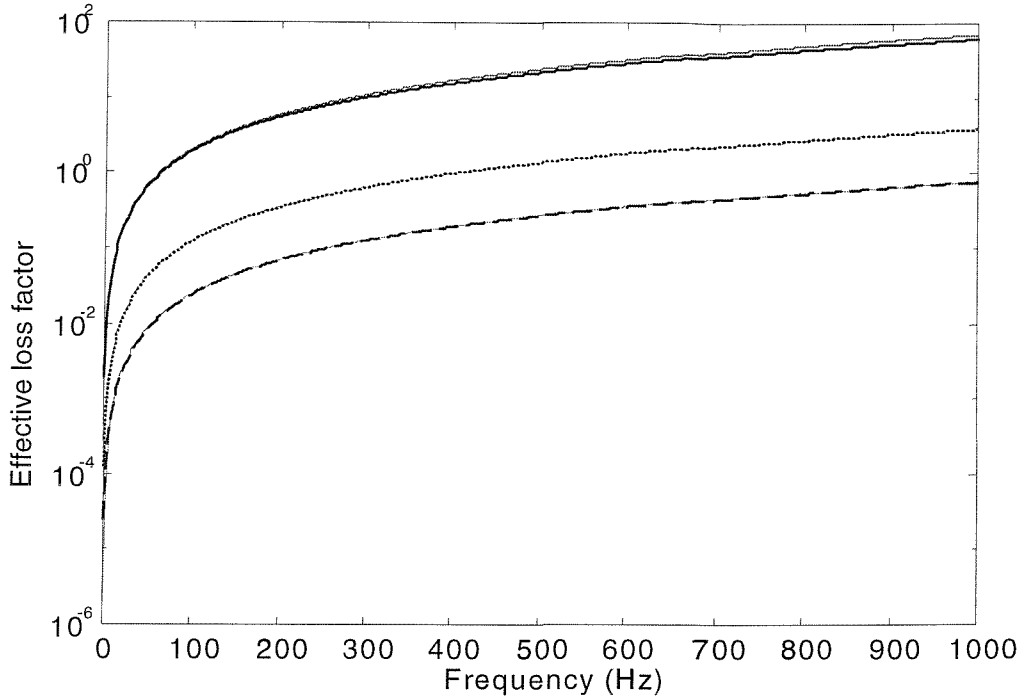

Figure 5.16 Effective loss factors induced to the first three modes of the beam ($k_p/k_b = 5.6$): 1st, ——— ; 2nd, ... ; 3rd, – – – ; by equation (5.50), ——— .

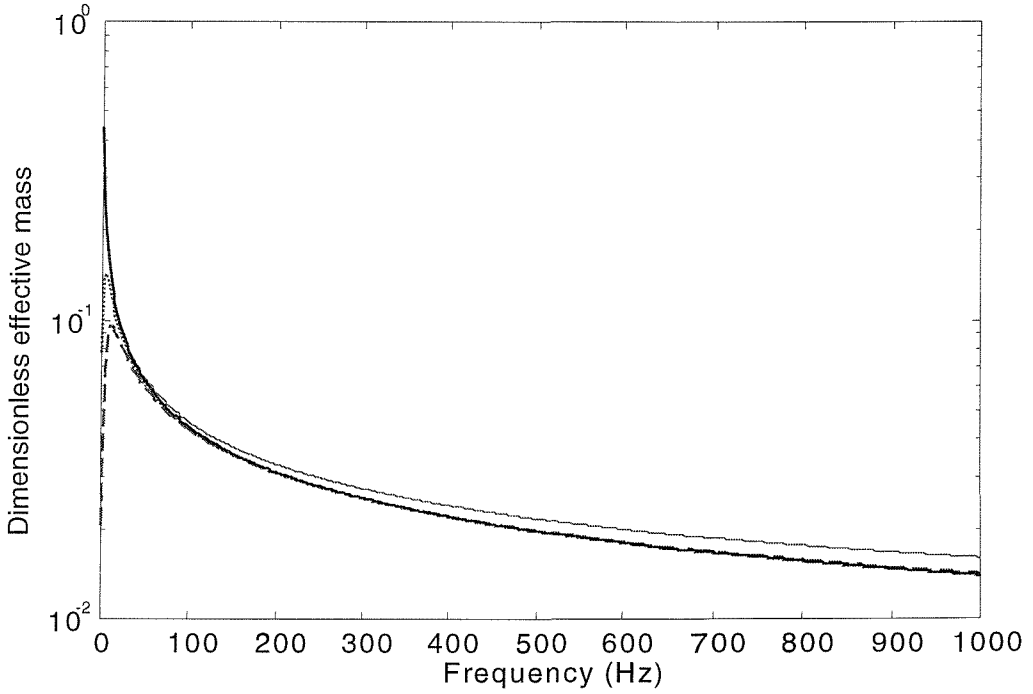

Figure 5.17 Dimensionless effective mass added to the first three modes of the beam ($k_p/k_b = 5.6$); 1st,——— ; 2nd, ...; 3rd, – – – ; by equation (5.49), ——— .

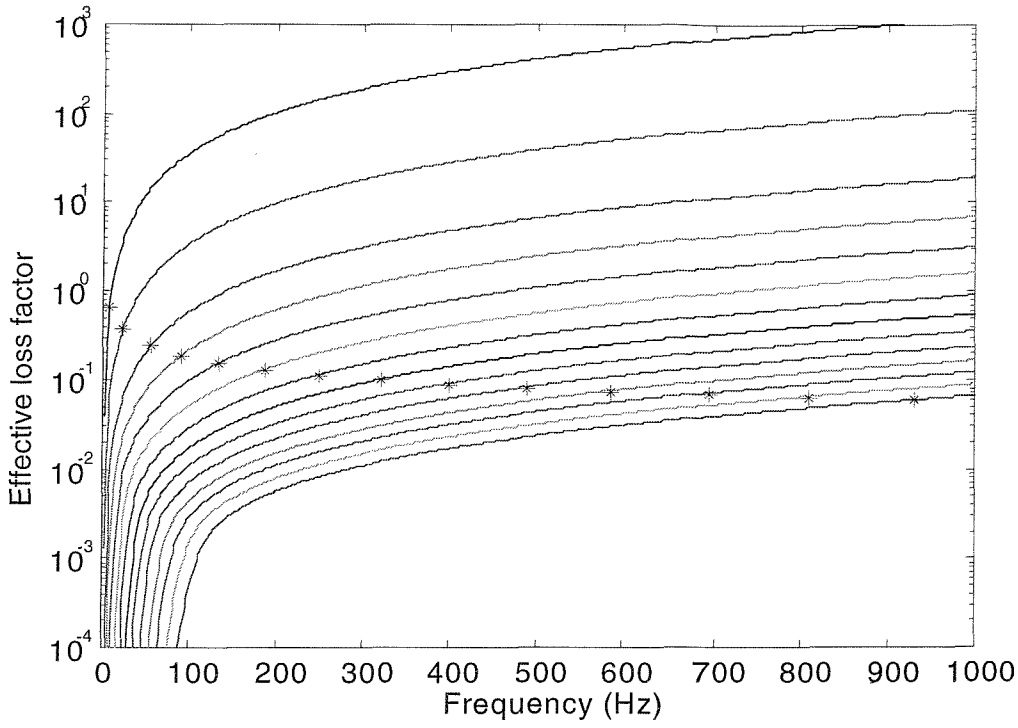

Figure 5.18 Effective loss factor induced to the first fourteen bending modes of the beam ($k_p/k_b = 5.6$): by equation (5.50), _____ (curves from upper to lower corresponding to the effective values added to the 1st to 14th modes of the beam, respectively); by $(m_p/m_b)(\lambda_p/\pi)$ at the beam resonances $\omega \approx \omega_{b,n}$, *.

Chapter 6

VIBRATION OF A FINITE BEAM ATTACHED TO A FINITE PLATE WITH THE SAME MODE SHAPES ALONG THE COUPLING LINE

6.1 INTRODUCTION

In the Mode/FT approach, one key point is to decompose the interface forces/displacements between the beam and the plate in terms of the uncoupled natural modes of the beam. The force equilibrium and displacement compatibility can then be enforced at the interface region to provide the coupling relations between the beam modes and plate wave motions in a quite simple manner, due to the orthogonal properties of these mode shape functions. Similar approaches are therefore expected to extend to beam/plate coupling cases, where a finite beam is attached to a finite plate. For simplicity, a special case of a finite beam attached to a finite plate is considered in this chapter, where the beam and the plate are assumed to have the same mode shapes along the coupling line, as shown in Figure 6.1. The beam is attached to the rectangular plate parallel to one pair of the opposite edges of the plate. The boundary conditions of the beam and of the plate (normal to the coupling) are assumed to be the same and also the plate boundary conditions are assumed allow the plate modes be written using separation of variables. In this case, the analytical expressions for the FRFs of the beam and the transmitted power to the plate can be determined very simply by the conventional modal analysis method. The derivation procedure is given below.

This chapter provides an analytical methodology for the development of a so-called 'mode-based' approach to deal with the vibration of a general complex built-up structure, which will be described in Part III.

6.2 MODAL ANALYSIS OF THE BEAM AND THE PLATE COMPONENTS

The source beam and the receiver plate are separately illustrated as Figures 6.2 and 6.3, respectively, where $F_0\delta(x-\xi)$ is the external force acting on the beam at point $x=\xi$, $w_b(x)$ and $w_p(x)\delta(y-y_0)$ are the displacements of the beam and the plate, respectively,

occurring along the interface line, and $f_b(x)$ and $f_p(x)\delta(y-y_0)$ are the interface force applied to the beam and the plate, respectively.

By modal analysis theory [11], the displacement of the beam can then be defined as

$$w_b(x)=F_0\sum_n b_n\phi_n(x)\phi_n(\xi)+\sum_n b_n\phi_n(x)\int_0^{L_b} f_b(x_0)\phi_n(x_0)dx_0 \tag{6.1}$$

where L_b is the length of the beam and $\phi_n(x)$ is the nth normalized mode shape of the beam so that

$$\int_0^{L_b}\phi_n(x)\phi_{n'}(x)dx=\begin{cases}1, n=n'\\0, n\neq n'\end{cases} \tag{6.2}$$

b_n here is the nth modal receptance of the beam (i.e. modal displacement per unit modal force)

$$b_n=\frac{1}{m_b}\frac{1}{\omega_n^{(b)^2}\left(1+j\eta_n^{(b)}\right)-\omega^2} \tag{6.3}$$

where m_b, $\omega_n^{(b)}$ and $\eta_n^{(b)}$ are, respectively, the mass per unit length, the nth natural frequency, and corresponding loss factor of the beam.

Similarly the displacement of the plate along the coupling region $y=y_0$ can be determined by

$$w_p(x)\delta(y-y_0)=\sum_m p_m\varphi_m(x,y_0)\int_{L_x}\int_{L_y} f_p(x)\delta(y-y_0)\varphi_m(x,y)dxdy \tag{6.4}$$

where $L_x=L_b$ and L_y correspond to the lengths of the plate along and normal to the coupling direction, and $\varphi_m(x,y)$ is the mth normalized mode shape of the plate so that

$$\int_0^{L_y}\int_0^{L_x}\varphi_m(x,y)\varphi_{m'}(x,y)dxdy=\begin{cases}1, m=m'\\0, m\neq m'\end{cases} \tag{6.5}$$

p_m is the mth modal receptance of the plate, given as

$$p_m=\frac{1}{m_p}\frac{1}{\omega_m^{(p)^2}\left(1+j\eta_m^{(p)}\right)-\omega^2} \tag{6.6}$$

where m_p, $\omega_m^{(p)}$ and $\eta_m^{(p)}$ are, respectively, the mass density, the mth natural frequency, and corresponding loss factor of the plate. Here, it is assumed that $\varphi_m(x,y)$ can be separated into the form

$$\varphi_m(x,y)=\psi_k(x)\chi_r(y) \tag{6.7}$$

where $\psi_k(x)$ and $\chi_r(y)$ are the kth and rth normalized mode shape functions of the plate along the x- and y- directions, respectively, i.e.,

$$\int_0^{L_x}\psi_k(x)\psi_{k'}(x)dx=\begin{cases}1, k=k'\\0, k\neq k'\end{cases} \tag{6.8}$$

$$\int_0^{L_y}\chi_r(y)\chi_{r'}(y)dy=\begin{cases}1, r=r'\\0, r\neq r'\end{cases} \tag{6.9}$$

Since in the case of Figure 6.1, the beam and the plate mode shapes have the same spatial variation along the coupling line, i.e.,

$$\phi_n(x)=\psi_n(x) \tag{6.10}$$

Substituting equation (6.10) into (6.7) and then into (6.4), gives

$$w_p(x)\delta(y-y_0)=\sum_k\sum_r p_{k,r}\phi_k(x)\chi(y_0)\int_{L_x} f_p(x)\phi_k(x)\chi(y_0)dx \tag{6.11}$$

where

$$p_{k,r}=\frac{1}{m_p}\frac{1}{\omega_{k,r}^{(p)2}\left(1+j\eta_{k,r}^{(p)}\right)-\omega^2} \tag{6.12}$$

Equation (6.11) can then be re-written in the form

$$w_p(x)\delta(y-y_0)=\sum_k q_k\phi_k(x)\int_0^{L_x} f_p(x_0)\phi_k(x_0)dx_0 \tag{6.13}$$

where

$$q_k=\frac{1}{m_p}\sum_r\frac{\chi_r^2(y_0)}{\omega_{k,r}^{(p)2}\left(1+j\eta_{k,r}^{(p)}\right)-\omega^2} \tag{6.14}$$

Physically, q_k is the kth modal receptance of the plate along $y=y_0$, which depends on m_p, $\omega_{k,r}^{(p)}$ and $\chi_r(y)$.

6.3 DYNAMIC RESPONSE OF THE BEAM/PLATE SYSTEM

The force equilibrium and displacement compatibility at the interface yield the relations

$$f_p(x)\delta(y-y_0)=-f_b(x)=f(x) \tag{6.15}$$

$$w_p(x)\delta(y-y_0)=w_b(x)=w(x) \tag{6.16}$$

Decompose $f(x)$ and $w(x)$ into the form

$$f(x)=\sum_n f_n\phi_n(x) \tag{6.17}$$

$$w(x)=\sum_n w_n\phi_n(x) \tag{6.18}$$

Substituting equations (6.15)-(6.18) into (6.1), respectively, yields

$$\sum_n w_n\phi_n(x)=\sum_n b_n f_n^{(\xi)}\phi_n(x)-\sum_n f_n b_n\phi_n(x) \tag{6.19}$$

where $f_n^{(\xi)}$ is the corresponding modal force, caused by the external force F_0, given by

$$f_n^{(\xi)}=F_0\phi_n(\xi) \tag{6.20}$$

Similarly, substituting equations (6.15)-(6.18) into (6.13), gives

$$\sum_n w_n\phi_n(x)=\sum_n q_n\phi_n(x)f_n \tag{6.21}$$

Multiplying both sides of equations (6.19) and (6.21) by $\phi_n(x)$ and integrating along the beam length, gives

$$w_n=b_n f_n^{(\xi)}-b_n f_n \tag{6.22}$$

$$w_n=q_n f_n \tag{6.23}$$

Equations (6.22) and (6.23) yield

$$f_n=\frac{b_n}{b_n+q_n}f_n^{(\xi)} \tag{6.24}$$

$$w_n=\frac{b_n}{1+b_n/q_n}f_n^{(\xi)} \tag{6.25}$$

The power transmitted to the plate from the beam can then be expressed as

$$P=\frac{1}{2}\mathrm{Re}\left\{\sum_n \int_0^{L_b}\left[f_n\phi_n(x)\right]^* j\omega\left[w_n\phi_n(x)\right]dx\right\}=\frac{1}{2}\mathrm{Re}\left\{j\omega\sum_n f_n^* w_n\right\} \tag{6.26}$$

Substituting equations (6.24) and (6.25) into (6.26), it gives

$$P=\frac{\omega}{2}\sum_n\left|\frac{b_n}{b_n+q_n}f_n^{(\xi)}\right|^2\mathrm{Im}\{q_n^*\} \tag{6.27}$$

where $\mathrm{Im}\{q_n^*\}$ can be given from equation (6.14) as

$$\mathrm{Im}\{q_n^*\}=\frac{1}{m_p}\sum_r\frac{\chi_r^2(y_0)\omega_{n,r}^{(p)2}\eta_{n,r}^{(p)}}{\left(\omega_{n,r}^{(p)2}-\omega^2\right)^2+\left(\omega_{n,r}^{(p)2}\eta_{n,r}^{(p)}\right)^2} \tag{6.28}$$

Equation (6.27) shows that the power can be taken as transmitted from each beam mode independently, and each mode corresponds to an interface-impedance which is determined by the summation of the modal impedances of the beam and the plate along the coupling line.

So far, analytical solutions for both the FRFs of the beam and the power transmitted to plate have been given, based on conventional modal analysis theory.

Equations (6.24) and (6.25) imply that when the beam and the plate have the same mode shapes along the coupling line, each individual beam mode $\phi_n(x)$ is coupled to only one set of plate modes $\phi_n(x)\chi_r(y_0)$, $r=1,2,3,\ldots$, so that the equations of motion of the beam and the plate for each n can actually be taken as uncoupled with each other. If that is not the case, however, each beam mode will couple to all sets of the plate modes, and the coupling situations will be very complicated. Therefore, Figure 6.1 can actually be regarded as a simplest coupling situation between a finite beam and a finite plate.

6.4 THE INTERACTIONS BETWEEN THE BEAM AND THE PLATE

Equations (6.24) and (6.25) show the coupling relation between the 'uncoupled' modes of the beam and the plate.

When the uncoupled beam has a modal receptance b_n of equation (6.3), it is changed, after coupling with the plate, to be

$$b_n'=\frac{b_n}{1+b_n/q_n} \tag{6.29}$$

Let equation (6.29) be re-expressed as

$$b_n' = \frac{1}{m_b \omega_n^{(b)2}\left(1+j\eta_n^{(b)}\right) - m_b\omega^2 + D_n} \tag{6.30}$$

where

$$D_n = \frac{1}{q_n} \tag{6.31}$$

Physically, D_n represents how the n th modal dynamic stiffness of the beam is affected by the presence of the plate modes. By writing equation (6.31) into a form

$$D_n = -D_{n1} + jD_{n2} \tag{6.32}$$

equation (6.30) can be re-expressed as

$$b_n' = \frac{1}{m_b \omega_n^{(b)2}\left[1+j\left(\eta_n^{(b)}+\eta_n'\right)\right] - \left(m_b + m_n'\right)\omega^2} \tag{6.33}$$

where

$$\eta_n' = \frac{D_{n2}}{m_b \omega_n^{(b)2}} \tag{6.34}$$

$$m_n' = \frac{D_{n1}}{\omega^2} \tag{6.35}$$

Therefore, the interaction effects by loading the plate to a stiff beam can be equivalently simulated as adding an effective loss factor (equation (6.34)) and effective mass (equation (6.35)) to each mode of the beam.

By the relations of equations (6.14), (6.31) and (6.32), this gives

$$D_{n1} = \frac{p_{n1}}{p_{n1}^2 + p_{n2}^2} \tag{6.36}$$

$$D_{n2} = \frac{p_{n2}}{p_{n1}^2 + p_{n2}^2} \tag{6.37}$$

where

$$p_{n1} = \frac{1}{m_p}\sum_r \frac{\chi_r^2(y_0)\left(\omega^2 - \omega_{n,r}^{(p)^2}\right)}{\left(\omega_{n,r}^{(p)^2} - \omega^2\right)^2 + \left(\omega_{n,r}^{(p)^2}\eta_{n,r}^{(p)}\right)^2} \tag{6.38}$$

$$p_{n2} = \frac{1}{m_p} \sum_r \frac{\chi_r^2(y_0)\omega_{n,r}^{(p)2}\eta_{n,r}^{(p)}}{\left(\omega_{n,r}^{(p)2} - \omega^2\right)^2 + \left(\omega_{n,r}^{(p)2}\eta_{n,r}^{(p)}\right)^2} \tag{6.39}$$

6.5 NUMERICAL EXAMPLES

In this section, numerical examples, as shown in Figure 6.1, are presented to demonstrate the accuracy and efficiency of this analytical approach. The same perspex material is used as in the numerical model as that in previous chapters, properties being given in Table 2.1. An external force excitation of magnitude of 1 is applied to the beam at a point $\xi = 0.73\text{m}$. System dimensions and coupling positions are listed in Table 6.1. Both the beam and the plate considered are simply supported.

6.5.1 The point mobility of the beam and the power transmitted to the plate

The analytical solutions for the dynamic response of the coupled beam and the power transmitted can be determined by equations (6.24), (6.25) and (6.26). In this subsection, these analytical results are compared to the numerical results of the conventional FRF-based sub-structuring method, where the line coupling is modelled by many discrete point couplings spaced at a quarter of the plate wavelength, as described in section 5.4.1.

Figures 6.4-6.7 compare the analytical and numerical results for the input mobility of the beam and the power transmitted to the plate, where the plate thicknesses are 0.010m and 0.005m, respectively. It is seen that the analytical and numerical results are almost exactly the same for both cases, but the computational cost of the former is much lower than that of the latter. When the plate thickness is 0.005m, for example, the computing time of the former is only about one twentieth of that of the latter. The reason is that the analytical approach can transfer a large number of physical DOFs into a small number of generalized DOFs by decomposing the interface force and displacement into a set of components of beam modes. At the same time it avoids having to calculate a matrix inversion, which is usually prohibitive when the matrix size is large. But this analytical approach has a significant limitation that the beam and the attached plate should have the same mode shapes along the coupling line.

6.5.2 Effective loss factor and effective mass

In section 6.4, the interactions between the beam and the plate were simulated as an effective loss factor and an effective mass induced to each individual mode of the beam

arising from the presence of the plate modes, as described in equations (6.34) and (6.35). Figures 6.8-6.9 then show the effective loss factor and effective mass added to the first three modes of the beam, respectively, where the attached plate thickness is 0.005m. Note that in Figure 6.9, a dimensionless mass is used, being m_n'/m_b. It is seen that more significant couplings occur to lower order modes of the beam than to the higher order ones. And also the effective loss factor of a given mode increases as frequency increases, while the effective mass decreases against frequency. These observations are quite similar to those found for a finite beam attached to an infinite plate in Chapter 5. The peak values of the effective loss factor are found to occur at the frequencies where D_{n2} tends to be maximum, which are related to the anti-resonance frequencies of the plate only but regardless of those of the beam. Physically, the plate can absorb more energy from the beam at these frequencies. Note that these peak frequencies are not necessarily the exact anti-resonance frequencies of the plate.

Figures 6.8-6.9 also give the effective loss factor and effective mass when the plate is extended uniformly to infinity, by the expressions given in Chapter 5. It is seen that the frequency-averaged effective damping and mass can be simply approximated by assuming the plate receiver as infinite.

6.6 SUMMARY

For a beam/plate coupled system, as shown in Figure 6.1, where the beam and the plate have the same mode shapes along the coupling line, an analytical solution for the vibration response of the system was given based on modal analysis theory. The advantage of this analytical approach is that a large number of physical DOFs at the interfaces can be reduced to a small number of generalized DOFs, by simply decomposing the interface force and displacement distributions into components of beam modes. As a result, this analytical approach was found much more efficient than the conventional FRF-based sub-structuring method, especially when the plate receiver has very short wavelengths.

Moreover, the interaction effects between the beam and the plate were simulated as the effective loss factor and effective mass induced to each individual mode of the beam arising from the presence of the plate modes. It was found that the lower the orders of the beam modes are, the bigger the induced loss factor and effective mass are. Also the effective damping in a given mode increases as frequency increases but the effective mass decreases. These are in good agreement with the results of a finite beam attached to an infinite plate described in Chapter 5.

Although this chapter concerns only the simplest coupling form of a finite beam attached to a finite plate, it helps to shed new light on developing a methodology to simplify the vibration predictions of general continuous couplings between a stiff source and a flexible receiver. This is the so-called 'mode-based' approach, which will be given in the next Chapter.

Table 6.1 System dimensions and coupling positions

Structure	Beam	Plate
Dimensions (m)	Length=2; Width=0.059; Height=0.068	Length=2; Width=0.9; Thickness=0.010/0.005
Coupling position (m)	$y_0 = 0.45$	
Wavenumber ratio	$k_p/k_b = 2.5,\ 3.5$	

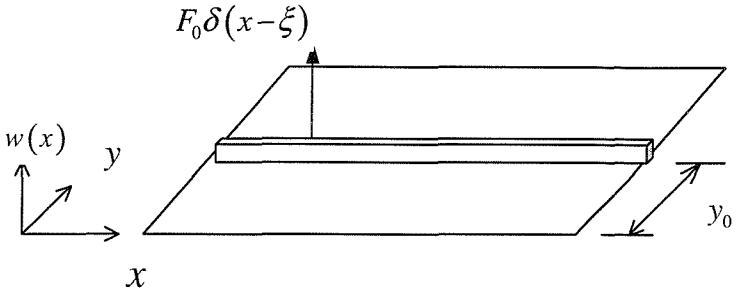

Figure 6.1 Line-coupled beam-plate system.

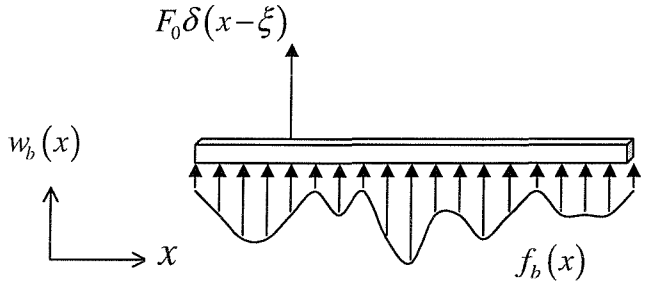

Figure 6.2 Dynamic illustration of the source beam.

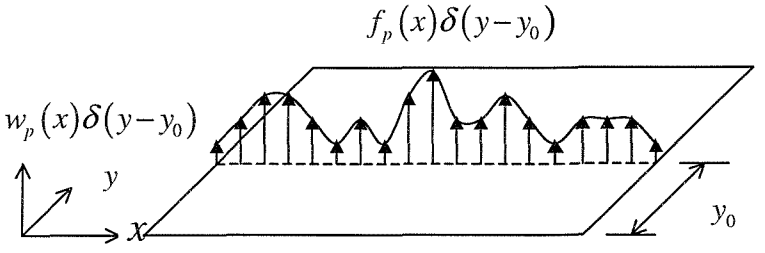

Figure 6.3 Dynamic illustration of the receiver plate.

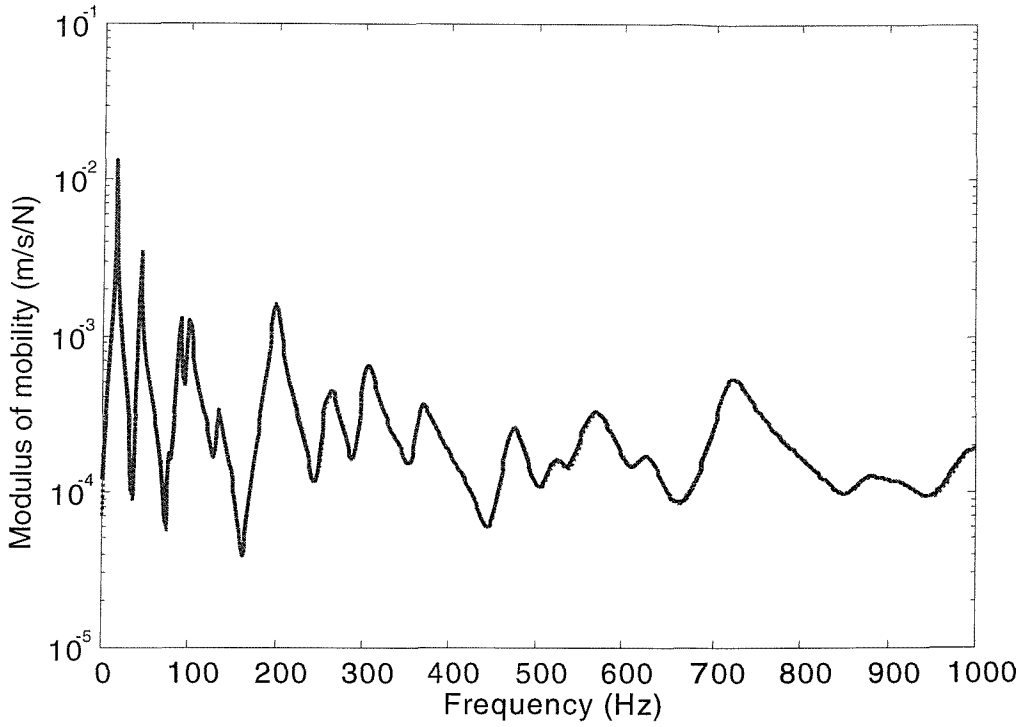

Figure 6.4 Point mobility of the beam at the excitation point when the plate thickness is 0.010m: numerical result, _____ ; analytical result, ...

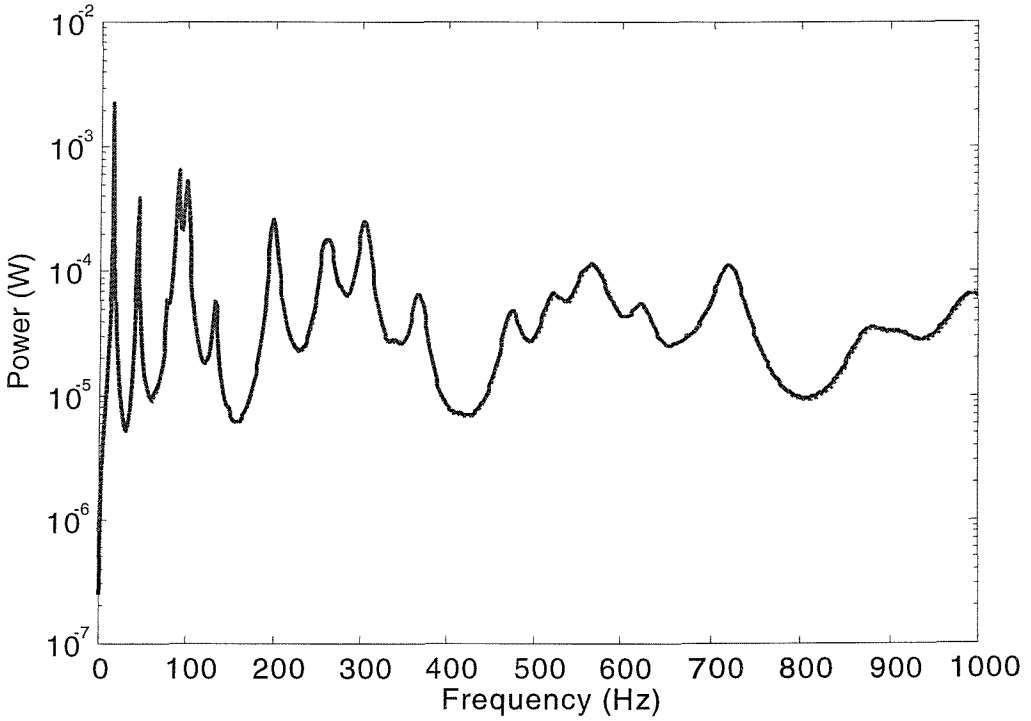

Figure 6.5 Power transmitted to the plate when the plate thickness is 0.010m: numerical result, _____ ; analytical result, ...

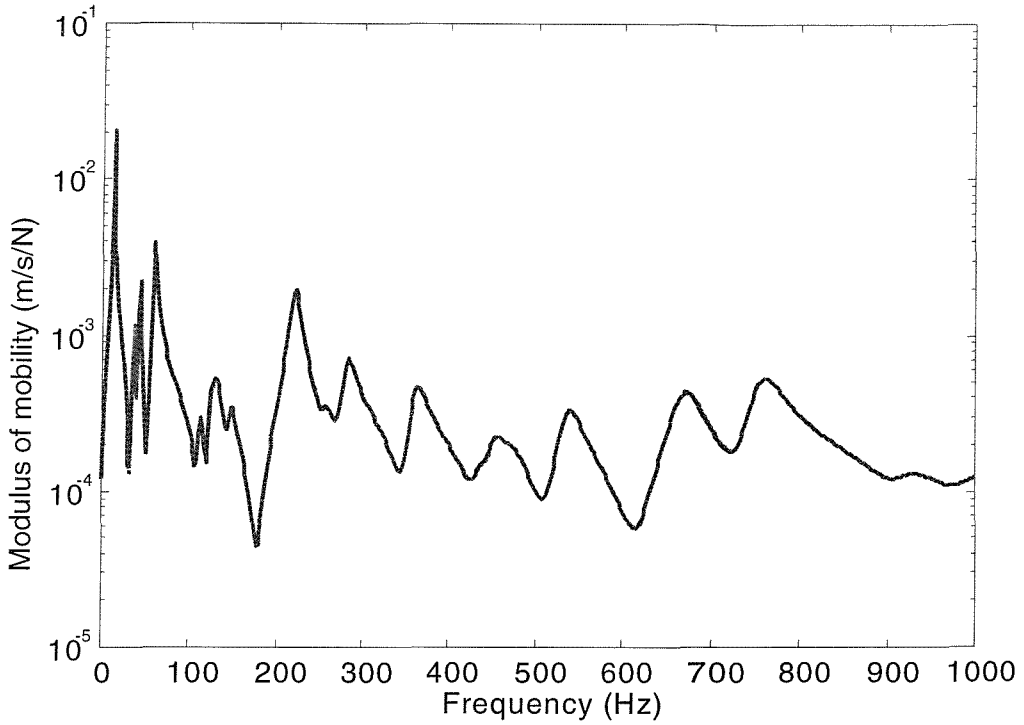

Figure 6.6 Point mobility of the beam at the excitation point when the plate thickness is 0.005m: numerical result, _____ ; analytical result, ...

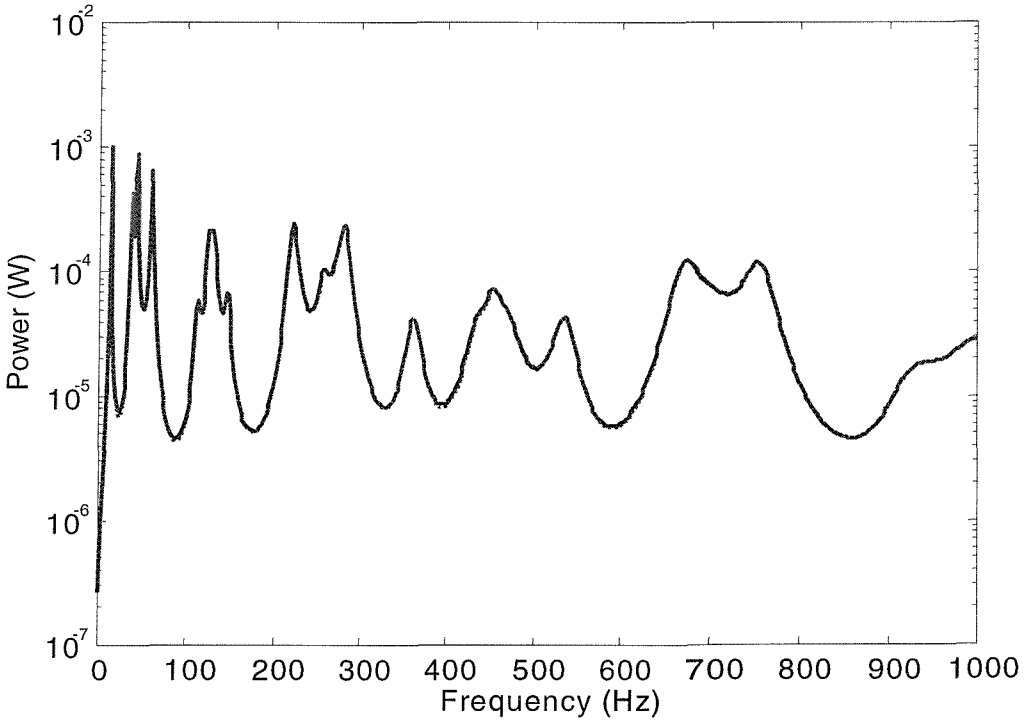

Figure 6.7 Power transmitted to the plate when the plate thickness is 0.005m: numerical result, _____ ; analytical result, ...

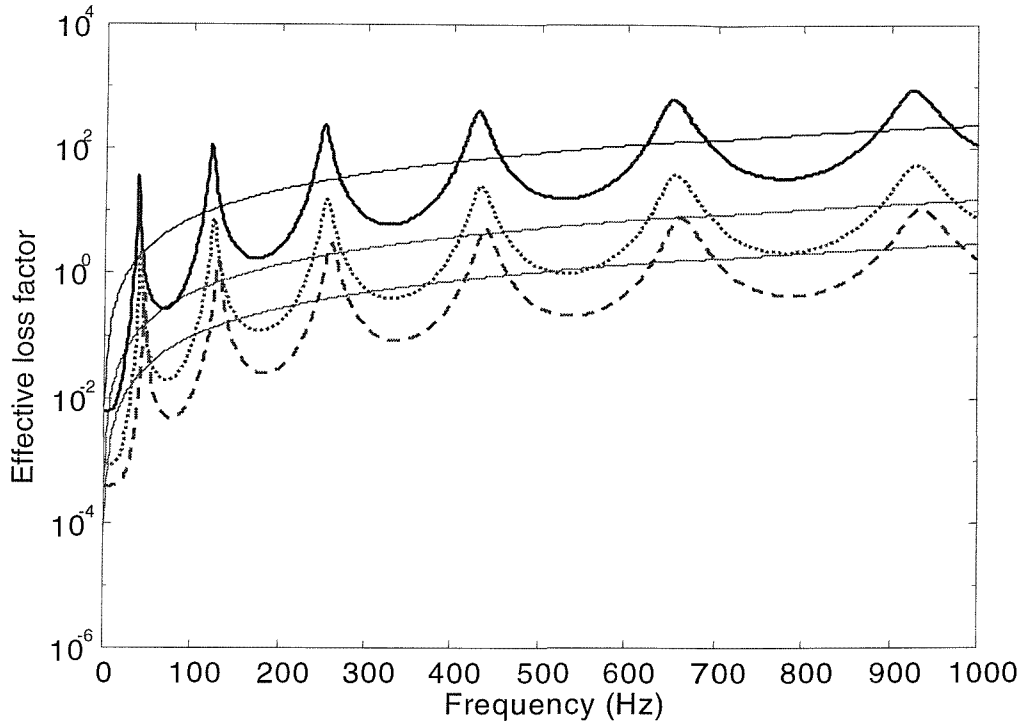

Figure 6.8 Effective loss factor induced to the first three modes of the beam when the plate is 0.005m: first, ____ ; second, ... ; third, - - - - ; results when the plate is infinite, ——— .

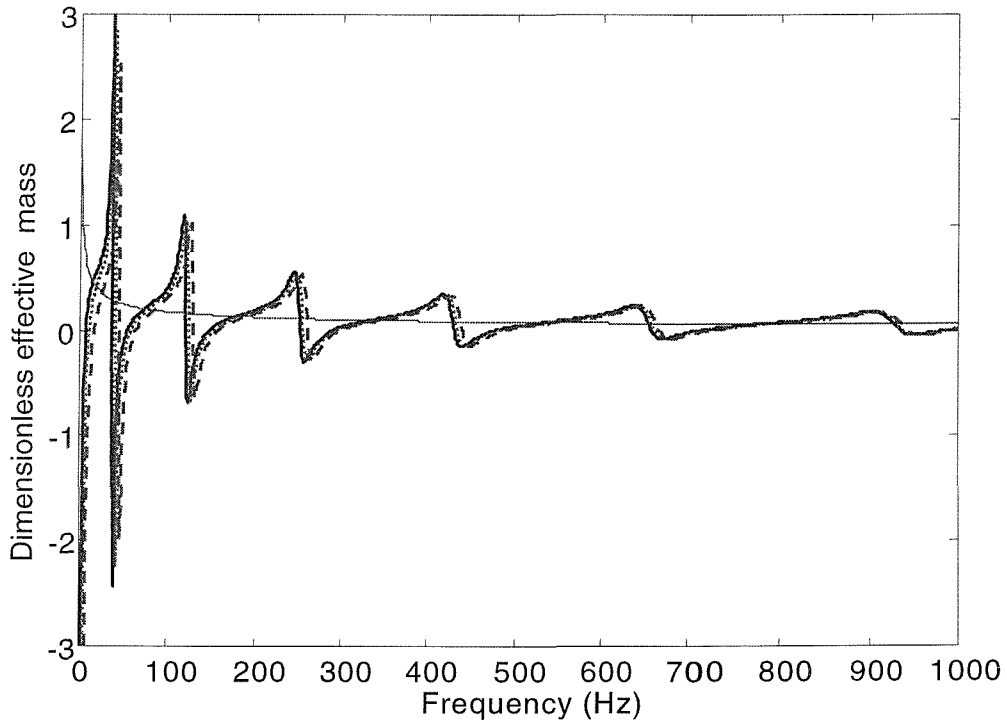

Figure 6.9 Dimensionless effective mass induced to the first three modes of the beam when the plate is 0.005m: first, ——— ; second, ... ; third, - - - - ; results when the plate is infinite, ____ .

Part III

GENERAL CONTINUOUS COUPLINGS: MODE-BASED APPROACH

Concerning the difficulty arising from limitations of the low-frequency finite element (FE) and high-frequency statistical (SEA) modelling methods in the so-called 'mid-frequency' range, a number of methods, being either conventional (Fourier Transform and wave analysis methods) or newly developed (Mode/FT approach, locally reacting impedance method, and mode-based analytical approach), have been used in Part II to deal with the vibration of a plate-stiffened beam system. However, these approaches only involve special cases of beam-stiffened plates so that certain significant simplifications can be made as appropriate. More general approaches are required for the vibration analysis of common complex built-up structures. In principle these structures can be viewed as constructed from many substructures with quite different dynamic properties, due to the differences in material and sectional properties, for example.

This part of the research is directed at developing a new technique to deal with the vibration of such a complex built-up system as a long-wavelength source coupled to a short-wavelength receiver through general continuous interfaces. It is proposed to meet the following two purposes: first, it can substantially reduce the system degrees of freedom (DOFs) so as to ameliorate significantly the relevant computational cost issue; and secondly, it has the ability to couple subsystems of different form, e.g. with big dynamic mismatch, within the same system model.

Based on the methodologies provided in Part II, a so-called 'mode-based approach' is developed in Chapter 7. It can and does meet the above two purposes: the system DOFs can be reduced by transferring the physical DOFs into generalized interface DOFs; and different subsystems may be modelled by different appropriate techniques for coupling, the choice being determined by the local dynamic properties of the individual subsystem of interest. The emphasis is put on predicting the frequency response functions (FRFs) of the stiff source and the coupling energy flow to the flexible receiver. Furthermore, the modal correlation between the source and the receiver, and hence the effective damping and mass, are analysed and compared to those of previous studies [1-2, 5-6].

Numerical application of this mode-based approach is performed in Chapter 8 on two kinds of beam-stiffened plate model: one with a straight beam and the other with an L-shaped beam. Results are compared with those from the Mode/FT approach and the locally reacting impedance method.

It is expected that the mode-based approach can form a flexible framework in that it might be further developed for built-up systems constructed from a number of connected subsystems.

Chapter 7

VIBRATION ANALYSIS OF A TYPICAL COMPLEX BUILT-UP STRUCTURE

7.1 INTRODUCTION

Based on the conventional modal analysis theory, an analytical solution was given in Chapter 6 for the vibration response of a beam/plate system in which the beam and the plate have the same mode shapes along the coupling line. Although it concerns only a special coupling form between a beam and a plate, this prediction procedure provides a methodology which can transfer a large number of physical DOFs into a small number of generalized DOFs by decomposing the interface forces/displacements in terms of a set of basis functions. Similar DOFs-reducing techniques have been described in other earlier research work, e.g., in Refs. [21-22], in which, the component coupling conditions are treated as generalized kinematic (for displacement) or natural (for force) boundary conditions. These boundary conditions (on discretized models) take the form of a finite number of constraints which can be treated through a direct elimination or the addition of Lagrange multipliers. Consequently, computationally efficient and robust direct elimination algorithm may be developed. However, such a reduction procedure may often lead to incompatible models, i.e., the interface deformations of the two components are described by the different number of DOFs, which can give poor predictions due to a so-called 'locking phenomenon' [21]. With this in mind, a mode-based approach is developed in this chapter to predict the vibration response of such a complex built-up structure consisting of a long-wavelength source structure and a short-wavelength receiver structure, as shown in Figure 7.1.

In what follows, the matrix form of the equation of motion of a continuous model is given by modal analysis theory in section 7.2. Then in section 7.3, the mode-based approach is described to predict the vibration response of the coupled system by introducing a set of complete and orthogonal basis functions along the interfaces. In the first instance both the dynamic properties of the source and the receiver are assumed known precisely. A precise solution for the FRFs of the source and the power transmitted to the receiver can then be given in terms of the generalised interface DOFs. Since

computational limitations can often place a restriction to provide a deterministic modal description to a given large flexible receiver structure, in section 7.4, an asymptotically simple standing wave receiver model is incorporated into the mode-based approach to provide estimations of the vibration response of the coupled system. Finally in section 7.5, the interaction effects between the source and the receiver are investigated and compared with the 'Resound' [1-2] and fuzzy structure theory [5-6].

Generally this mode-based approach has two main advantages: first, it can substantially reduce the system degrees of freedom (DOFs) by transferring the physical DOFs into generalized DOFs; and secondly, it can couple subsystems of different form within the same system model by modelling different subsystems by different appropriate techniques, the choice being determined by the local dynamic properties of the individual subsystem of interest.

7.2 EQUATION OF MOTION OF A CONTINUOUS MODEL: MODAL ANALYSIS

In the approach described here predictions are based on the conventional modal analysis of both the source and the receiver substructures when they are separated from each other. Modal analysis theory is therefore briefly reviewed in this section. The details can be found in many other works (e.g. Refs [11, 58]).

For a continuous undamped model, the general form of the equation of motion is given by

$$\rho(\mathbf{x})\ddot{w}(\mathbf{x})+L\left[w(\mathbf{x})\right]=F(\mathbf{x}) \tag{7.1}$$

where w is the displacement at a general location $\mathbf{x}$, $\rho(\mathbf{x})$ the mass density, L a differential (stiffness) operator of order $2p$ (where p is an integer) and F the applied force. As a continuous function of position $\mathbf{x}$, the system response $w(\mathbf{x})$ can be expressed in terms of a complete set of orthogonal functions of space under the prescribed natural boundary conditions of the structure, i.e., the mode shape functions, as

$$w(\mathbf{x})=\sum_n w_n\phi_n(\mathbf{x}) \tag{7.2}$$

where ϕ_n is the nth mode shape function of the structure and w_n is the associated generalized coordinate, or modal amplitude. The orthogonality property of ϕ_n gives

$$\int_V \rho(\mathbf{x})\phi_n(\mathbf{x})\phi_{n'}(\mathbf{x})d\mathbf{x} = 0\,,\ n \neq n' \tag{7.3}$$

Although theoretically an infinite number of modes are involved in any continuous structure, the modes required in practice are usually truncated to a convenient finite number, by a criterion of convergence. Combining equations (7.1), (7.2) and (7.3), the equation governing w_n is then given, in a matrix form, by

$$\mathbf{M}\ddot{\mathbf{w}}_\mathbf{n} + \mathbf{K}\mathbf{w}_\mathbf{n} = \mathbf{F}_\mathbf{n} \tag{7.4}$$

where $\mathbf{M}$ and $\mathbf{K}$ are, respectively, the mass and stiffness matrices, and $\mathbf{F}_\mathbf{n}$ is the generalized force vector.

The (n,n')th elements of $\mathbf{M}$ can, in general, be written in the form

$$M_{nn'} = \int_V \rho(\mathbf{x})\phi_n^{\,T}(\mathbf{x})\phi_{n'}(\mathbf{x})d\mathbf{x} \tag{7.5}$$

From equation (7.3), it is seen that $M_{nn'} = 0$, when $n \neq n'$.

The (n,n')th element of $\mathbf{K}$ is given by

$$K_{nn'} = \int_V \phi_{n'}^{\,T}(\mathbf{x})L\left[\phi_n(\mathbf{x})\right]d\mathbf{x} \tag{7.6}$$

Since ϕ_n satisfy the partial differential equation (equation (7.1)) with no forcing, it gives

$$L\left[\phi_n(\mathbf{x})\right] = \lambda_n\rho(\mathbf{x})\phi_n(\mathbf{x}) \tag{7.7}$$

λ_n here is the eigenvalue corresponding to eigenvector ϕ_n. When equation (7.7) is multiplied by $\phi_{n'}^{\,T}$ and integrated over V the domain of definition, using equation (7.5), it is easy to see that $K_{nn'} = 0$, when $n \neq n'$, i.e., ϕ_n satisfy a second orthogonality relation.

Therefore both $\mathbf{M}$ and $\mathbf{K}$ are diagonal. In the context below, the nth diagonal elements of $\mathbf{M}$ and $\mathbf{K}$ are simply represented by M_n and K_n, respectively, instead of M_{nn} and K_{nn}.

The nth element of general force vector $\mathbf{F}_\mathbf{n}$ is given by

$$F_n = \int_V F(\mathbf{x})\phi_n(\mathbf{x})d\mathbf{x} \tag{7.8}$$

The Fourier transform of equation (7.4) then gives

$$\mathbf{w_n} = \mathbf{Y_n F_n} \tag{7.9}$$

where $\mathbf{Y_n}$ is a diagonal matrix, whose nth diagonal element corresponds to the dynamic receptance of the nth mode of the structure. Let damping be included by assigning a complex value to the stiffness as $K_n(1+j\eta_n)$, where η_n is the damping loss factor associated with the nth mode of the structure. $\mathbf{Y_n}$ can then be given by

$$Y_n = \frac{1}{M_n\left[\omega_n^2(1+j\eta_n)-\omega^2\right]} \tag{7.10}$$

where $\omega_n = \sqrt{K_n/M_n}$ is the nth natural frequency of the structure ($\omega_n^2 = \lambda_n$). For convenience, $\phi_n(\mathbf{x})$ is usually mass-normalized in the form of $\Phi_n(\mathbf{x})$ such that

$$\int_V \rho(\mathbf{x})\Phi_n(\mathbf{x})\Phi_n(\mathbf{x})d\mathbf{x} = 1 \tag{7.11}$$

M_n and K_n can then be simplified as

$$M_n = 1,\ K_n = \omega_n^2 \tag{7.12}$$

Consequently, the nth modal force F_n and the modal receptance Y_n in equations (7.8) and (7.10), respectively, can be written as

$$F_n = \int_V F(\mathbf{x})\Phi_n(\mathbf{x})d\mathbf{x} \tag{7.13}$$

$$Y_n = \frac{1}{\omega_n^2(1+j\eta_n)-\omega^2} \tag{7.14}$$

From equations (7.9)-(7.14), the nth modal amplitude of the structure can be given as

$$w_n = Y_n F_n \tag{7.15}$$

Combining equations (7.2) and (7.15), the system response can consequently be expressed as a summation of a set of modal displacements. The above procedure is the conventional modal analysis for predicting the dynamic response of a continuous structure. In what follows, it is combined with an interface decomposition technique to predict the response of the built-up structure shown in Figure 7.1.

7.3 DYNAMIC ANALYSIS OF A GENERAL COMPLEX BUILT-UP STRUCTURE: MODE-BASED APPROACH

In principle, the mode-based approach can be divided into the following steps: (1) both the source and the receiver substructures are described in terms of their 'unloaded' modes, i.e., the modal properties when each individual substructure is separated from each other; (2) the interface forces/displacements are decomposed into a set of complete and orthogonal basis functions; (3) the equilibrium and continuity conditions are then enforced in terms of the basis functions. As a result, the vibration response of the built-up structure can be determined in a simple manner. Moreover, the modal correlations and hence the dynamic interactions between the source and the receiver across the interface can be found. Nevertheless, it can form a flexible framework by incorporation with different modelling strategies, e.g. the stiff source is described deterministic while the large flexible receiver is described asymptotically. The detailed procedure is given below.

7.3.1 Dynamic analysis of the source structure

The source substructure and its force loadings are shown in Figure 7.2, where $F_e\left(\mathbf{x}_s^e\right)$ and $F_I^s\left(\mathbf{x}_s^I\right)$ represent the external and interface forces acting at the local coordinates $\mathbf{x}_s^e$ and $\mathbf{x}_s^I$ of the source, respectively. By the modal analysis theory described in section 7.2, the displacement response w_s of the source at a general location $\mathbf{x}_s$, can be written as

$$w_s\left(\mathbf{x}_s\right)=\sum_n w_{s,n}\Phi_{s,n}\left(\mathbf{x}_s\right) \tag{7.16}$$

where $w_{s,n}$ is the nth generalized coordinate of the source, and $\Phi_{s,n}$ is its nth mass-normalized unloaded mode shape function, i.e.,

$$\int_{V_s} m_s\left(\mathbf{x}_s\right)\Phi_n\left(\mathbf{x}_s\right)\Phi_{n'}\left(\mathbf{x}_s\right)d\mathbf{x}_s=\begin{cases}1, n=n'\\ 0, n\neq n'\end{cases} \tag{7.17}$$

Here m_s is the mass distribution of the source substructure. Consequently, $w_{s,n}$ can be written, similar to equations (7.15), as

$$w_{s,n}=Y_{s,n}\left(f_{e,n}+f_{I,n}^s\right) \tag{7.18}$$

where $Y_{s,n}$ is the nth modal receptance of the uncoupled source, namely, the unloaded modal receptance of the source, and $f_{e,n}$ and $f_{I,n}^{s}$ are, respectively, the nth modal forces corresponding to $F_e\left(\mathbf{x}_{\mathrm{s}}^{\mathrm{e}}\right)$ and $F_I^s\left(\mathbf{x}_{\mathrm{s}}^{\mathrm{I}}\right)$, given by

$$Y_{s,n}=\frac{1}{\omega_{s,n}^2\left(1+j\eta_{s,n}\right)-\omega^2} \tag{7.19}$$

$$f_{e,n}=\int_{V_s^e} F_e\left(\mathbf{x}_{\mathrm{s}}^{\mathrm{e}}\right)\Phi_{s,n}\left(\mathbf{x}_{\mathrm{s}}^{\mathrm{e}}\right)d\mathbf{x}_{\mathrm{s}}^{\mathrm{e}} \tag{7.20}$$

$$f_{I,n}^{s}=\int_{V_s^I} F_I^s\left(\mathbf{x}_{\mathrm{s}}^{\mathrm{I}}\right)\Phi_{s,n}\left(\mathbf{x}_{\mathrm{s}}^{\mathrm{I}}\right)d\mathbf{x}_{\mathrm{s}}^{\mathrm{I}} \tag{7.21}$$

Here $\omega_{s,n}$ is the nth natural frequency of the uncoupled source (called the unloaded natural frequency), and V_s^e and V_s^I are, respectively, the region of the source over which the external and interface force loadings act. When a set of truncated mode shapes are used, equation (7.18) can then be written in matrix form as

$$\mathbf{w}_{\mathrm{s,n}}=\mathbf{Y}_{\mathrm{s,n}}\left(\mathbf{f}_{\mathrm{e,n}}+\mathbf{f}_{\mathrm{I,n}}^{\mathrm{s}}\right) \tag{7.22}$$

where $\mathbf{w}_{\mathrm{s,n}}$, $\mathbf{f}_{\mathrm{e,n}}$ and $\mathbf{f}_{\mathrm{I,n}}^{\mathrm{s}}$ are column vectors composed of $w_{s,n}$, $f_{e,n}$ and $f_{I,n}^{s}$, respectively, while $\mathbf{Y}_{\mathrm{s,n}}$ is a diagonal matrix whose nth diagonal element is $Y_{s,n}$. Substituting equations (7.18) into (7.16), the dynamic response of the source substructure can then be expressed in terms of its unloaded modes.

7.3.2 Dynamic analysis of the receiver structure

The same analytical procedure can be applied to the receiver substructure shown in Figure 7.3, where $F_I^r\left(\mathbf{x}_{\mathrm{r}}^{\mathrm{I}}\right)$ is the loaded interface force at the local coordinate $\mathbf{x}_{\mathrm{r}}^{\mathrm{I}}$ of the receiver. Let the displacement w_r at a general location $\mathbf{x}_{\mathrm{r}}$ of the receiver be expressed as

$$w_r\left(\mathbf{x}_{\mathrm{r}}\right)=\sum_m w_{r,m}\Psi_{r,m}\left(\mathbf{x}_{\mathrm{r}}\right) \tag{7.23}$$

where $w_{r,m}$ is the mth generalized coordinate of the receiver, and $\Psi_{r,m}$ is the mth unloaded mass-normalized mode shape of the receiver so that

$$\int_{V_r} m_r\left(\mathbf{x}_{\mathrm{r}}\right)\Psi_{r,m}\left(\mathbf{x}_{\mathrm{r}}\right)\Psi_{r,m'}\left(\mathbf{x}_{\mathrm{r}}\right)d\mathbf{x}_{\mathrm{r}}=\begin{cases}1, m=m'\\ 0, m\neq m'\end{cases} \tag{7.24}$$

Here m_r is the mass density of the receiver. $w_{r,m}$ is, therefore, governed, under the force loading condition of Figure 7.3, by

$$w_{r,m} = Y_{r,m} f_{I,m}^{r} \tag{7.25}$$

where $Y_{r,m}$ and $f_{I,m}^{r}$ are, respectively, the mth unloaded modal receptance of the receiver and the modal force caused by $F_I^r\left(\mathbf{x}_\mathbf{r}^\mathbf{I}\right)$. These are given by

$$Y_{r,m} = \frac{1}{\omega_{r,m}^2\left(1+j\eta_{r,m}\right)-\omega^2} \tag{7.26}$$

$$f_{I,m}^{r} = \int_{V_r^I} F_I^r\left(\mathbf{x}_\mathbf{r}^\mathbf{I}\right)\Psi_{r,m}\left(\mathbf{x}_\mathbf{r}^\mathbf{I}\right)d\mathbf{x}_\mathbf{r}^\mathbf{I} \tag{7.27}$$

Here $\omega_{r,m}$ is the mth unloaded natural frequency of the receiver and V_r^I represents the region of the receiver occupied by the interface. By modal truncation, equation (7.25) can then be written in a matrix form as

$$\mathbf{w}_{\mathbf{r,m}} = \mathbf{Y}_{\mathbf{r,m}}\mathbf{f}_{\mathbf{I,m}}^{\mathbf{r}} \tag{7.28}$$

where $\mathbf{w}_{\mathbf{r,m}}$ and $\mathbf{f}_{\mathbf{I,m}}^{\mathbf{r}}$ are column vectors composed of $w_{r,m}$ and $f_{I,m}^{r}$, respectively, and $\mathbf{Y}_{\mathbf{r,m}}$ is a diagonal matrix whose mth diagonal element is $Y_{r,m}$. Substituting equations (7.25) into (7.23), the dynamic response of the receiver is then expressed in terms of the unloaded modes of the receiver.

7.3.3 Decomposition of interface force/displacement

Let $\mathbf{x}_\mathbf{I}$ be the local coordinates of the interface, and $F_I\left(\mathbf{x}_\mathbf{I}\right)$ and $w_I\left(\mathbf{x}_\mathbf{I}\right)$ be, respectively, the interface forces and displacements. Now $F_I\left(\mathbf{x}_\mathbf{I}\right)$ and $w_I\left(\mathbf{x}_\mathbf{I}\right)$ are decomposed in terms of a set of complete basis functions $\mathrm{X}_k\left(\mathbf{x}_\mathbf{I}\right)$, as

$$F_I\left(\mathbf{x}_\mathbf{I}\right) = \sum_k f_{I,k}\mathrm{X}_{I,k}\left(\mathbf{x}_\mathbf{I}\right) \tag{7.29}$$

$$w_I\left(\mathbf{x}_\mathbf{I}\right) = \sum_k w_{I,k}\mathrm{X}_{I,k}\left(\mathbf{x}_\mathbf{I}\right) \tag{7.30}$$

where $f_{I,k}$ is the kth generalized interface force and $w_{I,k}$ is kth generalized interface coordinate. Here $\mathrm{X}_k\left(\mathbf{x}_\mathbf{I}\right)$ is orthogonal such that

$$\int_{V_I} \mathrm{X}_{I,k}(\mathbf{x}_\mathrm{I})\mathrm{X}_{I,k'}(\mathbf{x}_\mathrm{I})d\mathbf{x}_\mathrm{I} = \begin{cases} 1, k = k' \\ 0, k \neq k' \end{cases} \tag{7.31}$$

From equations (7.29) and (7.30), it is seen that the physical coupling DOFs of the built-up structure have been transferred into generalized coupling DOFs. This DOFs-transferring technique is potentially very useful to reduce the number of DOFs involved in the calculation.

Let the set of infinite basis functions be truncated to a convenient finite number. The force equilibrium and displacement compatibility conditions can then be enforced along the interface in a simple manner. The analytical procedure is described below.

7.3.4 Dynamic analysis of the coupled system

Let $\mathbf{T}_\mathrm{s}$ and $\mathbf{T}_\mathrm{r}$ represent transformation matrices which relate the local coordinates of $\mathbf{x}_\mathrm{s}^\mathrm{I}$, $\mathbf{x}_\mathrm{r}^\mathrm{I}$ and $\mathbf{x}_\mathrm{I}$ in the forms

$$\mathbf{x}_\mathrm{s}^\mathrm{I} = \mathbf{T}_\mathrm{s}\mathbf{x}_\mathrm{I} \tag{7.32}$$

$$\mathbf{x}_\mathrm{r}^\mathrm{I} = \mathbf{T}_\mathrm{r}\mathbf{x}_\mathrm{I} \tag{7.33}$$

where both $\mathbf{T}_\mathrm{s}$ and $\mathbf{T}_\mathrm{r}$ are orthogonal matrices [9, 18] so that $\mathbf{T}_\mathrm{s}^T = \mathbf{T}_\mathrm{s}^{-1}$ and $\mathbf{T}_\mathrm{r}^T = \mathbf{T}_\mathrm{r}^{-1}$. The boundary conditions at the interfaces give

$$F_I(\mathbf{x}_\mathrm{I}) = -F_I^s(\mathbf{x}_\mathrm{I}^\mathrm{s}) = F_I^r(\mathbf{x}_\mathrm{I}^\mathrm{r}) \tag{7.34}$$

$$w_I(\mathbf{x}_\mathrm{I}) = w_s(\mathbf{x}_\mathrm{I}^\mathrm{s}) = w_r(\mathbf{x}_\mathrm{I}^\mathrm{r}) \tag{7.35}$$

Substituting equations (7.34) into (7.21) and combining with equations (7.32) and (7.29), gives

$$f_{I,n}^s = -\sum_k f_{I,k} \int_{V_s^I} \Phi_{s,n}(\mathbf{x}_\mathrm{s}^\mathrm{I})\mathrm{X}_{I,k}(\mathbf{T}_\mathrm{s}^T\mathbf{x}_\mathrm{s}^\mathrm{I})d\mathbf{x}_\mathrm{s}^\mathrm{I} \tag{7.36}$$

For truncated sets of $\Phi_{s,n}$ and X_k, equation (7.36) can be expressed in a matrix form as

$$\mathbf{f}_\mathrm{I,n}^\mathrm{s} = -\boldsymbol{\alpha}_\mathrm{s}\mathbf{f}_\mathrm{I,k} \tag{7.37}$$

where $\mathbf{f}_\mathrm{I,k}$ is a column vector of $f_{I,k}$, and $\boldsymbol{\alpha}_\mathrm{s}$ is a $n \times k$ matrix, given by

$$\alpha_{s,nk} = \int_{V_s^I} \Phi_{s,n}(\mathbf{x}_\mathrm{s}^\mathrm{I})\mathrm{X}_{I,k}(\mathbf{T}_\mathrm{s}^T\mathbf{x}_\mathrm{s}^\mathrm{I})d\mathbf{x}_\mathrm{s}^\mathrm{I} \tag{7.38}$$

It is seen that $\boldsymbol{\alpha}_s$ can be regarded as a modal correlation matrix in that its (n,k)th term indicates the correlation between the source mode $\Phi_{s,n}$ and the basis function $\mathrm{X}_{I,k}$ across the interface. Equation (7.22) then becomes

$$\mathbf{w}_{s,n} = \mathbf{Y}_{s,n}\left(\mathbf{f}_{e,n} - \boldsymbol{\alpha}_s \mathbf{f}_{I,k}\right) \tag{7.39}$$

Similarly, substituting equations (7.34) into (7.27) and combining with equation (7.33), it follows that

$$f^r_{I,m} = \sum_k f_{I,k} \int_{V_r^I} \Psi_{r,m}\left(\mathbf{x}_r^{\mathrm{I}}\right) \mathrm{X}_{I,k}\left(\mathbf{T}_r^T \mathbf{x}_r^{\mathrm{I}}\right) d\mathbf{x}_r^{\mathrm{I}} \tag{7.40}$$

Let equation (7.40) be written in matrix form

$$\mathbf{f}^{\mathrm{r}}_{\mathrm{I,m}} = \boldsymbol{\alpha}_{\mathrm{r}} \mathbf{f}_{\mathrm{I,k}} \tag{7.41}$$

Here $\boldsymbol{\alpha}_r$ is a $m \times k$ matrix, whose (m,k)th element is

$$\alpha_{r,mk} = \int_{V_r^I} \Psi_{r,m}\left(\mathbf{x}_r^{\mathrm{I}}\right) \mathrm{X}_{I,k}\left(\mathbf{T}_r^T \mathbf{x}_r^{\mathrm{I}}\right) d\mathbf{x}_r^{\mathrm{I}} \tag{7.42}$$

The above relation indicates that $\boldsymbol{\alpha}^{\mathrm{r}}$ is a matrix representing the modal correlations between each individual receiver mode $\Psi_{r,m}$ and basis function $\mathrm{X}_{I,k}$ over the interface. Equation (7.28) then becomes

$$\mathbf{w}_{\mathrm{r,m}} = \mathbf{Y}_{\mathrm{r,m}} \boldsymbol{\alpha}_{\mathrm{r}} \mathbf{f}_{\mathrm{I,k}} \tag{7.43}$$

Combining equations (7.16) and (7.23) with equation (7.35), it follows that

$$\sum_n w_{s,n} \Phi_{s,n}\left(\mathbf{x}_s^{\mathrm{I}}\right) = \sum_m w_{r,m} \Psi_{r,m}\left(\mathbf{x}_r^{\mathrm{I}}\right) = \sum_k w_{I,k} \mathrm{X}_{I,k}\left(\mathbf{x}_{\mathrm{I}}\right) \tag{7.44}$$

Each side of equation (7.44) is multiplied by $\mathrm{X}_{I,k}\left(\mathbf{x}_{\mathrm{I}}\right)$ and integrated along the interface V_I. By the relation of equation (7.31), it follows that

$$w_{I,k} = \sum_n w_{s,n} \int_{V_I} \Phi_{s,n}\left(\mathbf{T}_s \mathbf{x}_{\mathrm{I}}\right) \mathrm{X}_{I,k}\left(\mathbf{x}_{\mathrm{I}}\right) d\mathbf{x}_{\mathrm{I}} \tag{7.45}$$

$$w_{I,k} = \sum_m w_{r,m} \int_{V_I} \Psi_{r,m}\left(\mathbf{T}_r \mathbf{x}_{\mathrm{I}}\right) \mathrm{X}_{I,k}\left(\mathbf{x}_{\mathrm{I}}\right) d\mathbf{x}_{\mathrm{I}} \tag{7.46}$$

The above equations yield

$$\boldsymbol{\beta}_{\mathrm{s}} \mathbf{w}_{\mathrm{s,n}} = \boldsymbol{\beta}_{\mathrm{r}} \mathbf{w}_{\mathrm{r,m}} = \mathbf{w}_{\mathrm{I,k}} \tag{7.47}$$

where $\boldsymbol{\beta}_s$ is a $k \times n$ matrix and $\boldsymbol{\beta}_r$ is a $k \times m$ matrix, given by

$$\beta_{s,kn} = \int_{V_I} \mathrm{X}_{I,k}(\mathbf{x}_\mathbf{I}) \Phi_{s,n}(\mathbf{T}_s \mathbf{x}_\mathbf{I}) d\mathbf{x}_\mathbf{I} \tag{7.48}$$

$$\beta_{r,km} = \int_{V_I} \mathrm{X}_{I,k}(\mathbf{x}_\mathbf{I}) \Psi_{r,m}(\mathbf{T}_r \mathbf{x}_\mathbf{I}) d\mathbf{x}_\mathbf{I} \tag{7.49}$$

Comparing equations (7.48) and (7.49) with (7.38) and (7.42), it follows that

$$\boldsymbol{\alpha}_s = \boldsymbol{\beta}_s^{\,T}, \quad \boldsymbol{\alpha}_r = \boldsymbol{\beta}_r^{\,T} \tag{7.50}$$

Combining equations (7.39), (7.43), (7.47) and (7.50), the interface force and displacement distributions in terms of generalised coordinates can be found

$$\mathbf{f}_{I,k} = \left[\mathbf{A}_s + \mathbf{A}_r\right]^{-1} \boldsymbol{\alpha}_s^{\,T} \mathbf{Y}_{s,n} \mathbf{f}_{e,n} \tag{7.51}$$

$$\mathbf{w}_{I,k} = \mathbf{A}_r \left[\mathbf{A}_s + \mathbf{A}_r\right]^{-1} \boldsymbol{\alpha}_s^{\,T} \mathbf{Y}_{s,n} \mathbf{f}_{e,n} \tag{7.52}$$

where

$$\mathbf{A}_s = \boldsymbol{\alpha}_s^{\,T} \mathbf{Y}_{s,n} \boldsymbol{\alpha}_s \tag{7.53}$$

$$\mathbf{A}_r = \boldsymbol{\alpha}_r^{\,T} \mathbf{Y}_{r,m} \boldsymbol{\alpha}_r \tag{7.54}$$

Physically, $\mathbf{A}_s$ and $\mathbf{A}_r$ provide the dynamic correlations (in matrix forms) between the source, the receiver and the interface. The (k,k')th entries of $\mathbf{A}_s$ and $\mathbf{A}_r$ are given by

$$A_{s,kk'} = \sum_n \alpha_{s,kn} \alpha_{s,k'n} Y_{s,n} \tag{7.55}$$

$$A_{r,kk'} = \sum_m \alpha_{r,km} \alpha_{r,k'm} Y_{r,m} \tag{7.56}$$

The (k,k')th element of $\mathbf{A}_s$ hence represents how the unloaded modal properties of the source collectively affect the kth generalised interface coordinate through the couplings between the source modes and the kth and k'th interface basis functions. Equation (7.56) gives the similar dynamic correlations between the receiver and the interface. Combining equations (7.39) and (7.51), the generalized coordinates of the source, after coupling to the receiver, can then be determined by

$$\mathbf{w}_{s,n} = \mathbf{Y}_{s,n} \left[\mathbf{I} - \boldsymbol{\alpha}_s \left(\mathbf{A}_s + \mathbf{A}_r\right)^{-1} \boldsymbol{\alpha}_s^{\,T} \mathbf{Y}_{s,n}\right] \mathbf{f}_{e,n} \tag{7.57}$$

Equation (7.57) indicates that the receiver substructure actually loads a dynamic modification matrix on the modal properties of the source substructure across the interface couplings.

Finally, the power transmitted to the receiver from the source through the interface can thus be expressed as

$$P_{tr} = \frac{1}{2}\mathrm{Re}\left\{\int_{V_I}\left[F_I\left(\mathbf{x}_\mathrm{I}\right)\right]^{*} j\omega w_I\left(\mathbf{x}_\mathrm{I}\right)d\mathbf{x}_\mathrm{I}\right\} = \frac{1}{2}\mathrm{Re}\left\{j\omega\sum_k w_{I,k} f_{I,k}^{*}\right\} \tag{7.58}$$

So far both the dynamic response of the coupled system and the power transmission within the system can be predicted. The above procedure is the newly developed mode-based approach.

It is seen that the key point of this mode-based approach is how to choose the set of basis functions appropriately for the purpose of interface force/displacement decomposition. Theoretically, the set of basis functions can be arbitrary, provided it is complete and orthogonal. In principle, the choices for the set of basis functions should meet the criteria of convenience, simplicity and accuracy, depending on the dynamic properties of the unloaded source and receiver structures as well as the coupling conditions between them. For example, when a stiff source structure is wholly attached to a large flexible receiver, which is very often in practice, the choice of the mode shape functions of the source, being a set of complete and orthogonal functions, is obviously one of the best. Other forms of basis functions may be also appropriate.

This mode-based approach can provide a very precise solution for the coupled responses of the system, provided the dynamic properties of the source and the receiver are precisely known and enough large numbers of modes and basis functions are used in the calculation. If that is not the case, however, there may be errors caused by the truncated sets of functions and by the uncertainties of the coupled system.

7.3.5 A special case: the simplest coupling form

It is interesting to look at a special coupling case when the source and the receiver mode shapes have the same spatial variations along the interface region so that

$$\mathrm{X}_{I,k}\left(\mathbf{x}_\mathrm{I}\right) = \Phi_{s,k}\left(\mathbf{x}_\mathrm{s}^\mathrm{I}\right) = \Psi_{r,k}\left(\mathbf{x}_\mathrm{r}^\mathrm{I}\right) \tag{7.59}$$

In this case, equations (7.38) and (7.42) give

$$\boldsymbol{\alpha}_\mathrm{s} = \boldsymbol{\alpha}_\mathrm{r} = \mathbf{I} \tag{7.60}$$

The generalized interface coordinates can then be written in a simple form as

$$f_{I,n} = \frac{Y_{s,n}}{Y_{s,n} + Y_{r,n}} f_{e,n} \tag{7.61}$$

$$w_{I,n} = \frac{Y_{s,n} Y_{r,n}}{Y_{s,n} + Y_{r,n}} f_{e,n} \tag{7.62}$$

Equations (7.61) and (7.62) imply that for each individual substructure, its loaded modes (i.e., after coupling to the other substructure) remain uncoupled from each other. In this sense, equation (7.59) can be regarded as the simplest coupling form between a source and a receiver. The beam/plate case considered in Chapter 6 corresponds to just such a coupling situation.

7.3.6 The dynamic interactions between a stiff source and a flexible receiver

Equation (7.57) gives the dynamic response of the source substructure when the dynamic contributions arising from the presence of the receiver are included. In this subsection the dynamic effects of a flexible receiver on a stiff source are considered, being relevant to many practical built-up structures.

7.3.6.1 *The modified dynamic modal stiffness matrix*

Let $n = k$ so that $\boldsymbol{\alpha}_s$ is a square matrix. Equation (7.57) can then be written as

$$\mathbf{w}_{s,n} = \mathbf{Y}_{s,n}\left[\mathbf{I} - \left(\mathbf{Y}_{s,n} + \mathbf{Y}_{rs}^{\mathbf{I}}\right)^{-1}\mathbf{Y}_{s,n}\right]\mathbf{f}_{e,n} = \left[\mathbf{Y}_{s,n}^{-1} + \left(\mathbf{Y}_{rs}^{\mathbf{I}}\right)^{-1}\right]^{-1}\mathbf{f}_{e,n} \tag{7.63}$$

where $\mathbf{Y}_{rs}^{\mathbf{I}}$ is given by

$$\mathbf{Y}_{rs}^{\mathbf{I}} = \left(\boldsymbol{\alpha}_r \boldsymbol{\alpha}_s^{-1}\right)^T \mathbf{Y}_{r,m}\left(\boldsymbol{\alpha}_r \boldsymbol{\alpha}_s^{-1}\right) \tag{7.64}$$

It is seen from equation (7.63) that $\mathbf{Y}_{rs}^{\mathbf{I}}$ has the same units as $\mathbf{Y}_{r,m}$. While $\mathbf{Y}_{s,n}^{-1}$ represents the unloaded dynamic modal stiffness matrix of the source, $\mathbf{Y}_{s,n}^{-1} + \left(\mathbf{Y}_{rs}^{\mathbf{I}}\right)^{-1}$ is the loaded dynamic modal stiffness matrix of the source substructure. Therefore $\left(\mathbf{Y}_{rs}^{\mathbf{I}}\right)^{-1}$ is in effect the dynamic stiffness modification matrix introduced to the source substructure by the presence of the receiver. Consequently, the (n,n)th diagonal element of $\left(\mathbf{Y}_{rs}^{\mathbf{I}}\right)^{-1}$ may be regarded as the *direct* modification to the nth mode of the source, i.e., through the couplings between the nth source mode and the receiver modes across the interface,

whereas the (n,n')th off-diagonal element is the *indirect* modification to the nth mode of the source, i.e., through the couplings between n'th source mode and the receiver modes (since the loaded nth and n'th source modes are usually coupled with each other).

A perturbation relation can be developed from equation (7.63) by letting

$$\mathbf{Y} = \mathbf{Y}_{s,n} + \mathbf{Y}_{rs}^{I} \tag{7.65}$$

Equation (7.65) can then be expressed in a perturbation form as

$$\mathbf{Y} = diag[\mathbf{Y}]\left\{\mathbf{I} + \left(diag[\mathbf{Y}]\right)^{-1}\delta[\mathbf{Y}]\right\} \tag{7.66}$$

where $diag[\mathbf{Y}]$ is a diagonal matrix comprising the diagonal elements of $\mathbf{Y}$ while $\delta[\mathbf{Y}]$ is a full matrix comprising the off-diagonal elements of $\mathbf{Y}$, i.e., the 'perturbation matrix' of $\mathbf{Y}$. $\mathbf{Y}^{-1}$ can thus be simply calculated by using a power-series expansion [3, 33-34].

It is known that the vibration of the source structure tends to be largely controlled by its unloaded modal properties as the flexibility of the receiver substructure increases. Therefore, it is quite reasonable to suppose that the coupling relations between the loaded modes of the source are generally not very strong when the receiver substructure is relatively very flexible. Consequently, one may assume that $\left(\mathbf{Y}_{rs}^{I}\right)^{-1}$ is strongly diagonally dominated for a stiff source and flexible receiver. (The validity of this assumption will be furthermore discussed in Chapter 8.) Under such circumstances, the loaded dynamic response of the source, from equation (7.63), can be simply approximated as

$$w_{s,n} \approx \frac{Y_{s,n}}{1 + Y_{s,n}/Y_{rs,n}^{I}} f_{e,n} \tag{7.67}$$

where $Y_{rs,n}^{I}$ is the nth diagonal element of $\mathbf{Y}_{rs}^{I}$, given by

$$Y_{rs,n}^{I} = \sum_{m} \alpha_{nm}^{2} Y_{r,m} \tag{7.68}$$

Here α_{nm} is the (n,m)th element of matrix $\boldsymbol{\alpha}_{r}\boldsymbol{\alpha}_{s}^{-1}$. Equation (7.67) indicates that for a very flexible receiver, the perturbation matrix $\delta[\mathbf{Y}]$ can be simply taken as zero.

7.3.6.2 Effective mass and effective loss factor

From equation (7.67), the dynamic modifications to a stiff source, arising from the presence of a very flexible receiver, can then be treated as effective mass and effective

loss factor added to each individual mode of the source. Let equation (7.68) be re-expressed as

$$Y^{I}_{rs,n} = -p'_{n1} - jp'_{n2} \tag{7.69}$$

where both p'_{n1} and p'_{n2} are real. Combining equations (7.26), (7.68) and (7.69), it follows that

$$p'_{n1} = \sum_{m} \frac{\alpha^2_{nm}\left(\omega^2 - \omega^2_{r,m}\right)}{\left(\omega^2_{r,m} - \omega^2\right)^2 + \left(\omega^2_{r,m}\eta_r\right)^2} \tag{7.70}$$

$$p'_{n2} = \sum_{m} \frac{\alpha^2_{nm}\omega^2_{r,m}\eta_r}{\left(\omega^2_{r,m} - \omega^2\right)^2 + \left(\omega^2_{r,m}\eta_r\right)^2} \tag{7.71}$$

Substituting equations (7.19) and (7.69)-(7.71) into (7.67), gives

$$w_{s,n} \approx \frac{1}{\left[\omega^2_{n,s}\left(1 + j\eta_s\right) - \omega^2\right] + \dfrac{1}{-p'_{n1} - jp'_{n2}}} f_{e,n} \tag{7.72}$$

The above equation can be re-expressed into the form

$$w_{s,n} \approx \frac{1}{\omega^2_{s,n}\left(1 + j\eta_s\right) - \omega^2 - D_{n1} + jD_{n2}} f_{e,n} \tag{7.73}$$

where

$$D'_{n1} = \frac{p'_{n1}}{p'^2_{n1} + p'^2_{n2}} \tag{7.74}$$

$$D'_{n2} = \frac{p'_{n2}}{p'^2_{n1} + p'^2_{n2}} \tag{7.75}$$

The dynamic modifications to the source by the receiver can then be interpreted as an effective loss factor η_n and effective non-dimensional mass m_n induced to each individual mode of the source such that

$$w_{s,n} \approx \frac{1}{\omega^2_{s,n}\left[1 + j\left(\eta_s + \eta_n\right)\right] - \left(1 + m_n\right)\omega^2} f_{e,n} \tag{7.76}$$

where

$$m_n = \frac{D'_{n1}}{\omega^2} \tag{7.77}$$

$$\eta_n = \frac{D'_{n2}}{\omega_{s,n}^2} \tag{7.78}$$

Note that the effective mass given in equation (7.77) is the ratio between the induced effective mass and the unloaded modal mass of the source (i.e., when it is uncoupled to the receiver). Therefore, m_n here can preferably be called 'dimensionless effective mass'. Equation (7.78) shows that the effective loss factor induced to any rigid body mode of the source tends to infinity, due to $\omega_{s,n} = 0$ for these modes. Therefore, the motion of the rigid body modes of the source can be greatly affected by the attached receiver, as would be expected.

7.4 VIBRATION APPROXIMATION BY THE MODE-BASED APPROACH

The above mode-based prediction procedure requires that both the source and the receiver substructures are defined precisely, i.e., in terms of their unloaded modes. However, it is increasingly difficult, or even impossible, to give such a deterministic description for dynamically very flexible substructures due to the large number of modes and uncertainties in the material properties, or boundary conditions, for example. The mode-based approach therefore needs to accommodate substructures whose dynamic properties are not known exactly.

7.4.1 Approximation of a short-wavelength structure

For a short-wavelength structure, which usually implies high mode count and relatively large modal overlap, perhaps also with some uncertainties in its material properties, two main issues arise [1-2]: first, the computational cost of FEA is generally prohibitive, due to the large number of degrees of freedom that may be required; and secondly, the system response becomes increasingly sensitive to geometrical imperfections as the wavelength of the response decreases so that even a highly detailed deterministic mathematical model based on the nominal system properties may not yield a reliable response prediction.

It is known in Ref. [11] that at frequencies high compared with the fundamental resonance frequency, the generated vibration response tends to be less sensitive to the detailed boundary conditions, sizes and shape, especially for points remote from their boundaries where the dynamic boundary effects (e.g., either evanescent waves or standing wave effects) can be ignored. Under such circumstances, the response can be regarded as a sum of propagating waves which are sinusoidal in nature. Consequently, the response solution can be obtained in form of a set of sinusoidal functions. Here, therefore, instead

of an exact description, the short-wavelength structure is described in an asymptotic (or statistical) way, e.g. as a simple standing wave model. (The dynamic boundary effects in the boundary zone, as a separated issue, however, will not be discussed here. Some relevant research may be found in Ref. [59].)

7.4.2 Vibration approximation of a stiff source /flexible receiver system

In a common arrangement of a built-up structure shown in Figure 7.1, the source substructure is taken to be well-defined with a low mode-count and long-wavelength, while the receiver substructure is relatively much more flexible with a high mode-count and short wavelength. Given the statistical description of the flexible receiver, the mode-based approach can then be used to estimate the broad features of the vibration response of the structure in a simple manner.

When the receiver is statistically approximated by a simple standing wave system, the generated modes can be estimated based on the wavelength within a subsystem, while the natural frequencies can be estimated from the free wavenumber within the subsystem.

The spatial correlation between the receiver modes can also be estimated analytically by making certain assumptions about the receiver mode shapes. Consequently, this yields

$$\Psi'_{r,m}(\mathbf{x}_r) \approx \frac{1}{\sqrt{m_r(\mathbf{x}_r)}} \prod_{\kappa} \sqrt{\frac{2}{L_{r,\kappa}}} \sin\left(\frac{m_\kappa \pi x_{r,\kappa}}{L_{r,\kappa}} + \theta_{r,\kappa}\right) \tag{7.79}$$

where $m_r(\mathbf{x}_r)$ is the mass distribution of the receiver substructure at a general location $\mathbf{x}_r$, κ is the number of the dimensions of the receiver structure (e.g. $\kappa = 2$ for a plate and $\kappa = 3$ for a volume), $L_{r,\kappa}$ is the length of the receiver of each dimension and $\theta_{r,\kappa}$ are the associated phase angles. The exact value of $\theta_{r,\kappa}$ tends to be of less importance as the wavelength of the receiver decreases, especially in a frequency average sense. In the high frequency range, $\theta_{r,\kappa}$ can be reasonably assumed to be random [36].

The mth natural frequency, for a receiver structure with a 4th order differential equation of motion (e.g. a plate-like structure), may be approximated by

$$\omega_{r,m} \approx \sum_{\kappa} \sqrt{\frac{D_r}{m_r}} \left(\frac{m_\kappa \pi}{L_{r,\kappa}}\right)^2 \tag{7.80}$$

where D_r corresponds to the stiffness of the receiver. For a receiver with a 2nd order differential equation of motion, such as a membrane-like structure

$$\omega_{r,m} \approx \sqrt{\sum_{\kappa} \frac{D_r}{m_r} \left(\frac{m_\kappa \pi}{L_{r,\kappa}} \right)^2} \tag{7.81}$$

Such a statistical receiver model can then be easily incorporated into the mode-based prediction procedure to estimate both the dynamic response of the source and the power transmitted to the receiver. Provided sufficient number of assumed modes $\Psi'_{r,m}$ are involved and the interfaces are located far enough from the boundaries, the predicted results can quite accurately represent the broad features of the vibration response of the coupled system, especially in a frequency average sense.

Given the transmitted power to the receiver structure, the total energy level of the receiver, when time and frequency averaged, can then be determined as below.

7.4.3 The mean-square response of the receiver

From the power transmitted to the receiver, the total energy level of the receiver, when time and frequency averaged, can then be approximated by incorporating it in an energy flow model as

$$E_r = \frac{P_{tr}}{\eta_r \omega} \tag{7.82}$$

In the above equation it is assumed [12-14] that (1) the kinetic energy and the potential energy, when time averaged, are equal (which is true at high frequencies); (2) sufficient number modes (typically 5) of the receiver subsystem are resonant with the frequency band of excitation; (3) energy is not created in the coupling between the subsystems; and (4) the damping loss factor is equal for all modes within a subsystem. The mean square velocity response of the receiver averaged over time, frequency and space, is thus given by

$$\left\langle \overline{v_r^2} \right\rangle = \frac{E_r}{M_r} = \frac{P_{tr}}{\eta_r \omega M_r} \tag{7.83}$$

where M_r is the total mass of the receiver. The result of (7.83) may be further used to predict the sound level radiated to the surroundings from the receiver, for example.

In equation (7.83) it has been tacitly assumed [11] that the mean square velocity can be defined and measured meaningfully. For example, it is not the case for a plate that is so large and so heavily damped that the velocities at different locations differ by more than an order of magnitude.

7.4.4 Other approximation approaches: the Mode/FT approach and the locally reacting impedance method

As well as a statistical simple standing wave model, a very flexible receiver can also be approximated as extended uniformly to infinity. Consequently, the Mode/FT approach and the locally reacting impedance method, described in Chapter 5, may also be appropriate, e.g. in the case of a source beam joins a very flexible plate receiver by a straight line. These will be discussed by numerical examples in Chapter 9.

7.5 DISCUSSION OF RESULTS

From the above analysis, it is seen that this mode-based approach can provide either a very precise solution of the built-up structure when the dynamics of both the source and the receiver are exactly known, or an approximate one by involving a statistical simple standing wave model to simulate the short-wavelength deformations of the flexible receiver. This procedure is similar to that in the 'Resound' method [1-2] in that the solution consists of a deterministic model of the long-wavelength (global) response and a statistical model of the short-wavelength (local) response. However, the mode-based approach contains relatively very few assumptions. The main one required is that the interface locations are far from the boundaries of the receiver when a statistical model of section 7.4.2 is to be used.

The mode-based approach also reveals that the dynamic interactions between a stiff source and a flexible receiver can be mainly taken as adding effective mass and effective damping to the source substructure by the presence of the receiver. These conclusions are in line with those obtained from the 'Resound' [1-2] and fuzzy structure [5-6] theories. The detailed comparisons are given below.

7.5.1 Effective mass and damping induced by a 'fuzzy-like' receiver

When the receiver structure is much more flexible than the source and has a high modal overlap such that it behaves as a set of fuzzy attachments to the source, by the 'resound' theory [1], the following approximate relations are taken to hold

$$\mathrm{Re}\left\{\sum_m Y_{r,m}\right\} = \sum_m \frac{\omega_{r,m}^2 - \omega^2}{\left(\omega_{r,m}^2 - \omega^2\right)^2 + \left(\omega_{r,m}^2 \eta_r\right)^2} \approx 0 \qquad (7.84)$$

$$\mathrm{Im}\left\{\sum_m Y_{r,m}\right\}=\sum_m \frac{-\omega_{r,m}^2\eta_r}{\left(\omega_{r,m}^2-\omega^2\right)^2+\left(\omega_{r,m}^2\eta_r\right)^2}\approx-\frac{\pi n_r}{2\omega} \tag{7.85}$$

where n_r is the modal density of the receiver. When it is assumed that $\Psi_m\left(\mathbf{x}_\mathrm{r}^\mathrm{I}\right)$ are independent of the order number m, at least over the restricted range of the resonant modes, α_{nm}^2 term in equation (7.68) may be replaced by its average value

$$\alpha_n^2=E\left[\alpha_{nm}^2\right] \tag{7.86}$$

Substituting equations (7.84)-(7.86) into (7.70) and (7.71), yields

$$p_{n1}'\approx 0 \tag{7.87}$$

$$p_{n2}'\approx\frac{\pi n_r}{2\omega}\alpha_n^2 \tag{7.88}$$

Consequently, equations (7.77) and (7.78) give

$$m_n'\approx 0 \tag{7.89}$$

$$\eta_n'\approx\frac{1}{\omega_{s,n}^2}\frac{2}{\pi n_r}\frac{\omega}{\alpha_n^2} \tag{7.90}$$

It is seen that the dynamic interactions between a stiff source and a relatively very flexible receiver can be mainly taken as adding effective damping to each mode of the source. Also the induced effective damping tends to be independent of the internal damping of the receiver substructure itself.

Similar conclusions can also be obtained by another approximation procedure, as used in Ref. [6]. It is known that for a flexible receiver behaving in a 'fuzzy' manner, its resonances are very often close enough such that

$$\omega_{r,m+1}-\omega_{r,m}<<\eta_r\omega_{r,m} \tag{7.91}$$

In this case, equations (7.70) and (7.71) yield the following approximations

$$p_{n1}'\approx 0 \tag{7.92}$$

$$p_{n2}'\approx\sum_m\frac{\alpha_{nm}^2}{\omega_{r,m}^2\eta_r} \tag{7.93}$$

By combining with equation (7.86), equation (7.93) can be further simplified as

$$p'_{n2} \approx \alpha_n^2 \sum_m \frac{1}{\omega_{r,m}^2 \eta_r} \approx \alpha_n^2 m(\omega) E\left[\frac{1}{\omega_{r,m}^2 \eta_r}\right] \tag{7.94}$$

where $m(\omega)$ is the number of modes of the receiver resonating within the frequency range of $\omega \pm \omega\eta/2$, and $E\left[1/\omega_{r,m}^2 \eta_r\right]$ represents the mean value of $1/\omega_{r,m}^2 \eta_r$ within the range of $\omega \pm \omega\eta/2$. When the modal density of the receiver n_r varies little over the narrow frequency band, $m(\omega)$ is given by

$$m(\omega) \approx \int_{\omega - \frac{\eta_r \omega}{2}}^{\omega + \frac{\eta_r \omega}{2}} n_r d\omega \approx \eta_r \omega n_r \tag{7.95}$$

Let $E\left[1/\omega_{r,m}^2 \eta_r\right]$ be approximated by

$$E\left[\frac{1}{\omega_{r,m}^2 \eta_r}\right] \approx \frac{1}{\eta_r \omega}\left(\int_{\omega - \frac{\eta_r \omega}{2}}^{\omega + \frac{\eta_r \omega}{2}} \frac{1}{\omega_{r,m}^2 \eta_r} d\omega_{r,m}\right) \approx \frac{1}{\eta_r \omega^2} \tag{7.96}$$

Equation (7.94) can then give

$$p'_{n2} \approx \frac{n_r}{\omega} \alpha_n^2 \tag{7.97}$$

As equation (7.92) gives $m'_n \approx 0$, equation (7.97) gives

$$\eta'_n \approx \frac{1}{\omega_{s,n}^2} \frac{1}{n_r} \frac{\omega}{\alpha_n^2} \tag{7.98}$$

It is seen that equations (7.90) and (7.98) differ by a factor of $\pi/2$. This is caused by the non-rigorous approximation procedure used for predicting p'_{n2} in equation (7.88) or (7.97). This can be overcome by replacing the half-power bandwidth $\omega \pm \omega\eta/2$ by the noise bandwidth $\omega \pm \pi\omega\eta/4$. In addition, the influence of the $\pi/2$ factor is expected to be insignificant when the induced effective damping value is small, e.g., for the higher-ordered modes of the source whose $\omega_{s,n}$ are usually very big.

Although the effective damping in the case of fuzzy attachments is given in a very simple form, it can hardly be used directly in practice due to the difficulty arising in estimating α_n^2 in equation (7.86). For beam/plate coupling cases, however, it is suggested

that the effective damping is estimated by assuming a locally reacting model as described in Chapter 5.

7.5.2 Comparison with the 'Resound' [1] and fuzzy theory [5-6]

In 'Resound' theory [1], the degrees of freedoms of a complex dynamic system are partitioned into a 'global' set and a 'local' set. The presence of the local modes acts to damp the global modes. As a result, the local degrees of freedom is considered to produce an effective loss factor of the form

$$\eta_n^{eff} \approx \frac{\pi\omega}{2}\sum_{r=1}^{N_S} j_{rnn}^2 v_r \tag{7.99}$$

In above equation N_S is the number of the subsystems contained in the complete system, v_r is the modal density of subsystem r, and $j_{rnn'}^2$ represents the average value of $j_{rnn'}^2(k)$ given by

$$j_{rnn'}^2(k) = \int_{V_r}\int_{V_r} \rho(\mathbf{x})\rho(\mathbf{x}')\phi_n^{gT}(\mathbf{x})R_r(\mathbf{x},\mathbf{x}',k)\phi_{n'}^{gT}(\mathbf{x}')d\mathbf{x}d\mathbf{x}' \tag{7.100}$$

$$R_r(\mathbf{x},\mathbf{x}',k) = \phi_{j(k,r)}^{l}(\mathbf{x})\phi_{j(k,r)}^{lT}(\mathbf{x}') \tag{7.101}$$

where k is the local mode of the subsystem r, and the symbol $j(k,r)$ is used to indicate the position of this mode in the total sequence of local mode shapes, $\phi_n^g(\mathbf{x})$ and $\phi_{j(k,r)}^{l}(\mathbf{x})$ are, respectively, the mass-normalized global and local modes. In equation (7.99), only $n = n'$ elements are involved. Equation (7.99) is extremely simple in form but there could be some difficulty involved in predicting the term $j_{rnn'}^2$.

In fuzzy theory of Ref. [5], a simplified model is considered. The master structure is taken as a rectangular plate in a rigid baffle, which faces an unbounded fluid medium on the external side. On the internal side is a fuzzy structure, consisting of a random array of point-attached spring-mass systems. The apparent damping (units of force per unit area divided by velocity) imposed on the master structure by the added fuzzy substructure can be simply approximated as

$$R_{F,appar} \approx \frac{\pi\omega^2}{2}\frac{d\bar{m}_F}{d\omega} \tag{7.102}$$

where $\bar{m}_F(\omega)$ is a smoothed-out total mass, per unit plate area, of all those attached oscillators which have their natural frequencies less than a given value ω.

In Ref. [6], the system considered consists of a large, rigid, and dissipationless mass M to which are attached N small sprung masses. A simple expression for the damping induced in a main structure by attached small sprung masses is given, by a relatively simple, deterministic derivation procedure, as

$$\eta = \frac{\pi}{2}\frac{m_0 f}{M} \tag{7.103}$$

where $m_0 df$ is the incremental mass of sprung masses resonating at frequencies between f and $f + df$.

It is seen that none of the above effective damping expressions are exactly agreed with each other, due to different model descriptions and simplifications/assumptions used in the approximating procedure. Despite of the differences in these expressions, however, they all indicate that the effective damping increases as frequency increases, and is independent of the internal damping of the fuzzy attachments.

7.6 SUMMARY

In this chapter a mode-based approach was presented for a general complex built-up system consisting of a long-wavelength source and a short-wavelength receiver. In summary the steps are as follows:

- The source and the receiver substructures are described in terms of their uncoupled natural modes, i.e., the modal properties of each individual substructure when it is separated from the other.
- The interface force distribution between the source and the receiver is decomposed into a complete set of orthogonal basis functions. In principle, the basis functions should meet the criteria of convenience, simplicity and accuracy.
- The equilibrium and compatibility boundary conditions at the interface are enforced in terms of the generalized interface coordinates.
- The dynamic response of the source/receiver system and the power transmitted to the receiver can then be determined in a simple manner.
- The mode-based approach is able to accommodate both deterministic and statistical models, in that a large flexible structure is described asymptotically as a simple standing wave model, for example. (Note that the assumption of a simple standing wave model requires that the interface positions are far away from the

boundaries of the given receiver structure so that the influences of the near field wave motions can be ignored.)

- The mode-based approach can be further extended to more general cases, where more than one type of wave motion may be involved, for example.

The dynamic interactions between a stiff source and a large flexible receiver were investigated, which were revealed as adding effective damping and effective mass to the dynamic properties of the source, arising from the presence of the receiver. Expressions were given, being the effective loss factor and effective mass to each individual mode of the source. Results are compared to those of 'Resound' and fuzzy structure theory, where a 'fuzzy'-like receiver structure was assumed. It was found that they agreed well on the key result that fuzzy attachments add damping to the master structure but this is independent of the loss factor of the attachments, although detailed results differed.

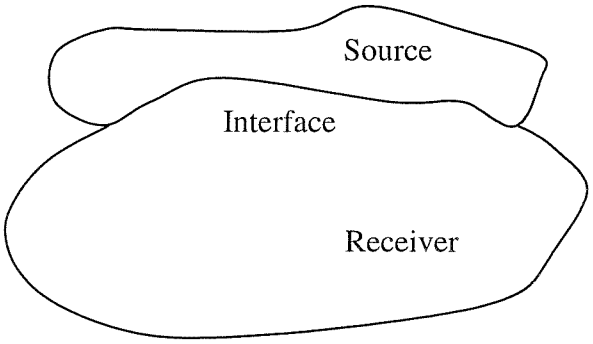

Figure 7.1 Illustration of a typical built-up structure.

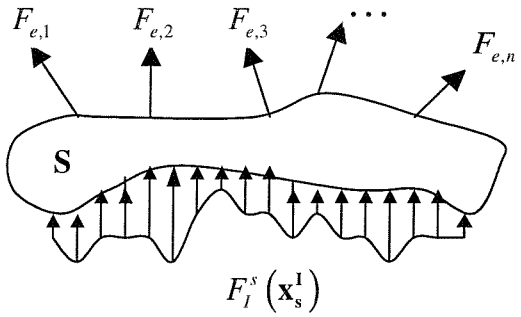

Figure 7.2 Dynamic illustration of the source.

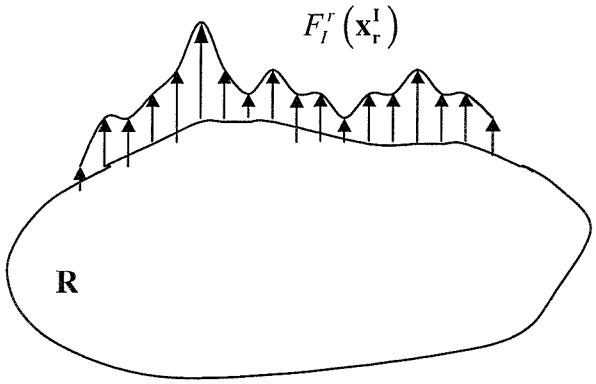

Figure 7.3 Dynamic illustration of the receiver.

Chapter 8

APPLICATION OF THE MODE-BASED APPROACH: NUMERICAL EXAMPLES OF BEAM/PLATE COUPLED SYSTEM

8.1 INTRODUCTION

In Chapter 7 a mode-based approach was presented to predict the mid-frequency vibration of complex built-up structures, in which a large number of physical DOFs of the system can be reduced into a relatively small number of generalised DOFs, and also an asymptotic simple standing wave model of the flexible substructure can be easily incorporated into the prediction procedure, instead of a deterministic description. Following the theoretical analysis, this chapter is intended to demonstrate the validity and efficiency of the mode-based approach by numerical examples, together with a comparison with the solutions based on the Mode/FT approach and the locally reacting impedance method. Being broadly representative of a structure with a broad mid-frequency range, the numerical models involved are beam-stiffened plates, as shown in Figure 8.1. The beam is relatively very stiff compared with the attached large plate. A point force of $F_0\delta(\mathbf{r}-\xi)$ is applied directly on the beam at a point of $\mathbf{r}=\xi$ ($\mathbf{r}$ is the local coordinates of the beam).

For completeness, the expressions for the vibration response of the coupled system from the mode-based approach, the Mode/FT approach and the locally reacting impedance method are briefly described in sections 8.2 and 8.3. Meanwhile, the close relations between these three approaches are discussed. Their corresponding effective mass and damping predictions are given in section 8.4. Numerical results follow in section 8.5. Two coupling situations are involved, one with a straight beam and the other with an L-shaped beam, as shown in Figures 8.2 and 8.3, respectively.

8.2 APPLICATION OF THE MODE-BASED APPROACH

For a beam-stiffened plate model as shown in Figure 8.1, the interface basis functions may be simply chosen as the set of beam mode functions, i.e.,

$$X_n(\mathbf{r}) = \Phi_n(\mathbf{r}) \tag{8.1}$$

In this case, X_n can most easily satisfy the criteria of convenience, simplicity and accuracy. As a result, the dynamic response of the coupled beam/plate system can be predicted by using the expressions given in section 7.3 of Chapter 7. Let

$$\mathbf{x}_I = \mathbf{x}_s^I = \mathbf{r} \tag{8.2}$$

Equations (8.1) and (8.2) yield

$$\mathbf{T}_s = \boldsymbol{\alpha}_s = \mathbf{I} \tag{8.3}$$

The force and displacement distributions $F_I(\mathbf{r})$ and $w_I(\mathbf{r})$, in equations (7.51) and (7.52), can then be simplified as

$$\mathbf{f}_{I,n} = \left[\mathbf{Y}_{s,n} + \mathbf{A}_r\right]^{-1} \mathbf{Y}_{s,n}\mathbf{f}_{e,n} \tag{8.4}$$

$$\mathbf{w}_{I,n} = \mathbf{A}_r\left[\mathbf{Y}_{s,n} + \mathbf{A}_r\right]^{-1} \mathbf{Y}_{s,n}\mathbf{f}_{e,n} \tag{8.5}$$

where the nth column element of modal force vector $\mathbf{f}_{e,n}$ is given by

$$f_{e,n} = F_0\Phi_n(\xi) \tag{8.6}$$

and the (n,n')th element of the dynamic modal correlation matrix $\mathbf{A}_r$ (equation (7.54)) is given by

$$A_{r,nn'} = \sum_m \alpha_{r,nm}\alpha_{r,n'm}Y_{r,m} \tag{8.7}$$

where

$$\alpha_{r,nm} = \int_{L_b} \Phi_n(\mathbf{r})\Psi_m(\mathbf{r})d\mathbf{r} \tag{8.8}$$

Equation (8.8) indicates the modal correlations between each individual mode of the beam and the plate due to the couplings. It is quite similar to form of a so-called 'modal correlation coefficient', which was given in [1] to describe the correlations between the local modes in a subsystem of interest. As a result, $\mathbf{A}_r$ is now equal to the dynamic modification matrix $\mathbf{Y}_{rs}^I$ (equation (7.64)), which reveals how the plate modal receptance and the mode-correlations between the beam and the plate act to modify the beam modal stiffness and furthermore the dynamic response of the beam.

Re-write equation (8.5) as

$$\mathbf{w}_{\mathrm{I,n}} = \left[\mathbf{Y}_{\mathrm{s,n}} + \mathbf{A}_{\mathrm{r}} - \mathbf{Y}_{\mathrm{s,n}}\right]\left[\mathbf{Y}_{\mathrm{s,n}} + \mathbf{A}_{\mathrm{r}}\right]^{-1} \mathbf{Y}_{\mathrm{s,n}}\mathbf{f}_{\mathrm{e,n}} \tag{8.9}$$

It follows that

$$\mathbf{w}_{\mathrm{I,n}} = \mathbf{Y}_{\mathrm{s,n}}\left[\mathbf{I} - \left(\mathbf{Y}_{\mathrm{s,n}} + \mathbf{A}_{\mathrm{r}}\right)^{-1} \mathbf{Y}_{\mathrm{s,n}}\right]\mathbf{f}_{\mathrm{e,n}} \tag{8.10}$$

Comparing to equation (7.57), it is seen that equation (8.10) is just the modal amplitudes $\mathbf{w}_{\mathrm{s,n}}$ of the beam, i.e.,

$$\mathbf{w}_{\mathrm{s,n}} = \mathbf{w}_{\mathrm{I,n}} \tag{8.11}$$

The beam displacement response at a general position $\mathbf{r}$ and the transmitted power to the receiver can then be determined, from equations (8.4) and (8.10), as

$$w_s(\mathbf{r}) = \sum_n \mathbf{w}_{\mathrm{s,n}} \Phi_n(\mathbf{r}) \tag{8.12}$$

$$P_{tr} = \frac{1}{2}\mathrm{Re}\left\{ j\omega \sum_n f_{I,n}^{*} w_{s,n} \right\} \tag{8.13}$$

The above two expressions can provide very precise solutions if the dynamic properties of both the beam and the plate are known exactly and also the numbers of the local modes of the beam and the plate used are big enough to meet the criterion of convergence [20].

8.2.1 Vibration approximation based on a simple-standing-wave plate model

As far as many practical plate-stiffened beam systems concerned, the plate receivers usually have very short-wavelength waves and high mode-counts, and also maybe possess some uncertainties in either the material properties or the boundary conditions or both. In this case an asymptotic description of the plate is more appropriated.

When the plate receiver is estimated by a simple standing wave model, from equation (7.79), the normalized mode shape functions can be written as

$$\Psi_{r,m}(\mathbf{x}_{\mathrm{r}}) \approx \frac{1}{\sqrt{m_r}}\left(\sqrt{\frac{2}{L_x^r}}\sin\frac{m_1\pi x}{L_x^r}\right)\left(\sqrt{\frac{2}{L_y^r}}\sin\frac{m_2\pi y}{L_y^r}\right) \tag{8.14}$$

where L_x^r and L_y^r are, respectively, the lengths used for the plate in the x- and y-directions, m_r is the mass per unit area of the plate, and the phase angles $\theta_{r,\kappa}$ are assumed to be zeros.

The corresponding natural frequencies can then be expressed as

$$\omega_{r,m} \approx \sqrt{\frac{D_r}{m_r}}\left[\left(\frac{m_1\pi}{L_x^r}\right)^2+\left(\frac{m_2\pi}{L_y^r}\right)^2\right] \tag{8.15}$$

Substituting equations (8.14) and (8.15) into (8.4) and (8.5), the vibration response of the couple beam/plate system can then be approximated in a simple manner.

The above analysis indicates that this mode-based approximate approach can be used to deal with the vibration of a general plate-stiffened beam, in that the shape of the beam structure of interest may be arbitrary and the complex geometry of the plate may be ignored.

8.3 APPLICATIONS OF THE MODE/FT APPROACH AND THE LOCALLY REACTING IMPEDANCE METHOD

Except for a simple standing wave model, a large flexible plate can also be simply described as a uniformly extended infinite [11, 47-48] and/or a locally reactive model. Consequently, the Mode/FT approach and locally reacting impedance method developed in Chapter 5 can be used very simply to provide approximate results for the vibrations of the beam-stiffened plate system. Since the Mode/FT approach was developed when the beam component was assumed to be straight and uniform, this may restrict its application to such coupling cases as shown in Figure 8.3.

Theoretically, these approximations have generally acceptable accuracy when the beam/plate system has a big dynamic mismatch (which could be either in terms of mobility or wavenumber or both), at least in a frequency average sense.

8.3.1 Vibration approximation based on an infinite plate model

When a straight and uniform beam is attached to a very flexible plate, as shown in Figure 8.2, the force and displacement distributions of the beam can be estimated, by the Mode/FT approach, as

$$f_{I,n} \approx \frac{Y_{s,n}}{Y_{s,n}+1/(j\omega Z_n)} f_{e,n}, \tag{8.16}$$

$$w_{s,n} \approx \frac{Y_{s,n}}{1+j\omega Y_{s,n} Z_n} f_{e,n} \tag{8.17}$$

where Z_n represents a modification value to the dynamic impedance of the nth mode of the beam by the presence of the plate, determined by the mode shape functions of the

beam $\Phi_{s,n}$ and the line dynamic stiffness of the plate $Z_p(k)$ in the wavenumber domain. These were given in equations (5.11) and (5.27). Then the FRF response of the stiff beam and the power transmitted to the plate can be estimated by substituting equations (8.16) and (8.17) into (8.12) and (8.13).

Comparing equation (8.17) with (8.5), it is seen that for a very flexible plate receiver, the dynamic modification matrix $\mathbf{A}_r$ can be regarded as diagonal such that

$$A_{r,nn} \approx \frac{1}{j\omega Z_n}, \; A_{r,nn'} \approx 0, (n \neq n') \tag{8.18}$$

Equation (8.18) indicates that the '*indirect*' dynamic modifications to each individual mode of the beam loaded by the plate modes are ignorable when the plate is very flexible. It implies, therefore, that the dynamic modification matrix $\mathbf{Y}_{rs}^{I}$ in equation (7.64) tends to be diagonal as the flexibility of the plate increases. This is in a good agreement with the assumption made in Chapter 7 for equation (7.67). Consequently, the dynamic response expressions derived by the mode-based approach can be simplified.

8.3.2 Vibration approximation based on a locally reacting plate model

Especially, when the plate receiver is relatively very flexible compared to the beam, i.e., the dynamic mismatch between the interface properties of the beam and the plate is big enough, the plate can be simply treated as a locally reacting model, where the plate-loaded dynamic stiffness modification to each individual mode of the beam Z_n can be taken as the same, being determined by only the plate properties of D_p and k_p, but regardless of the mode shape functions of the beam $\Phi_{s,n}$, as given in equation (5.46). This means that the dynamic modification matrix $\mathbf{Y}_{rs}^{I}$ in equation (7.64) tends to be diagonal and also each diagonal element value tends to be the same.

8.4 EFFECTIVE MASS AND DAMPING

It has been shown in the previous chapters that the dynamic interactions between a stiff beam and a flexible plate can be equivalently simulated as adding effective mass and damping to each mode of the beam.

By the mode-based approach (section 7.3.6.2 of Chapter 7), the effective non-dimensional mass and loss factor were given, respectively, as

$$m_n = \frac{D''_{n1}}{\omega^2} \tag{8.19}$$

$$\eta_n = \frac{D''_{n2}}{\omega^2_{s,n}} \tag{8.20}$$

where D''_{n1} and D''_{n2} depend on the model used for the plate receiver, given by

$$D''_{n1} = \frac{p''_{n1}}{p''^2_{n1} + p''^2_{n2}} \tag{8.21}$$

$$D''_{n2} = \frac{p''_{n2}}{p''^2_{n1} + p''^2_{n2}} \tag{8.22}$$

where

$$p''_{n1} = \sum_m \frac{\alpha^2_{r,nm}\left(\omega^2 - \omega^2_{r,m}\right)}{\left(\omega^2_{r,m} - \omega^2\right)^2 + \left(\omega^2_{r,m}\eta_r\right)^2} \tag{8.23}$$

$$p''_{n2} = \sum_m \frac{\alpha^2_{r,nm}\omega^2_{r,m}\eta_r}{\left(\omega^2_{r,m} - \omega^2\right)^2 + \left(\omega^2_{r,m}\eta_r\right)^2} \tag{8.24}$$

By the Mode/FT approach (section 5.2.4 of Chapter 5), these effective mass and damping can be written, respectively, as

$$D''_{n1} \approx \frac{1}{2\pi}\int_{-k_p}^{-k_p} \left|\Phi_{s,n}(k)\right|^2 \left[2D_p\left(k_p^2 - k^2\right)\sqrt{k_p^2 + k^2}\right] dk \tag{8.25}$$

$$D''_{n2} \approx \frac{1}{2\pi}\int_{-k_p}^{-k_p} \left|\Phi_{s,n}(k)\right|^2 \left[2D_p\left(k_p^2 + k^2\right)\sqrt{k_p^2 - k^2}\right] dk \tag{8.26}$$

Here, $\Phi_{s,n}(k)$ corresponds to the Fourier Transform of the mass-normalised mode shape function of the beam. Therefore, equations (8.25) and (8.26) are a little different from (5.36) and (5.37). In equation (8.25) the integral terms in $\left(-\infty, -k_p\right)$ and in $\left(k_p, +\infty\right)$ have been ignored due to $\left|\Phi_{s,n}(k)\right| \to 0$ in these two wavenumber ranges.

By the locally reacting method (section 5.3.1 of Chapter 5), equations (8.25) and (8.26) become

$$D''_{n1} = D''_{n2} = \frac{2k_p^3 D_p}{m_b} = \frac{2m_p\omega^2}{m_b k_p} \tag{8.27}$$

Physically, the 'dissipated' power by the effective damping represents the power transmitted from the beam to the plate, and the effective mass modifies the dynamic response of the beam.

When the plate receiver is so flexible that it can be taken as a fuzzy attachment to the vibration of the beam, the effective loss factor and effective mass can be simply estimated by substituting equation (8.27) into (8.19) and (8.20). Under such circumstances, the effective loss factor depends on the mass density and the wavenumber of the plate regardless of the internal damping of the plate, while the effective mass can be neglected due to $m_n \approx 2m_p/(m_b k_p)$.

8.5 NUMERICAL RESULTS

Given the above solutions, numerical investigations are performed into beam/plate coupling models. In the first instance, the source beam concerned is straight, and then L-shaped, as shown in Figures 8.2 and 8.3, respectively. Calculations are made by the mode-based approach, the Mode/FT approach and locally reacting impedance method, respectively, for both the point-mobility of the beam and the power transmitted to the plate. These results are then compared with those of the conventional FRF-based sub-structuring method. The calculated results for the effective mass and damping by using these three newly developed approaches are also compared and discussed.

All the numerical models concerned here are of perspex, the material properties being given in Table 2.1. All the beam models and the plate models involved are simply supported. (The natural frequencies and mode shapes of the L-shaped beam are given in Appendix VI. Those for a simply supported beam and a simply supported rectangular plate have been given in Appendix I and II.) The dimensions and the coupling positions of the beam/plate models of Figures 8.2 and 8.3 are respectively given in Tables 8.1 and 8.2. For both coupling cases, the plate thickness and the plate material loss factor are varied, so as to indicate how the flexibility and the material damping of the receiver can affect the accuracy and efficiency of the predictions of the mode-based approach. In the calculation the first 20 modes of the beam models are included, while for the plate models, the numbers of the modes involved are 1500, 2400 and 4800, respectively, corresponding to $h_p = 0.010$ m, 0.005m and 0.002m.

The relevant modal overlap factors ($MOF = n\omega\eta$) of the beam and the plate models (corresponding to a loss factor of 0.05) are given in Figure 8.4. (Note that the modal

overlap factors of the straight- and L-shaped beams are actually very close to each other for the cases concerned here.) It is seen that the beams have much lower modal overlap than the plates. Therefore, the assembled system can be taken as dominated by typical mid-frequency vibration in very broad range of frequency.

8.5.1 Straight beam cases

For the numerical model given in Figure 8.2, Figures 8.5-8.10 compare the predicted results for the point-mobility (at the driving point) of the beam and power transmitted to the plate, when the plate thicknesses are 0.010m, 0.005m and 0.002, respectively.

It is found that the mode-based analytical results are almost the same as those of the FRF-based sub-structuring method, but the former cost much lower than the latter. For example, when the plate thickness is 0.005m ($k_p/k_b = 3.5$), the computational cost of the mode-based analytical method was only about one thirtieth of that of the FRF-based sub-structuring method. When the plate thickness is 0.002m ($k_p/k_b = 5.6$), this computational cost ratio decreased to one fiftieth. The main reason is that the former can reduce the large number of physical DOFs of the coupling system into a relatively small number of generalized interface DOFs by using an interface decomposition technique. This advantage is particularly significant when the plate has very short-wavelengths (in which case the DOFs required by conventional FRF method can be increased to an incredibly large number). The results corresponding to the Mode/FT method and locally reacting impedance method are also shown in Figures 8.5-8.10. It is seen that both of them can be used to predict in a simple way the frequency-averaged response of the system. Especially when $k_p/k_b >> 2$ (e.g. $k_p/k_b = 5.6$), the locally reacting impedance method is the most attractive to provide very good predictions as shown in Figures 8.7 and 8.10, where the results of Mode/FT method and locally reacting method are indistinguishable.

It is also found that the frequencies at which the maximum dynamic response (of the beam) and the power transmitted (to the plate) occur tend to be around both the resonance of beam $\omega_{s,n}$ and the resonances of the plate $\omega_{r,m}$ at which the modal correlation function α_{nm} (between the nth mode of the beam and the mth mode of the plate) happens to be a maximum. However, when there exists $\alpha_{nm} \approx 0$ corresponding to $\omega_{r,m}$, both the dynamic response of the beam and the power transmitted to the plate tend to be their minimum at these resonance frequencies.

Figures 8.11 compares the point-mobility values at the driving point of the beam before and after it is attached to different plate models. It is seen that the vibration pattern of the beam has been changed by the presence of the plate in that the resonance frequencies are shifted and at the same time the peak amplitudes of the FRF responses are reduced compared with those of the unloaded beam component. These may be explained by the concepts of 'effective mass' and 'effective damping' induced on the beam by the presence of the plate. It is also observed that the influences of the plate on the vibration pattern of the beam decrease as frequency and/or the plate flexibility increase. This trend is also reflected by such a phenomena that when the plate is very flexible compared with the beam, the main broad features of the response spectra are largely controlled by the stiff beam while only the small 'wrinkles' on these spectra are sensitive to the exact properties of the plate. This implies that the dynamic interactions between the beam and the plate decrease as the dynamic mismatch of the coupled system increases. When the plate receiver is much more flexible than the beam (e.g. $k_p/k_b = 5.6$), the plate can be taken as adding only effective damping to the beam. In this case, the plate can actually be taken as a fuzzy-like attachment to the beam vibration [1-2, 5-6].

Figures 8.12-8.17 show the effective loss factor and dimensionless effective mass induced to the first three orders of the beam modes when the flexibility of the plate attached is varied, expressions being given in equations (8.21)-(8.24). Three general trends can be found: first, for lower orders of the beam modes, the effective mass and damping added are larger; second, the effective damping in a given mode increases as frequency increases whereas the effective mass decreases against frequency; and third, when the plate is much more flexible than the beam, the effective mass loaded to the beam can almost be taken as zero. Consequently, the influences of the plate on the vibration of the beam can be taken as loading effective damping only, as expected. The individual peak values of the effective mass and loss factor occur at the frequencies which are close to the natural frequencies of the plate, but also where the modal correlation functions between the beam mode and the corresponding plate modes happen to be minimum. This indicates that the positions of these peaks depend on the modal properties of the plate, the coupling position on the plate, and the beam mode shape functions, but are independent of the other properties of the beam

Moreover, the results corresponding to equations (8.25) and (8.26) are shown in Figures 8.12-8.15, and those corresponding to equation (8.27) are shown in Figures 8.16-8.17. It is seen from Figures 8.12-8.15 that the frequency average values of the effective

damping and mass can be simply predicted by assuming the plate as an infinite model. When the plate behaves as a fuzzy-like attachment, as shown in Figures 8.16-8.17, the effective damping and mass can be even more simply estimated by assuming the plate as a locally reacting model.

Figures 8.18-8.23 compare the effective mass and loss factors induced to the first beam mode when the loss factor of the plate is varied between 0.01, 0.05 and 0.1 in the cases of $k_p/k_b = 2.5$, 3.5 and 5.6, respectively. It is quite obvious that as the loss factor (and thus the modal overlap factor) of the plate increases, the effective mass and damping induced tend to be closer to the results of an extended infinite plate (i.e., the modal overlap factor of the plate $MOF_p = \infty$), which just corresponds to the frequency averaged effective mass/damping. This observation implies that the induced damping and mass tend to be independent of the internal damping of the plate in terms of their frequency average level. Especially when the modal overlap of the plate is very high, so that it behaves like an infinite structure, e.g. the case shown in Figures 8.20 and 8.23, the effective loss factor can be reasonably treated as independent of the internal damping of the plate while the effective mass can be ignored.

8.3.2 L-shaped beam cases

The same numerical investigations are made for the model shown in Figure 8.3 as those for the one of Figure 8.2. The mode shape functions of the simply supported L-shaped beam are given in the Appendix VI, one rigid mode being included. It is assumed that the beam applies no torsional constraints to the plate, due to the fact that the main coupling interactions between the beam and the plate are in bending motions. However, more general cases, which may consist of more than one type of wave motion, can still be accommodated within the same approach.

Figures 8.24-8.29 compare the results of different methods for the point mobility of the beam (at the driving point) and the power transmitted to the plate, where the plate thicknesses are respectively 0.010m, 0.005m and 0.002m (i.e., $k_p/k_b = 2.4$, 3.5 and 5.6). It is seen that the results of the mode-based analytical method and the FRF-based sub-structuring method tend to agree well as frequency increases and/or the plate flexibility increases, although relatively big differences can be observed at the low frequency region and/or where the plate receiver is not very flexible compared with the source beam (i.e., $k_p/k_b = 2.4$). These differences may be caused by the errors arising from the choice of the

basis functions and the limited numbers used for the interface decomposition, in which case, the mode-based 'analytical' approach may actually provide an 'approximate' solution.

It is known that the dynamic interactions between a beam and a plate decrease as the dynamic mismatch of the system increases. As a result, the system response tends to be less affected by the interface when the plate is relatively very flexible compared with the beam. With this in mind, it is reasonable to expect that such kind of basis-function-associated errors may only be significant when the frequency of interest is low and/or the plate is not very flexible compared with the beam. This can explain well the trend in Figures 8.24-8.29, i.e., the mode-based results and the FRF-based ones get closer as the flexibility of the plate increases. From the relatively bigger differences (or errors) observed in Figures 8.24-8.29 than in Figures 8.5-8.10, however, it can be reasonably expected that the interface dynamic distribution along the L-shaped beam is a little more complex than that along the straight-shaped beam.

The choice of the basis interface functions (used for interface decomposition) is, therefore, closely related to the performance of the mode-based approach, especially when the dynamic interactions between the beam and the plate are relatively strong, e.g. the case of $k_p/k_b = 2.4$. In principle, the mode shape functions of the source structure may be simply taken as the set of basis functions, where the loading effects of the receiver on the source is not very strong, such that the presence of the receiver cannot greatly change the vibration behaviour of the source, but a somewhat modification.

Figures 8.24-8.29 also compare the results when the plate receivers are described, respectively, as a 'different' simple standing wave model and a locally reacting model, where the so-called 'different' wave model is realized by extending the dimensions of the plate to 3m in the $x-$direction and 2m in the $y-$direction, but keeping the other conditions of the system unchanged. It is seen that the results corresponding to the assumed 'large' plates are quite close to those corresponding to the true plates for all the three cases of interest. This can be explained by such a fact that the dynamic properties of a flexible structure tend to those of a uniformly extended infinite structure. As a result, neither the dimensions nor the boundary conditions of the plate are important for determining the vibration response of a stiff beam/flexible plate system. Under such circumstances, therefore, it is reasonable to describe a large flexible receiver structure as a simple standing wave model. Consequently, the mode-based approach can be used to provide a fairly good approximation for both the FRF response of the beam and the power

transmitted to the plate, at least in frequency average level. The results corresponding to locally reacting plate models are found suitable for the predictions of FRFs of the beam, as shown in Figures 8.24-8.26. For the power transmitted to the plates, however, it might be only useful for rough frequency average predictions, unless the plate receiver is much more flexible than the beam, as shown in Figure 8.29.

Figure 8.30 compares the point mobility results of the beam before and after coupling with the plate when $k_p/k_b = 2.4$, 3.3 and 5.3, respectively. This is quite similar to Figure 8.11 in how the flexibility of the plate can affect the vibration pattern of the beam. Again the plate can be taken as a sort of fuzzy-like attachment of the beam structure in the case of $k_p/k_b = 5.3$.

Figures 8.31-8.36 show the effective dimensionless mass and loss factor induced to the first three elastic modes of the beam, when $k_p/k_b = 2.4$, 3.3 and 5.3, respectively. (The rigid mode of the 'unloaded' beam is now taken as substantially 'supressed', since the induced effective damping to this mode tends to be infinity from equation (8.20).) The same trends are observed as those found in the straight beam case in Figures 8.12-8.17. The results corresponding to the assumed large plate models (i.e., extended to 3m in the $x-$direction and 2m in the $y-$direction) as well as locally reacting plate models are also given in Figures 8.31-8.36. It is seen that as the plate gets more flexible, the exact dimensions of the plate tend to be less important to the effective mass/damping of the beam, as expected. However, the locally reacting solutions (equations (8.27)) in the case of the L-beam seem only applicable to predict roughly the broadband frequency average of the effective mass/damping, even for the case of $k_p/k_b = 5.3$. The main reason is that the L-beam is located a little closer to the boundaries of the plate, especially the beam part along the $x-$direction which only has a distance of 0.13m to one edge of the plate. (This distance is equivalent to the wavelength of the 0.002m thick plate at frequency 453Hz, or the wavelength of the 0.005m thick plate at frequency of 1133Hz.) Figure 8.37 then gives the effective damping results when the L-beam is attached to a large $3\times2\times0.002m^3$ plate where $x_1 = 1\text{m}$ and $y_1 = 0.8\text{m}$. It is seen that agreements between the two sets of results (mode-based and locally reacting) are substantially improved. This reveals that the assumption of a simple standing wave model is only valid when the source structure is far from the boundaries of the receiver.

Investigations have also been made for the influences of the internal damping of the plate on the effective mass/damping of the L-beam. Similar trends are observed as those of the straight beam. For brevity the relevant figures are not given here.

8.4 SUMMARY

In this chapter the mode-based approach was applied to predicting the vibrations of plate-stiffened beam systems. The set of beam modes were chosen as the basis functions used for interface decomposition. Consequently, the dynamic response of the coupled beam and the power transmitted to the plate can then be expressed in terms of unloaded modal properties of the beam and the plate as well as the modal correlation matrix between them. Numerical examples were given where both a straight- and an L-shaped beam were considered. The predicted results were given for both the point-mobility of the beam and the power transmitted to the plate and comparisons were made with the exact results determined by the conventional FRF-based sub-structuring method. Very good agreements were observed between the two sets of results.

Three approximate techniques were applied to describe the large and flexible plate models, i.e., simple standing wave models, infinite models and locally reacting models. (Note that the assumption of a simple standing wave model requires that the interface positions are far away from the boundaries of the given receiver structure so that the influences of the near field wave motions can be ignored.) Predictions for the vibration response of a stiff beam/flexible plate system were then made, respectively, by the mode-based approach, Mode/FT approach and locally reacting impedance approach.

Comparisons showed that both the Mode/FT and the locally reacting impedance methods were quite useful for straight beam coupling cases, whereas for the L-beam coupling cases, the mode-based approach was more appropriate. However, the locally reacting impedance method may still be quite useful when the plate receiver is very flexible compared with the source beam, as in this case the dynamic interactions between the beam and the plate are not very significant.

Furthermore, the effective mass and damping added to the beam models were investigated. For both the straight and L-shaped beam cases, three general trends were observed: (1) the lower the orders the beam modes are, the greater is the effective mass/damping added; (2) the effective damping for a given mode increases as frequency increases whereas the effective mass decreases against frequency; and (3) when the plate is much more flexible than the beam so that it behaves as a fuzzy-like attachment, the

plate can be taken as loading only effective damping to the beam whereas the effective mass can be neglected. Also it was found that the induced effective mass/damping values tend to be independent of the internal damping of the plate in a frequency average sense. Especially when the modal overlap of the plate is very high, so that it behaves like an infinite structure, the effective loss factor can be reasonably treated as independent of the internal damping of the plate while the effective mass can be ignored.

Table 8.1 System dimensions and coupling positions of Figure 8.2

Structure	**Beam**	**Plate**
Dimensions (m)	Length $L_b = 2$, Width $t_b = 0.059$, Height $h_b = 0.068$.	Length $L_x^{(p)} = 2$, Width $L_y^{(p)} = 0.9$, Thickness $h_p = 0.010/0.005/0.002$.
Coupling positions (m)	$x_1 = 0.03$, $y_1 = 0.3$, $\theta = 10^\circ$. $x_2 = x_1 + L_b \cos\theta$, $y_2 = y_1 + L_b \sin\theta$	
Driving point (m)	$\xi = 0.73$	
Wavenumber ratio	$k_p / k_b = 2.5/3.5/5.6$	

Table 8.2 System dimensions and coupling positions of Figure 8.3

Structure	**Beam**	**Plate**
Dimensions (m)	Length $L_x^{(b)} = 1.31$, Length $L_y^b = 0.69$, Width $t_b = 0.060$, Height $h_b = 0.060$.	Length $L_x^{(p)} = 2$, Width $L_y^{(p)} = 0.9$, Thickness $h_p = 0.010/0.005/0.002$.
Coupling positions (m)	$x_1 = 0.27$, $y_1 = 0.13$.	
Driving point (m)	$\xi = 0.22$	
Wavenumber ratio	$k_p / k_b = 2.4/3.3/5.3$	

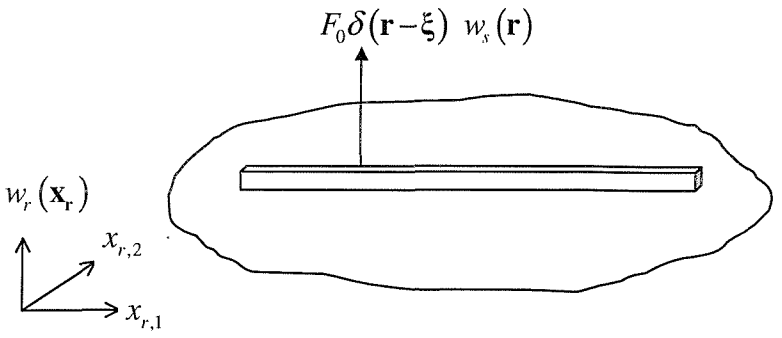

Figure 8.1 Beam-stiffened plate model.

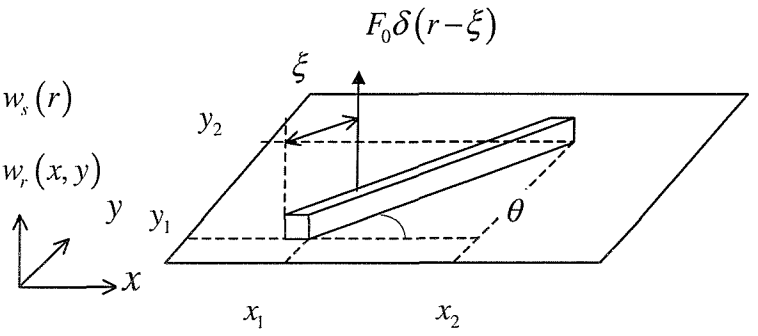

Figure 8.2 Straight beam and plate model.

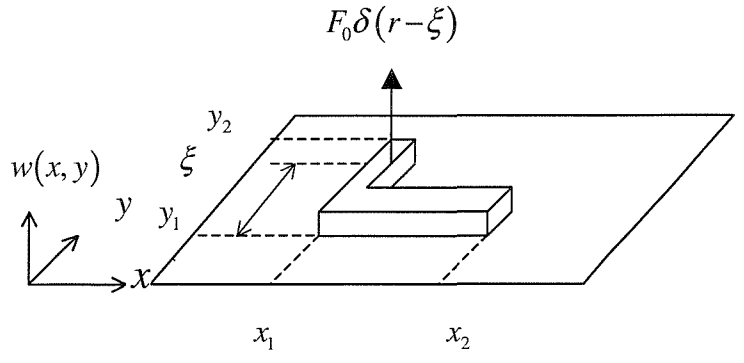

Figure 8.3 L-shaped beam and plate model.

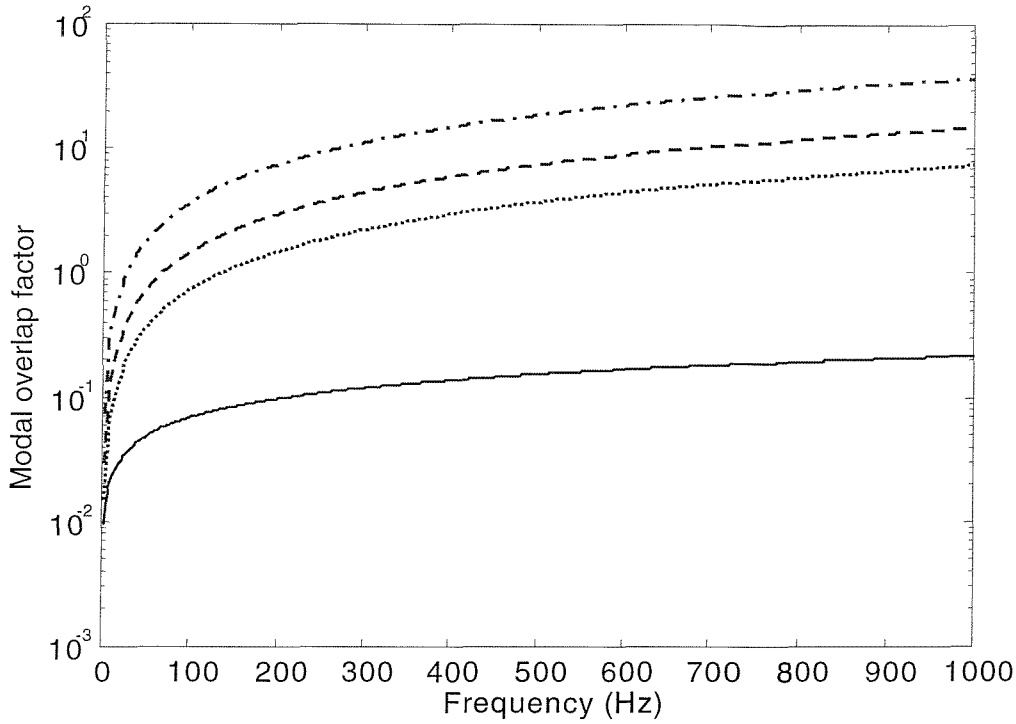

Figure 8.4 Modal overlap factors of the beam and the plate when the system material loss factor is 0.05: beam (——), plate (..... 0.010m thick, - - - 0.005m thick, - · - 0.002m thick).

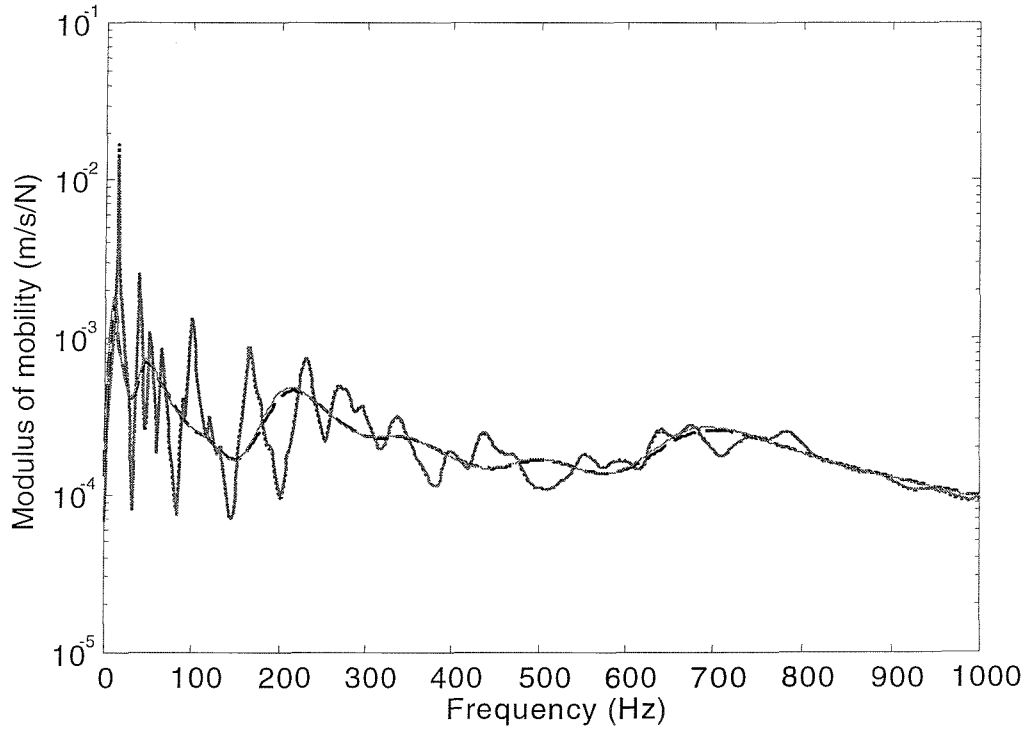

Figure 8.5 Point mobility of the beam at the excitation point when the plate thickness is 0.010m: mode-based (——), exact (·····), Mode/FT (— —) and locally reacting method (——).

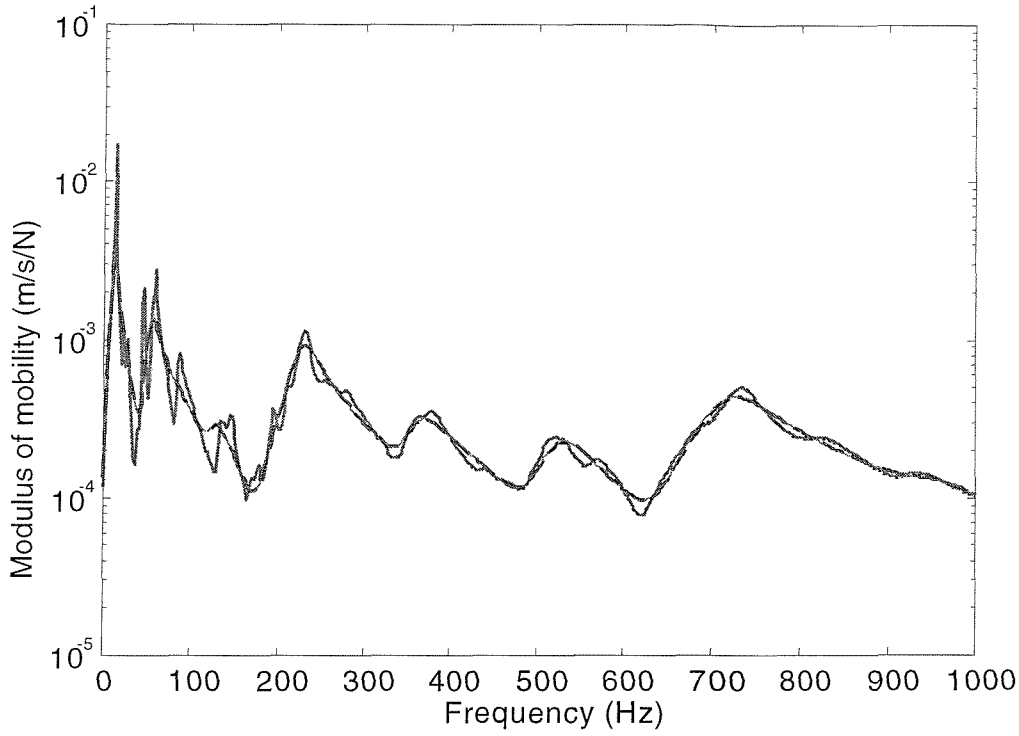

Figure 8.6 Point mobility of the beam at the excitation point when the plate thickness is 0.005m: mode-based (——), exact (.....), Mode/FT (— —) and locally reacting method (——).

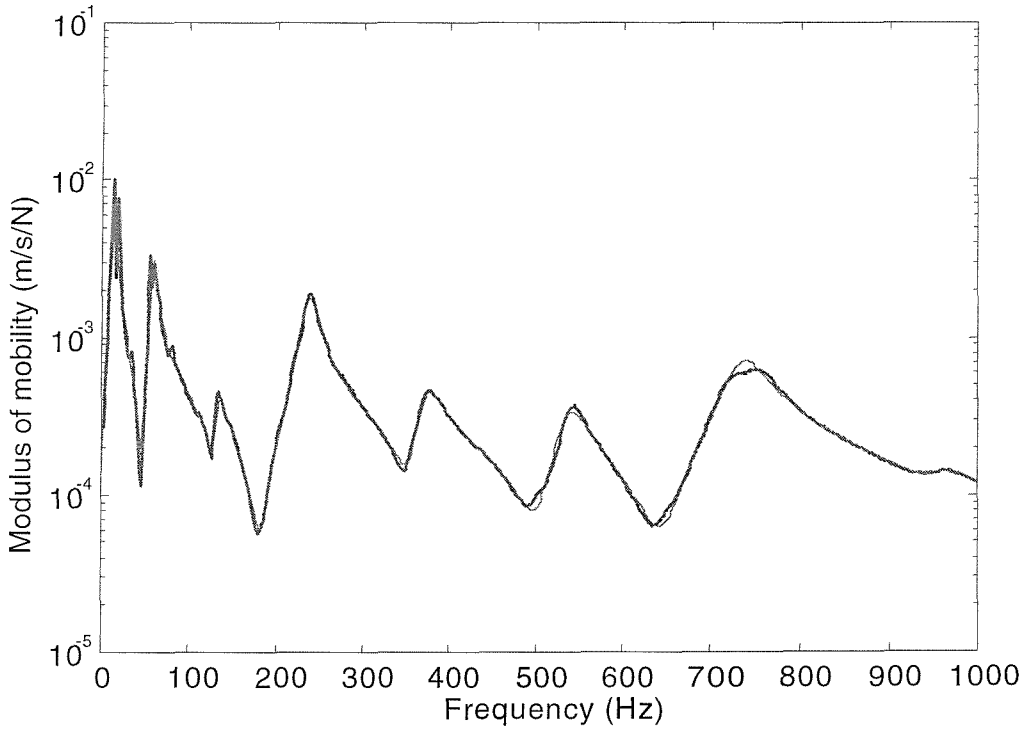

Figure 8.7 Point mobility of the beam at the excitation point when the plate thickness is 0.002m: mode-based (——), exact (.....), Mode/FT (— —) and locally reacting method (——).

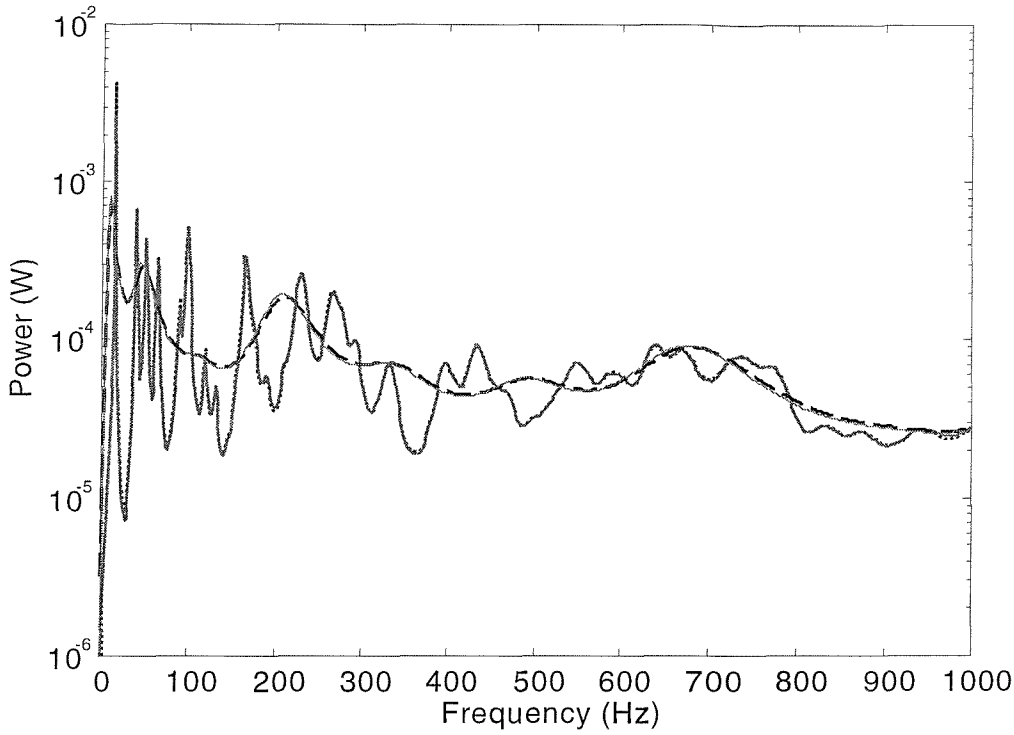

Figure 8.8 Power transmitted to the plate when the plate thickness is 0.010m: mode-based (——), exact (.....), Mode/FT (— —) and locally reacting method (——).

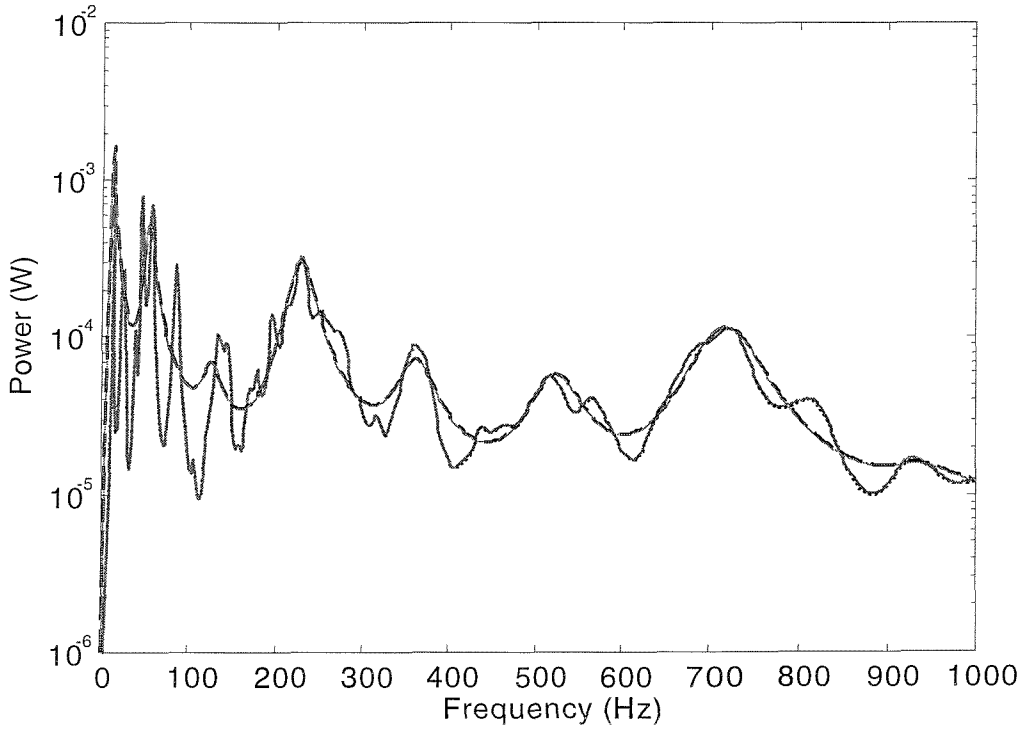

Figure 8.9 Power transmitted to the plate when the plate thickness is 0.005m: mode-based (——), exact (.....), Mode/FT (— —) and locally reacting method (——).

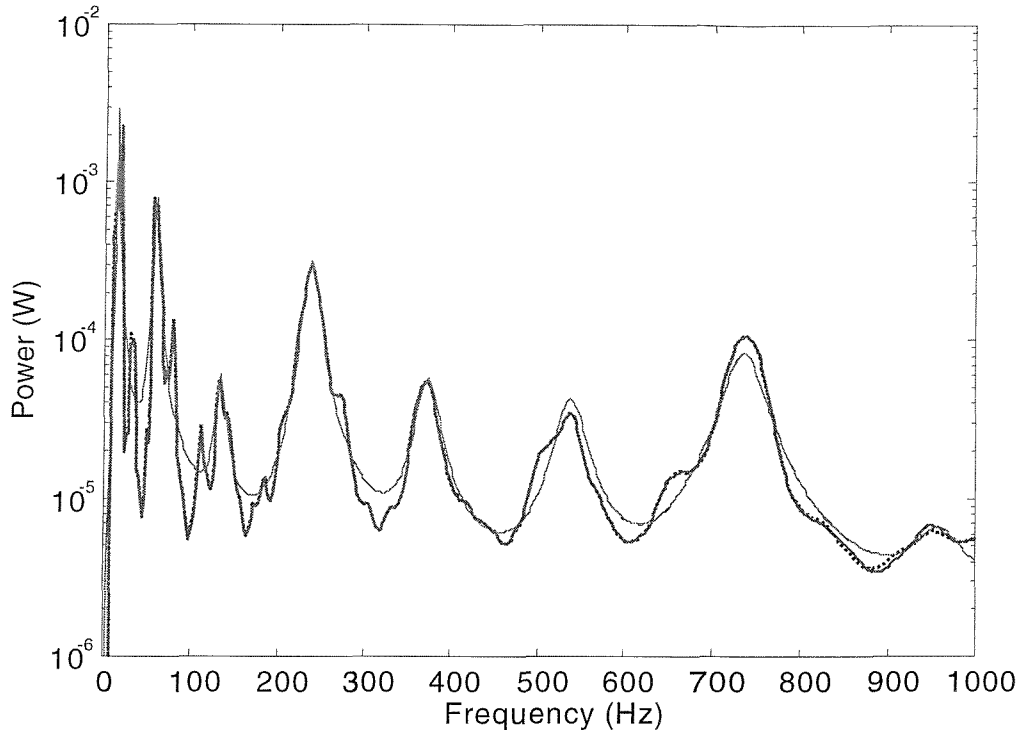

Figure 8.10 Power transmitted to the plate when the plate thickness is 0.002m: mode-based (——), exact (·····), Mode/FT (— —) and locally reacting method (——).

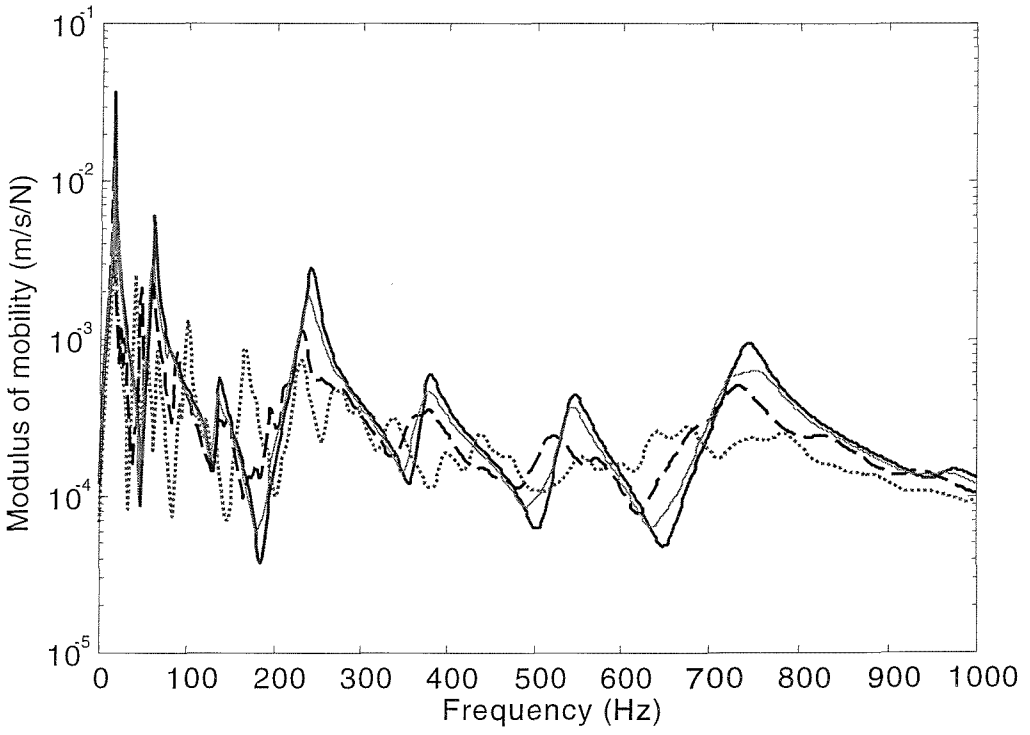

Figure 8.11 Point mobility results of the beam at the excitation point: before coupling (——), after coupling (····· , 0.010m thick plate; - - - , 0.005 thick plate; ____ , 0.002m thick plate).

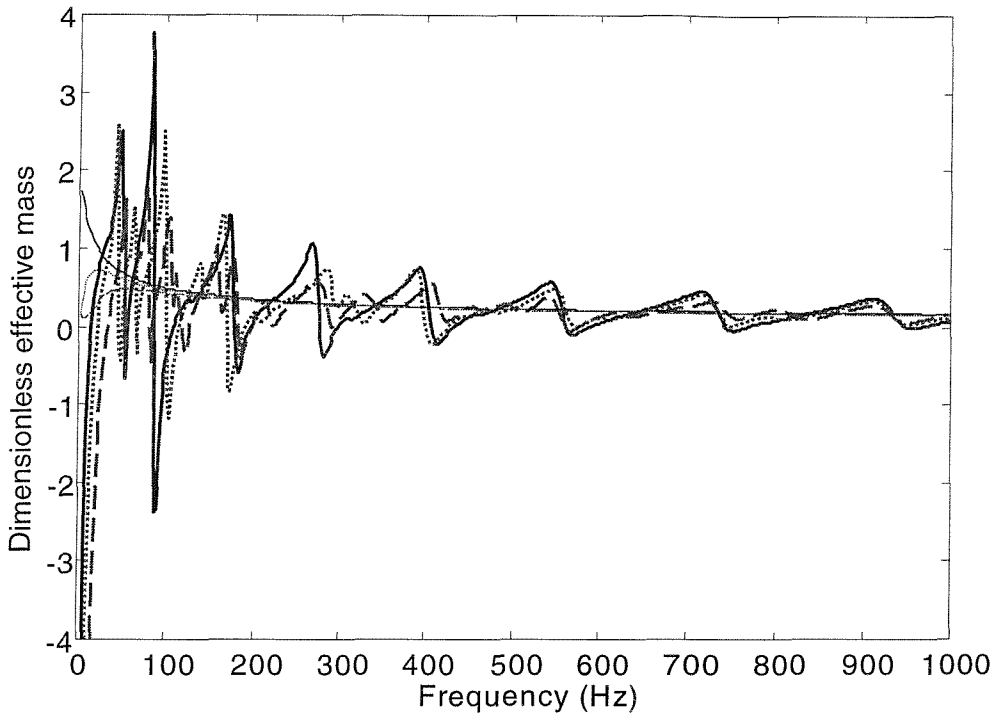

Figure 8.12 Dimensionless effective mass added to the first three modes of the beam ($k_p/k_b = 2.5$): 1st mode (equations (8.21-8.24) ____, equation (8.25) ____); 2nd (equations (8.21-8.24)..... , equation (8.25) .....); 3rd (equations (8.21-8.24) - - - , equation (8.25) -----).

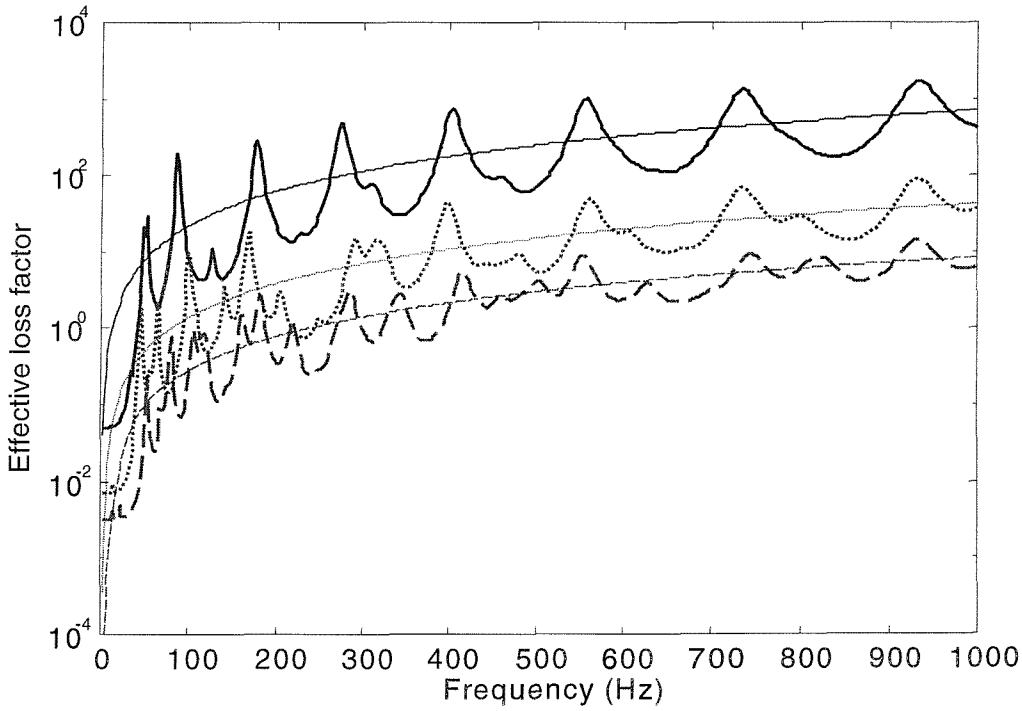

Figure 8.13 Effective loss factor added to the first three modes of the beam ($k_p/k_b = 2.5$): 1st (equations (8.21-8.24) ____, equation (8.26) ____) ; 2nd (equations (8.21-8.24) ..... , equation (8.26) .....); 3rd (equations (8.21-8.24) - - -, equation (8.26)-----).

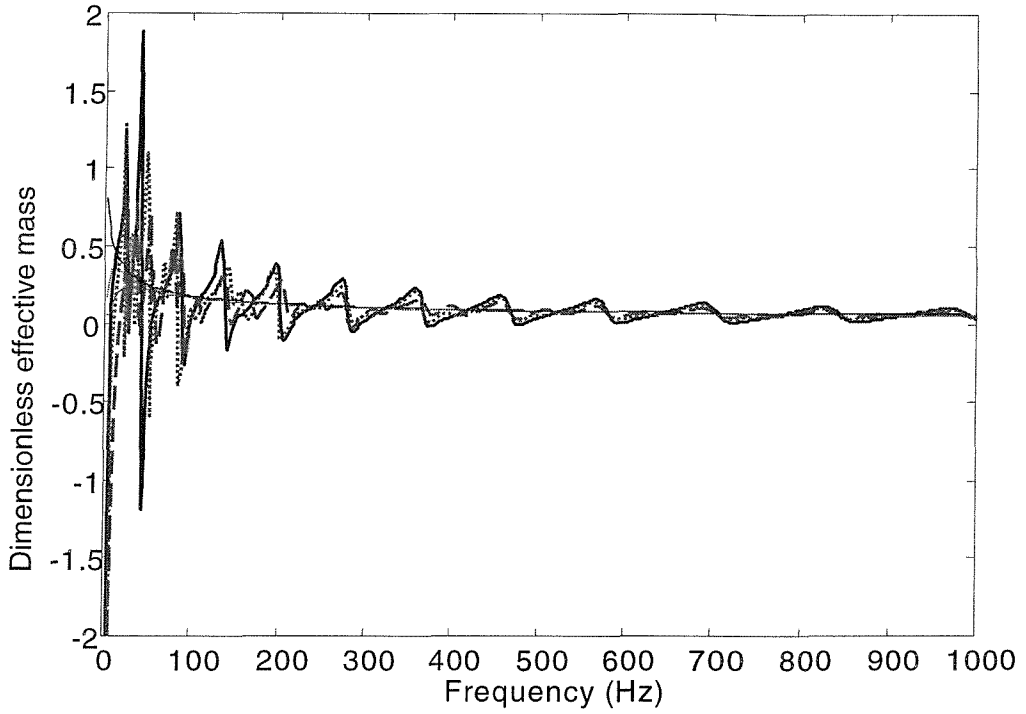

Figure 8.14 Dimensionless effective mass added to the first three modes of the beam ($k_p/k_b = 3.5$): 1st mode (equations (8.21-8.24) ____, equation (8.25) .....); 2nd (equations (8.21-8.24)..... , equation (8.25) ____); 3rd (equations (8.21-8.24) - - - , equation (8.25) -----).

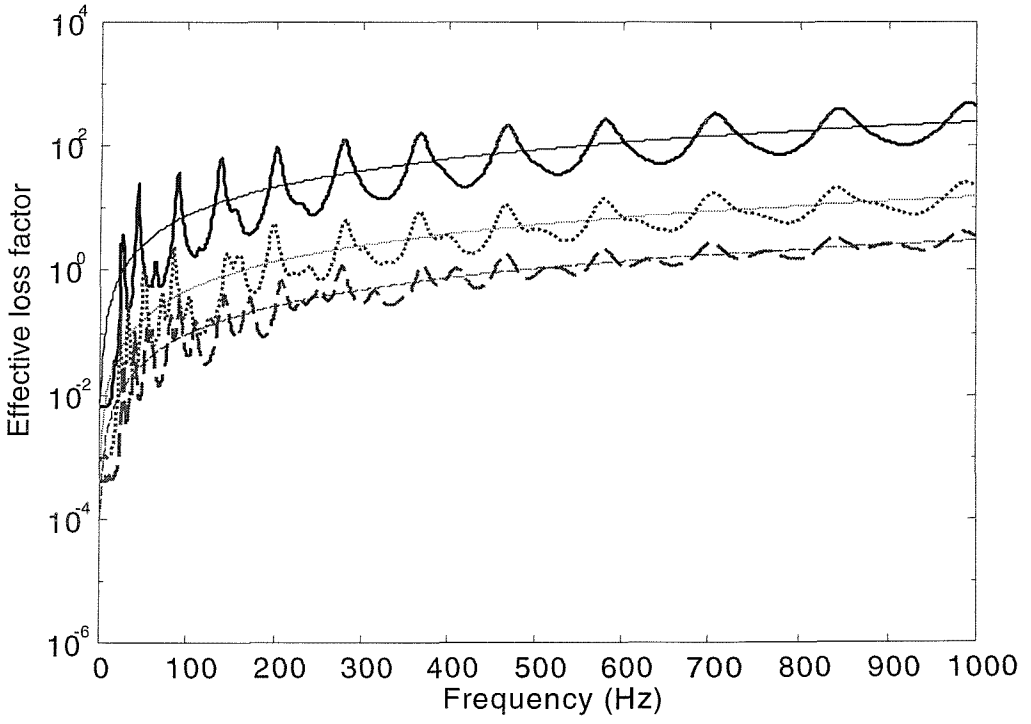

Figure 8.15 Effective loss factor added to the first three modes of the beam ($k_p/k_b = 3.5$): 1st (equations (8.21-8.24) ____, equation (8.26) ____) ; 2nd (equations (8.21-8.24) ..... , equation (8.26) ____); 3rd (equations (8.21-8.24) - - -, equation (8.26)-----).

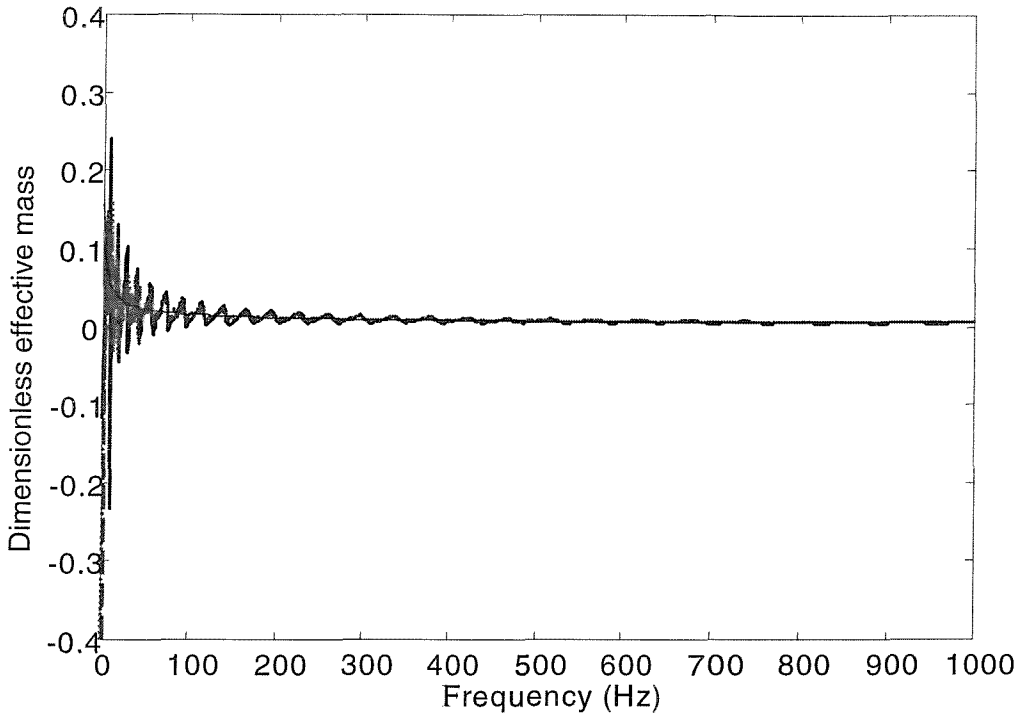

Figure 8.16 Dimensionless effective mass added to the first three modes of the beam ($k_p/k_b = 5.6$): 1st mode (equations (8.21-8.24) ____, equation (8.27) .....); 2nd (equations (8.21-8.24)..... , equation (8.27) ____); 3rd (equations (8.21-8.24) - - - , equation (8.27) -----·).

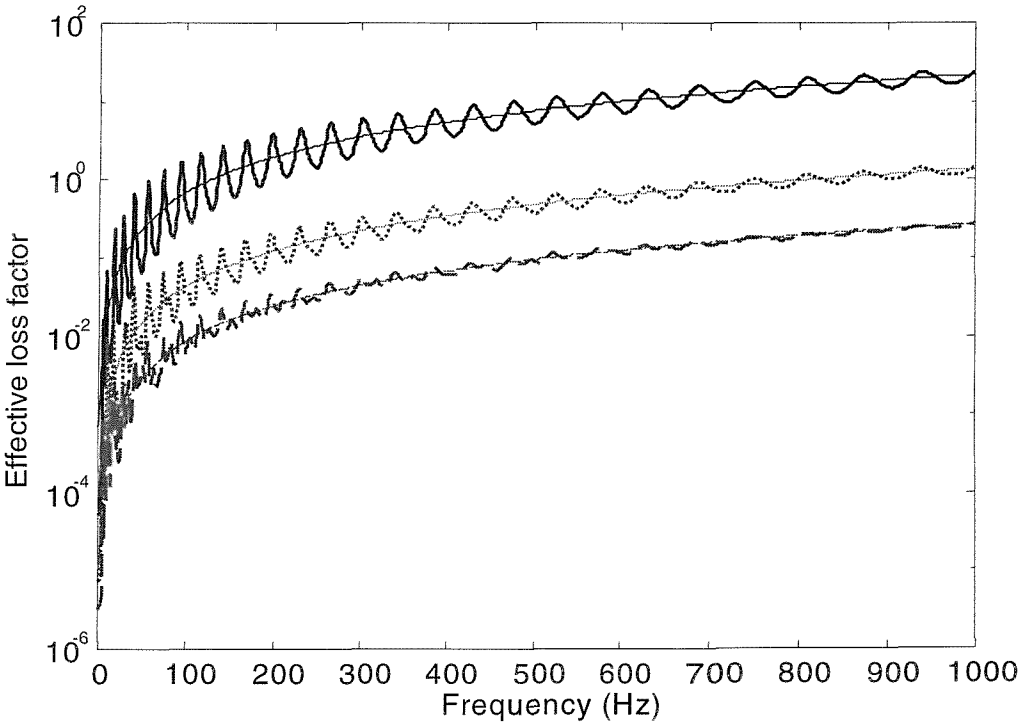

Figure 8.17 Effective loss factor added to the first three modes of the beam ($k_p/k_b = 5.6$): 1st (equations (8.21-8.24) ____, equation (8.27) ____) ; 2nd (equations (8.21-8.24) ..... , equation (8.27) ____); 3rd (equations (8.21-8.24) - - -, equation (8.27)-----·).

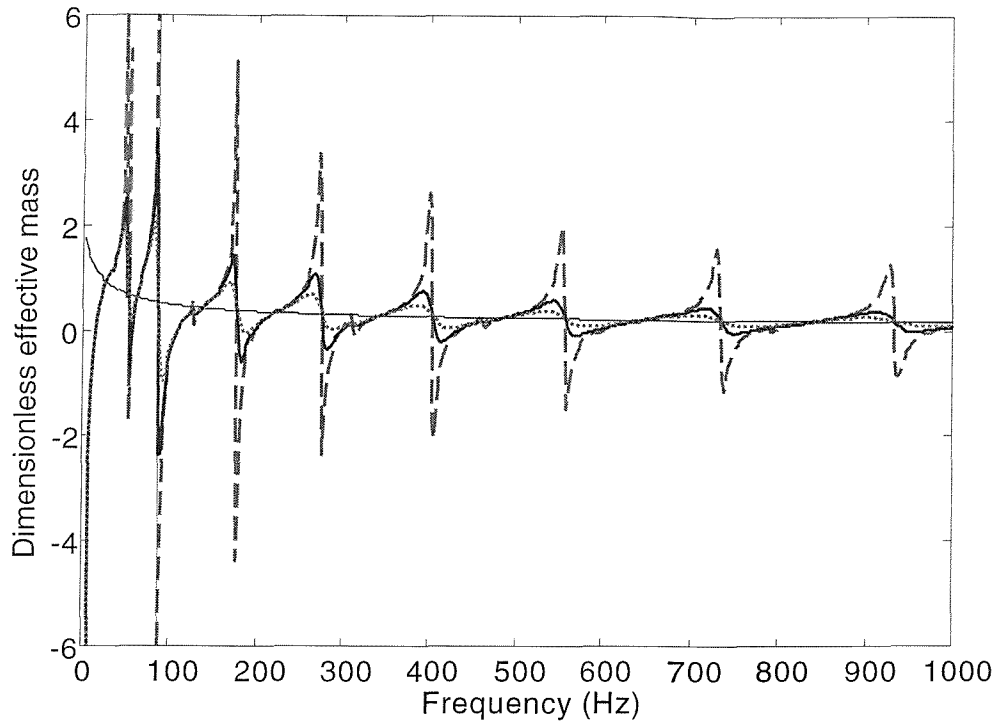

Figure 8.18 Dimensionless effective mass added to the first mode of the beam ($k_p/k_b = 2.5$): $\eta_p = 0.01$, _ _ _ ; $\eta_p = 0.05$, ____ ; $\eta_p = 0.1$, ...; $MOF_p = \infty$, ____ .

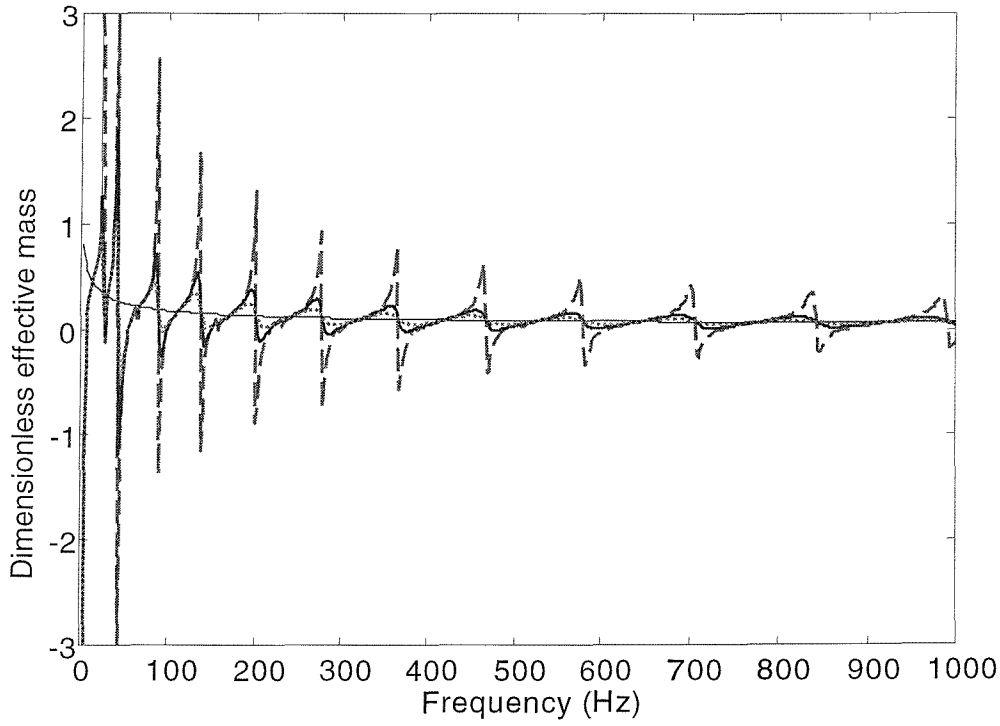

Figure 8.19 Dimensionless effective mass added to the first mode of the beam ($k_p/k_b = 3.5$): $\eta_p = 0.01$, _ _ _ ; $\eta_p = 0.05$, ____ ; $\eta_p = 0.1$, ...; $MOF_p = \infty$, ____ .

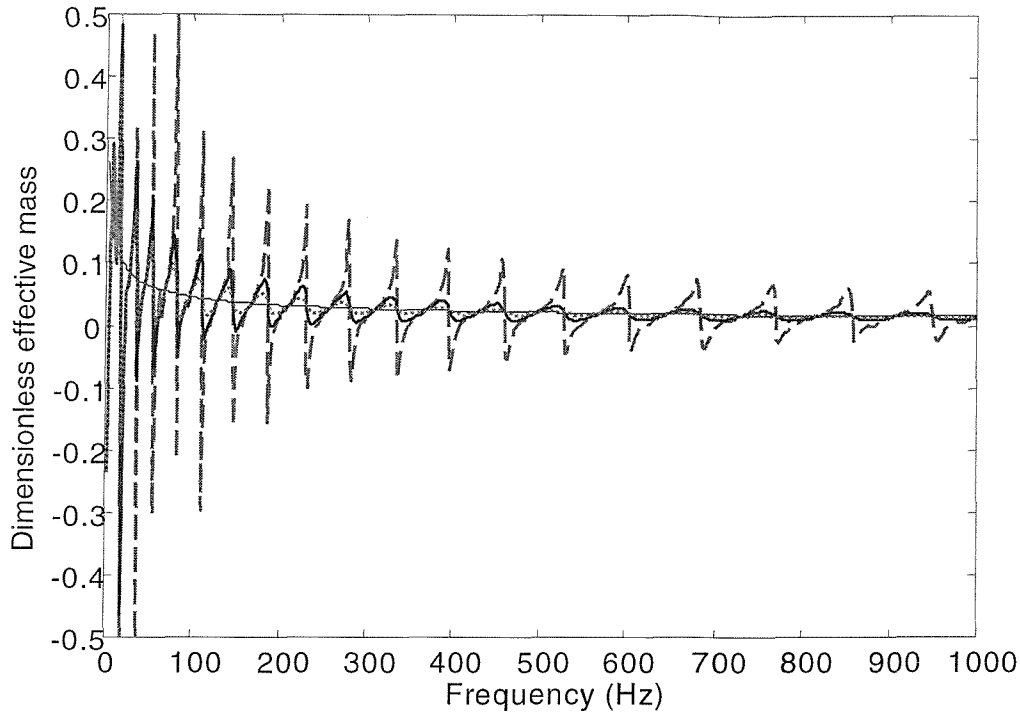

Figure 8.20 Dimensionless effective mass added to the first mode of the beam ($k_p/k_b = 5.6$): $\eta_p = 0.01$, _ _ _ ; $\eta_p = 0.05$, ____ ; $\eta_p = 0.1$, ...; $MOF_p = \infty$, ____ .

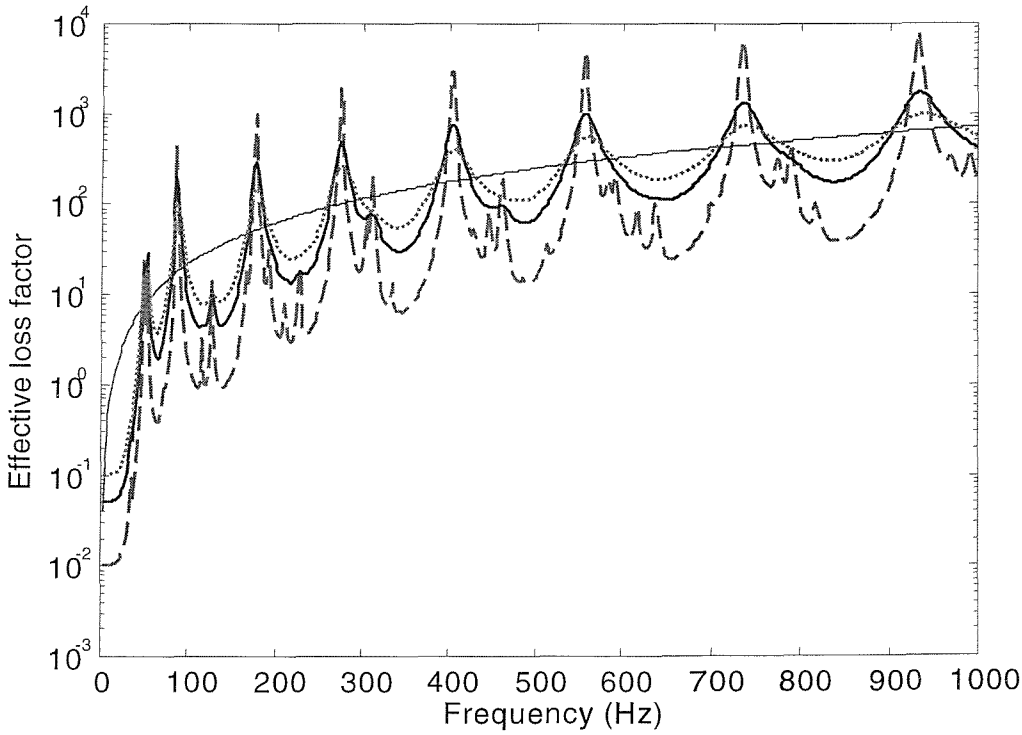

Figure 8.21 Effective loss factor added to the first order mode of the beam ($k_p/k_b = 2.5$): $\eta_p = 0.01$, _ _ _ . ; $\eta_p = 0.05$, ____ ; $\eta_p = 0.1$, ...; $MOF_p = \infty$, ____ .

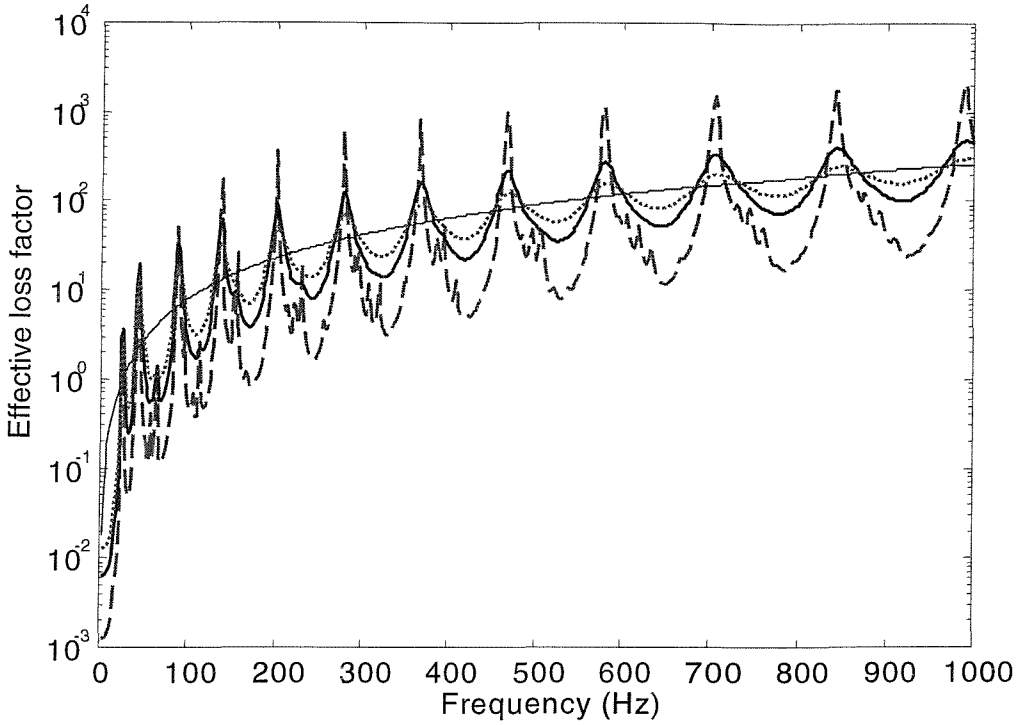

Figure 8.22 Effective loss factor added to the first order mode of the beam ($k_p/k_b = 3.5$): $\eta_p = 0.01$, - - - - ; $\eta_p = 0.05$, ——— ; $\eta_p = 0.1$, ...; $MOF_p = \infty$, ——— .

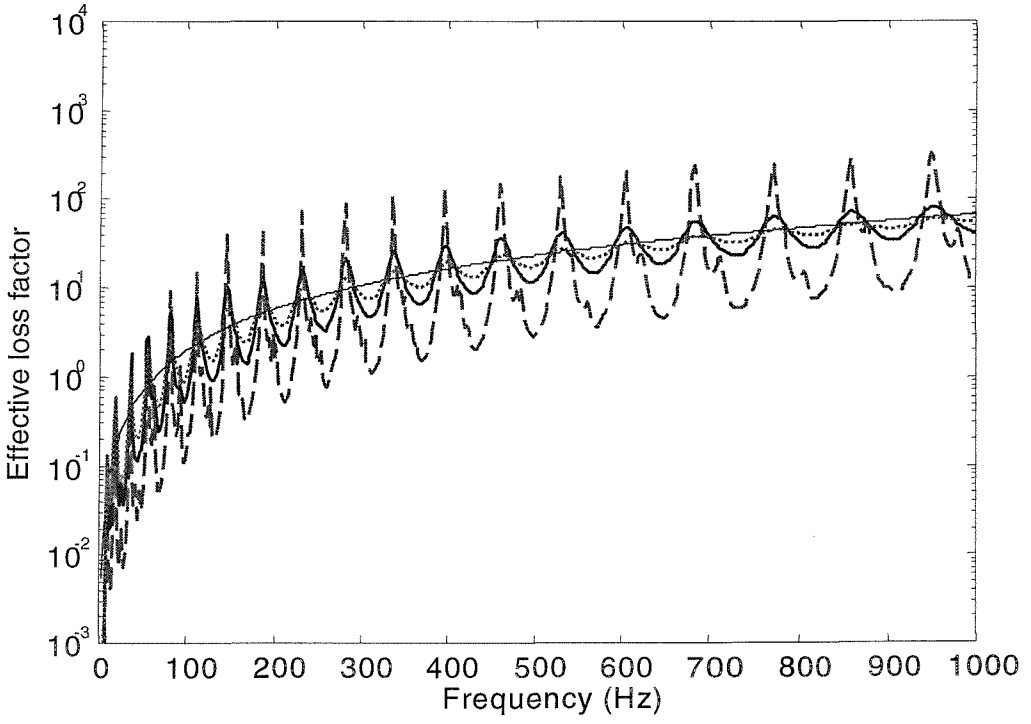

Figure 8.23 Effective loss factor added to the first order mode of the beam ($k_p/k_b = 5.6$): $\eta_p = 0.01$, - - - - ; $\eta_p = 0.05$, ——— ; $\eta_p = 0.1$, ...; $MOF_p = \infty$, ——— .

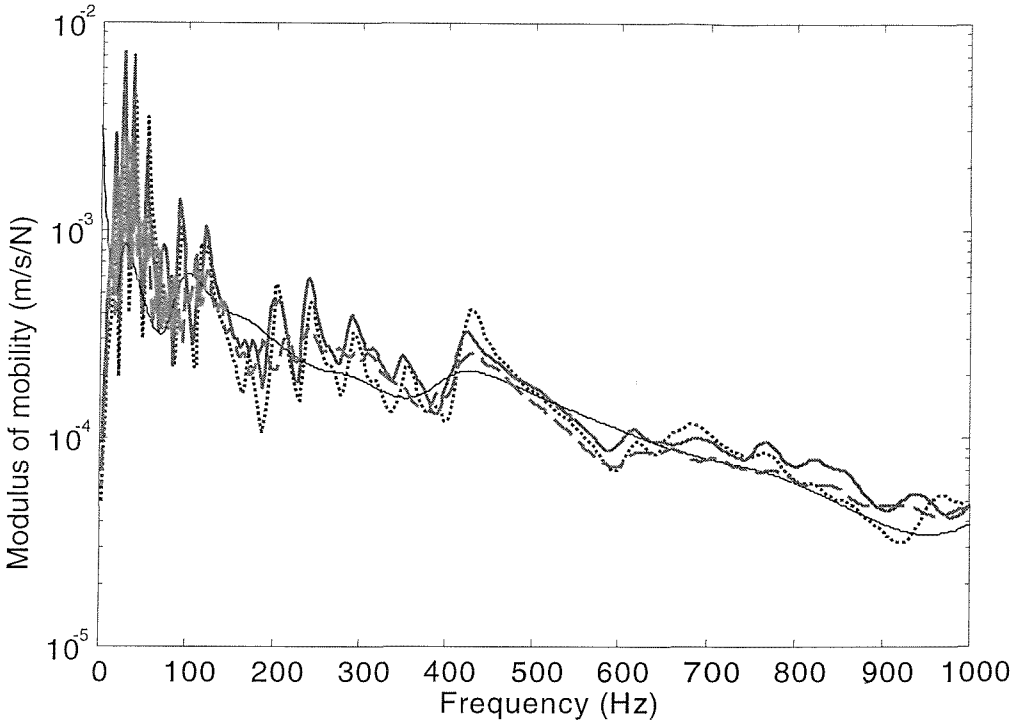

Figure 8.24 Point mobility of the L-beam at the excitation point when $k_p/k_b = 2.4$: mode-based (true plate ____ , larger plate _ _); exact (·····), and locally reacting method (——).

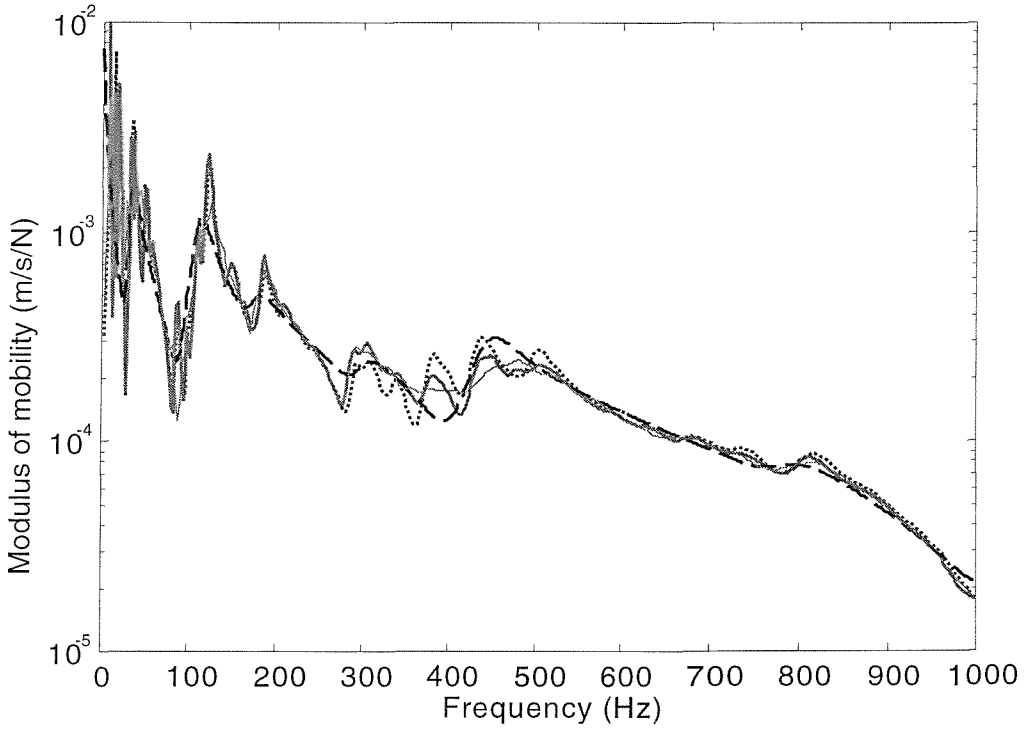

Figure 8.25 Point mobility of the L-beam at the excitation point when $k_p/k_b = 3.3$: mode-based (true plate —— , larger plate — —); exact (·····), and locally reacting method (——).

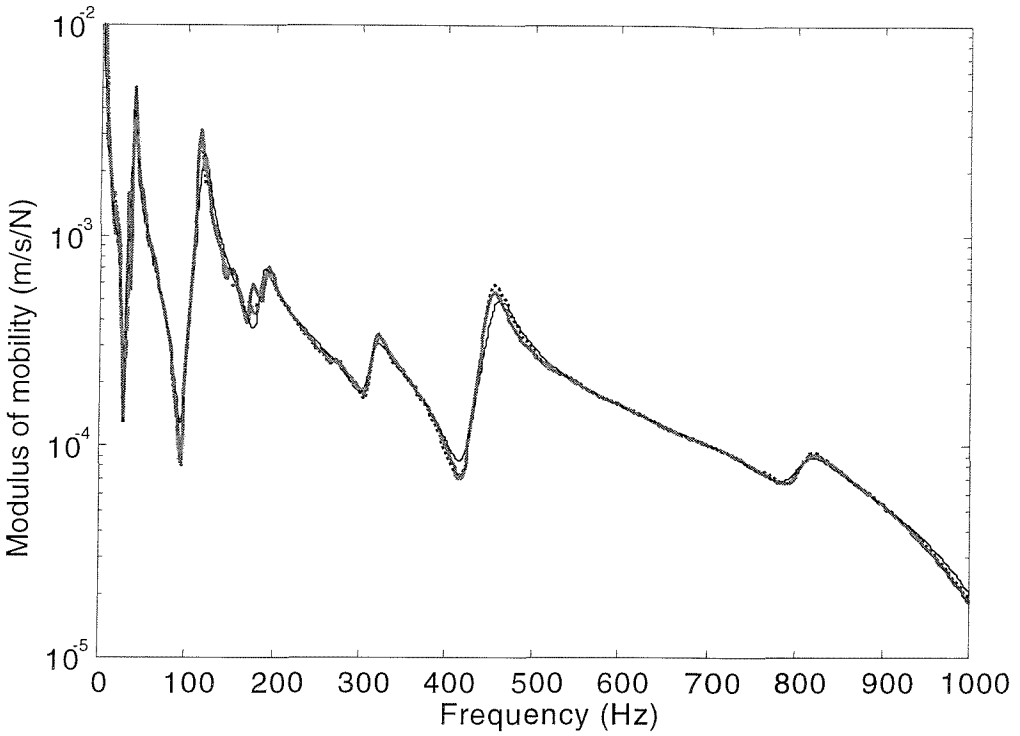

Figure 8.26 Point mobility of the L-beam at the excitation point when $k_p/k_b = 5.3$: mode-based (true plate ——— , larger plate — —); exact (·····), and locally reacting method (———).

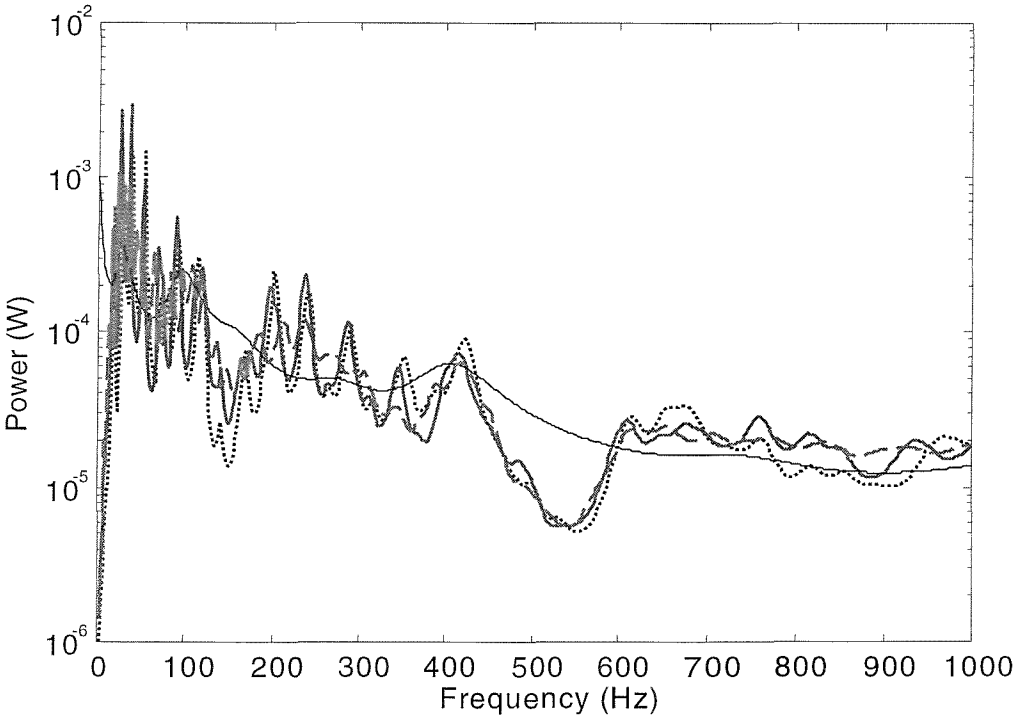

Figure 8.27 Power transmitted to the plate when $k_p/k_b = 2.4$: mode-based (true plate ——— , large plate — —); exact (·····); locally reacting method (———).

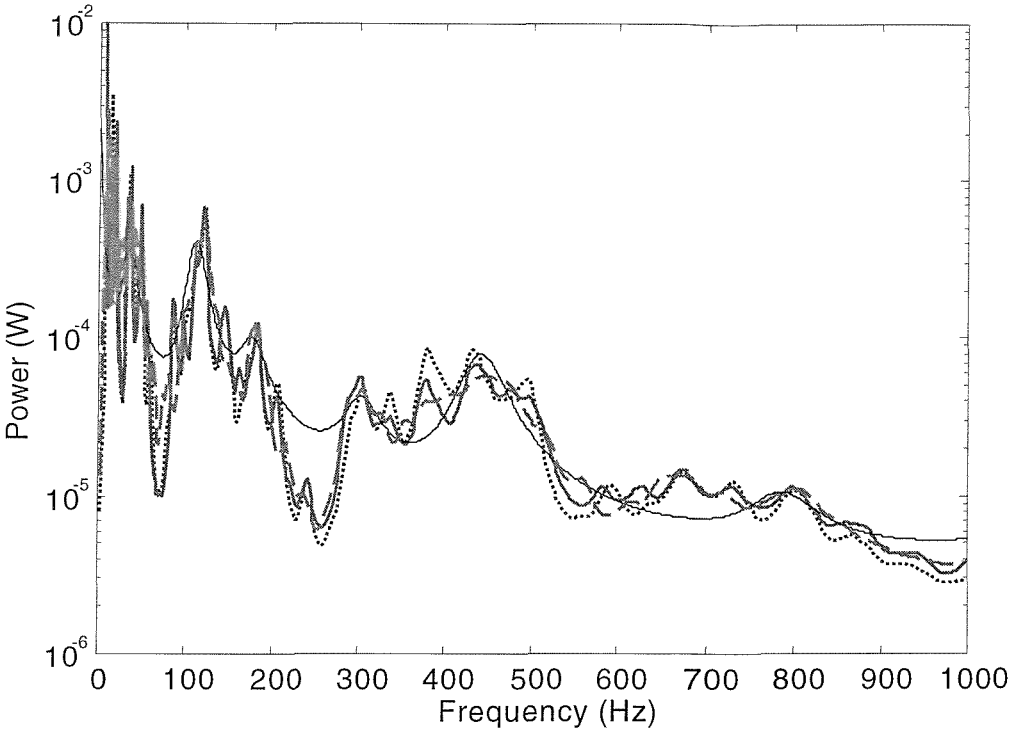

Figure 8.28 Power transmitted to the plate when $k_p/k_b = 3.3$: mode-based (true plate ——— , large plate – –); exact (·····); locally reacting method (——).

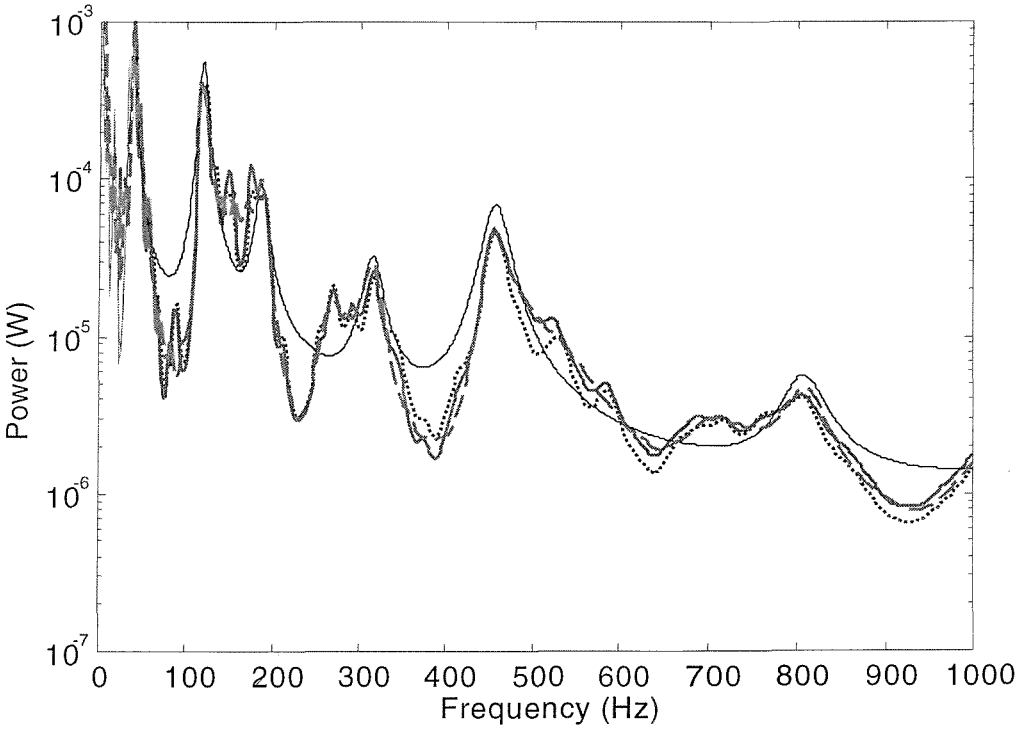

Figure 8.29 Power transmitted to the plate when $k_p/k_b = 5.3$: mode-based (true plate ——— , large plate – –); exact (·····); locally reacting method (——).

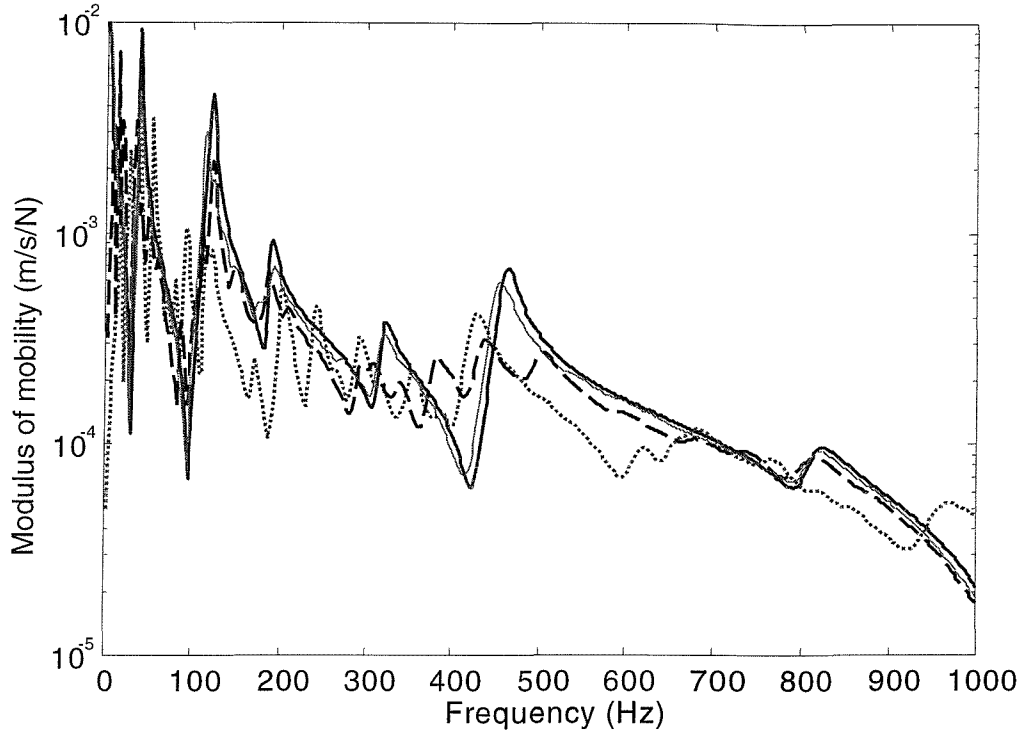

Figure 8.30 Point mobility results of the L-beam at the excitation point: before coupling (——), after coupling (0.010m thick plate ....., 0.005 thick plate - - - , 0.002m thick plate ——).

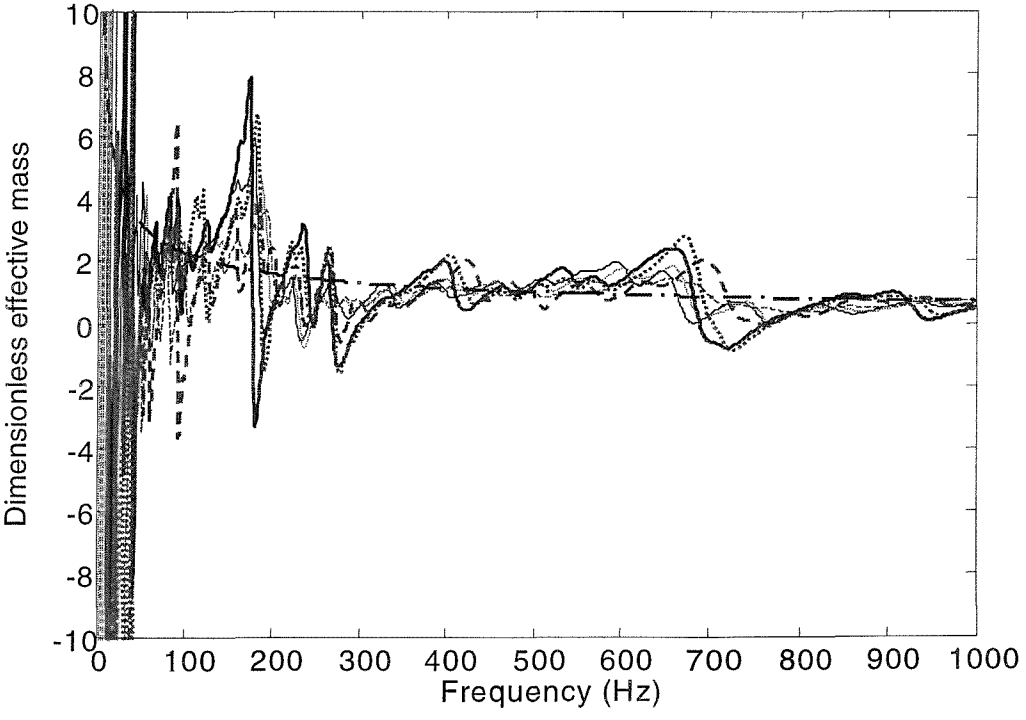

Figure 8.31 Dimensionless effective mass added to the first three modes of the L-beam ($k_p/k_b = 2.4$): 1st (true plate ____ , large plate____); 2nd (true plate ....., large plate.....); 3rd (true plate _ _ _, large plate_____); locally reacting plate (— · —)

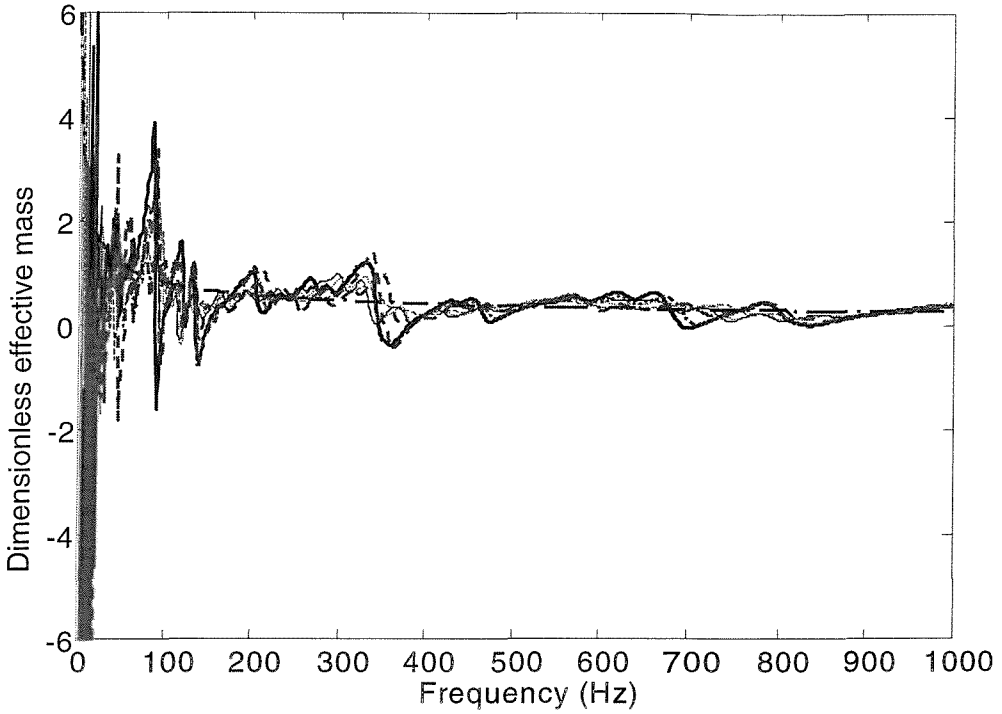

Figure 8.32 Dimensionless effective mass added to the first three modes of the L-beam ($k_p/k_b = 3.3$): 1st (true plate ____ , large plate ____); 2nd (true plate ....., large plate.....); 3rd (true plate _ _ _, large plate_____); locally reacting plate (— · —)

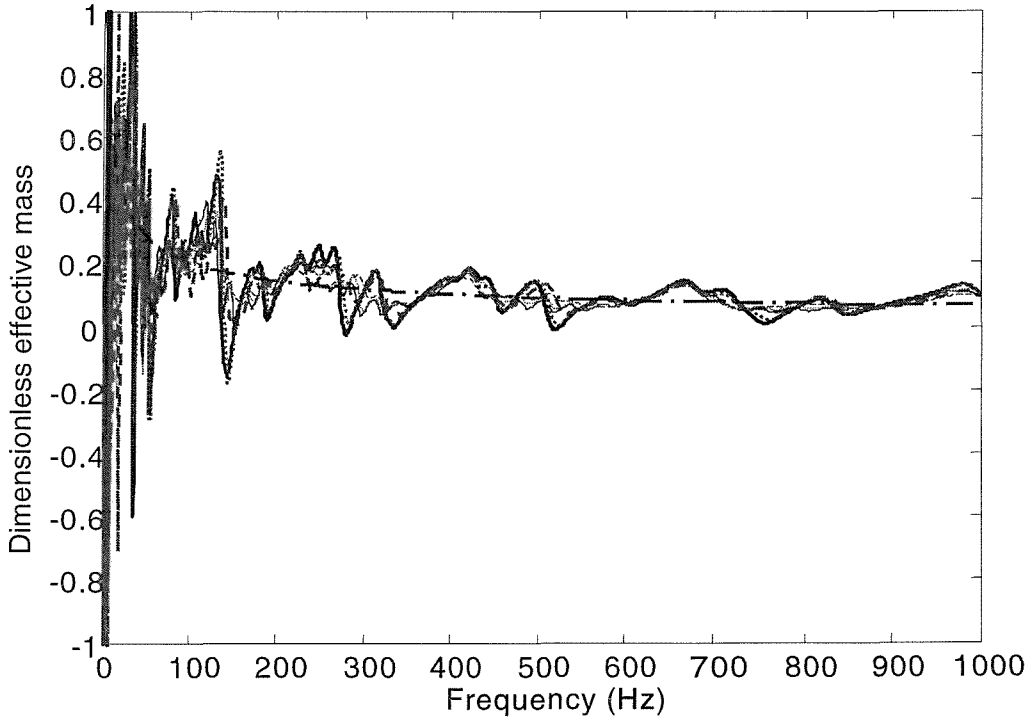

Figure 8.33 Dimensionless effective mass added to the first three modes of the L-beam ($k_p/k_b = 5.3$): 1st (true plate ____ , large plate ____); 2nd (true plate ....., large plate.....); 3rd (true plate _ _ _, large plate_____); locally reacting plate (— · —)

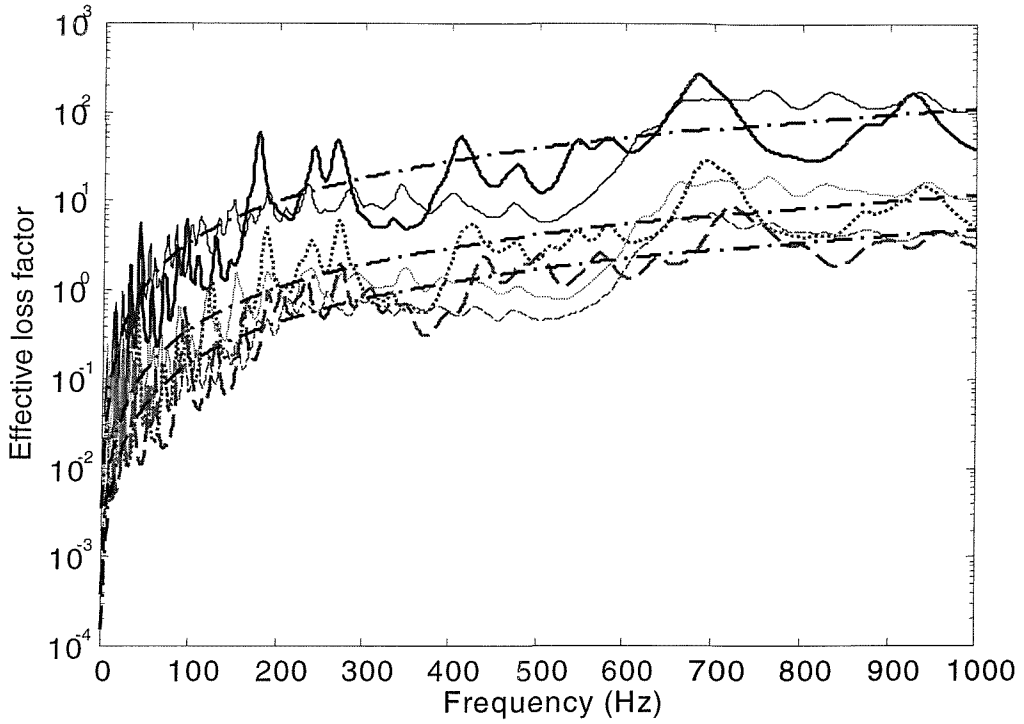

Figure 8.34 Effective loss factor added to the first three modes of the L-beam ($k_p/k_b = 2.4$): 1st mode (true plate ——— , large plate ———); 2nd (true plate ·····, large plate———); 3rd (true plate – – –, large plate -----); locally reacting plate (— · —)

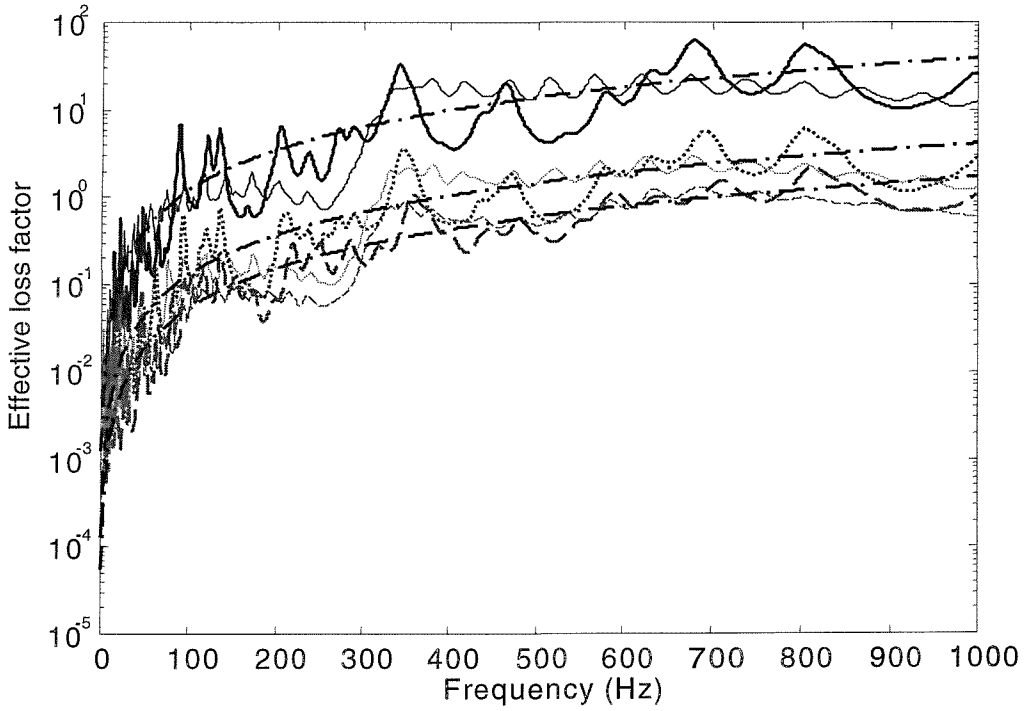

Figure 8.35 Effective loss factor added to the first three modes of the L-beam ($k_p/k_b = 3.3$): 1st mode (true plate ——— , large plate ———); 2nd (true plate ·····, large plate———); 3rd (true plate – – –, large plate -----); locally reacting plate (— · —).

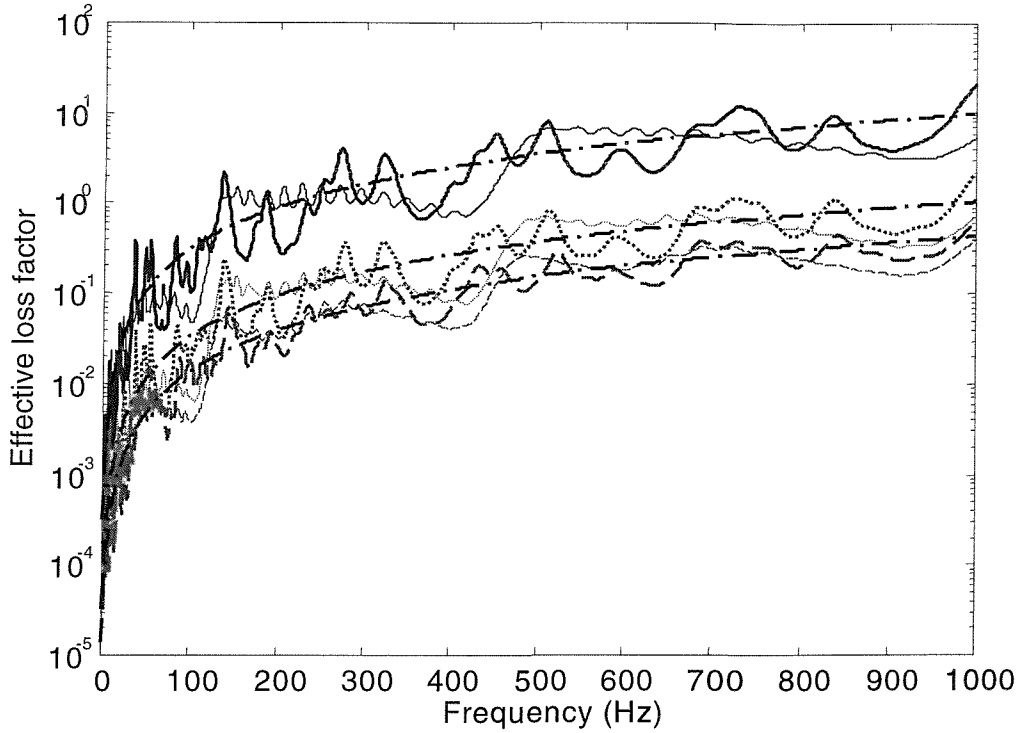

Figure 8.36 Effective loss factor added to the first three modes of the L-beam ($k_p/k_b = 5.3$): 1st mode (true plate ——— , large plate ———); 2nd (true plate ·····, large plate·····); 3rd (true plate - - - , large plate -----); locally reacting plate (— · —).

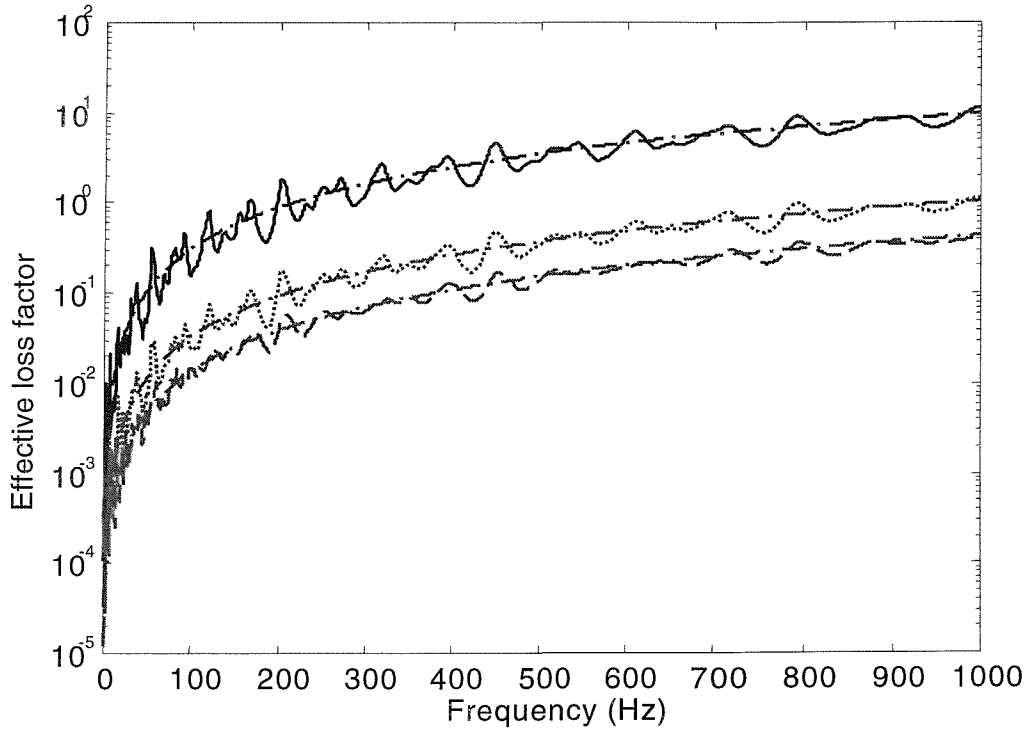

Figure 8.37 Effective loss factor added to the first three modes of the L-beam by the $3\times2\times0.002\text{m}^3$ plate: simple standing wave plate (1st ____ , 2nd ····· , 3rd - - -); locally reacting plate (— · —).

Part IV

EXPERIMENTAL RESULTS

All the numerical investigations in the previous parts illustrated that for a complex structure built-up from both long- and short-wavelength substructures, the main features of the vibration response of the structure tend to be largely controlled by the dynamic properties of the long-wavelength substructures while the knowledge of the short-wavelength ones is only important for the exact details of the response. Consequently, it is appropriate to describe the long-wavelength substructures deterministically while the short-wavelength ones can be described statistically, so as to understand the dynamic behaviour of the coupled structure in a way that is simple and practical but with acceptable accuracy. Based on such a fact that the dynamics of a flexible structure become less affected by its boundary conditions, sizes and shapes as the wavelength decreases, three approximate techniques were given in Part II and Part III for continuous coupling cases. These are the mode-based approach, the Mode/FT approach and the locally reacting impedance method in which the short-wavelength substructure is asymptotically described, respectively, as a simple standing wave model, an infinite model, or even more simply, as a locally reacting model.

In this final part of the thesis, a laboratory experiment is arranged on beam-stiffened plate models to round off these theoretical developments. The measurement results, together with the numerical investigations made in previous chapters, can then provide a sound verification for both the validity and practicality of these three approximate approaches.

Chapter 9

LABORATORY MEASUREMENTS ON A BEAM-STIFFENED PLATE MODEL

9.1 INTRODUCTION

This chapter describes measurements intended to verify experimentally the main theoretical developments made in the previous chapters. These are (1) when a receiver is relatively very flexible compared to a source, the vibration response of the coupled structure can be simply approximated by assuming the receiver either as a simple standing wave model, or as an infinite model or a locally reacting model; (2) the more flexible the receiver is, the more accurate these approximate results are; and (3) the internal damping of the receiver tends to have less effect on the dynamic response of the coupled structure as the flexibility of the receiver increases. The main contents of this chapter can be divided into the following parts: a description of the experimental models and arrangements, a presentation of the measurement results and a discussion of the practicality and limitations of the approximating methods, and finally a summary of the chapter.

9.2 EXPERIMENTAL MODELS AND ARRANGEMENTS

The laboratory measurements were made on similar beam-stiffened plate models as those described in previous numerical cases. The physical configuration is given in Figure 9.1, where the beam model is entirely attached to the rectangular plate by strong adhesives (car body filler) in a symmetrical manner above and below the plate. In this case, the neutral axis of the beam lies in the mid-plane of the plate so that the dynamic effects arising from the longitudinal coupling of the system can be taken as relatively very small compared to that of the flexural coupling. Consequently, the system vibration can be simply treated as involving only flexural wave motions. Such a coupling relation was realised by cutting the beam model along its length into two parts, each with half the height of the beam, and then gluing them exactly symmetrically to the surfaces of both sides of the plate. All the beam and plate components are made of aluminium whose material properties are given in Table 9.1. Their dimensions and the coupling positions are given in Table 9.2, which were

chosen to let the constructed systems be characterised with the mid-frequency vibration properties for a very broad frequency region, as the beam model has a relatively very low modal density compared to those of the plate models. The frequency range of interest was 0-2000Hz, in which appropriate numbers of resonances of the beam and the plates were contained. Four experimental arrangements were involved by attaching the same beam to four different plates, which were (1) a 2mm thick plate; (2) a 2mm plate with certain damping sheets added; (3) a 1mm thick plate; and (4) a 1mm thick plate with certain damping sheets added.

During the measurements, the experimental models were freely suspended by soft strings because free boundaries are much easier to simulate in the test condition than are clamped or grounded ones. An external point excitation force, provided by a random source, was excited directly onto the beam and hence vibrational power was transmitted from the beam to the plate. (Note that the choice of the force driving point of the beam should avoid the positions at or very close to a node of one or more of the beam modes. Here $\xi = 0.25\text{m}$ is used). The measurements were made of the point-mobility of the beam (at the driving point) and the power transmitted to the plate (by measuring the time and spatial averaged surface velocity of the plate). The experimental arrangement is shown in Figure 9.2. A pseudo random force signal, generated from Polytec Scanning Vibrometer (PSV), was applied to the beam through a shaker. The input force and the velocity response of the beam at the driving point were, respectively monitored by an attached force transducer (PCB Piezotronics 208C01 SN 19041) and the laser scanning head of the PSV.

9.3 MEASUREMENT RESULTS AND DISCUSSION

It is necessary to know the dynamic properties of each individual component of the structure when separate to get a better understanding of the vibration behaviour of the complete structure. Therefore, the first step of the measurements consisted of the point-mobility of each individual beam and plate component before the responses of the constructed beam-stiffened plate models were measured.

9.3.1 Point-mobility of the beam component

The point-mobility of the beam component at $\xi = 0.25m$ was measured by replacing the beam-stiffened plate in Figure 9.2 by the freely suspended beam. (The two parts of the beam models were glued together firmly by strong car body filler.) The measurement

result is plotted in Figure 9.3. It is seen that the beam has only a few of resonances within the frequency range of interest and is a typical low mode-count structure.

A comparison was shown in Figure 9.3 with the theoretical prediction obtained by using the natural frequencies and mode shapes of a free-free beam (which are given in Appendix VII). It is seen that the two plots are quite different for the first two flexural modes but tend to agree well for the later modes. The main reason is that the boundary conditions of the beam components involved in the above two plots were actually not exactly the same. For the experimental one the result was measured when the beam model was freely suspended, whereas for the theoretical one the result was predicted based on an ideal free-free beam. As a result, differences occurred both for the resonance frequencies and response amplitudes. However, such boundary influences tend to be small as frequency increases, as shown in Figure 9.3. Besides, it can also be observed that the experimental plot seemed have extra small resonance peaks not shown in the theoretical one. These insignificant resonances may be explained as those corresponding to the bending motion of the beam along another direction, perhaps together with some torsion motion of the beam. Since the cross section area of the beam is almost square, the resonances of these two sets of bending motions of the beam are quite close with each. However, it is quite obvious that for the excitation case of Figure 9.2, the bending motion along the excitation force direction dominated the beam vibration.

9.3.2 Point-mobility of the plate components

The point-mobility of each plate component at the off-centre point $(0.300, 0.197)\text{m}$, when it was freely suspended by two soft strings, was measured using a similar experimental set-up to that given in Figure 9.2. Four different plates, as described in section 9.2, were measured. Two thicknesses (2mm and 1mm) were used to vary the flexibility of the plates, which correspond to modal densities 0.056 and 0.11 per Hz, respectively. Damping sheets were used to vary the plate damping. The increased damping loss factor of each plate, in this experiment, was determined experimentally by measuring the input power P to the plate and the plate mean-square velocity response $\langle \overline{v^2} \rangle$, and then using the relation $\eta = P / \left(\omega M \langle \overline{v^2} \rangle \right)$, where M is the total mass of the plate. The input power was measured from the product of the force and the corresponding velocity response spectra, while the mean square velocity response was measured by using laser scanning. Figure 9.4 gives the experimentally estimated internal loss factor result (solid line) for the 1mm thick

plate when damping sheets were pasted onto the plate. When assumed frequency independent, the internal loss factor of the plate here may be estimated as $\eta_p \approx 0.03$. The same experimental result was obtained for the damping loss factor of the 2mm thick plate (with damping sheets attached). For brevity, it is not given here.

The measured mobility results are plotted in Figures 9.5-9.8 corresponding to these four plates, where a running frequency average was taken to smooth the responses curves. The bandwidth used was 40Hz so that each bandwidth may contain several modes. It is seen that there are many discrete modes within the frequency range of interest, especially for the 1mm thick plate. When the plate was heavily damped, however, these distinctive resonances became unclear. The mobility plots drifting downwards at higher frequencies in Figures 9.7-9.8 can be explained by the mass loading effects of the force transducer [41-42].

Figures 9.5-9.8 also show the running-frequency-average results of the theoretical predictions when the plates were assumed as a simple standing wave model and a uniformly extended infinite plate. It can be observed that the three sets of results tend to get closer as the wavelength of the plate gets short and/or the damping of the plate increases. Such a trend implies that the boundary conditions of a structure tend to be of less importance as its wavelength gets short. Actually, when the wavelength is short enough, the changes of boundary conditions may often cause only a slight shift in resonance frequencies of the structure but have little effects on the envelopes of its spectrum [48]. Moreover, when the half power bandwidth of the resonance is greater than the spacing between the modes (due to heavy damping, for example), the structure tends to exhibit 'infinite' behaviour [47]. (Or alternatively, the 'infinite' behaviour occurs when the frequency is above that at which the envelopes of the peaks and the troughs in the real components of mobility coincide [48]). By the above criteria, therefore, it is quite reasonable, especially in a frequency average sense, simply to describe a high mode-count plate asymptotically as a simple standing wave model or an infinite model, as appropriate. Consequently, the mode-based approach and the Mode/FT approach are expected to give a reasonable estimation for the vibration response of such beam-stiffened plate models. These will be described and discussed below.

9.3.3 Vibrations of the beam-stiffened plates

The above measurements show that there were quite big dynamic mismatches (e.g., in terms of wavenumbers and/or modal densities) between the individual properties of the

beam and the plates in that the former had a very low mode-count while the latter had a relatively much higher mode-count. Therefore, when such beam and plate components were coupled to each other, as shown in Figure 9.1, the built-up structure was actually dominated by the mid-frequency characteristics for a very broad range of frequency. The construction of the experimental beam-stiffened plates has been described in Section 9.2. Four beam-stiffened plates were involved in the measurements, corresponding to changes in either the thickness or the damping of the plate. The measurements were mainly made of the point-mobility at the driving point of the beam and the power transmitted to the plate.

The mobility measurement procedure was the same as that for the disconnected beam. For the power measurements, the spatially averaged mean-square velocity spectrum $\left\langle \overline{v_p^2} \right\rangle$ was measured directly by using the PSV Scanning Head. The power can then be obtained from [11]

$$P = \eta_p \omega m_p S_p \left\langle \overline{v_p^2} \right\rangle \tag{9.1}$$

where m_p, S_p and η_p are respectively the mass density, the surface area and the material loss factor of the plate.

For ease of comparisons between the experimental and theoretical results, the power was expressed in terms of power per unit force spectrum input (measured at the beam driving point), i.e., normalized to the force input as

$$P_0 = \frac{\eta_p \omega m_p S_p \left\langle \overline{v_p^2} \right\rangle}{\frac{1}{2}\left|F_\xi\right|^2} \tag{9.2}$$

The measurement results are shown in Figures 9.9-9.16, together with those estimated by the mode-based approach (assuming a simple standing wave plate) and the Mode/FT approach (assuming an infinite plate). These results are compared and discussed below.

9.3.3.1 Point-mobility of the beam

Figures 9.9-9.12 show, respectively, the point mobility results of the beam when it was attached to the four different plates. It can be seen clearly that the measurements and the theoretical predictions converge as the flexibility of the plate increases and/or the modal overlap factor of the plate increases. Big differences between the measurement and theoretical results occur in low frequency range where the plate modal overlap is much

less than unity. This is because that at these frequencies the plate tends to exhibit discrete resonant behaviour and its boundary conditions have a significant effect on these resonances. Hence neither a simple standing wave model nor an infinite model is appropriate to describe the dynamics of the plate asymptotically. As the frequency increases (i.e., the wavelength of the plate decreases), however, the boundary conditions of the plate become less important. When the plate modal overlap factor is close to or bigger than unity, the plate dynamic behaviour tends to be that of a simple standing wave model, whose mode shapes can be estimated from the wavelength within the plate and the natural frequencies from the free wavenumber of the plate. Consequently, the mode-based approach can give a quite good approximation for the vibration response of the beam-stiffened plate. When the modal overlap factor of the plate is big enough, e.g. more than 2 or 3, the plate tends to exhibit obvious infinite behaviour. In this case, the Mode/FT approach can be very useful to estimate the vibration response of the coupled structure. (Here, the modal overlap factor of the 1mm thick plate with extra damping becomes greater than 2 when the frequency is over 600Hz, however, for the 2mm thick plate with extra damping, its modal overlap factor is less than 2 up to the frequency at 1200Hz.)

Figures 9.13-9.14 compare the measured point-mobility results of the beam when it was, respectively, attached to the 2mm and 1mm plates without and with damping sheets attached. It is seen that in Figure 9.13 the damping of the plate has an obvious effect on the FRFs of the beam for the 2mm thick plate, while such an effect is relatively much smaller for the 1mm thick plate in Figure 9.14. This observation agrees well with the theoretical studies presented in previous chapters 4-8, i.e., the influence of the internal damping of the plate on the dynamic response of the beam tends to be less important as the flexibility and/or mode count of the plate increase.

9.3.3.2 Power transmitted from the beam to the plate

Figures 9.15-9.20 are the plots corresponding to the power transmitted from the beam to the four different plates. It is seen that the flexibility and damping of the plate receiver have similar influences on the power transmitted to the plate to those on the dynamics of the beam. However, greater errors occurred than those observed in Figures 9.9-9.14. This implies that the transmitted power is more sensitive to the boundary conditions of the plate than the dynamic properties of the beam. Since equation (9.1) is only valid for a high-mode-count receiver structure [10, 12], the experimental results for the power transmitted to the plate in the lower frequency range may not represent the actually power

transmission within the system. This is one important reason to explain the big differences between the measurements and the theoretical approximations.

The measured input power (to the beam) results are also given in Figures 9.17-9.18. It is seen that at higher frequencies, the differences between the input and transmitted power tend to be smaller. This indicates that the power dissipated by the beam is relatively very small compared with that transmitted to the plate, as expected.

9.4 SUMMARY

This chapter was intended to verify experimentally the practicality of the theoretical developments made in previous chapters 5, 7 and 8. Beam-stiffened plate models were considered, due to the typical dynamic mismatch between the beam and plate components. Measurements were made to both the point-mobility of the beam and the power transmitted to the plate, and then compared with the theoretical predictions by the mode-based approach, Mode/FT approach where the plate receiver was assumed, respectively, as a simple standing wave model and an infinite model. The influences of the flexibility and damping of the plate on the vibration response of the coupled structure were investigated. The results shown are quite encouraging and meet all our theoretical expectations. It is worth noting from the measurements that equation (9.1) is more valid when the receiver structure fulfils a flexible SEA model as described in section 7.4.3. In other cases, power should be measured from the product of the force and some structural frequency response spectra [48].

Table 9.1 Material properties of aluminium

Young's modulus (GN/m^2)	Poisson's ratio	Density (kg/m^3)	Loss factor (Nominal)
71	0.33	2700	0.005

Table 9.2 The dimensions and coupling positions of the beam-stiffened plate

Structure	**Beam**	**Plate**
Dimensions (m)	Length $L_b = 0.598$, Width $t_b = 0.0122$, Height $h_b = 0.006 \times 2$.	Length $L_x^{(p)} = 0.700$, Width $L_y^{(p)} = 0.500$, Thickness $h_p = 0.002 / 0.001$.
Coupling positions (m)	$x_1 = 0.046$, $y_1 = 0.319$; $x_2 = 0.618$, $y_2 = 0.137$	
Driving point (m)	$\xi = 0.25$	
Wavenumber ratio	$k_p / k_b = 2.4 / 3.4$	
Modal density (1/Hz)	0.056 ($h_p = 0.002$)/0.11 ($h_p = 0.001$)	

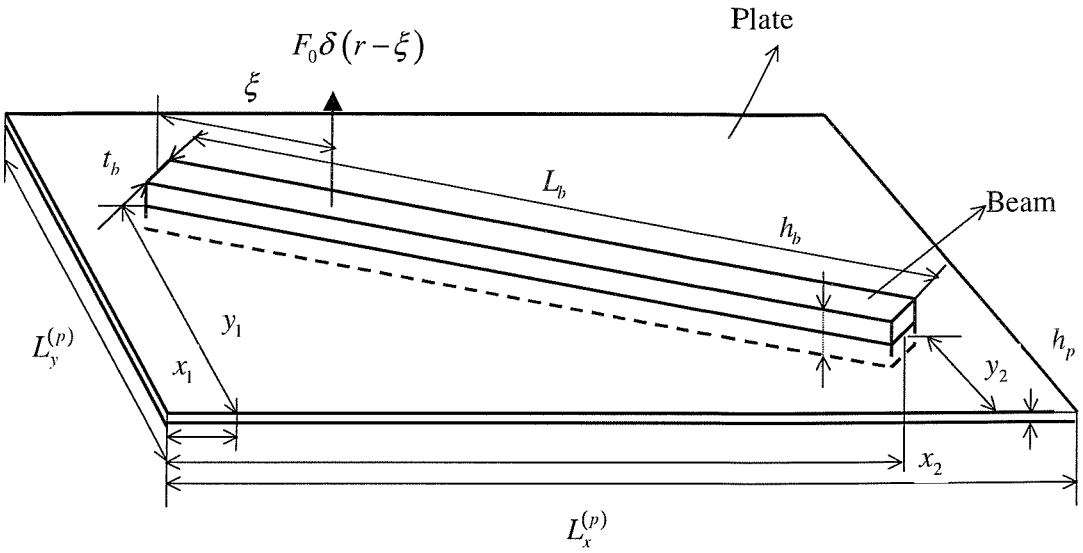

Figure 9.1 The beam-stiffened plate experimental model.

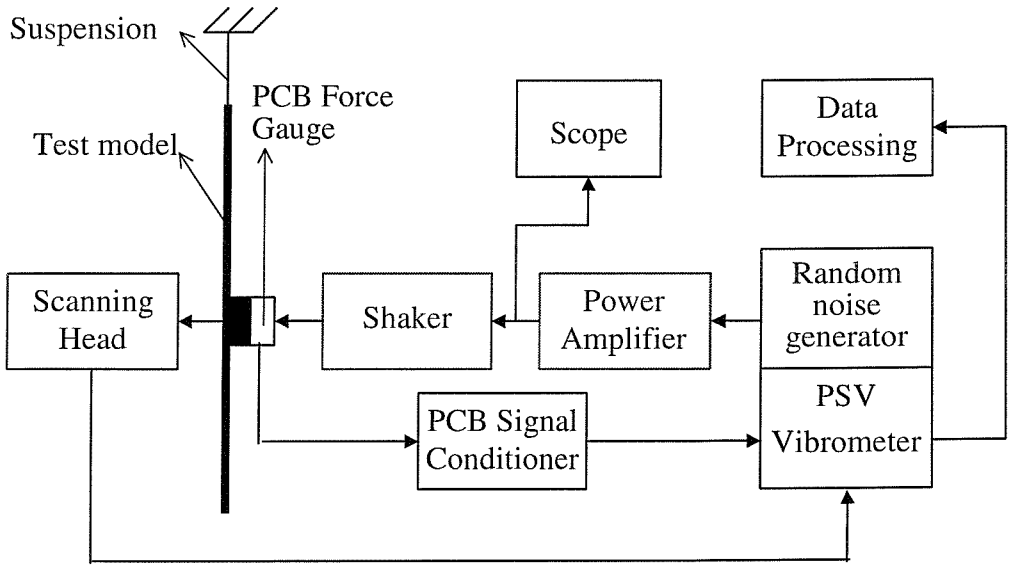

Figure 9.2 Experimental arrangement of the measurement system.

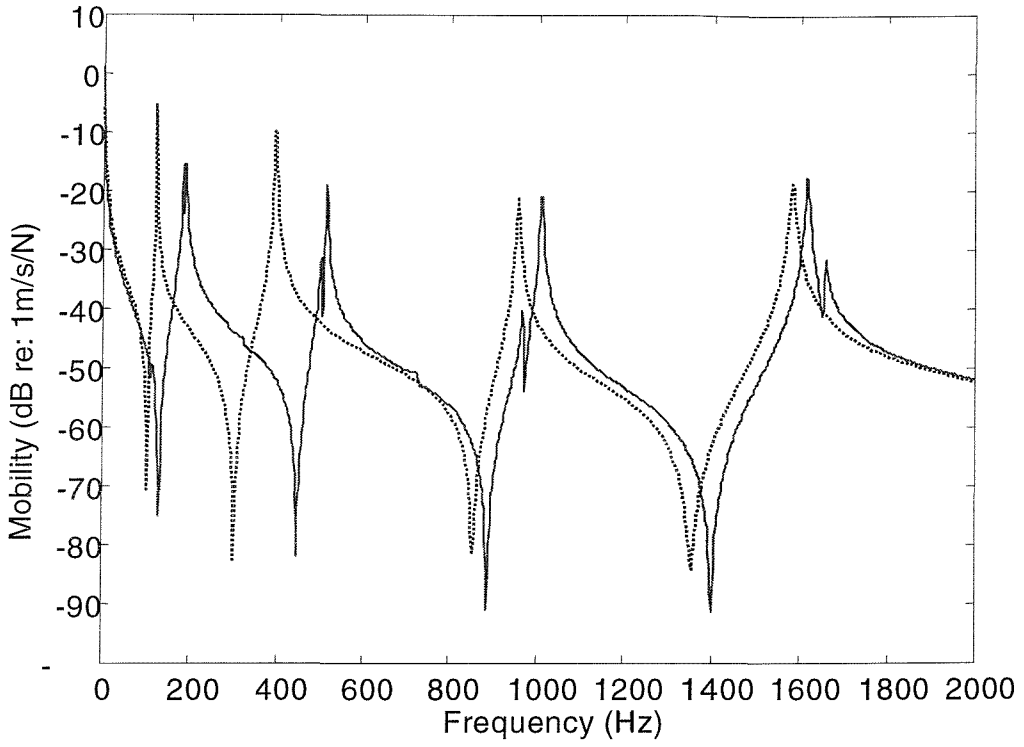

Figure 9.3 Point mobility of the separated beam component at the driving point: theoretical, ... ; measured, _____ .

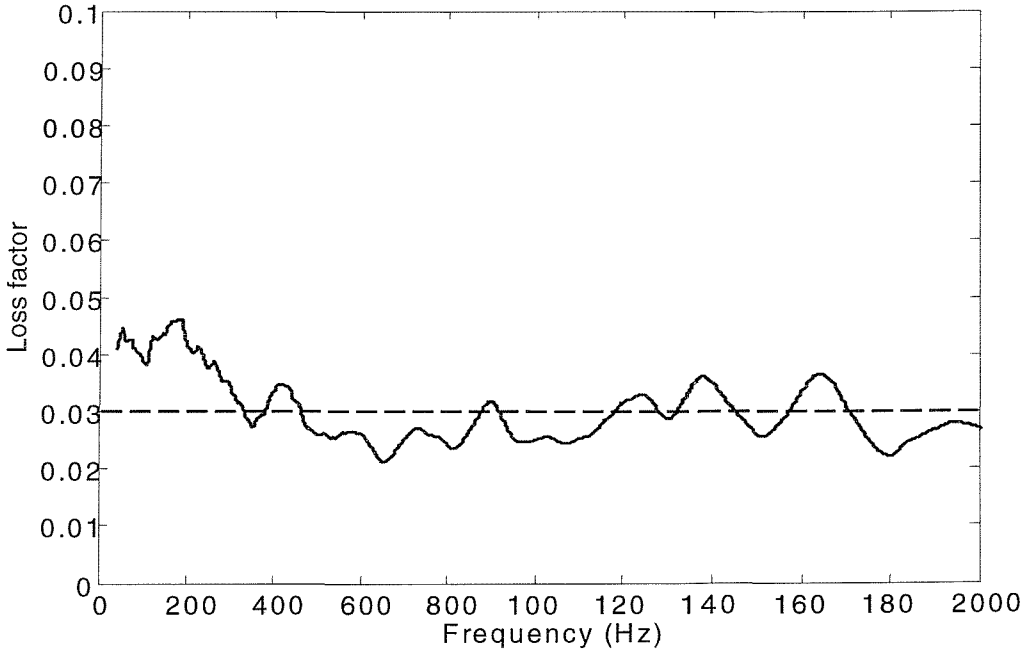

Figure 9.4 Experimentally estimated loss factor of the 1mm thick plate, _____ .

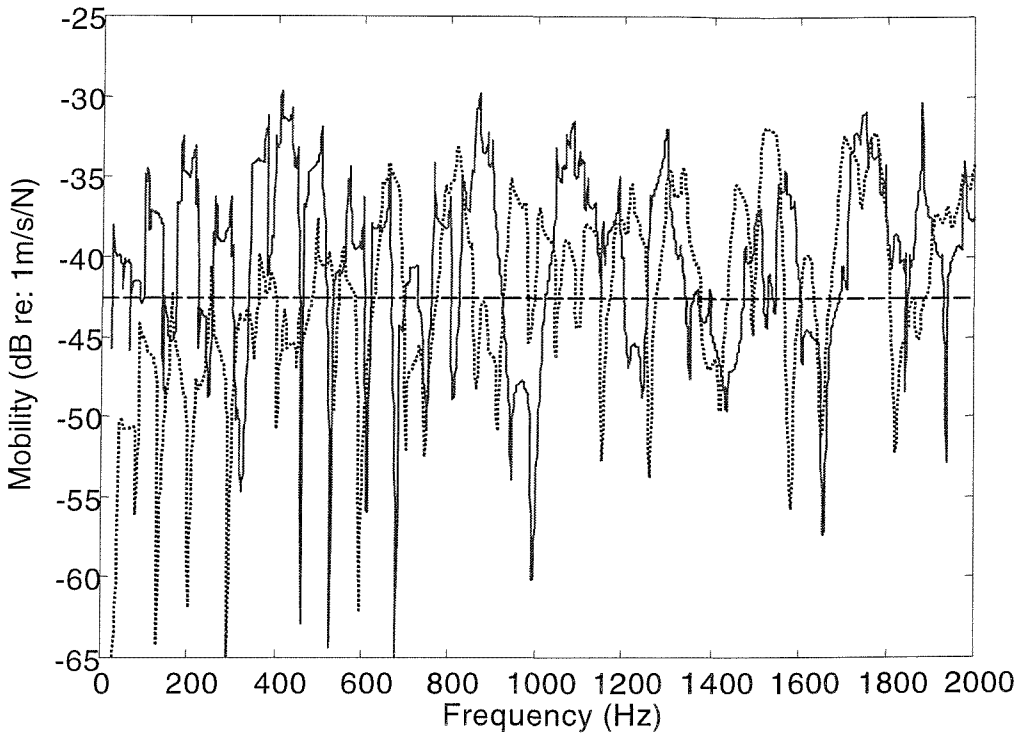

Figure 9.5 Point-mobility of the 2mm thick plate ($\eta_p \approx 0.005$): theoretical (a simple standing wave model, ... ; an infinite model, ____); measured, ——.

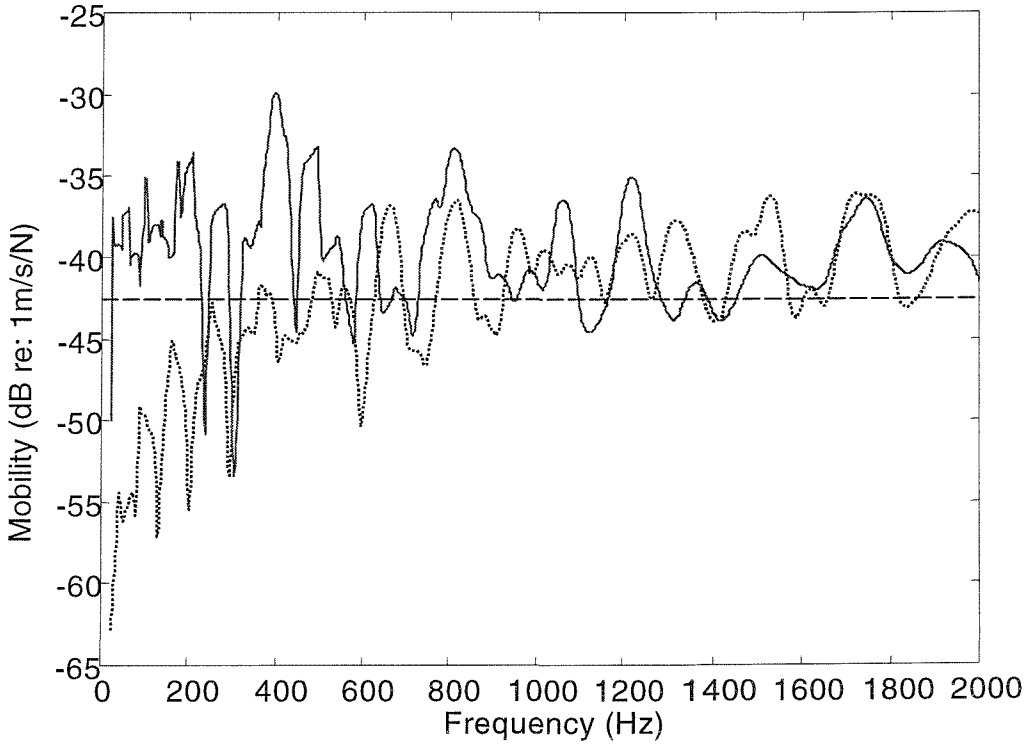

Figure 9.6 Point-mobility of the 2mm thick plate with damping sheets attached ($\eta_p \approx 0.03$): theoretical (a simple standing wave model, ... ; an infinite model, ----); measured, —— .

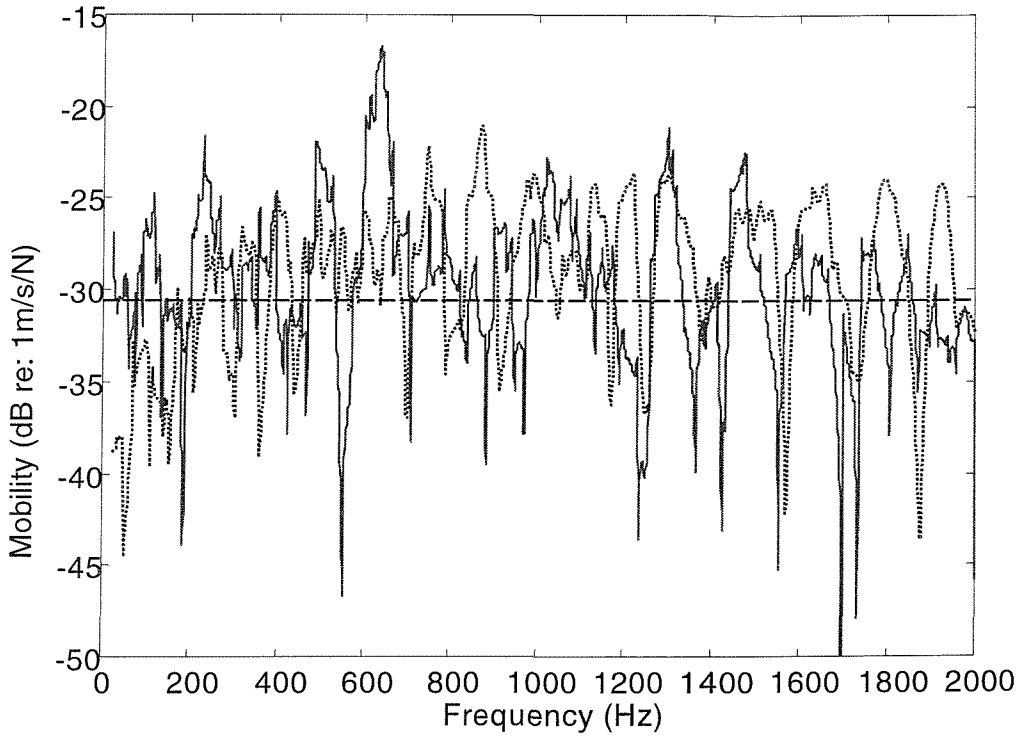

Figure 9.7 Point-mobility of the 1mm thick plate ($\eta_p = 0.005$): theoretical (a simple standing wave model, ... ; an infinite model, ____); measured, ——

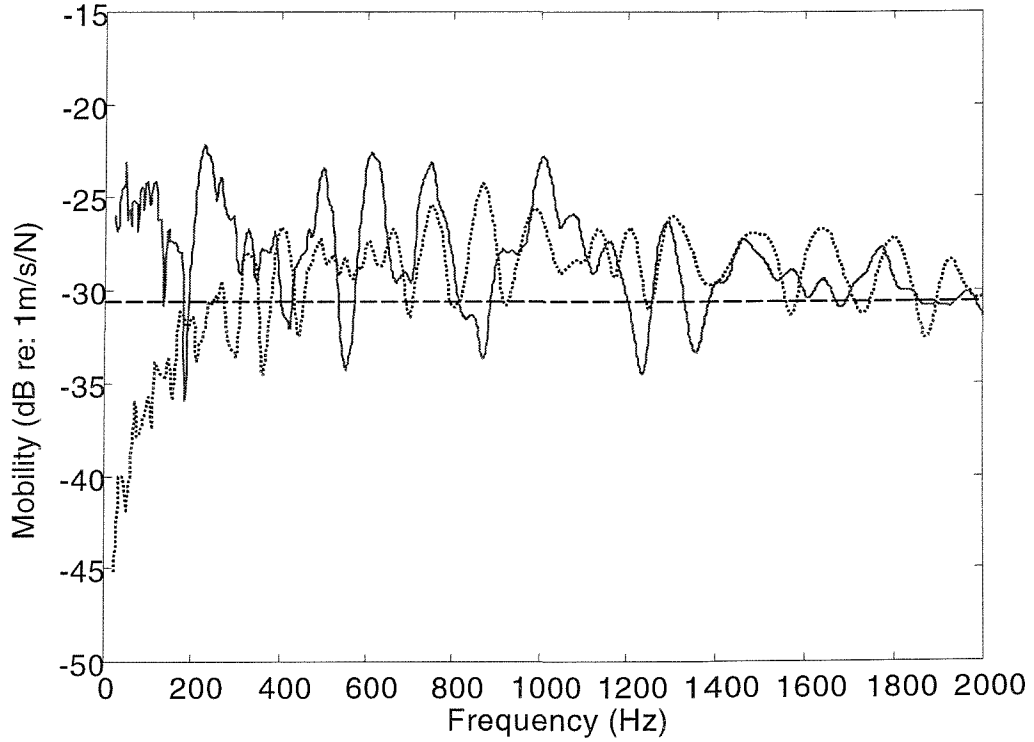

Figure 9.8 Point-mobility of the 1mm thick plate with damping sheets attached ($\eta_p \approx 0.03$): theoretical (a simple standing wave model, ... ; an infinite model, ----); measured, —— .

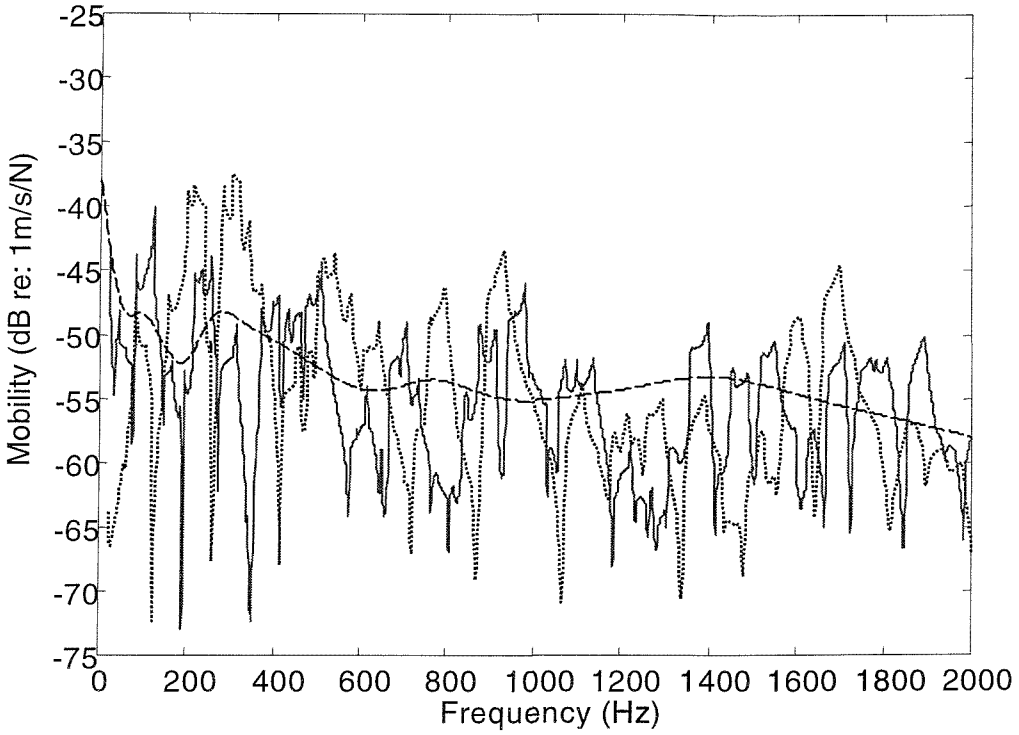

Figure 9.9 Point-mobility of the beam when attached to the 2mm plate ($\eta_p = 0.005$): theoretical (mode-based, ... ; Mode/FT, ____); measured, _____ .

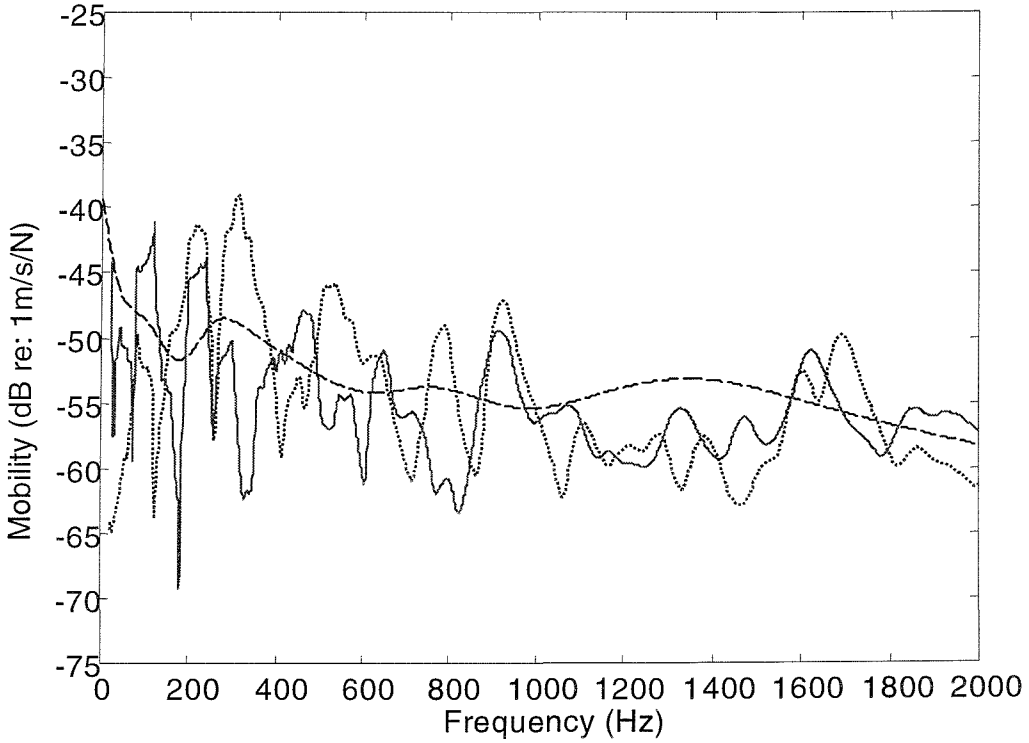

Figure 9.10 Point-mobility of the beam when attached to the 2mm plate ($\eta_p \approx 0.03$): theoretical (mode-based, ... ; Mode/FT, ____); measured, _____ .

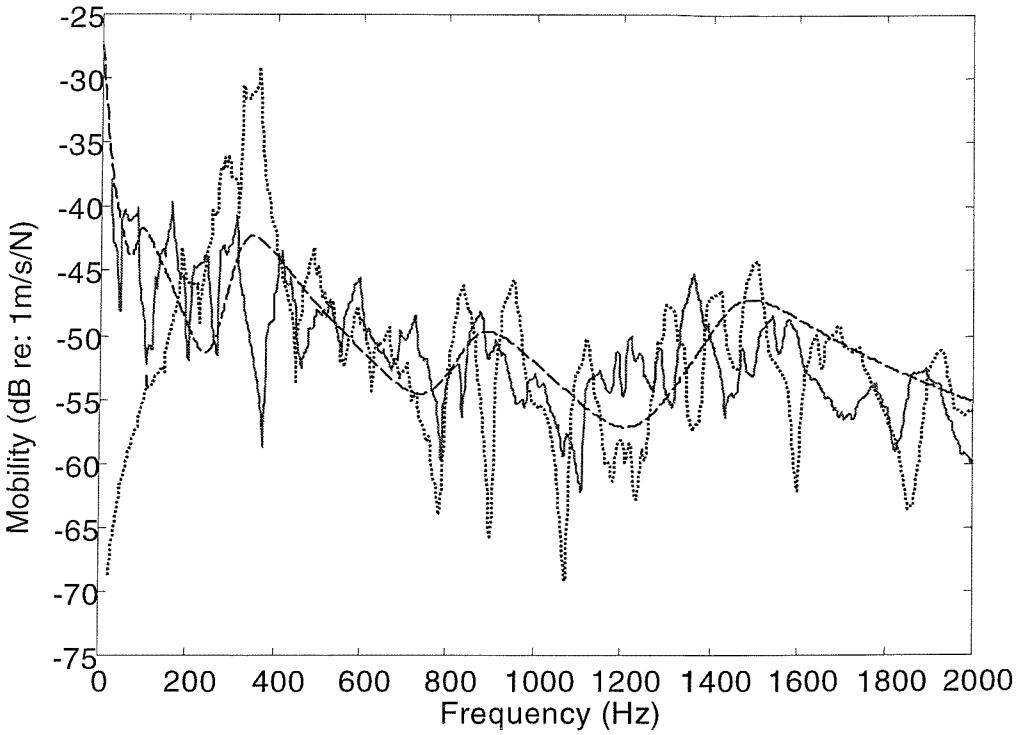

Figure 9.11 Point-mobility of the beam when attached to the 1mm plate ($\eta_p = 0.005$): theoretical (mode-based, ... ; Mode/FT, ____); measured, _____ .

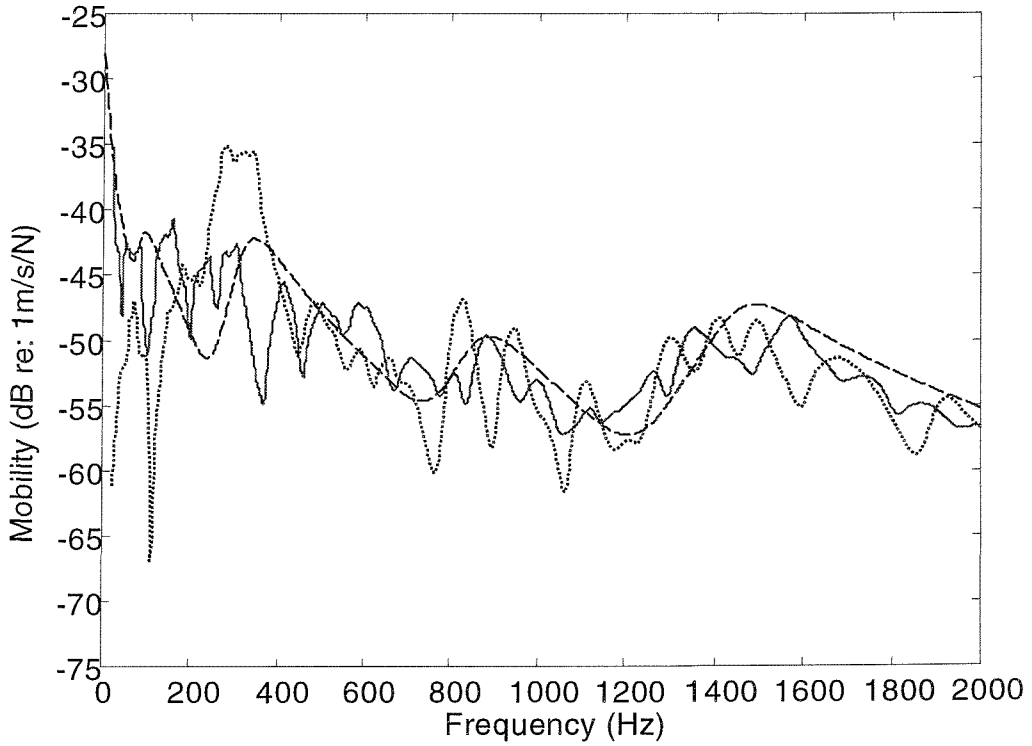

Figure 9.12 Point-mobility of the beam when attached to the 1mm plate ($\eta_p \approx 0.03$): theoretical (mode-based, ... ; Mode/FT, ____); measured, _____ .

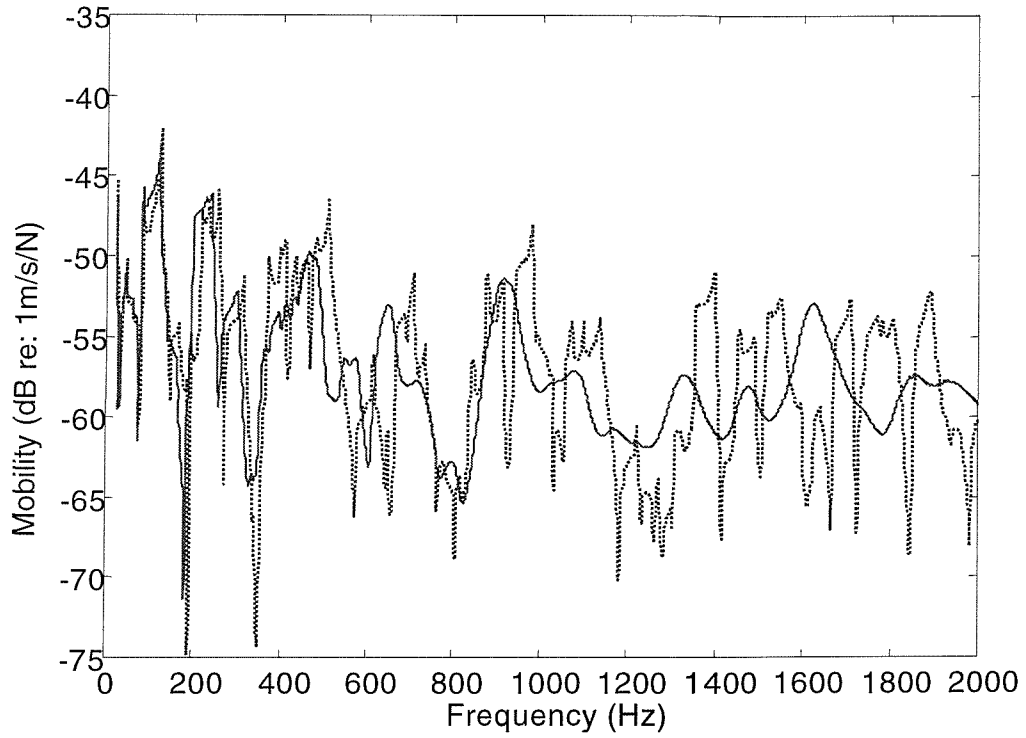

Figure 9.13 Measured point-mobility results of the beam when it was attached to the 2mm thick plate: $\eta_p = 0.005$, ... ; $\eta_p \approx 0.03$, ——— .

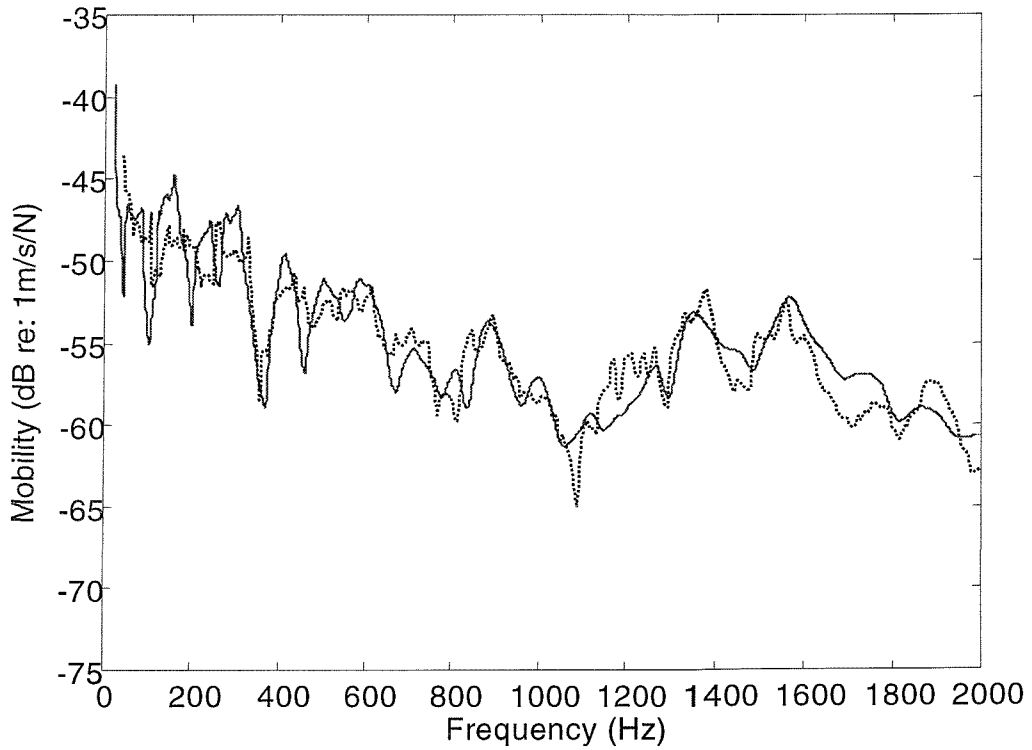

Figure 9.14 Measured point-mobility results of the beam when it was attached to the 1mm plate: $\eta_p = 0.005$, ... ; $\eta_p \approx 0.03$, ——— .

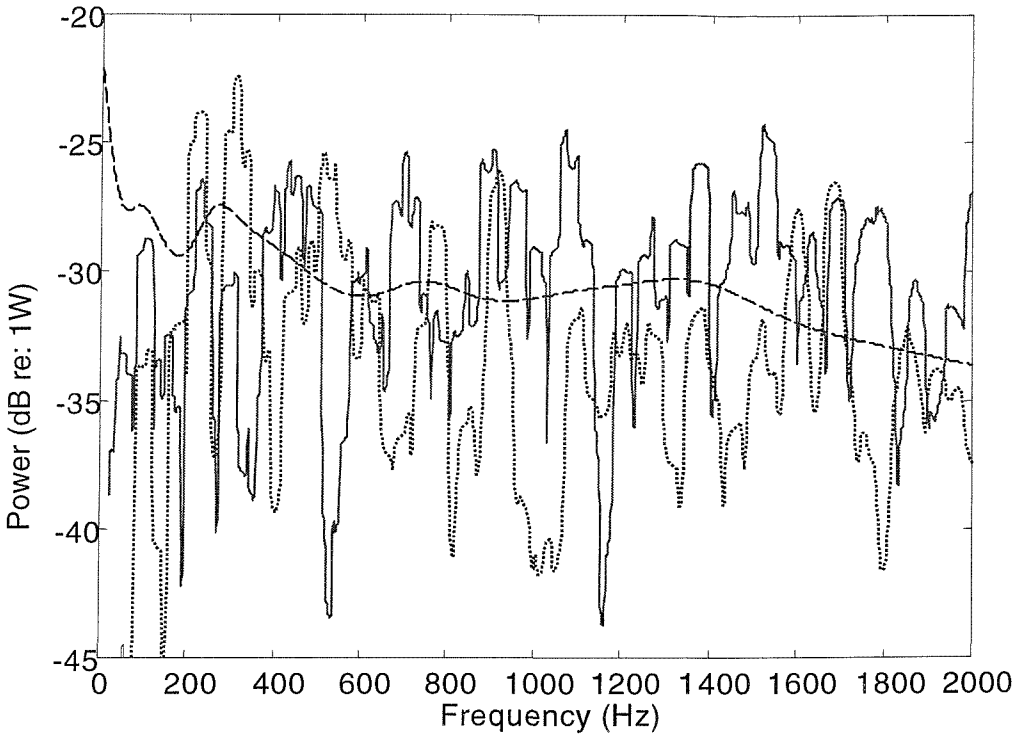

Figure 9.15 Power transmitted to the 2mm thick plate ($\eta_p = 0.005$): theoretical (mode-based, ... ; Mode/FT, ----); measured, ——— .

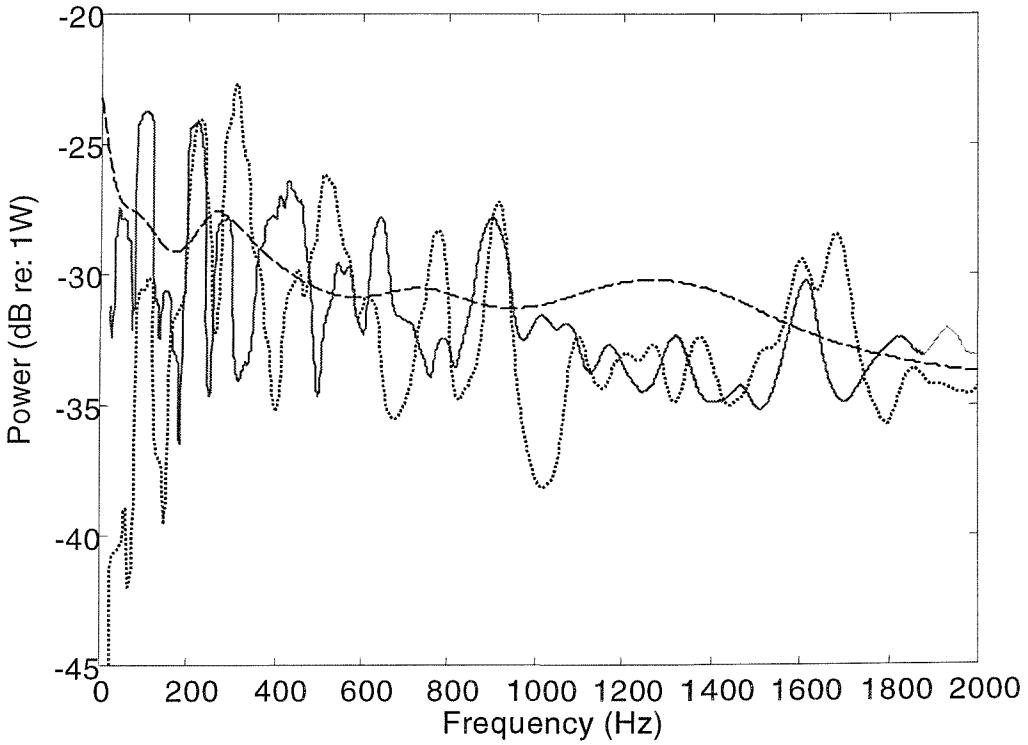

Figure 9.16 Power transmitted to the 2mm thick plate ($\eta_p = 0.03$): theoretical (mode-based, ... ; Mode/FT, ----); measured, ——— .

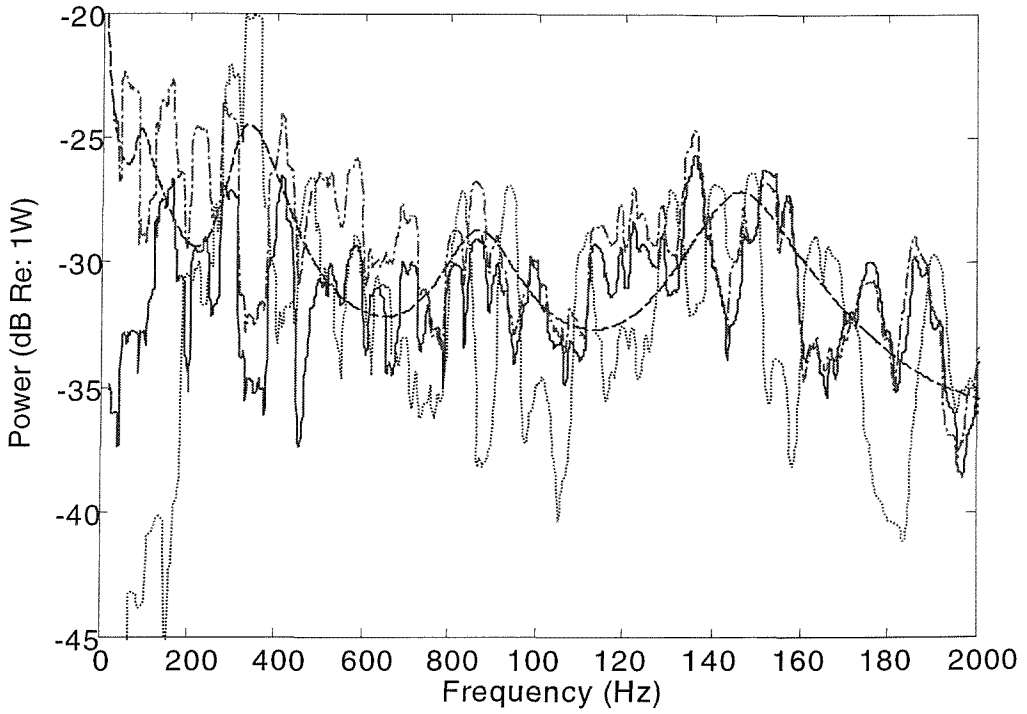

Figure 9.17 Power transmitted to the 1mm thick plate ($\eta_p = 0.005$): theoretical (mode-based, ... ; Mode/FT, -----); measured, ——— . Input power to the coupled system, _.-._.- .

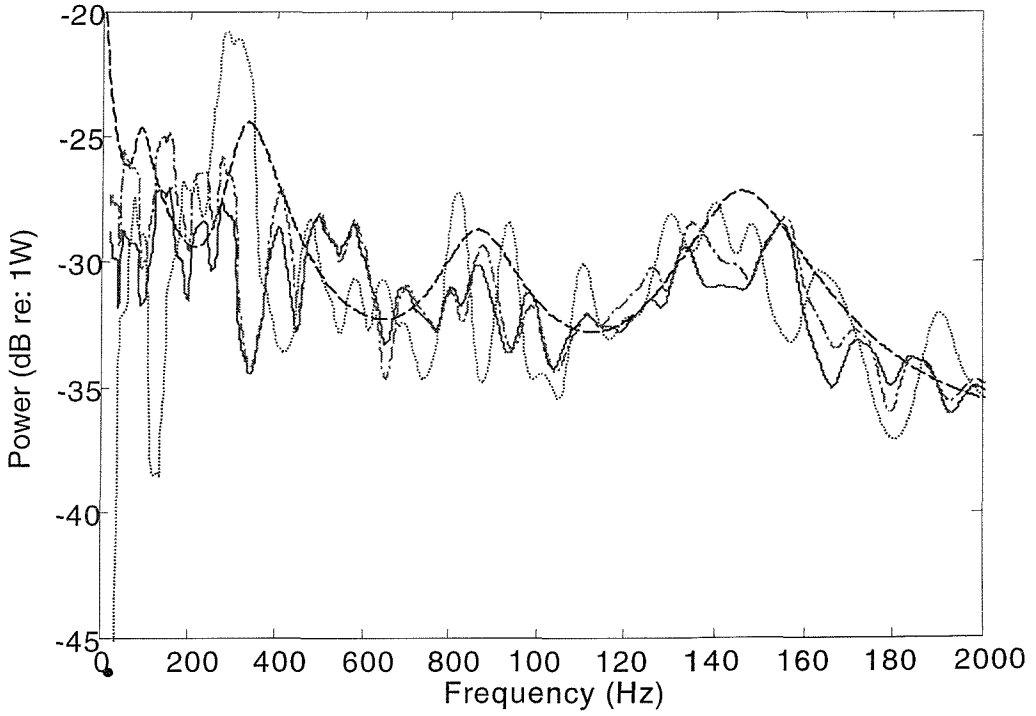

Figure 9.18 Power transmitted to the 1mm thick plate ($\eta_p = 0.03$): theoretical (mode-based, ... ; Mode/FT, -----); measured, ——— . Input power to the coupled system, _.-._.- .

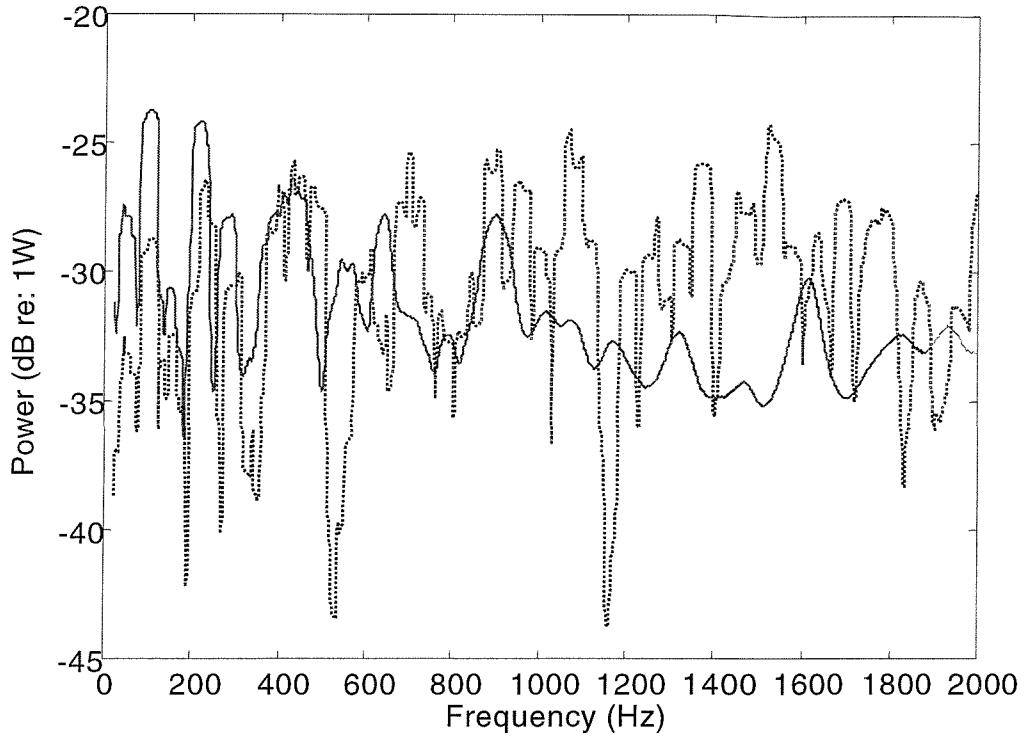

Figure 9.19 Measured power transmission from the beam to the 2mm thick plate: $\eta_p = 0.005$, ... ; $\eta_p \approx 0.03$, ——— .

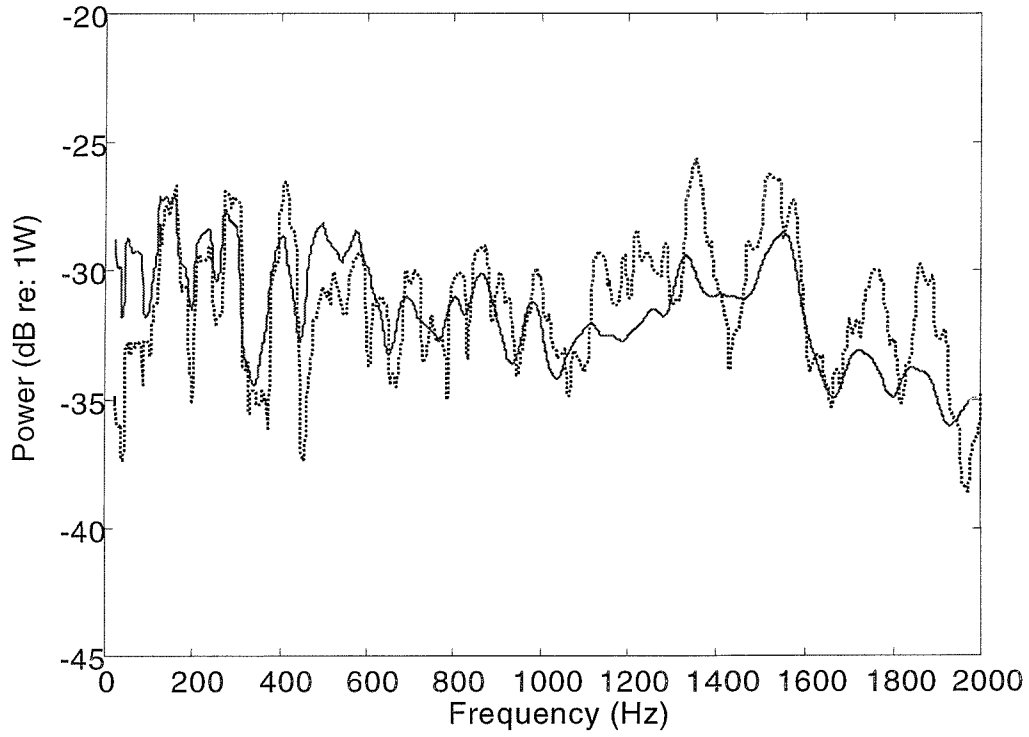

Figure 9.20 Measured power transmission from the beam to the 1mm thick plate: $\eta_p = 0.005$, ... ; $\eta_p \approx 0.03$, ——— .

Chapter 10

CONCLUSIONS

The thesis is presented in four parts. The first part concerned discrete point coupling cases between a stiff source and a flexible receiver. The second part investigated a foundation consisting of a beam-stiffened plate. The third part involved a general complex built-up system consisting of a long-wavelength (low mode count) source and a short-wavelength (high mode count) receiver. Finally, the main theoretical developments were experimentally verified in part 4. The results were given at the end of each chapter. For completeness the main conclusions are briefly summarised below.

10.1 DISCRETE POINT COUPLINGS

Considering an issue on prediction and control of the power transmitted from a resiliently mounted machine to a flexible foundation due to the complex nature of the coupled system, a concept of 'power modes' was introduced and then used to estimate the power transmitted to a flexible receiver from an array of point force excitations in Chapter 2. Based on the power mode theory, the vibrational power transmitted by N discrete point forces was regarded as the power transmitted by N independent power modes following eigen-decomposition of the real part of the mobility matrix of the receiving structure. Simple expressions were developed for approximating the upper and lower bounds and the mean value of the transmitted power in terms of these power modes. It also has been shown that these approximations can be extended to more general cases, including that where both force and moment excitations are applied to the structure and where there are velocity source excitations. Finally numerical results were presented for the case of a plate excited at a number of points.

It is known that only under ideal, limiting cases, such as are considered here, can those source mobilities be neglected. In practice, however, the mobilities of the source may be important and thus have to be included. This leads to the application of the power mode technique to estimating the power transmission between a stiff source and a flexible receiver through discrete couplings. These were given in Chapter 3. In the first instance, only translational coupling motion of the system was considered, where the coupling degrees of freedom of a source/receiver system were all of the same sense and acted in the

same direction, e.g. normal to the surface of a plate-like receiver. Then a more general source/receiver system was considered, where both the translational and rotational motions of the system were involved, by applying a matrix scaling technique. Approximations were developed for the upper and lower bounds and the frequency average of the transmitted power. These depend only on the point mobilities of the source and receiver, and thus the amount of data required is reduced substantially compared to an exact description. This power mode approach was particularly useful when the mobility mismatch between the source and the receiver is big enough.

In principle, the power mode approach has two main advantages: first, it allows expressions for the upper and lower bounds and the mean value of the transmitted power to be developed in a simple manner; and secondly, it can involve both the translational and rotational motions of the system.

10.2 STRAIGHT LINE COUPLINGS

For continuous coupling studies in this thesis, vibration problems of a beam-stiffened plate system, consisting of a directly excited stiff beam attached to a large flexible plate, is particularly of interest, being broadly representative of the machinery foundation. When the difference between the wavelengths of the long wave stiff beams and the short wave flexible plates is very large, (which is very often for most relevant practical cases), the vibration around the structure is largely controlled by the long-wavelength stiff beam, but with some modifications or damping effects from the attached short-wavelength flexible plate. Under such circumstances, the frequency-response-functions (FRFs) of the source beam and the power transmitted to the plate are most relevant for a better understanding of the whole vibration properties of the coupled system.

This part of thesis concerns three cases of plate-stiffened beam systems in the first instance: (1) an infinite beam attached to an infinite plate in chapter 4, (2) a finite beam attached to an infinite plate in chapter 5 and (3) a finite beam attached to a finite plate when the beam and the plate have the same mode shapes along the coupling in chapter 6. Certain analytical/approximate methods are developed to predict simply and accurately the frequency response of the stiff beam and the power transmitted to the plate. Moreover, the interacting effects between the beam and the plate are investigated, being the effective loss factor and the effective mass added to the beam by the presence of the plate. Although only special cases of beam/plate coupling systems are involved in this part of study, it provides new methodologies, both analytical and approximate, on which the vibration of a

general stiff beam/flexible plate system can be predicted in a much simpler manner. This finally leads to Part III for predicting the vibration of a stiff source/flexible receiver system with general continuous couplings. The conclusions are respectively described below.

10.2.1 An infinite beam attached to an infinite plate

In this case, both Fourier Transform (FT) and wave analysis methods were used to give an analytical solution for the dynamic response of the coupled system. It was shown that only the beam wave motion with $k_b < k_p$ should be taken into account for predicting the power transmitted to the plate. When the wavenumber ratio between the beam and the plate is big enough, e.g. $k_p/k_b > 2$, the locally reacting impedance method can be used to approximate simply and accurately both the dynamic response of the beam and the power transmission to the plate. Moreover, it has been shown that the interacting effects between the beam and the plate may be viewed as adding an effective mass and an effective damping to each wave propagating in the beam. The energy 'dissipated' by the effective damping represents the energy transmitted from the beam to the plate. When the plate receiver is much more flexible than the source beam (e.g. behaves in a fuzzy manner to the beam), the induced effective loss factor depends on the wavenumber of the plate as well as the mass ratio between the beam and the plate, but is independent of the internal damping of the plate, being in good agreement with fuzzy structure theory. The effective mass is almost equivalent to the plate mass in a strip of width equal to one third of the plate wavelength in this case. Since the mass density of the plate m_p is usually relatively very small, the effective mass added is consequently very small. Therefore, the main effect of loading a fuzzy-like plate to a stiff beam can be viewed as adding effective damping to the beam dynamics.

10.2.2 A finite beam attached to an infinite plate

In chapter 5, a combined Mode/FT approach was developed to predict the vibration response of the coupled system. The displacement of the plate beyond the beam was set equal to zero by applying fictitious forces in the plate. The interface force and displacement distributions between the beam and the plate were first decomposed into a set of components in terms of beam modes, and then the force equilibrium and displacement compatibility (at the interface region) were enforced in the wavenumber domain by the conventional Fourier Transforms. As a result, the relation between the

modal coordinates of the beam and the wave motions of the plate can be determined. Finally both the FRFs of the beam and power transmitted to the plate can be predicted simply. The performance of this Mode/FT approach was assessed numerically against the conventional FRF-based sub-structuring method, by modelling the interface as discrete point couplings spaced at no more than a quarter of the plate wavelength apart. Very good approximations were found both for the dynamic response of the beam and the power transmission to the plate. The close relations between the Mode/FT approach and the locally reacting impedance method were also discussed. It was found that the results of these two methods meet very well when the plate receiver is relatively very flexible compared to the beam. Moreover, the interactions between the beam and the plate were analysed, being that the plate mainly added an effective loss factor and an effective mass to each mode of the beam. Two general trends were observed: (1) the lower the orders of the beam modes are, the bigger the induced loss factor and effective mass; (2) the effective damping of a given mode increases as frequency increases while the effective mass decreases. As far as a fuzzy-like plate receiver concerned, it is only important to consider the induced effective damping whereas the effective mass can be ignored. Also it was found that the effective damping is independent of the internal damping of the plate. This agrees well with the fuzzy structure theory.

10.2.3 A finite beam attached to a finite plate when the beam and the plate have the same mode shapes along the couplings

An analytical solution for the vibration response of the system was given based on modal analysis theory for this special coupling case. The advantage of this analytical approach is that a large number of physical DOFs at the interfaces can be reduced to a small number of generalized DOFs, simply by decomposing the interface force and displacement distributions into components of beam modes. As a result, this analytical approach was found much more efficient than the conventional FRF-based sub-structuring method, especially when the plate receiver has very short wavelengths. Moreover, the interactions between the beam and the plate were simulated as the effective loss factor and effective mass induced in each individual mode of the beam arising from the presence of the plate modes. These effective damping and mass were found to be in good agreement with those obtained from the case of a finite beam attached to an infinite plate. Although this analytical solution concerns only the simplest coupling form between a finite beam and a finite plate, it helps to shed light on developing a new methodology to simplify the

vibration predictions for general continuous couplings between a stiff source and a flexible receiver, which is the so-called 'mode-based' approach described in Part III.

10.3 GENERAL CONTINUOUS COUPLINGS

In this part of the research a mode-based approach was presented for a general complex built-up system consisting of a long-wavelength source and a short-wavelength receiver. The source and the receiver substructures are described separately in terms of their uncoupled natural modes (with free-free interface). The interface displacements between the source and the receiver are then decomposed into a complete set of orthogonal basis functions. In principle, the basis functions should meet the criteria of convenience, simplicity and accuracy. The dynamic response of the source/receiver system and the power transmitted to the receiver can then be determined analytically by enforcing the equilibrium and compatibility boundary conditions at the interface in terms of the generalized interface coordinates. The mode-based approach is able to accommodate both deterministic and statistical models, in that a large flexible structure is described asymptotically as a simply standing wave model, for example. But the assumption of a simple standing wave model requires that the interface positions are far away from the boundaries of the given receiver structure so that the influences of the near field wave motions can be ignored. This mode-based approach can be further extended to more general cases, where more than one type of wave motions may be involved, for example. The dynamic interactions between a stiff source and a large flexible receiver were investigated, in a form of dynamic stiffness modification matrix loaded on the source by presence of the receiver. Expressions were given for the effective loss factor and effective mass induced in each individual mode of the source by the receiver. Results were compared to those of 'Resound' [1] and fuzzy structure [5-6] theory, when a fuzzy-like receiver structure was assumed. It was found that they agreed well on the key result that fuzzy attachments add damping to the master structure which is independent of the internal damping of the attachments.

Numerical examples were given on plate-stiffened beam systems where both a straight- and an L-shaped beam were considered. Three approximate techniques were applied to describe the large and flexible plate models, i.e., simple standing wave models, infinite models and locally reacting models. Accordingly, vibration response predictions were made, respectively, by the mode-based approach, Mode/FT approach and locally reacting impedance method, and the associated results were compared against the 'exact' results determined by the conventional FRF-based sub-structuring method. It was found that both

the Mode/FT and locally reacting impedance methods were quite useful for straight beam coupling cases, whereas for the L-beam coupling cases, the mode-based approach was more appropriate. The plate-loaded effective mass and effective damping on the beam models were found with very similar dynamic properties as those described in previous chapters. It was also shown that the effective mass/damping tend to be independent of the internal damping of the plate in frequency average level. Especially when the modal overlap of the plate is so high that it exhibits non-resonant behaviour, the effective damping can be reasonably treated as independent of the internal damping of the plate.

10.4 EXPERIMENTAL RESULTS

As the final part of this thesis, laboratory measurements were arranged to verify experimentally the practicality of the main theoretical developments of the thesis. Freely suspended beam-stiffened plate models were set up. Measurements were made on both the point-mobility of the beam and the power transmitted to the plate, and then compared with the theoretical predictions by the mode-based approach and the Mode/FT approach where the plate receiver was assumed, respectively, as a simple standing wave model and an infinite model. The influences of the flexibility and damping of the plate on the vibration response of the coupled structure were investigated. The results shown were quite encouraging and in agreement with the theoretical expectations.

10.5 FURTHER RESEARCH WORK

It is expected that the mode-based approach can be developed for built-up structures which may consist of more than two substructures rather than only a single stiff source and a single flexible receiver. Once a generalized mode-based approach is established, the vibration response of and the power transmitted between each individual subsystem can be obtained in a simple manner. In addition, the dynamic interactions, then the coupling strength among directly and indirectly coupled subsystems, can be quantified.

Such a generalized mode-based approach could be potentially very useful in two research areas: first, it may be used to refine the conventional FEA methods to be much less computationally expensive by reducing significantly the DOFs involved; secondly, it provides a novel tool to determine the coupling loss factors (CLF) between each individual subsystem in a rigorous and systematic way. The effects of 'remote' subsystems on the 'local' energy flow may also be quantified. As a result, a so-called 'SEA-like' method may be developed to be applicable for strong coupling regime where

classical SEA was seen to be unsatisfied, namely, the traditional SEA may be reformulated with less restrictive assumptions.

Furthermore, when the uncertainties and variations of each subsystem are involved in the dynamic interaction quantification procedure, it is possible to estimate the variability of SEA-like parameters and system response predictions.

Ideally, the generalized mode-based approach, by combining with the conventional FEA and SEA methods, shall be able to provide a rigorous and systematic technique for predicting vibration properties in the mid-frequency range.

REFERENCES

1 R. S. Langley and P. Bremner 1999 *Journal of Acoustical Society of America* 105, 1657-1671. A hybrid method for the vibration analysis of complex structural-acoustic systems.

2 P. J. Shorter, B. K. Gardner and P. G. Bremner 2002 *Fifth World Congress on Computational Mechanics, July 7-12, Vienna, Austria.* A hybrid method for full spectrum noise and vibration prediction.

3 B. R. Mace and P. J. Shorter 2001 *Journal of Sound and Vibration* 242, 793-811. A local modal/perturbational method of estimating frequency response statistics of built-up structures with uncertain properties. doi: 10.1006/jsvi. 2000. 3389

4 C. Soize 1993 *Journal of the Acoustical Society of America* 94, 849-865. A model and numerical method in the medium frequency range for vibroacoustic predictions using the theory of structural fuzzy.

5 A. D. Pierce, V. W. Sparrow and D. A. Russell 1995 *Trans ASME Journal of Vibration and Acoustics* 117, 339-348. Fundamental structural-acoustic idealisations for structures with fuzzy internals.

6 M. Strasberg and D. Feit 1996 *Journal of the Acoustical Society of America* 99, 335-344. Vibration damping of large structures induced by attached small resonant structures.

7 L. Ji, B. R. Mace and R. J. Pinnington 2001 Institute of Sound and Vibration Research Technical Memorandum ISVR 877. Power transmission to flexible receiver by force sources.

8 L. Ji, B. R. Mace and R. J. Pinnington 2001 Institute of Sound and Vibration Research Technical Memorandum ISVR 876. Vibration power transmission between long-wavelength sources and short-wavelength receivers.

9 M. Petyt 1990 Introduction to finite element vibration analysis. Cambridge, MA: Cambridge University Press.

10 M. Lalanne, P. Berthier and J. D. Hagopian 1984 Mechanical Vibrations for Engineers. Chichester: Wiley.

11 L. Cremer, M. Heckl and E. E. Ungar 1988 Structure-Borne Sound. Berlin: Springer-Verlag, Second Edition.

12 F. J. Fahy 1994 *Phil. Trans. R. Soc. Lond. A* 346, 431-447. Statistical energy analysis: a critical overview.

13 B. R. Mace Structural Acoustics: Mechanical Vibrations at Higher Frequencies

14 R. H. Lyon and R. G. Dejong 1995 Theory and Application of Statistical Energy Analysis. Boston: Butterworth-Heinemann, Second Edition.

15 C. B. Burroughs, R. W. Fischer and F. R. Kern 1997 *Journal of Acoustical Society of America.* An introduction to statistical energy analysis.

16 J. Woodhouse 1981 *Applied Acoustics.* An introduction to Statistical energy analysis of structural vibration.

17 D. G. Crighton, A. P. Dowling, J. E. Williams, M. Heckl and F. G. Leppington 1992 Model Methods in Analytical Acoustics. Berlin: Springer-verlag.

18 R. R. Craig Jr 1995 *Trans ASME Journal of Vibrations and Acoustics* 117, 207-213. Substructure methods in vibration.

19 R. R. Craig Jr 1987 *International Journal of Analytical and Experimental Modal Analysis* 2, 59-72. A review of time-domain and frequency-domain component-mode synthesis methods.

20 J. T. Xing, W. G. Price and Q. H. Du 1996 *Phil. Trans. R. Soc. Lond.* A 354, 259-295. Mixed finite element substructure - subdomain methods for the dynamical analysis of coupled fluid-solid interaction problems.

21 E. Balmes 1996 *IMAC*, 204-210. Use of generalized interface degrees of freedom in component mode synthesis.

22 G. Kergoulay, E. Balmes, and D. Clouteau 2000 *ISMA* 25. Model reduction for efficient FEM/BEM coupling.

23 K. Shankar and A. J. Keane 1995 *Journal of Sound and Vibration* 185, 867-890. Energy flow predictions in a structure of rigidly joined beams using receptance theory.

24 K. Shankar and A. J. Keane 1997 *Journal of Sound and Vibration* 201, 491-513. Vibrational energy flow analysis using a substructure approach: the application of receptance theory to FEA and SEA.

25 M. Heckl 1961 *Journal of the Acoustical Society of America* 33, 640-651. Wave propagation on beam-plate systems.

26 R. M. Grice and R. J. Pinnington 2000 *Journal of Sound and Vibration* 230, 825-849. A method for the vibration analysis of built-up structures, Part I: Introduction and analytical analysis of the plate stiffened beam.

27 R. M. Grice and R. J. Pinnington 2000 *Journal of Sound and Vibration* 230, 851-875. A method for the vibration analysis of built-up structures, Part II: Analysis of the plate stiffened beam using a combination of finite element analysis and analytical impedance.

28 R. M. Grice and R. J. Pinnington 2000 *Journal of Sound and Vibration* 232, 449-471. Vibration analysis of a thin plate box using a finite element model which accommodates only in-plane motion.

29 R. J. Pinnington and D. C. R. Pearce 1990 *Journal of Sound and Vibration* 142, 461-479. Multipole expansion of the vibration transmission between a source and a receiver.

30 R. J. Pinnington, R. A Fulford and M. Terry 1996 *Proceedings of inter-noise 96*, 1587-1592. The use of polar mobility for predicting the coupled response of machine mounting system.

31 L. Meirovitch 1967 Analytical methods in vibrations. Macmillan Company, New York.

32 J. Su, A. T. Moorhouse and B. M. Gibbs 1995 *Journal of Sound and Vibration* 185, 737-741. Towards a practical characterisation for structure-borne sound sources based on mobility techniques. doi: 10. 1006/jsvi. 1995. 0415

33 H. R. Schwarz, H. Rutishauser, and E. Stiefel 1973 Numerical Analysis of Symmetric Matrices. Prentice-Hall, INC. Englewood Cliffs, N. J.

34 J. H. Wilkinson 1965 The Algebraic Eigenvalue Problem. Clarendon Press. Oxford

35 S. J. Elliott and M. E. Johnson 1993 *Journal of the Acoustical Society of America* **94**, 2194-2204. Radiation modes and the active control of sound power.

36 A. T. Moorhouse and B. M. Gibbs 1993 *Journal of Sound and Vibration* 167, 223-237. Prediction of the structure-borne noise emission of machines: development of a methodology.

37 B. A. T. Petersson 1993 *Journal of Sound and Vibration* 160, 43-66. Structural acoustic power transmission by point moment and force excitation, Part I: Beam- and frame-like structures.

38 B. A. T. Petersson 1993 *Journal of Sound and Vibration* 160, 67-91. Structural acoustic power transmission by point moment and force excitation, Part II: Plate-like structures.

39 A. T. Moorhouse and B. M. Gibbs 1998 *Acustica united with Acta Acustica* (84)5, 843-853. Simplified characterisation of multiple point excited structures using mobility matrix eigenvalues and eigenvectors.

40 A. T. Moorhouse 1999 *Proceedings of inter-noise 99*, 789-794. A mobility matrix simulation for force and moment excitation of structures.

41 E. E. Ungar and C. W. Dietrich 1966 *Journal of Sound and Vibration* 4, 224-241. High-frequency vibration isolation.

42 E. Bodewig 1959 Matrix Calculus. Amsterdam: North-Holland Publishing Company.

43 R. W. Ramirez 1985 The FFT Fundamentals and Concepts. Prentice-hall, Inc. Englewood cliffs. N.J.

44 Q. W. De 1978 Handbook of Mechanical Vibration.

45 D. J. Ewins 1984 Modal Testing: Theory and Practice. Research Study Press LTD. Letchworth, Hertfordshire, England.

46 K. G. McConnell 1995 Vibration Testing: Theory and Practice. John Wiley & Sons Inc.

47 E. J. Skudrzyk 1958 *Journal of the Acoustical Society of America* 30, 1140-1152. Vibrations of a system with a finite or an infinite number of resonances.

48 R. J. Pinnington 1982 Vibrational power transmission between sources and substructures. Ph. D Thesis, ISVR, University of Southampton.

49 N. H. Farag and J. Pan 1997 *Journal of the Acoustical Society of America* 102, 315-325. Dynamic response and power flow in the three-dimensional coupled beam structures. I. Analytical modelling.

50 J. T. Xing 1984 Some theoretical and computational aspects of finite element method and sub-structure sub-domain technique for dynamic analysis of the coupled fluid-solid interaction problems, Ph.D. thesis (in Chinese), the Department of Engineering Mechanics, Tsinghua University, Beijing, PRC.

51 J. Pan, J. Q. Pan and C. H. Hansen 1992 *Journal of the acoustical society of America* 92, 985-907. Total power flow from a vibrating rigidly body to a thin panel through multiple elastic mounts.

52 Y. K. Koh and R. G. White 1996 *Journal of Sound and Vibration* 196, 469-493. Analysis and control of vibrational power transmission to machinery supporting structures subjected to a multi-excitation system, Part 1: Driving point mobility matrix of beams and rectangular plates.

53 D. A. Thomas 1958 *Journal of the Acoustical Society of America* 30, 220-221. Characteristic impedances for flexure waves in thin plates.

54 G. B. Arfken and H. J. Weber 2001 Mathematical Methods for Physicists. San Diego: A Harcount Science and Technology Company, Fifth Edition.

55 T. C. Lim and J. Li 2000 *Journal of Sound and Vibration* 231(4), 1135-1157. A theoretical and computational study of the FRF-based sub-structuring technique applying enhanced least square and TSVD approaches.

56 P. A. Nelson and S. H. Yoon 2000 *Journal of Sound and Vibration* 233(4), 643-668. Inverse methods for source strength estimation.

57 J. T. Xing and W. G. Price 2003 *The Eighth International Conference on Recent Advances in Structural Dynamics (RASD), Southampton, UK.* A substructure approach to power flow analysis and application to engineering structures.

58 L. Meirovitch 1997 *Principles and Techniques of Vibrations.* New Jersey: Prentice-Hall, Inc.

59 M. W. Bonilha and F. J. Fahy 1998 *Journal of Sound and Vibration* 214(3), 443-467. On the vibration field correlation of randomly excited flat plate structures, I: Theory.

60 R. Courant 1956 Methods of Mathematical Physics. Institute of Mathematical Sciences, New York University.

61 I. Dyer 1960 *Journal of the Acoustical Society of America* 32, 1290-1297. Moment impedance of plates.

Appendix I

MODES OF A SIMPLY SUPPORTED THIN RECTANGULAR PLATE

A1.1 Natural modes and natural frequencies of the plate

For a thin rectangular plate bounded by four edges $x=0$, $x=l_x$, $y=0$ and $y=l_y$, as shown in Figure A1.1, the natural modes (mass-normalized) and natural frequencies are given by [11]

$$\Phi_{mn}(x,y)=\sqrt{\frac{4}{M_p}}\sin\frac{m\pi x}{l_x}\sin\frac{n\pi y}{l_y} \tag{A1.1}$$

$$\omega_{mn}=\sqrt{\frac{D_p}{m_p}}\left[\left(\frac{m\pi x}{l_x}\right)^2+\left(\frac{n\pi x}{l_y}\right)^2\right] \tag{A1.2}$$

where m_p and D_p are respectively the mass distribution (mass per unit area) and the bending stiffness of the plate, M_p is the total mass of the plate, and m and n are integers which give the orders of the modes.

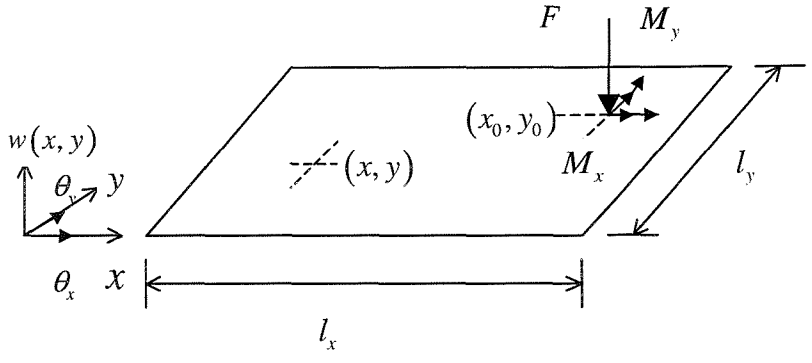

Figure A1.1 Simply supported thin rectangular plate

A1.2 Input- and transfer- mobilities of the plate

Let F and M_x and M_y represent respectively the harmonic force and moment excitations at the point (x_0, y_0), and w and θ_x and θ_y correspond to the displacement and rotational

responses at an arbitrary point (x, y). In Ref. [11], it is shown that the plate responses corresponding to the force excitation F can be determined by

$$w^F(x,y) = F\sum_{m=1}^{\infty}\sum_{n=1}^{\infty}\frac{\Phi_{mn}(x_0,y_0)\Phi_{mn}(x,y)}{\omega_{mn}^2(1+j\eta)-\omega^2} \tag{A1.3}$$

$$\theta_x^F(x,y) = \frac{\partial w^F}{\partial y} = F\sum_{m=1}^{\infty}\sum_{n=1}^{\infty}\frac{\Phi_{mn}(x_0,y_0)\frac{\partial}{\partial y}\left[\Phi_{mn}(x,y)\right]}{\omega_{mn}^2(1+j\eta)-\omega^2} \tag{A1.4}$$

$$\theta_y^F(x,y) = -\frac{\partial w^F}{\partial x} = -F\sum_{m=1}^{\infty}\sum_{n=1}^{\infty}\frac{\Phi_{mn}(x_0,y_0)\frac{\partial}{\partial x}\left[\Phi_{mn}(x,y)\right]}{\omega_{mn}^2(1+j\eta)-\omega^2} \tag{A1.5}$$

For the moment excitation M_x, the plate responses are given by [11, 51-52]

$$w^{M_x}(x,y) = M_x\sum_{m=1}^{\infty}\sum_{n=1}^{\infty}\frac{\frac{\partial}{\partial y}\left[\Phi_{mn}(x,y)\right]_{\substack{x=x_0\\y=y_0}}\Phi_{mn}(x,y)}{\omega_{mn}^2(1+j\eta)-\omega^2} \tag{A1.6}$$

$$\theta_x^{M_x}(x,y) = \frac{\partial w^{M_x}}{\partial y} = M_x\sum_{m=1}^{\infty}\sum_{n=1}^{\infty}\frac{\frac{\partial}{\partial y}\left[\Phi_{mn}(x,y)\right]_{\substack{x=x_0\\y=y_0}}\frac{\partial}{\partial y}\left[\Phi_{mn}(x,y)\right]}{\omega_{mn}^2(1+j\eta)-\omega^2} \tag{A1.7}$$

$$\theta_y^{M_x}(x,y) = -\frac{\partial w^{M_x}}{\partial x} = -M_x\sum_{m=1}^{\infty}\sum_{n=1}^{\infty}\frac{\frac{\partial}{\partial y}\left[\Phi_{mn}(x,y)\right]_{\substack{x=x_0\\y=y_0}}\frac{\partial}{\partial x}\left[\Phi_{mn}(x,y)\right]}{\omega_{mn}^2(1+j\eta)-\omega^2} \tag{A1.8}$$

The plate responses corresponding to the moment excitation M_y, similar to equations (A1.6)-(A1.8), can be written as

$$w^{M_y}(x,y) = -M_y\sum_{m=1}^{\infty}\sum_{n=1}^{\infty}\frac{\frac{\partial}{\partial x}\left[\Phi_{mn}(x,y)\right]_{\substack{x=x_0\\y=y_0}}\Phi_{mn}(x,y)}{\omega_{mn}^2(1+j\eta)-\omega^2} \tag{A1.9}$$

$$\theta_x^{M_y}(x,y) = \frac{\partial w^{M_y}}{\partial y} = -M_y\sum_{m=1}^{\infty}\sum_{n=1}^{\infty}\frac{\frac{\partial}{\partial y}\left[\Phi_{mn}(x,y)\right]_{\substack{x=x_0\\y=y_0}}\frac{\partial}{\partial x}\left[\Phi_{mn}(x,y)\right]}{\omega_{mn}^2(1+j\eta)-\omega^2} \tag{A1.10}$$

$$\theta_y^{M_y}(x,y) = -\frac{\partial w^{M_y}}{\partial x} = M_y\sum_{m=1}^{\infty}\sum_{n=1}^{\infty}\frac{\frac{\partial}{\partial x}\left[\Phi_{mn}(x,y)\right]_{\substack{x=x_0\\y=y_0}}\frac{\partial}{\partial x}\left[\Phi_{mn}(x,y)\right]}{\omega_{mn}^2(1+j\eta)-\omega^2} \tag{A1.11}$$

The force and moment transfer-mobilities can therefore be determined from the above equations as

$$Y_{tr}^{F\dot{w}} = \frac{j\omega w^{F}(x,y)}{F} \tag{A1.12}$$

$$Y_{tr}^{F\dot{\theta}_x} = \frac{j\omega \theta_x^{F}(x,y)}{F} \tag{A1.13}$$

$$Y_{tr}^{F\dot{\theta}_y} = \frac{j\omega \theta_y^{F}(x,y)}{F} \tag{A1.14}$$

$$Y_{tr}^{M_x\dot{w}} = \frac{j\omega w^{M_x}(x,y)}{M_x},\ Y_{tr}^{M_y\dot{w}} = \frac{j\omega w^{M_y}(x,y)}{M_y} \tag{A1.15}$$

$$Y_{tr}^{M_x\dot{\theta}_x} = \frac{j\omega \theta_x^{M_x}(x,y)}{M_x},\ Y_{tr}^{M_y\dot{\theta}_y} = \frac{j\omega \theta_y^{M_y}(x,y)}{M_y} \tag{A1.16}$$

$$Y_{tr}^{M_x\dot{\theta}_y} = \frac{j\omega \theta_y^{M_x}(x,y)}{M_x},\ Y_{tr}^{M_y\dot{\theta}_x} = \frac{j\omega \theta_x^{M_y}(x,y)}{M_y} \tag{A1.17}$$

The force and moment input-mobility terms $Y_{in}^{(\ )}$ can be determined by letting (x,y) in equations (A1.12)-(A1.17) be replaced by (x_0,y_0). For brevity, these expressions are not repeated here.

It is seen then that

$$Y_{in}^{F\dot{\theta}_x} = Y_{in}^{M_x\dot{w}},\ Y_{tr}^{F\dot{\theta}_x} = Y_{tr}^{M_x\dot{w}} \tag{A1.18}$$

$$Y_{in}^{F\dot{\theta}_y} = Y_{in}^{M_y\dot{w}},\ Y_{tr}^{F\dot{\theta}_y} = Y_{tr}^{M_y\dot{w}} \tag{A1.19}$$

$$Y_{in}^{M_x\dot{\theta}_y} = Y_{in}^{M_y\dot{\theta}_x},\ Y_{tr}^{M_x\dot{\theta}_y} = Y_{tr}^{M_y\dot{\theta}_x} \tag{A1.20}$$

A1.3 Dynamic responses of the plate: Mobility matrix

A mobility matrix can be formed to obtain the dynamic response of the plate when subjected to external force and moment excitations.

For example when the plate is excited simultaneously by F_1, M_{x1} and M_{y1} at (x_1,y_1), and F_2, M_{x2} and M_{y2} at (x_2,y_2), the dynamic responses at these two points can be expressed as

$$\begin{Bmatrix} \dot{w}_1 \\ \dot{\theta}_{x1} \\ \dot{\theta}_{y1} \\ \dot{w}_2 \\ \dot{\theta}_{x2} \\ \dot{\theta}_{y2} \end{Bmatrix} = \begin{bmatrix} Y_{in}^{F\dot{w}} & Y_{in}^{M_x\dot{w}} & Y_{in}^{M_y\dot{w}} & Y_{tr}^{F\dot{w}} & Y_{tr}^{M_x\dot{w}} & Y_{tr}^{M_y\dot{w}} \\ Y_{in}^{F\dot{\theta}_x} & Y_{in}^{M_x\dot{\theta}_x} & Y_{in}^{M_y\dot{\theta}_x} & Y_{tr}^{F\dot{\theta}_x} & Y_{tr}^{M_x\dot{\theta}_x} & Y_{tr}^{M_y\dot{\theta}_x} \\ Y_{in}^{F\dot{\theta}_y} & Y_{in}^{M_x\dot{\theta}_y} & Y_{in}^{M_y\dot{\theta}_y} & Y_{tr}^{F\dot{\theta}_y} & Y_{tr}^{M_x\dot{\theta}_y} & Y_{tr}^{M_y\dot{\theta}_y} \\ Y_{tr}^{F\dot{w}} & Y_{tr}^{M_x\dot{w}} & Y_{tr}^{M_y\dot{w}} & Y_{in}^{F\dot{w}} & Y_{in}^{M_x\dot{w}} & Y_{in}^{M_y\dot{w}} \\ Y_{tr}^{F\dot{\theta}_x} & Y_{tr}^{M_x\dot{\theta}_x} & Y_{tr}^{M_y\dot{\theta}_x} & Y_{in}^{F\dot{\theta}_x} & Y_{in}^{M_x\dot{\theta}_x} & Y_{in}^{M_y\dot{\theta}_x} \\ Y_{tr}^{F\dot{\theta}_y} & Y_{tr}^{M_x\dot{\theta}_y} & Y_{tr}^{M_y\dot{\theta}_y} & Y_{in}^{F\dot{\theta}_y} & Y_{in}^{M_x\dot{\theta}_y} & Y_{in}^{M_y\dot{\theta}_y} \end{bmatrix} \begin{Bmatrix} F_1 \\ M_{x1} \\ M_{y1} \\ F_2 \\ M_{x2} \\ M_{y2} \end{Bmatrix} \tag{A1.21}$$

From equations (A1-18)-(A1.20), it is seen that the mobility matrix in equation (A1.21) is symmetric.

A1.4 Matrix scaling and input power

Let the real part of the mobility matrix in equation (A1.21) be scaled by a diagonal matrix $\mathbf{D}_c = diag\left[\left(\mathrm{Re}\{Y_{nn}\}\right)^{-1}\right]$. The input power can then be approximated by the power mode approach as described in Chapter 2.

Appendix II

MODES OF A SIMPLY SUPPORTED EULER-BERNOULLI BEAM

A1.1 Natural modes and natural frequencies of the beam

For an Euler-Bernoulli beam with both ends simply supported, its natural modes (mass-normalized) and natural frequencies are given by [11]

$$\Phi_n(x)=\sqrt{\frac{2}{m_b L_b}}\sin\frac{n\pi x}{L_b} \tag{A2.1}$$

$$\omega_n=\sqrt{\frac{D_b}{m_b}}\left(\frac{n\pi x}{L_b}\right)^2 \tag{A2.2}$$

where m_b and D_b are respectively the mass distribution (mass per unit length) and bending stiffness of the beam, L_b is the length of the beam, and n is the order of the beam mode.

A1.2 Input- and transfer-mobilities of the beam

Let F_0 and M_0 represent respectively the harmonic force and moment excitations at the point x_0, and w and θ correspond to the displacement and rotational responses at an arbitrary point x. Similar to Appendix I, the beam responses corresponding to the force excitation F_0 are given by

$$w_F(x)=F_0\sum_{n=1}^{\infty}\frac{\Phi_n(x_0)\Phi_n(x)}{\omega_n^2(1+j\eta)-\omega^2} \tag{A2.3}$$

$$\theta_F(x_0)=\frac{\partial w_F(x)}{\partial x}=F_0\sum_{n=1}^{\infty}\frac{\Phi_n(x_0)\frac{\partial}{\partial x}\left[\Phi_n(x)\right]}{\omega_n^2(1+j\eta)-\omega^2} \tag{A2.4}$$

The beam responses corresponding to the moment excitation M_0 are given by

$$w_M(x)=M_0\sum_{n=1}^{\infty}\frac{\frac{\partial}{\partial x}\left[\Phi_n(x)\right]_{x=x_0}\Phi_n(x)}{\omega_n^2(1+j\eta)-\omega^2} \tag{A2.5}$$

$$\theta_M(x)=\frac{\partial w_M(x,y)}{\partial x}=M_0\sum_{n=1}^{\infty}\frac{\frac{\partial}{\partial x}\left[\Phi_n(x)\right]_{x=x_0}\frac{\partial}{\partial x}\left[\Phi_n(x)\right]}{\omega_n^2(1+j\eta)-\omega^2} \tag{A2.6}$$

The force and moment transfer-mobilities can therefore be determined from the above equations as

$$Y_{tr}^{(F\dot{w})}(x)=\frac{j\omega w_F(x)}{F_0} \tag{A2.7}$$

$$Y_{tr}^{(F\dot{\theta})}(x)=\frac{j\omega\theta_F(x)}{F_0} \tag{A2.8}$$

$$Y_{tr}^{(M\dot{w})}=\frac{j\omega w_M(x)}{M_0} \tag{A2.9}$$

$$Y_{tr}^{(M\dot{\theta})}(x)=\frac{j\omega\theta_M(x)}{M_0} \tag{A2.10}$$

The input-mobility terms $Y_{in}^{(\ )}$ can be obtained by letting x in equations (A2.7)-(A2.10) be replaced by x_0. It is seen then that

$$Y_{in}^{(M\dot{w})}=Y_{in}^{(F\dot{\theta})},\ Y_{tr}^{(M\dot{w})}=Y_{tr}^{(F\dot{\theta})} \tag{A2.11}$$

The above are the modal-summation solution for the input- and transfer-mobilities of the beam.

A2.3 Dynamic responses of the beam: Mobility matrix

When the beam is excited simultaneously by F_1 and M_1 at x_1 and F_2 and M_2 at x_2, the dynamic responses at these two points can be obtained by

$$\begin{Bmatrix}\dot{w}_1\\ \dot{\theta}_1\\ \dot{w}_2\\ \dot{\theta}_2\end{Bmatrix}=\begin{bmatrix}Y_{in}^{(F\dot{w})} & Y_{in}^{(M\dot{w})} & Y_{tr}^{(F\dot{w})} & Y_{tr}^{(M\dot{w})}\\ Y_{in}^{(F\dot{\theta})} & Y_{in}^{(M\dot{\theta})} & Y_{tr}^{(F\dot{\theta})} & Y_{tr}^{(M\dot{\theta})}\\ Y_{tr}^{(F\dot{w})} & Y_{tr}^{(M\dot{w})} & Y_{in}^{(F\dot{w})} & Y_{in}^{(M\dot{w})}\\ Y_{tr}^{(F\dot{\theta})} & Y_{tr}^{(M\dot{\theta})} & Y_{in}^{(F\dot{\theta})} & Y_{in}^{(M\dot{\theta})}\end{bmatrix}\begin{Bmatrix}F_1\\ M_1\\ F_2\\ M_2\end{Bmatrix} \tag{A2.12}$$

From equation (A2.11), it is seen that the mobility matrix in equation (A2.12) is symmetric.

Appendix III

THE FORCED RESPONSE OF A THIN INFINITE PLATE IN BENDING

A3.1 Boundary conditions of the thin infinite plate

The analytical solution for the input- and transfer-mobilities of a point-excited thin infinite plate in bending is found by assuming the following:

a) The displacement must be axially symmetric;

b) At the excitation point, the angular rotation or slope must vanish by symmetry;

c) At the excitation point, the sum of the shear forces must be equal to the exciting force;

d) The displacements at large distance from the excitation point must behave like a decaying wave (i.e., the Sommerfeld 'radiation condition' [11]).

A3.2 Force input- and transfer-mobilities of the plate [11, 53]

The differential equation for small transverse displacements w of a thin plate under no tension, neglecting losses, rotary inertia, and transverse shear flexibility, is

$$D_p \Delta\Delta w + m_p \frac{\partial^2 w}{\partial t^2} = 0 \qquad \text{(A3.1)}$$

where Δ is the Laplace Operator in the plane of the plate and m_p is the mass density of the plate. For vibrations that are harmonic (sinusoidal time-variations), by introducing the bending wavenumber $k = \sqrt[4]{m_p \omega^2 / D_p}$, equation (A3.1) reduces to

$$\Delta\Delta w - k^4 w = 0 \qquad \text{(A3.2)}$$

The general solution, obtained from the above equation, may be written as

$$w(r) = C_1 H_0^{(2)}(kr) + C_2 H_0^{(2)}(-jkr) \qquad \text{(A3.3)}$$

where $H_0^{(2)}$ is the zero-order Hankel function of the second kind, and $C_2 H_0^{(2)}(-jkr)$ term represents an exponentially decaying nearfield.

When the plate is excited by a harmonic force F_0 at the original point $r=0$, by the boundary conditions (b) and (c) in section A3.1, the plate transverse and rotational displacements w and θ at an arbitrary point with a distance r to the original point can be determined by [11]

$$w^F(r)=\frac{F_0}{j8D_pk^2}\left[H_0^{(2)}(kr)+j\frac{2}{\pi}K_0(kr)\right] \tag{A3.4}$$

$$\theta^F(r)=\frac{\partial w}{\partial r}=\frac{F_0}{j8D_pk}\left[H_1^{(2)}(kr)-j\frac{2}{\pi}K_1(kr)\right] \tag{A3.5}$$

where $H_0^{(2)}$ and $H_1^{(2)}$ are respectively the zero- and the first-order Hankel functions of the second kind, while K_0 and K_1 are the zero- and first-order modified Bessel functions of the second kind. At $r=0$, w and θ are respectively

$$w^F(0)=\frac{F_0}{8jD_pk^2} \tag{A3.6}$$

$$\theta^F(0)=0 \tag{A3.7}$$

As a result, the force input- and transfer-mobilities of an infinite thin plate can be determined by

$$Y_{in}^{(F\dot{w})}=\frac{j\omega w(0)}{F_0},\ Y_{tr}^{(F\dot{w})}=\frac{j\omega w(r)}{F_0} \tag{A3.8}$$

$$Y_{in}^{(F\dot{\theta})}=0,\ Y_{tr}^{(F\dot{\theta})}=\frac{j\omega\theta(r)}{F_0} \tag{A3.9}$$

A3.3 Moment input- and transfer-mobilities of the plate [11, 61]

Let the localized moment M_0 at $r=0$ be considered as applied over a disk of radius a located in the plate. The disk may be assumed to be infinitely rigid and massless. The plate can thus be taken as excited by two oppositely directed point forces F and $-F$, applied at two neighbouring points $r=a$ and $r=-a$, with $M_0=2aF$. In view of equation (A3.4), the plate response, at an arbitrary point with a distance r to the original point, corresponding to this system of excitation forces is given by

$$w^M(r)=\frac{F}{8jD_pk^2}\left[\Pi(k(r-a))-\Pi(k(r+a))\right] \tag{A3.10}$$

where Π represents a propagation function as

$$\Pi(x)=H_0^{(2)}(x)+j\frac{2}{\pi}K_0(x) \tag{A3.11}$$

In the expansion of equation (A3.10) for small arguments, when only the lower order terms are indicated, it gives

$$\Pi\left(k(r-a)\right)\approx 1+2k^2(r-a)^2\left[\alpha_1+\alpha_2\ln\frac{1}{2}\gamma k(r-a)-\frac{1}{2}\alpha_2\ln(-j)\right] \tag{A3.12}$$

$$\Pi\left(k(r+a)\right)\approx 1+2k^2(r+a)^2\left[\alpha_1+\alpha_2\ln\frac{1}{2}\gamma k(r+a)-\frac{1}{2}\alpha_2\ln(-j)\right] \tag{A3.13}$$

where α_1, α_2 and γ are defined as

$$\alpha_1=-\frac{1}{4}-\frac{j}{2\pi},\ \alpha_2=\frac{j}{2\pi},\ \gamma=1.781 \tag{A3.14}$$

By differentiating equation (A3.10) with respect to r and letting $a\to 0$, the rotational displacements of the plate, can be written as

$$\theta(r)\approx\frac{M_0}{8jD_p}\left[H_0^{(2)}(kr)-\frac{1}{kr}H_1^{(2)}(kr)+j\frac{2}{\pi}\left(K_0(kr)+\frac{1}{kr}K_1(kr)\right)\right] \tag{A3.15}$$

At $r=0$, the plate rotational displacement, after some manipulation, is given by [11]

$$\theta(0)\approx\frac{M_0}{j16D_p}\left[1-j\frac{4}{\pi}\ln\frac{1}{2}\gamma ka\right] \tag{A3.16}$$

From equations (A3.15) and (A3.16), the moment input- and transfer mobilities can be determined by

$$Y_{in}^{(M\dot{\theta})}=\frac{j\omega\theta(0)}{M_0},\ Y_{tr}^{(M\dot{\theta})}=\frac{j\omega\theta(r)}{M_0} \tag{A3.17}$$

It is clear that the moment input-mobility depends upon the size of applied 'point'. In fact the practical values of ka are usually much less than 10^{-1}. In Ref. [61], it is pointed out that the successful application of the above results requires the two conditions: (1) $(kh_p)^2<<1$ (h_p is the thickness of the plate) to retain the thin plate assumption; (2) $(\pi a/h_p)^2>>1$ to neglect the transverse shear effects in the plate. Thus the appropriate value of a should meet both $\pi a/h>>1$ and $ka<10^{-1}$.

Appendix IV

WAVENUMBER OF THE BEAM AFTER IT IS COUPLED TO A LOCALLY REACTING PLATE

Based on the analytical procedure given in Chapter 4, it is seen when a beam is coupled to a locally reacting plate, the wavenumber of the beam can be simply determined by

$$k_b' \approx \sqrt[4]{\frac{m_b\omega^2 - j\omega Z_p}{D_b}} \tag{A4.1}$$

where

$$Z_p \approx \frac{2m_p\omega}{k_p}(1+j) \tag{A4.2}$$

The real part of k_b', from the above two equations, is given as

$$k_b' \approx \sqrt[4]{\frac{m_b\omega^2}{D_b} + \frac{2D_p k_p^3}{D_b}} \tag{A4.3}$$

Equation (A1.3) can then be re-written as

$$k_b' \approx k_b \sqrt[4]{1 + \frac{2D_p k_p^4}{D_b k_b^4}\frac{1}{k_p}} = k_b \sqrt[4]{1 + \left(\frac{m_p\omega^2}{m_b\omega^2}\right)\frac{2}{k_p}} \tag{A4.4}$$

where $k_b \approx \sqrt[4]{m_b\omega^2/D_b}$. It finally yields

$$k_b' \approx k_b \sqrt[4]{1 + \frac{m_p\lambda_p}{m_b\pi}} \tag{A4.5}$$

The locally reacting condition $k_p/k_b' > 2$ given in Refs. [26-27] can then be estimated as

$$\frac{k_p}{k_b} > 2\left(\sqrt[4]{1 + \frac{m_p\lambda_p}{m_b\pi}}\right) \tag{A4.6}$$

When the plate component is relatively very flexible compared to the beam such that

$$\frac{m_p\lambda_p}{\pi} << m_b \tag{A4.7}$$

equation (A1.5) gives

$$k_b' \approx k_b \tag{A4.8}$$

In this case, the locally reacting condition $k_p/k_b' > 2$ may be simply determined by $k_p/k_b > 2$.

Appendix V

FRF-BASED SUB-STRUCTURING METHOD FOR A GENERAL SOURCE-RECEIVER SYSTEM

To model the dynamic characteristic of complex built-up structures, the frequency response function (FRF)-based sub-structuring technique is found to be a rather convenient and attractive [23-24]. The fundamental concept of this technique is to utilize the individual uncoupled component FRFs to construct the total system response based on dynamic compliance formulation. Figure A5.1 illustrates a general source-receiver system, of which, both the source and the receiver has, in general, infinite number of degrees of freedom, and the two structures coupled at a finite number of points. The connections between the source and the receiver can be either rigid or flexible with dynamic stiffness characteristics. For simplicity, here, these coupling stiffness terms have been assumed to be included as part of one component.

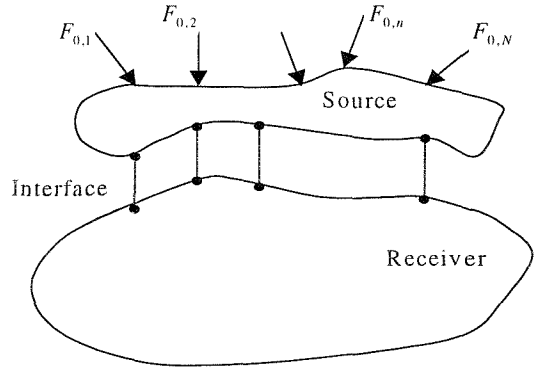

Figure A5.1 a general source-receiver system

Let $\bar{\mathbf{M}}_{0S}$ be the mobility matrix of the source from the excitation coordinates to the coupling points when it separated from the receiver, and $\bar{\mathbf{M}}_S$ and $\bar{\mathbf{M}}_R$ be the mobility matrices of the uncoupled source and receiver at the interface coupling points. When the source structure is excited by a set of external forces $\mathbf{F}_0$, the dynamic response of the coupled system can be obtained by applying compatibility and equilibrium between the interface DOFs and forces, as below.

For the source structure, there is

$$\mathbf{V}_S = \bar{\mathbf{M}}_{0S}\mathbf{F}_0 + \bar{\mathbf{M}}_S\mathbf{F}_S \qquad \text{(A5.1)}$$

where $\mathbf{V}_S$ and $\mathbf{F}_S$ are respectively the velocity and force vectors of the source structure at the interface points.

For the receiver structure, there is

$$\mathbf{V}_R = \bar{\mathbf{M}}_R \mathbf{F}_R \tag{A5.2}$$

where $\mathbf{V}_R$ and $\mathbf{F}_R$ are respectively the velocity and force vectors of the receiver structure at the interface points.

The compatibility and equilibrium boundary conditions at the interface give

$$\mathbf{V}_S = \mathbf{V}_R, \ \mathbf{F}_S = -\mathbf{F}_R \tag{A5.3}$$

The dynamic responses of the receiver at the coupling positions are then given by

$$\mathbf{F}_R = \left[\bar{\mathbf{M}}_S + \bar{\mathbf{M}}_R\right]^{-1} \bar{\mathbf{M}}_{0S} \mathbf{F}_0 \tag{A5.4}$$

$$\mathbf{V}_R = \bar{\mathbf{M}}_R \left[\bar{\mathbf{M}}_S + \bar{\mathbf{M}}_R\right]^{-1} \bar{\mathbf{M}}_{0S} \mathbf{F}_0 \tag{A5.5}$$

Consequently, the power transmitted from the source to the receiver can be written as

$$P_{tr} = \frac{1}{2} \mathrm{Re}\left\{ \mathbf{F}_0{}^H \left[\left(\bar{\mathbf{M}}_S + \bar{\mathbf{M}}_R\right)^{-1} \bar{\mathbf{M}}_{0S} \right]^H \bar{\mathbf{M}}_R \left[\left(\bar{\mathbf{M}}_S + \bar{\mathbf{M}}_R\right)^{-1} \bar{\mathbf{M}}_{0S} \right] \mathbf{F}_0 \right\} \tag{A5.6}$$

Equation (A5.6) is the general expression of the power transmission from the source to the receiver. It can be re-written as

$$P_{tr} = \frac{1}{2} \mathrm{Re}\left\{ \mathbf{V}_{sf}{}^H \left(\left[\bar{\mathbf{M}}_S + \bar{\mathbf{M}}_R\right]^{-1} \right)^H \bar{\mathbf{M}}_R \left[\bar{\mathbf{M}}_S + \bar{\mathbf{M}}_R\right]^{-1} \mathbf{V}_{sf} \right\} \tag{A5.7}$$

where $\mathbf{V}_{sf} = \bar{\mathbf{M}}_{0S} \mathbf{F}_0$ is the free velocity vector of the source structure at its interface points when it is uncoupled from the receiver structure.

The FRF-based sub-structuring method has the advantage of being able to incorporate experimental FRFs directly into its spectral formulations. However, it inherently requires several matrix inversion calculations, which provide two major computational difficulties: one is the amplification of errors in the FRF-matrix inversion process, and the other is that the inversion computation could be very expensive for the large interface DOF cases, e.g., line coupling. The first difficulty can be overcome by applying least squares (LS) and singular value decomposition (SVD) approaches [55-56], while the second problem can be ameliorated by modern high-speed digital computers.

Appendix VI

NATURAL FREQUENCIES AND MODE SHAPES OF AN L-SHAPED BEAM

When an L-shaped beam is excited by an external point force F_0, as shown in Figure A6.1, the dynamic response of the beam structure can be determined using the modal summation approach.

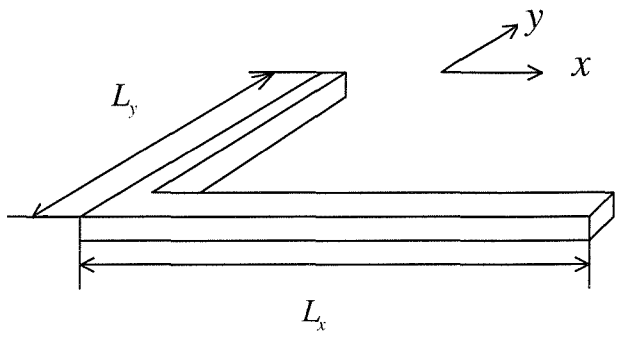

Figure A6.1 The L-shaped beam model

Let the "L"-shaped beam be viewed as two beam components rigidly connected at one joint, and the other ends of the beam components keep being described by their original boundary conditions, as shown in Figure A6.2. Here both the other ends of the beam components are simply supported, and also both the components of the beam are assumed to be uniform with same material properties and constant square cross sections.

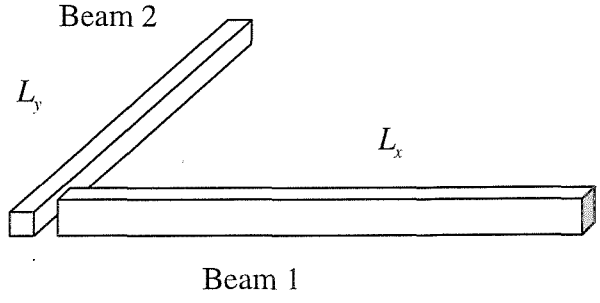

Figure A6.2 Decomposition of the L-shape beam

The displacements, deformations and stresses at the joint end of the L-beam are given in Figure A6.3.

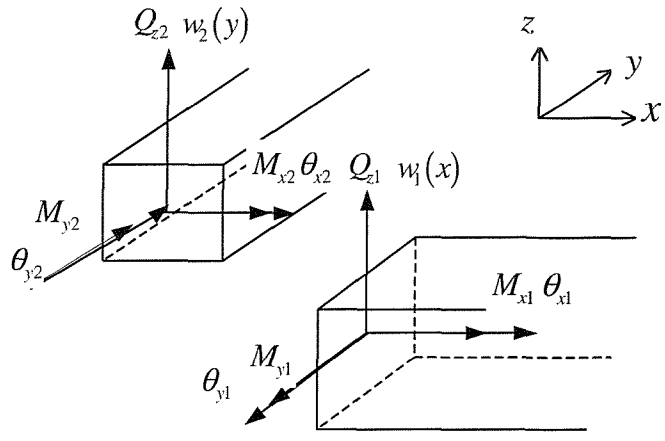

Figure A6.3 Displacements, deformations and stresses at the joint end of the L-beam

The equations of free flexural and torsional motions of the beams have the well-known forms as [10]

$$D\frac{\partial^4 w_1}{\partial x^4}+m\frac{\partial^2 w_1}{\partial t^2}=0 \tag{A6.1}$$

$$T\frac{\partial^2 \theta_{x1}}{\partial x^2}-J_x\frac{\partial^2 \theta_{x1}}{\partial t^2}=0 \tag{A6.2}$$

$$D\frac{\partial^4 w_2}{\partial y^4}+m\frac{\partial^2 w_2}{\partial t^2}=0 \tag{A6.3}$$

$$T\frac{\partial^2 \theta_{y2}}{\partial y^2}-J_y\frac{\partial^2 \theta_{y2}}{\partial t^2}=0 \tag{A6.4}$$

where $w_1(x)$, $w_2(y)$, $\theta_{x1}(x)$ and $\theta_{y2}(y)$ are the flexural and torsional displacements of the beam components 1 and 2 in z-direction, x-direction and y-directions, respectively, D and T are the flexural and torsional stiffness of the beam components, respectively, and m, J_x and J_y are the mass distribution, the mass moment of the inertia per unit length about the x- and y- directions, respectively. Since it is assumed that the two beam components have the same square cross sections, $J_x = J_y = J$. The complementary solutions of the above equations then give

$$w_1(x)=A_1\cosh(kx)+B_1\sinh(kx)+C_1\cos(kx)+D_1\sin(kx) \tag{A6.5}$$

$$w_2(y) = A_2\cosh(ky) + B_2\sinh(ky) + C_2\cos(ky) + D_2\sin(ky) \tag{A6.6}$$

$$\theta_{x1}(x) = E_1\cos(k_t x) + F_1\sin(k_t x) \tag{A6.7}$$

$$\theta_{y2}(y) = E_2\cos(k_t y) + F_2\sin(k_t y) \tag{A6.8}$$

where $k = \sqrt{m\omega^2/D}$ and $k_t = \sqrt{J/T\omega}$ are the corresponding bending and torsional wavenumbers of the beam components, respectively.

Enforcing force equilibrium and displacement compatibility at the joint end of the L-beam, yields

$$w_1(x)\big|_{x=0} = w_2(y)\big|_{y=0} \tag{A6.9}$$

$$Q_{z1}(x)\big|_{x=0} = -Q_{z2}(y)\big|_{y=0} \tag{A6.10}$$

$$\theta_{y1}(x)\big|_{x=0} = -\theta_{y2}(y)\big|_{y=0} \tag{A6.11}$$

$$M_{y1}(x)\big|_{x=0} = M_{y2}(y)\big|_{y=0} \tag{A6.12}$$

$$\theta_{x1}(x)\big|_{x=0} = \theta_{x2}(y)\big|_{y=0} \tag{A6.13}$$

$$M_{x1}(x)\big|_{x=0} = -M_{x2}(y)\big|_{y=0} \tag{A6.14}$$

where Q_{z1} and Q_{z2} are the shear forces at the cross sections of beam 1 and 2, respectively, given as

$$Q_{z1}(x) = D\frac{\partial^3 w_1}{\partial x^3} \tag{A6.15}$$

$$Q_{z2}(y) = D\frac{\partial^3 w_2}{\partial y^3} \tag{A6.16}$$

M_{y1} and M_{x2} are the bending moments at the cross sections of beam 1 and 2, respectively, given as

$$M_{y1} = -D\frac{\partial^2 w_1}{\partial x^2} \tag{A6.17}$$

$$M_{x2} = -D\frac{\partial^2 w_2}{\partial y^2} \tag{A6.18}$$

M_{x1} and M_{y2} are the torsional moments at the cross sections of beam 1 and 2, respectively, given as

$$M_{x1} = T\frac{\partial \theta_{x1}}{\partial x} \tag{A6.19}$$

$$M_{y2} = T\frac{\partial \theta_{y2}}{\partial y} \tag{A6.20}$$

θ_{y1} and θ_{x2} are the angular rotation of the beam at the cross sections of beam 1 and 2, respectively, given as

$$\theta_{y1} = \frac{\partial w_1}{\partial x} \tag{A6.21}$$

$$\theta_{x2} = \frac{\partial w_2}{\partial y} \tag{A6.22}$$

The boundary conditions at the other two simply supported ends of the beam components are

$$w_1(x)\Big|_{x=L_x} = 0 \tag{A6.23}$$

$$w_2(y)\Big|_{y=L_y} = 0 \tag{A6.24}$$

$$M_{y1}(x)\Big|_{x=L_x} = 0 \tag{A6.25}$$

$$M_{x2}(y)\Big|_{y=L_y} = 0 \tag{A6.26}$$

$$M_{x1}(x)\Big|_{x=L_x} = 0 \tag{A6.27}$$

$$M_{y2}(y)\Big|_{y=L_y} = 0 \tag{A6.28}$$

Combining equations (A6.5), (A6.6) and (A6.9), gives

$$A_1 + C_1 = A_2 + C_2 \tag{A6.29}$$

Combining equations (A6.5), (A6.6), (A6.10), (A6.15) and (A6.16), gives

$$B_1 - D_1 = -(B_2 - D_2) \tag{A6.30}$$

Combining equations (A6.5), (A6.8), (A6.12), (A6.17) and (A6.19), gives

$$-Dk^2(A_1 - C_1) = Tk_t F_2 \tag{A6.31}$$

Combining equations (A6.5), (A6.8), (A6.11) and (A6.21), gives

$$k\left(B_1 + D_1\right) = -E_2 \tag{A6.32}$$

Combining equations (A6.6), (A6.7), (A6.14), (A6.18) and (A6.19), gives

$$Dk^2\left(A_2 - C_2\right) = Tk_t F_1 \tag{A6.33}$$

Combining equations (A6.6), (A6.7), (A6.13) and (A6.22), gives

$$k\left(B_2 + D_2\right) = E_1 \tag{A6.34}$$

Combining equations (A6.5) and (A6.23), (A6.6) and (A6.24), respectively, yields

$$A_1 \cosh\left(kL_x\right) + B_1 \sinh\left(kL_x\right) + C_1 \cos\left(kL_x\right) + D_1 \sin\left(kL_x\right) = 0 \tag{A6.35}$$

$$A_2 \cosh\left(kL_y\right) + B_2 \sinh\left(kL_y\right) + C_2 \cos\left(kL_y\right) + D_2 \sin\left(kL_y\right) = 0 \tag{A6.36}$$

Combining equations (A6.5), (A6.17), and (A6.25), yields

$$A_1 \cosh\left(kL_x\right) + B_1 \sinh\left(kL_x\right) - C_1 \cos\left(kL_x\right) - D_1 \sin\left(kL_x\right) = 0 \tag{A6.37}$$

Combining equations (A6.6), (A6.18) and (A6.26), yields

$$A_2 \cosh\left(kL_y\right) + B_2 \sinh\left(kL_y\right) - C_2 \cos\left(kL_y\right) - D_2 \sin\left(kL_y\right) = 0 \tag{A6.38}$$

Combining equations (A6.7), (A6.8), (A6.19), (A6.20), (A6.27) and (A6.28), gives

$$-E_1 \sin\left(k_t L_x\right) + F_1 \cos\left(k_t L_x\right) = 0 \tag{A6.39}$$

$$-E_2 \sin\left(k_t L_y\right) + F_2 \cos\left(k_t L_y\right) = 0 \tag{A6.40}$$

From equations (A6.35) and (A6.37), it yields

$$A_1 = -\tanh\left(kL_x\right) B_1 \tag{A6.41}$$

$$C_1 = -D_1 \tan\left(kL_x\right) \tag{A6.42}$$

From equations (A6.36) and (A6.38), it yields

$$A_2 = -\tanh\left(kL_y\right) B_2 \tag{A6.43}$$

$$C_2 = -D_2 \tan\left(kL_y\right) \tag{A6.44}$$

From equations (A6.39) and (A6.40), it follows that

$$F_1 = E_1 \tan\left(k_t L_x\right) \tag{A6.45}$$

$$F_2 = E_2 \tan\left(k_t L_y\right) \tag{A6.46}$$

Equations (A6.32) and (A6.34) yield

$$\left(B_1 + D_1\right) + \left(B_2 + D_2\right) = \frac{1}{k}\left(E_1 - E_2\right) \tag{A6.47}$$

Combining equations (A6.30) and (A6.47), it follows

$$B_1 + B_2 = D_1 + D_2 = \frac{1}{2k}\left(E_1 - E_2\right) \tag{A6.48}$$

Equations (A6.31) and (A6.33) yield

$$\left(A_1 - C_1\right) + \left(A_2 - C_2\right) = \frac{Tk_t}{Dk^2}\left(F_1 - F_2\right) \tag{A6.49}$$

Combining equations (A6.29) and (A6.49), it gives

$$A_1 - C_2 = A_2 - C_1 = \frac{Tk_t}{2Dk^2}\left(F_1 - F_2\right) \tag{A6.50}$$

Combining equations (A6.31), (A6.41) and (A6.42), it follows

$$-\tanh\left(kL_x\right)B_1 + \tan\left(kL_x\right)D_1 = -\frac{Tk_t}{Dk^2}F_2 \tag{A6.51}$$

Combining equations (A6.32) and (A6.51), it gives

$$-\tanh\left(kL_x\right)\left(\frac{E_2}{k} + D_1\right) + \tan\left(kL_x\right)D_1 = -\frac{Tk_t}{Dk^2}F_2 \tag{A6.52}$$

Substituting equation (A6.46) into (A6.52), it gives

$$D_1 = -C_{01}E_2 \tag{A6.53}$$

where

$$C_{01} = \frac{1}{k}\frac{\tanh\left(kL_x\right) + \dfrac{Tk_t}{Dk}\tan\left(k_t L_y\right)}{\tanh\left(kL_x\right) + \tan\left(kL_x\right)} \tag{A6.54}$$

Substituting equation (A6.53) into (A6.42), it gives

$$C_1 = \tan\left(kL_x\right)C_{01}E_2 \tag{A6.55}$$

Then equations (A6.32) and (A6.55) yield

$$B_1 = \left(-\frac{1}{k} + C_{01}\right)E_2 \tag{A6.56}$$

Equations (A6.41) and (A6.56) yield

$$A_1 = \tanh\left(kL_x\right)\left(\frac{1}{k} - C_{01}\right)E_2 \tag{A6.57}$$

Similarly, combining equations (A6.33), (A6.43) and (A6.44), it gives

$$-\tanh\left(kL_y\right)B_2 + \tan\left(kL_y\right)D_2 = \frac{Tk_t}{Dk^2}F_1 \tag{A6.58}$$

Combining equations (A6.34) and (A6.58), it yields

$$-\tanh\left(kL_y\right)\frac{E_1}{k} + \left[\tanh\left(kL_y\right) + \tan\left(kL_y\right)\right]D_2 = \frac{Tk_t}{Dk^2}F_1 \tag{A6.59}$$

Substituting equation (A6.45) into (A6.59), it gives

$$D_2 = C_{02}E_1 \tag{A6.60}$$

where

$$C_{02} = \frac{1}{k}\frac{\tanh\left(kL_y\right) + \frac{Tk_t}{Dk}\tan\left(k_tL_x\right)}{\tanh\left(kL_y\right) + \tan\left(kL_y\right)} \tag{A6.61}$$

Substituting equation (A6.44) into (A6.60), it gives

$$C_2 = -\tan\left(kL_y\right)C_{02}E_1 \tag{A6.62}$$

Combining equations (A6.34) and (A6.60), it follows

$$B_2 = \left(\frac{1}{k} - C_{02}\right)E_1 \tag{A6.63}$$

Substituting equation (A6.43) into (A6.63), it gives

$$A_2 = -\tanh\left(kL_y\right)\left(\frac{1}{k} - C_{02}\right)E_1 \tag{A6.64}$$

Substituting equations (A6.55), (A6.57), (A6.62) and (A6.64) into (A6.29), it gives

$$C'_{01}E_2 + C'_{02}E_1 = 0 \tag{A6.65}$$

where

$$C'_{01} = \frac{\tanh\left(kL_x\right)}{k} - \left[\tanh\left(kL_x\right) - \tan\left(kL_x\right)\right]C_{01} \tag{A6.66}$$

$$C'_{02} = \frac{\tanh(kL_y)}{k} - \left[\tanh(kL_y) - \tan(kL_y)\right] C_{02} \tag{A6.67}$$

Substituting equations (A6.53), (A6.56), (A6.60) and (A6.63) into equation (A6.30), and then combining with equation (A6.65), the frequency equation of the L-shaped beam can be written as

$$\frac{1}{k}\left[C'_{01} + C'_{02}\right] = 2\left[C_{01}C'_{02} + C_{02}C'_{01}\right] \tag{A6.68}$$

The natural frequencies of the L-shaped beam can then be determined by solving the set of roots ω_n of equation (A6.68) by the relations

$$\omega_n = \sqrt{\frac{EI}{m}} k_n^2 = \sqrt{\frac{T}{J}} k_{t,n}, \quad n = 1, 2, \ldots \tag{A6.69}$$

Consequently, the elastic mode shape functions of the beam components can be expressed as

$$\phi_n(x) = A_n^{(1)} \cosh(k_n x) + B_n^{(1)} \sinh(k_n x) + C_n^{(1)} \cos(k_n x) + D_n^{(1)} \sin(k_n x) \tag{A6.70}$$

$$\varphi_n(y) = A_n^{(2)} \cosh(k_n y) + B_n^{(2)} \sinh(k_n y) + C_n^{(2)} \cos(k_n y) + D_n^{(2)} \sin(k_n y) \tag{A6.71}$$

where

$$A_n^{(1)} = -\frac{C'_{02}}{C'_{01}} \tanh(k_n L_x) \left(\frac{1}{k_n} - C_{01} \right) \tag{A6.72}$$

$$B_n^{(1)} = \frac{C'_{02}}{C'_{01}} \left(\frac{1}{k_n} - C_{01} \right) \tag{A6.73}$$

$$C_n^{(1)} = -\frac{C'_{02}}{C'_{01}} \tan(k_n L_x) C_{01} \tag{A6.74}$$

$$D_n^{(1)} = \frac{C'_{02}}{C'_{01}} C_{01} \tag{A6.75}$$

$$A_n^{(2)} = -\tanh(k_n L_y) \left(\frac{1}{k_n} - C_{02} \right) \tag{A6.76}$$

$$B_n^{(2)} = \frac{1}{k_n} - C_{02} \tag{A6.77}$$

$$C_n^{(2)} = -\tan(k_n L_y) C_{02} \tag{A6.78}$$

$$D_n^{(2)} = C_{02} \tag{A6.79}$$

And the torsional mode shapes of the beam components are

$$\theta_n(x) = E_n^{(1)} \cos\left(k_{t,n} x\right) + F_n^{(1)} \sin\left(k_{t,n} x\right) \tag{A6.80}$$

$$\theta_n(y) = E_n^{(2)} \cos\left(k_{t,n} y\right) + F_n^{(2)} \sin\left(k_{t,n} y\right) \tag{A6.81}$$

where

$$E_n^{(1)} = 1 \tag{A6.82}$$

$$F_n^{(1)} = \tan\left(k_{t,n} L_x\right) \tag{A6.83}$$

$$E_n^{(2)} = -\frac{C'_{02}}{C'_{01}} \tag{A6.84}$$

$$F_n^{(2)} = -\frac{C'_{02}}{C'_{01}} \tan\left(k_{t,n} L_y\right) \tag{A6.85}$$

Combining equations (A6.70) and (A6.71), the nth elastic mode shape function of the beam can be re-written as

$$\Psi_n(x,y) = \begin{cases} \phi_n(x) & 0 \le x \le L_x, y = 0 \\ \varphi_n(y) & 0 \le y \le L_y, x = 0 \end{cases}, \tag{A6.86}$$

Except the above elastic mode shape functions, a complete set of mode shape functions of the L–shaped beam considered here also include a rigid mode, which is defined as

$$\Psi_0(x,y) = \begin{cases} 1 - \dfrac{x}{L_x}, 0 \le x \le L_x, y = 0 \\ 1 - \dfrac{y}{L_y}, 0 \le y \le L_y, x = 0 \end{cases} \tag{A6.87}$$

and the associated natural frequency $\omega_0 = 0$.

So far a complete set of mode shapes Ψ_n as well as the associated natural frequencies ω_n have been derived for an L-shaped beam with simply supported boundary conditions. Ψ_n, of course, can be furthermore normalized as required.

Especially, when $L_x = L_b, L_y = 0$, i.e., a straight beam with both ends simply supported, no torsion waves are included so that $k_t = 0$. By the relations given in

equations (A6.54), (A6.61), (A6.66) and (A6.67), the frequency equation (A6.68) becomes $C'_{01}=0$, i.e.,

$$\frac{\tanh\left(kL_b\right)}{k}=\left[\tanh\left(kL_b\right)-\tan\left(kL_b\right)\right]\frac{1}{k}\frac{\tanh\left(kL_b\right)}{\tanh\left(kL_b\right)+\tan\left(kL_b\right)} \tag{A6.88}$$

which yields

$$\tan\left(kL_b\right)=0 \Rightarrow \sin\left(kL_b\right)=0 \tag{A6.89}$$

The above equation is just the frequencies of a straight beam with both ends simply supported, being given by

$$k_n=\frac{n\pi}{L_b} \tag{A6.90}$$

Appendix VII

NATURAL MODES AND NATURAL FREQUENCIES OF A FREE-FREE BEAM

A7.1 Natural frequencies of the beam

For an Euler-Bernoulli free-free beam (i.e., with both ends free), in Ref. [40], the natural frequencies of the beam can be determined by solving the following equation

$$1-\cosh(kL_b)\cos(kL_b)=0 \tag{A7.1}$$

where k is the wavenumber of the beam and L_b is the length of the beam. The set of roots of equation (A7.1) therefore can be obtained as

$$k_1 L_b = 4.730 \tag{A7.2}$$

$$k_n L_b \approx \left(n+\frac{1}{2}\right)\pi \quad n \geq 2 \tag{A7.3}$$

By the relation $k=\sqrt[4]{m_b\omega^2/D_b}$, where m_b and D_b are respectively the mass distribution (mass per unit length) and bending stiffness of the beam, the nth natural frequency of the beam can be given as

$$\omega_n \approx \sqrt{\frac{D_b k_n^2}{m_b}} \tag{A7.4}$$

A7.2 Natural modes of the beam

The nth natural mode of a free-free beam is give by [40]

$$\phi_n(x)=\cosh(k_n x)+\cos(k_n x)-E_n\left[\sinh(k_n x)+\sin(k_n x)\right] \tag{A7.5}$$

where

$$E_n=\frac{\sinh(k_n L_b)+\sin(k_n L_b)}{\cosh(k_n L_b)-\cos(k_n L_b)} \tag{A7.6}$$

It should be noted that the expression ϕ_n given in equation (A7.5) is not in a normalized form.

Appendix VIII

LIST OF PUBLICATIONS

1 L. Ji, B. R. Mace and R. J. Pinnington 2001 *Institute of Sound and Vibration Research Technical Memorandum ISVR* 877. Power transmission to flexible receiver by force sources.

2 L. Ji, B. R. Mace and R. J. Pinnington 2001 *Institute of Sound and Vibration Research Technical Memorandum ISVR* 876. Vibration power transmission between long-wavelength sources and short-wavelength receivers.

3 L. Ji, B. R. Mace and R. J. Pinnington 2002 *Institute of Acoustics Spring Conference*, March 25-27, Salford, United Kingdom. A power mode technique for estimating power transmission to a flexible receiver.

4 L. Ji, B. R. Mace and R. J. Pinnington 2002 *ISMA International Conference on Noise and Vibration Engineering*, September16-18, Leuven, Belgium. A power mode approach for estimating power transmission between a stiff source and a flexible receiver.

5 L. Ji, B. R. Mace and R. J. Pinnington 2003 *Journal of Sound and Vibration* 265, 387-399. A power mode approach to estimating vibrational power transmission by multiple sources.

6 L. Ji, B. R. Mace and R. J. Pinnington. *Journal of Sound and Vibration.* Estimation of power transmission to a flexible receiver from a stiff source using a power mode approach. (Accepted as P/182/02, YJSVI 5827)

7 L. Ji, B. R. Mace and R. J. Pinnington. *Tenth International Congress on Sound and Vibration, ICSV10*, July 7-10, Stockholm, Sweden. A mode-based approach to the vibration analysis of coupled long- and short-wavelength subsystems.

8 L. Ji, B. R. Mace and R. J. Pinnington 2003 *Eighth International Conference on Recent Advances in Structural Dynamics*, July 14-16, Southampton, United Kingdom. Vibration approximation for a complex built-up system consisting of both long-wavelength and short-wavelength substructures.

9 L. Ji, B. R. Mace and R. J. Pinnington. *Journal of Sound and Vibration*. A hybrid mode/Fourier Transform approach to estimating the vibration of beam-stiffened plate systems. (Accepted as P/066/03 in May 2003)

10 L. Ji, B. R. Mace and R. J. Pinnington. *Journal of Sound and Vibration*. A mode-based approach for the dynamic analysis of built-up structures. (Submitted to JSV in September 2003)